

Textile Reinforced Concrete: Design Methodology and Novel Reinforcement

Fahed Abdullah S Alrshoudi

Submitted in accordance with the requirements for the degree of
Doctor of Philosophy

The University of Leeds
School of Civil Engineering

The candidate confirms that the work submitted is his own and that appropriate credit has been given where reference has been made to the work of others.

This copy has been supplied on the understanding that it is copyright material and that no quotation from the thesis may be published without proper acknowledgement.

ACKNOWLEDGMENT

I would like to express my sincere gratitude to the supervisors, Prof Phil Purnell and Prof John Forth for their great patience in guiding me and for their useful advice during the various stages of the research.

I wish to thank the technical staff (Marvin Wilman, Steve Holmes and Peter Flatt) who facilitated so much of this work.

My thanks go to the FORMAX Company for supplying me the reinforcement material that it is used in this study.

I would like to extend my acknowledgment to King Saud University for their financial support.

I'd like to dedicate this work with all my love and appreciation

To

My wonderful parents Abdullah Alrshoudi and Hessa Almoqbel

To

My brothers and sister

To

My wife and children for their enormous patience and support

To

Whom I will be deeply indebted for the rest of my life

ABSTRACT

Fibre reinforcement has been used to reinforce concrete members for decades. It has combined well with concrete to help control cracking and increase toughness and other properties such as corrosion resistance. The use of traditional fibre reinforcement has led to the development of a new material called textile reinforcement (multifilament continuous fibre) which can also be used as the main reinforcement instead of steel reinforcement. This study experimentally investigates concrete beams reinforced only with carbon textile material (TRC beams).

The tensile strength of textile reinforcement and pull out strength of TRC were measured. Four-point bending tests were performed on 76 beams (small and large scale beams). Several parameters such as volume fraction and reinforcement layout were studied in order to investigate their effect on TRC beam behaviour. The results showed that with the correct layout and geometry of textile reinforcement, these reinforced concrete beams, providing they had sufficient cover thickness, would perform well. Also, the results confirmed that the bond between the concrete and textile reinforcement plays a vital role in TRC beam performance. The behaviour of the TRC beams was compared with that of the steel reinforced concrete (SRC) beams; a major advantage of the TRC beam was the reduced crack widths.

This study finishes by proposing a design methodology for TRC beams. Guidance covers flexural design, predictions for moment-curvature, and predictions for crack width of TRC beams.

TABLE OF CONTENTS

1- ACKNOWLEDGMENT	iii
2- ABSTRACT	v
3- Table of Contents	vi
4- List of Tables	xii
5- List of Figures	xv
6- Notations	xxii
7- Abbreviation	xxvii
CHAPTER 1	1
INTRODUCTION	1
1.1 Background.....	1
1.2 Textile reinforced concrete (TRC)	3
1.3 Research aim and objectives	5
1.4 Outline of thesis	6
CHAPTER 2	8
LITERATURE REVIEW	8
2.1 Historical background.....	8
2.2 Fibre reinforced concrete (FRC).....	8
2.2.1 FRC behaviour	9
2.2.2 Fibre-matrix interaction	10
2.2.3 FRC flexural moment	13
2.2.4 Efficiency factors of fibre reinforced concrete.....	15
2.2.5 Mechanics of FRC.....	18
2.3 Textile reinforced concrete (TRC)	21
2.3.1 Cementitious matrix	22
2.3.1.1 Fine grained concrete	23
2.3.2 Textile reinforcement.....	25
2.3.3 Textile properties.....	28
2.3.4 Textile geometry.....	30
2.3.5 Textile reinforced concrete behaviour	32
2.3.5.1 TRC tensile strength	33
2.3.5.2 Textile pull out.....	34
2.3.5.3 Stress-strain behaviour of TRC.....	39
2.3.5.4 Cracking.....	40

2.3.6	Bending moment behaviour of TRC	41
2.3.7	Efficiency of textile reinforced concrete (TRC)	43
2.3.8	Bond.....	44
2.4	Design method	47
2.4.1	Flexural design of TRC	48
2.4.1.1	Papanicolaou's method.....	49
2.4.1.2	Voss's method	51
2.5	TRC manufacturing methods	55
2.5.1	Hand lay-up.....	56
2.5.2	Pultrusion	57
2.5.3	Filament winding	57
2.5.4	Module process.....	57
2.6	TRC applications.....	58
2.6.1	Façade panels.....	58
2.6.2	Decentralised wastewater treatment plants	58
2.6.3	Integrated formwork	60
2.6.4	Various applications	60
2.7	Conclusion	62
CHAPTER 3.....		65
MATERIALS AND METHOD		65
3.1	Introduction	65
3.2	Materials.....	65
3.2.1	Cement	65
3.2.2	Fly ash	66
3.2.3	Silica fume.....	68
3.2.4	Fine aggregate	69
3.2.5	Coarse aggregate	69
3.2.6	Water	70
3.2.7	Superplasticisers.....	70
3.2.8	Reinforcement.....	71
3.2.8.1	Steel reinforcement.....	71
3.2.8.2	Textile reinforcement	72
3.3	Preliminary work.....	76
3.3.1	Trial mixes.....	76
3.4	Casting and curing	77

3.5	Mechanical Testing	79
3.5.1	Compression test	79
3.5.2	Tensile test.....	80
3.5.3	Pull out test	82
3.5.4	Flexural test.....	83
3.6	Experimental programme	86
3.6.1	Notation.....	89
3.6.1.1	Small scale beams	89
3.6.1.1.1	Biaxial textile	89
3.6.1.1.2	Tow textile (uni-axial textile).....	94
3.6.1.1.3	Chopped fibre.....	97
3.6.1.1.4	Plain concrete	97
3.6.1.1.5	Steel.....	97
3.6.1.2	Large scale beams.....	97
3.6.1.2.1	Woven fabric	98
3.6.1.2.2	Tow textile (Uni-axial direction)	99
3.6.1.2.3	Steel.....	102
CHAPTER 4	104
RESULTS	104
4.1	Introduction	104
4.2	Tensile testing of reinforcement	104
4.3	Pull out test	106
4.4	Four point bending test	107
4.4.1	Small scale beams	107
4.4.1.1	Plain concrete	107
4.4.1.2	Biaxial textile (woven fabric).....	109
4.4.1.3	Tow textile (uni-axial textile).....	122

4.4.1.4	Chopped fibre	129
4.4.1.5	Steel.....	130
4.4.2	Large scale beams.....	133
4.4.2.1	Biaxial textile (woven fabric).....	133
4.4.2.2	Tow textile (uniaxial textile).....	135
4.4.2.3	Steel.....	141
CHAPTER 5	143
	DISCUSSION and ANALYSIS	143
5.1	The effect of textile geometry and lay out	143
5.1.1	The effect of the voids ratio of a textile.....	143
5.1.2	The effect of layering reinforcement.....	145
5.1.3	The effect of cover thickness.....	147
5.1.4	The effect of the orientation	148
5.1.5	The effect of the increase in the number of layers	149
5.1.6	The effect of weft rovings	150
5.1.7	The effect of the volume fraction	152
5.1.8	The effect of the cross sectional area	153
5.1.9	The effect of a change in geometry.....	154
5.1.10	FRC vs TRC.....	156
5.2	Influence of reinforcement type	159
5.3	Large scale beam.....	161
5.3.1	The effect of anchored roving.....	161
5.3.2	The effect of layering.....	163
5.3.3	The effect of volume fraction.....	165
5.3.4	The effect of cross sectional area	166
5.3.5	The effect of increase in the number of layers	168
5.3.6	The effect of cover thickness.....	170
5.4	Conclusions.....	174
CHAPTER 6	176
	Textile reinforced concrete (TRC) versus Steel reinforced concrete (SRC)	176
6.1	Flexural behaviour.....	176
6.1.1	Moment curvature	176
6.1.2	Comparison of TRC and SRC beams containing identical reinforcement areas	179

6.1.3	Comparison of TRC and SRC beams containing identical reinforcement stiffness	182
6.1.4	Cracking	185
6.1.4.1	First crack	185
6.1.4.2	Crack spacing	187
6.1.4.3	Crack development	189
6.1.4.4	Crack width	192
6.1.5	Tension stiffening	195
6.2	Conclusions.....	198
Chapter 7	200
	Textile Reinforced Concrete Design Methodology	200
7.1	Design concepts.....	200
7.1.1	Design assumptions.....	201
7.2	Analysis and design of carbon textile reinforced concrete	202
7.2.1	Tension failure.....	202
7.2.2	TRC beam behaviour	204
7.2.2.1	Uncracked section	204
7.2.2.2	Cracked section	206
7.2.3	Design of TRC beams using tension control	208
7.2.3.1	Bond efficiency factor.....	213
7.2.3.1.1	Volume fraction	214
7.2.3.1.2	Textile geometry.....	216
7.2.4	Reduction factor	217
7.2.5	Moment-curvature prediction.....	218
7.2.6	Predicting crack width	221
7.3	Examples	221
7.4	Conclusions.....	229
CHAPTER 8	231
	CONCLUSIONS and RECOMMENDATIONS FOR FUTURE STUDIES.....	231
8.1	Introduction	231
8.2	Conclusions.....	231
8.3	Recommendations for further study	234

Reference..... 236

LIST OF TABLES

Table 2-1 Matrix components (Brameshuber <i>et al.</i> 2006).	24
Table 3-1 Manufacturer data sheet of chemical compositions and physical properties of OPC.	66
Table 3-2 Manufacturer data sheet of chemical compounds and physical properties.	67
Table 3-3 Manufacturer data sheet of the chemical compounds and physical properties	68
Table 3-4 Sieve analyses results of fine aggregate.....	69
Table 3-5 Sieve analysis results of coarse aggregate 10 mm.	70
Table 3-6 Technical data of Sika®ViscoCrete 25MP.	71
Table 3-7 25 mm carbon textile properties of biaxial reinforcement (C50k, 260, 0/90).	73
Table 3-8 50 mm roving (warp and weft) spacing of carbon textile properties of biaxial reinforcement (C50k, 150, 0/90).....	74
Table 3-9 Carbon textile properties of tow (uniaxial) reinforcement (C24k).	75
Table 3-10 Carbon textile properties of tow (uniaxial) reinforcement (C50k).	75
Table 3-11 Matrix compositions.	77
Table 3-12 Properties of different mixes at preliminary stage of fine concrete.	78
Table 3-13 Properties of different mixes at preliminary stage of normal concrete.	79
Table 4.1 The results of plain concrete.	108
111	
Table 4.4 The results of uni-axial roving with 50k filaments reinforced beams.	123
Table 4.5 The results of uni-axial roving with 24k filaments reinforced beams.	124
Table 4.6 The results of chopped fibre reinforced concrete beams.....	132
Table 4.7 The results of steel reinforced concrete beams.....	132
Table 4.8 Fabric reinforced concrete beam result.	133
Table 4.9 Edge straight uni-axial tow textile reinforced beam.	135

Table 4.10 Results of anchored uni-axial tow reinforced beam.....	138
Table 4.11 Results of steel reinforced beam.....	141
Table 5-1 Average ultimate load and deflection of a bi-axial textile in both directions.....	145
Table 5-2 Average ultimate load and deflection of a layered bi-axial TRC beam.....	146
Table 5-3 Average ultimate load and deflection of different TRC cover thicknesses.....	147
Table 5-4 Ultimate load and deflection of $\pm 45^0$ TRC.....	148
Table 5-5 Average ultimate load and deflection of TRC for different numbers of layers.....	150
Table 5-6 Average ultimate load and deflection of uni and bi-axial TRC beams.....	151
Table 5-7 The bond efficiency factor for various fibre geometries.....	155
Table 5-8 Average ultimate load and deflection of FRC and TRC beams.....	157
Table 5-9 Straight and anchored textile reinforced concrete.....	161
Table 5-10 Results for TRC with different layers of the same cross sectional area.....	164
Table 5-11 Result of changing volume fraction.....	166
Table 5-12 Results for increased cross sectional area.....	167
Table 5-13 The effect of increasing the number of rovings.....	169
Table 5-14 Flexural results for different cover thicknesses.....	171
Table 6-1 First crack load and deflection of steel reinforced concrete, and textile reinforced concrete.....	187
Table 6-2 The development in number of cracks and average crack length of TRC and SRC.....	191
Table 6-3 Crack width with increasing applied load for the SRC and TRC beams.....	194
Table 7-1 The bond efficiency factor for various volume fractions and numbers of layers.....	215
Table 7-2 The bond efficiency factor for various fibre geometries.....	216
Table 7-3 Measured and calculated crack width of a TRC beam.....	222
Table 7-4 Measured crack width of a TRC beam and calculated crack width based on the new proposed equation.....	225

Table 7-5 The results for calculated and experimental nominal moment.

..... 228

LIST OF FIGURES

Figure 1-1 Corroded steel reinforced concrete beam (www.adbengineering.com).	2
Figure 1-2 Textile reinforced concrete beam: a) 0.8 x magnification, b) 5 x magnification.	2
Figure 1-3 Textile reinforcement.	3
Figure 1-4 Fine grained concrete.	4
Figure 1-5 Comparison between different systems of reinforcement.	5
Figure 2-1 Stress-strain behaviour of FRC: a) Strain-softening; b) Strain- hardening (Naaman 2007).	10
Figure 2-2 Fibre pull out test results of a sample cured for 3 days and fibre embedded length 20 mm (Mobasher and Li 1996).....	13
Figure 2-3 Stresses and strains of a cracked fibre reinforced concrete beam (Hannant 2003).	14
Figure 2-4 a) Stress block at elastic flexural in tension and compression. b) Stress block at elastic in compression and plastic in tension (Hannant 2003).	15
Figure 2-5 Length and orientation efficiency factor (Purnell 2010c).	17
Figure 2-6 Two types of fibre failure (Purnell 2010c).....	17
Figure 2-7 Stress-strain model for FRC (Aveston, Cooper and Kelly 1971).....	19
Figure 2-8 Various kinds of fibres (ITP, TU Dresden).....	25
Figure 2-9 Different types of woven textile, a) Multi-axial carbon, b and e) Biaxial carbon, c) Biaxial glass, d) Glass-carbon fabric.	27
Figure 2-10 Mechanical properties of various textile materials (ITP, TU Dresden).	29
Figure 2-11 Load-strain of two layers of carbon and glass textile reinforced concrete, respectively (Hegger <i>et al.</i> 2006b).....	29
Figure 2-12 Different fabric structures: a) weft insertion knit fabric, b) short weft knit fabric, and c) woven fabric (Peled and Bentur 2000).	32
Figure 2-13 Load bearing capacity of different forms of textile, such as filaments and roving (Hegger <i>et al.</i> 2006c).	34
Figure 2-14 Specimen for the one sided strand pull out test (Banholzer 2006).....	36
Figure 2-15 Specimen responses to pull out test (Banholzer 2006).....	36

Figure 2-16 Active filament versus displacement diagram $N_F(\Omega)$ and pull out load versus displacement $P(\Omega)$ for specimens A to D (Banholzer 2006).....	37
Figure 2-17 Failure mechanism of a strand embedded in a cement based matrix under a pull out load (Banholzer 2006).	37
Figure 2-18 Bond layer model (Hegger, Bruckermann and Chudoba 2004).....	38
Figure 2-19 Stress-strain behaviour of textile reinforced concrete under uniaxial loading (Hegger <i>et al.</i> 2006c).....	40
Figure 2-20 Flexural behaviour of different geometries of PE at $V_f = 5.7\%$ (Peled and Bentur 2003).	42
Figure 2-21 Influence of the density of weft rovings on flexural strength (Peled and Bentur 2003).	43
Figure 2-22 The internal strain in the roving (Jesse <i>et al.</i> 2008).	46
Figure 2-23 Inner and outer bond (Reinhardt <i>et al.</i> 2006b).	46
Figure 2-24 Woven fabric embedded in cement matrix (Peled, Bentur and Yankelevsky 1998).	47
Figure 2-25 Beam details.	49
Figure 2-26 Strain profile of the cross section of the roving (Papanicolaou and Papantoniou 2010): a) strain distribution in a coated roving; b) uncoated roving; c) simplification of strain distribution in an uncoated roving.....	51
Figure 2-27 Beam details.	51
Figure 2-28 Influence of the change in textile direction on load bearing capacity (Hegger and Voss 2004).	53
Figure 2-29 Ratio between ultimate tensile strength under bending moment and tensile loading (Voss <i>et al.</i> 2006a).	54
Figure 2-30 Cement penetration of two methods of processing: a) and c) pultrusion, and b) and d) casting (Reinhardt <i>et al.</i> 2006a).	56
Figure 2-31 TRC façade panels on various buildings.....	59
Figure 2-32 TRC for decentralised wastewater treatment plants (ibac, IMB RWTH Aachen University + Fa.Mall).	60
Figure 2-33 TRC formwork elements integrated with steel reinforced concrete floors.....	61
Figure 2-34 Various applications of TRC by a) Prull (1995), b) Lieboldt <i>et al.</i> (2005), c) RWTH Aachen Germany.	61

Figure 3-1 Different types of carbon reinforcements.	72
Figure 3-2 Layout of biaxial carbon textile reinforcement with 2.5 cm looping size.	73
Figure 3-3 Layout of biaxial carbon textile reinforcement with 5 cm looping size.	74
Figure 3-4 Compression test setup.	80
Figure 3-5 Textile roving preparation before test.	81
Figure 3-6 The setup of tensile test of carbon roving.	81
Figure 3-7 Tensile test setup of steel rebar.	82
Figure 3-8 Pull-out test set-up a) straight edge b) anchored edge.	83
Figure 3-9 Set-up of four point bending test of small scale beam.	84
Figure 3-10 Experimental set-up of four point bending test of large scale beam.	85
Figure 3-11 Demecs setup.	85
Figure 3-12 Optical microscope.	86
Figure 3-13 Experimental programme for small scale beams.	87
Figure 3-14 Experimental programme for large scale beams.	88
Figure 3-15 Basic reinforcement details of small scale beam; a) biaxial textile reinforced concrete. b) tow textile reinforced concrete.	90
Figure 3-16 Top view of weft direction of textile reinforced concrete.	91
Figure 3-17 Biaxial textile reinforcement reinforced concrete in two separated layers of warp or weft direction.	92
Figure 3-18 25 mm cover thickness.	92
Figure 3-19 Top view of 5 cm woven fabric of textile reinforced concrete.	93
Figure 3-20 Cross section and side view of web reinforcement.	94
Figure 3-21 Different patterns of tows.	95
Figure 3-22 Longitudinal tows reinforced concrete beam.	96
Figure 3-23 Beam reinforcement default of large scale beam.	98
Figure 3-24 Top view of biaxial textile reinforced concrete beam.	99
Figure 3-25 Uniaxial textile reinforcement; a) 4UT ₈ -S-2.6, b) 4UT ₈ -S-L-2.6.	101
Figure 3-26 Uniaxial textile reinforced concrete at different layouts; a) 3UT _{12 or 15} -Anch-L ₃ -2.6, b) 3UT ₁₅ -Anch-L ₃ -2.6-C ₁₅	102

Figure 3-27 Steel reinforcement details.....	103
Figure 4-1 Tensile stress-strain behaviour of carbon tow, 50k.	105
Figure 4-2 Tensile stress-strain behaviour of 8 mm steel rebar.	105
Figure 4-3 Load-Deflection behaviour at mid-span of plain concrete beam.....	108
Figure 4-4 Load-Deflection behaviour at mid-span of woven fabric (2.5 cm) at warp direction reinforced beams.	112
Figure 4-5 Cracks pattern of beam reinforced by BT ₇ ,50k.	112
Figure 4-6 Load-Deflection behaviour at mid-span of woven fabric (2.5 cm) at weft direction reinforced beams.	113
Figure 4-7 Cracks pattern of beam reinforced by BT ₄₋₉₀ ,50k.	114
Figure 4-8 Load-Deflection behaviour at mid-span of different layers of woven fabric (2.5 cm) at warp direction reinforced beams.	115
Figure 4-9 Cracks pattern of beam reinforced by BT _{7-L} ,50k.	116
Figure 4-10 Load-Deflection behaviour at mid-span of different layers of woven fabric (2.5 cm) at weft direction reinforced beams.	117
Figure 4-11 Cracks pattern of beam reinforced by BT _{4-90-L} ,50k.	118
Figure 4-12 Load-Deflection behaviour at mid-span of woven fabric (2.5 cm) at weft direction reinforced beams with 2.5 cm cover.....	118
Figure 4-13 Cracks pattern of beam reinforced by BT _{3-90-C} ,50k.....	119
Figure 4-14 Load-Deflection behaviour at mid-span of woven fabric (2.5 cm) at ± 45 direction reinforced beams.	119
Figure 4-15 Load-Deflection behaviour at mid-span of woven fabric (5 cm) at warp direction reinforced beams.	120
Figure 4-16 Cracks pattern of beam reinforced by BT ₈ -5cm,50k.....	120
Figure 4-17 Load-Deflection behaviour at mid-span of web woven fabric (5 cm) at warp direction reinforced beams.	121
Figure 4-18 Cracks pattern of beam reinforced by BT _{3-W} ,50k.....	121
Figure 4-19 Load-Deflection behaviour at mid-span of uni-axial tow at the same volume fraction (0.31%) with different geometries.....	125
Figure 4-20 Cracks pattern of beam reinforced by UT _{b4} ,50k.....	125
Figure 4-21 Cracks pattern of beam reinforced by UT _{br4} ,50k.	126
Figure 4-22 Load-Deflection behaviour at mid-span of uni-axial tow at different quantity of fibre.....	127
Figure 4-23 Cracks pattern of beam reinforced by UT ₄ ,50k.	128

Figure 4-24 Cracks pattern of beam reinforced by UT ₇ ,50k.	128
Figure 4-25 Load-Deflection behaviour at mid-span of short fibre at different quantity.....	129
Figure 4-26 Cracks pattern of beam reinforced by short fibres T-1.08%,50k.	130
Figure 4-27 Load-Deflection behaviour at mid-span of steel reinforced concrete beam.	131
Figure 4-28 Cracks pattern of beam reinforced by steel.....	131
Figure 4-29 Load-Deflection behaviour at mid-span of woven textile at large scale beam.....	134
Figure 4-30 Cracks patterns of BT _(5cm) ¹⁴ -Anch-2.6-L, 50k.....	134
Figure 4-31 Load-Deflection behaviour at mid-span of uni-axial textile reinforcement at different layers.....	136
Figure 4-32 Cracks patterns of UT ₈ -2.6, 50k.....	136
Figure 4-33 Cracks patterns of UT ₈ -L-2.6, 50k.....	137
Figure 4-34 Load-Deflection behaviour at mid-span of anchored uni-axial reinforcement at different layouts.....	139
Figure 4-35 Crack patterns of different layouts of uni-axial textile reinforced concrete beams.....	140
Figure 4-36 Load-Deflection behaviour at mid-span of steel reinforced concrete beam.	141
Figure 4-37 Crack pattern of steel reinforced concrete.	142
Figure 5-1 The width of different reinforcement rovings.	145
Figure 5-2 Load-deflection behaviour at mid-span of textile reinforcement with and without weft rovings.	152
Figure 5-3 Load-deflection curves at mid-span for different roving geometries at the same volume fraction.	156
Figure 5-4 Load-deflection behaviour at mid-span of TRC vs FRC at 0.62% volume fraction.....	158
Figure 5-5 Load-deflection behaviour at mid-span of TRC vs FRC at 1.08% volume fraction.....	158
Figure 5-6 Load-deflection behaviour at mid-span of different types of reinforcement of the same area.	160
Figure 5-7 Reinforcement details of T ₈ , straight and anchored.	162
Figure 5-8 UT ₈ -Anch-2.6 cracks.....	162

Figure 5-9 Reinforcement details of UT ₈ -Anch-2.6 and UT ₁₂ -Anch-3L ₃ -2.6.....	164
Figure 5-10 Reinforcement details of UT ₁₂ -Anch-3L ₃ -2.6 and UT ₁₅ -Anch-3L ₃ -2.6.....	167
Figure 5-11 Load-deflection behaviour at mid-span of UT ₁₂ -Anch-3L ₃ -2.6 and UT ₁₅ -Anch-3L ₃ -2.6.....	168
Figure 5-12 Reinforcement details of UT ₈ -Anch-L-2.6 and UT ₁₂ -Anch-L-2.6.....	170
Figure 5-13 Different cover thicknesses of textile reinforcements.	171
Figure 5-14 Load-deflection behaviour at mid-span of TRC with different cover thicknesses.....	172
Figure 5-15 Cracking pattern of TRC with different cover thicknesses.....	174
Figure 6-1 Surface strain of TRC beams obtained by reading demec points.	177
Figure 6-2 Calculation of beam curvature.	177
Figure 6-3 Moment-curvature relationship of TRC and SRC beams.	178
Figure 6-4 Load-deflection behaviour at mid-span of uniaxial tow and steel reinforced concrete beams of the same area.	180
Figure 6-5 Failure mode of UT ₇ ,50k.....	180
Figure 6-6 Load-deflection behaviour at mid-span of uniaxial reinforcement (tow) and steel reinforced concrete beams.	182
Figure 6-7 Load-deflection behaviour at mid-span of uniaxial reinforcement of carbon (tow) and steel reinforced concrete beams of the same stiffness.	184
Figure 6-8 Failure mode of UT _{5.5} ,50k.....	185
Figure 6-9 Crack pattern of the steel reinforced concrete beam.	188
Figure 6-10 Crack pattern of the TRC beam.	189
Figure 6-11 Stress distribution between cracks (Forth and Martin 2014).	190
Figure 6-12 Definition of variables for the crack width calculations (Nilson, Darwin and Dolan 2009).	193
Figure 6-13 Tension stiffening of SRC beam.	197
Figure 6-14 Tension stiffening of TRC beam.....	198
Figure 7-1 Balanced section.....	204
Figure 7-2 Stress and strain distribution of an elastic section.	205

Figure 7-3a) Stress and strain distribution at elastic cracked section, b) at cracked transformed section (Nilson, Darwin and Dolan 2009). ...	207
Figure 7-4 Stress and strain distribution (ACI-440 2006).	210
Figure 7-5 Stress and strain distribution of a TRC control beam.	211
Figure 7-6 k_1 and k_2 relative to concrete strength.	213
Figure 7-7 Bond efficiency factor with volume fraction.	215
Figure 7-8 Bond efficiency factor and ultimate load with the same volume fraction ($V_f = 0.31$) and 4 layers for all beams with different geometries.	217
Figure 7-9 Normal distribution of designed capacity over the experimental capacity of beams reinforced by carbon textile.	218
Figure 7-10 Predicted moment-curvature of a TRC beam against 4 experimentally beams measured.	221
Figure 7-11 The relationship between the measured/calculated crack and the load of the TRC beam.	223

NOTATIONS

The following symbols are used in this thesis:

a : Depth of stress block;

A_c : Concrete area;

A_f : Fibre reinforcement area;

A'_f : Effective fibre reinforcement area;

A_s : Steel reinforcement area;

A_t : Textile reinforcement area;

b : Beam width;

c : The distance from extreme compression fibre to neutral axis;

c_b : The distance from extreme compression fibre to neutral axis at balanced strain condition;

d : The effective depth of reinforced beam;

D : The beam depth;

d_c : The concrete cover thickness until the centre of the bar closest to that face;

E_f : Modulus of elasticity of fibre;

E_m : Modulus of elasticity of matrix;

f'_c : cylinder compressive strength of concrete;

f_c : Stress of concrete;

F_{ctu} : The tensile strength of TRC;

f_{eff} : The effective tensile strength;

f_f :Fibre tensile stress;

f_{fu} : Ultimate tensile strength of fibre;

f_s : The steel stress at particular load;

f_y : yield strength of steel;

f_r :The modulus of rupture;

I_{cr} : The cracked moment of inertia;

I_{eff} : The effective moment of inertia;

I_g : The gross moment of inertia;

h : Height of beam;

k :The number of filaments in thousands in each roving;

k_r : Roving reduction factor;

k_b : Factor that represents the textile area in good contact with matrix;

k_s :Factor that represents the strain lag which accounts for the differentiation in strain between the inner and outer filaments;

$k_{0,\alpha}$: The factor for orientation of the reinforcement;

k_2 : The factor of biaxial load;

$k_{fl,p}$: The factor for bending loading;

l : The embedded length;

$l_{s,max}$: The maximum distance over which slip between the concrete and steel occurs;

M : Bending moment;

M_a : Service moment;

M_{cr} : Cracking moment;

M_n : Nominal moment;

M_u : External factored moment;

n : Modular ratio;

P : The pull out force;

P_n : Nominal load;

P_u : Ultimate load;

r : The radius of fibre;

V_f : Volume fraction of fibre;

$V_{f,crit}$: Critical volume fraction of fibre;

V_m : Volume fraction of matrix;

w : the crack width;

w/c : water-cement ratio;

y_t : The distance from centroid to the tension edge;

z : The internal lever arm;

β_1 : A coefficient depends on the compressive strength of concrete;

ε_c : Concrete strain;

ε_{cm} : The average concrete strain with $l_{s,max}$;

ε_{cs} : The concrete shrinkage strain;

ε_{cu} : The ultimate strain in the concrete;

ε_f : Tensile strain of fibre;

ε_{fu} : Ultimate tensile strain of fibre;

ε_m : Matrix strain;

ε_{mu} : The ultimate matrix strain;

ε_{sm} : The average steel strain with in $l_{s,max}$;

ε_y : The yield strain of steel;

ρ_{fb} : The balanced fibre reinforcement ratio;

ρ_f : The textile reinforcement ratio;

Φ : The strength reduction factor;

\emptyset : Beam moment-curvature;

τ : The interface bond strength;

τ_{au} : Shear adhesional stress;

τ_{fu} : Shear frictional resistant stress;

η : The efficiency factor;

η_l : The length efficiency factor;

η_o : The orientation efficiency factor;

η_τ : The bond efficiency factor;

σ_c : the composite stress;

σ_{cu} : The ultimate composite strength;

σ_f : the fibre stress;

σ_{fl} : Flexural tensile stress at un-cracked section;

σ_{fu} : The ultimate fibre strength;

σ_m : the matrix stress;

σ_{mu} : The ultimate matrix strength;

ABBREVIATION

The following symbols are used in this thesis:

FRC: Fibre reinforced concrete;

TRC: Textile reinforced concrete;

SRC: Steel reinforced concrete;

LVDT :Linear variable differential transformer;

MoR : Modulus of rupture;

CHAPTER 1

INTRODUCTION

1.1 Background

In recent times, there has been an increased demand for structures to be built with materials which have improved properties in terms of physical performance and durability; the new aim is for more sustainable, longer lasting, lower maintenance structures. Nowadays, governments spend too much money on existing structures. Most of the expense is related to the maintenance and repair of structural members which have deteriorated due to problems associated with the corrosion of steel reinforcements. Figure 1-1 shows a sample of corroded steel reinforced concrete. The cost of this kind of deterioration in terms of money, time, and inconvenience is relatively high. For example, the cost of corrosion in America is more than \$276 billion per year (Yang 2008) and in the UK 4-5% of Gross National Product (GNP) (Ghali, Sastri and Elboudjaini 2007). Finding a new material which would negate these sorts of problems/costs would therefore be of great benefit to society and the economy (Mobasher 2011).

Discontinuous fibres have been used inside the concrete, mainly as a form of secondary reinforcement, in order to control cracking. This is not a method for replacing the main steel reinforcement (Bentur and Mindess 2006). Fibre materials such as alkali-resistant glass and carbon fibre have been used for decades to strengthen and rehabilitate RC structural members. These materials do not corrode in the normal sense which could lead to several structural benefits, i.e. reduced cover dimensions and hence structural element thickness (Keil, Cuyper and Wastiels 2008). Recently, roving fibre has been investigated as a main reinforcement to replace steel reinforcement. Tysmans *et al.* (2009) stated that as the tensile strength of textile reinforcement is high, there is a possibility that it could be used as a main reinforcement instead of steel. Figure 1-2 shows a cross section of a concrete beam reinforced with textile material.



Figure 1-1 Corroded steel reinforced concrete beam
(www.adbengineering.com).

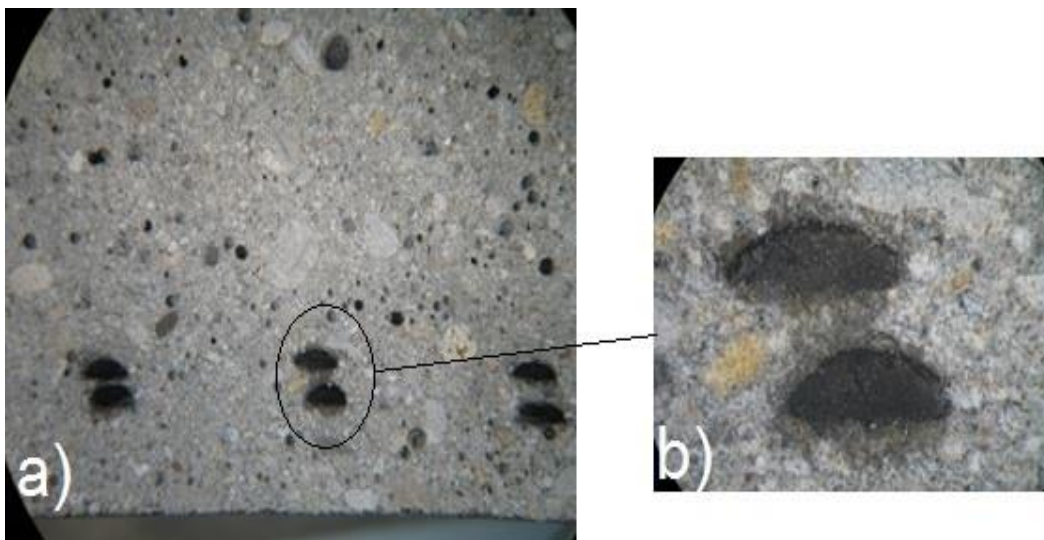


Figure 1-2 Textile reinforced concrete beam: a) 0.8 x magnification, b) 5 x magnification.

1.2 Textile reinforced concrete (TRC)

TRC is defined as a combination of a fine grained concrete and textile material (Häußler-Combe and Hartig 2006; Sickert *et al.* 2006; Steinigen *et al.* 2006). Figure 1-3 and Figure 1-4 show the textile reinforcement and fine grained concrete, respectively. The textile fabric could be alkali-resistant glass or carbon consisting of multifilament roving; the concrete is normally designed with 1 mm maximum aggregate size (Häußler-Combe and Hartig 2007). This combination provides a composite material that has many favourable features such as high tensile strength, corrosion resistance, thin cover, and reduced self-weight (Al-Jamous *et al.* 2006).

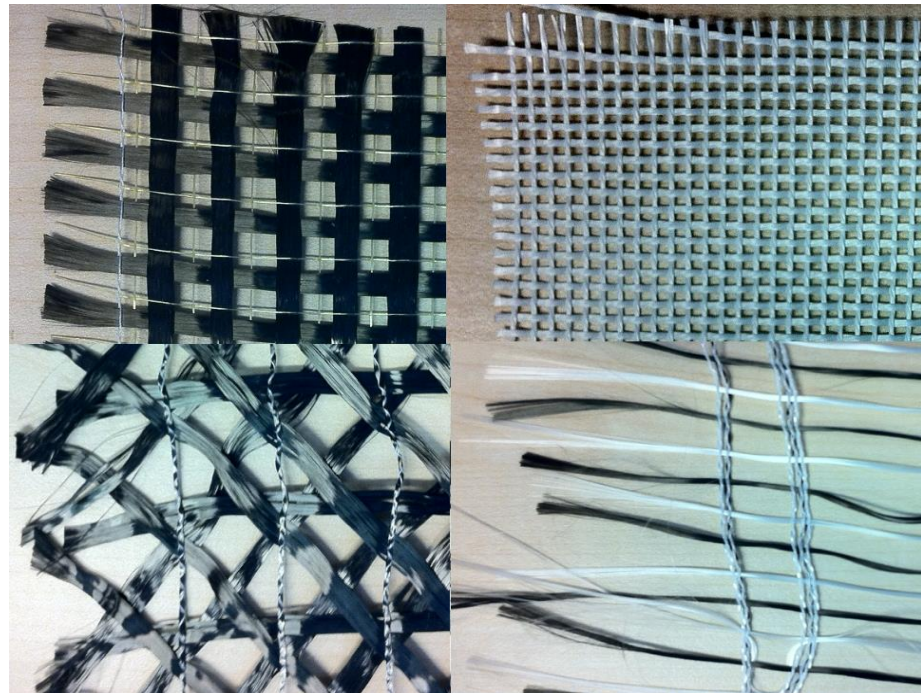


Figure 1-3 Textile reinforcement.



Figure 1-4 Fine grained concrete.

Textile reinforced concrete (TRC) has a major advantage over fibre reinforced concrete (FRC) because it can be placed where the stresses exist. Papanicolaou and Papantoniou (2010) stated that the properties of textile reinforced concrete can be fully utilized as it is located in the required place with enough quantity, while traditional fibres are randomly dispersed and oriented (which is less efficient). As a result of the random orientation of fibres (in FRC) the fibres are not fully utilized in terms of crack control, strengthening or stiffening (Swamy and Mangat 1974). Furthermore, for beams, the strength in the compression zone is not significantly affected by the presence of the fibres (Sri Ravindrarajah and Tam 1984). TRC combines some of the best features of chopped fibre RC and conventional steel reinforced concrete (Hegger *et al.* 2006c; see Figure 1-5). In addition to that, the volume fraction of TRC is much lower than for short fibre RC. More than 3% FRC is required to reinforce concrete effectively (Mobasher 2011). Therefore, TRC will lead to lower cost structures as the volume fraction required is lower (Cuypers and Wastiels 2006) as the use of fibre becomes more efficient.

In light of all these benefits, the better the understanding of the behaviour of these materials, the better they can be used in composite materials and,

therefore, the more they can benefit the construction industry (Ohno and Hannant 1994). However, more information on TRC behaviour is required before it can be safely used (Bramshuber and Brockmann 2006).

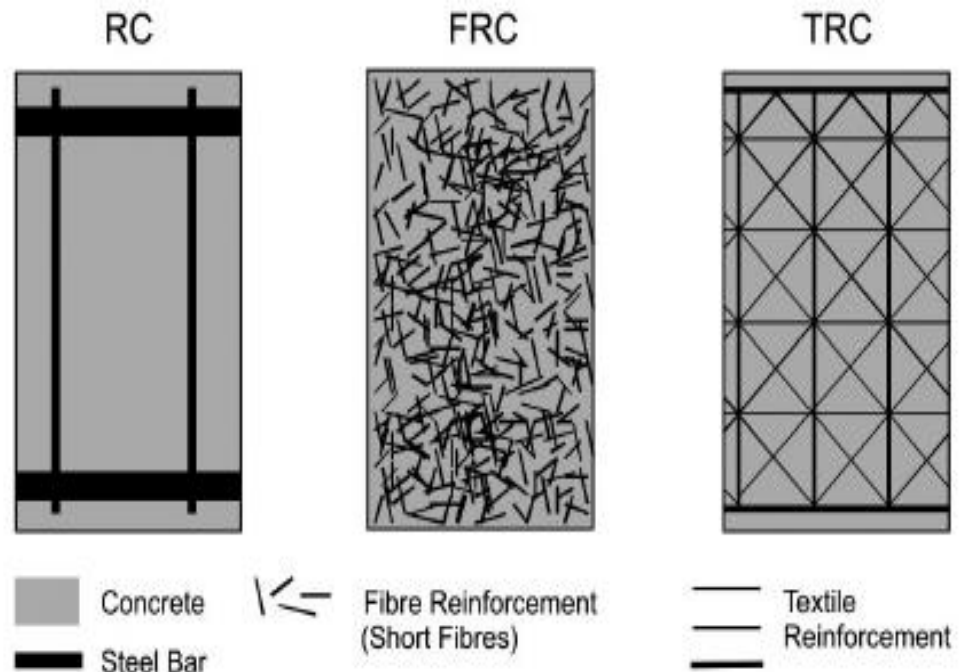


Figure 1-5 Comparison between different systems of reinforcement.

1.3 Research aim and objectives

The main aim of this study is to investigate the load-bearing behaviour of textile reinforced concrete (TRC) beams. An additional aim is to develop a new design methodology that could be used to design TRC beams. In order to achieve these aims, the following objectives are identified:

- 1) To study the effect of a variety of parameters on the flexural behaviour of TRC beams, such as:
 - Volume fraction of the fibre
 - Reinforcement area
 - Geometry and layout
 - Beam size

- Fabric type
 - Location of the reinforcement
 - Cover thickness
- 2) To provide a better understanding of the tensile strength of textile reinforcement.
 - 3) To investigate cracking behaviour (first crack, crack spacing, crack width) of TRC beams.
 - 4) To compare experimentally the textile reinforced concrete (TRC) beam results with the results for a steel reinforced concrete (SRC) beam.
 - 5) To investigate the tension stiffening of TRC beams and compare it with SRC beams.
 - 6) To investigate the bond efficiency factor between textile reinforcement and concrete.
 - 7) To collect the laboratory test results to establish a better understanding of the short term behaviour of TRC beams and also to use the experimental results to add to our current knowledge on textile reinforced concrete.

1.4 Outline of thesis

The study takes the form of eight chapters, including this introductory chapter. Chapter 2 is a literature review of the previously related topics to TRC. It commences by establishing a preliminary understanding of fibre reinforced concrete (FRC) before moving on to talk about TRC. Chapter 3 illustrates the measured properties of the materials and the experimental programme carried out in this study. Chapter 4 presents the results for the tested materials and beams. Chapter 5 discusses and analyses the tensile strength of carbon textile reinforcement, pull out strength, and the effect of changing different parameters on the behaviour of carbon textile reinforced concrete. Chapter 6 compares the performance of TRC beams with conventional SRC beams. The load-deflection behaviour of TRC and SRC beams, and stiffness and cracking behaviour, are the main performance criteria used in the comparison. Chapter 7 develops a design methodology that can be applied to safely design carbon textile reinforced concrete beams. In Chapter 8, the main findings and

conclusions of this research are presented, and recommendations for future work are provided.

CHAPTER 2

LITERATURE REVIEW

2.1 Historical background

The use of composite materials in construction dates back thousands of years as natural fibres were used to provide the strength of clay bricks. Each part of the world used the natural materials available in their county to reinforce the matrix. For example, in the Arabic Peninsula, straw was used to reinforce dried bricks and mud was used as cement between the bricks. However, the real change in the use of modern composite materials started at the beginning of the last century when asbestos cement was first produced. Johnston (2000) and Mobasher (2011) stated that asbestos cement was the first modern composite material used in construction since 1900 to produce cladding, roofing, etc.

Asbestos cement is Portland cement with 12 to 20% of volume fraction of asbestos fibre (Cheyreyzy *et al.* 1996). After the 1960s, for health and safety reasons, the application of asbestos cement was restricted as it can cause a terminal illness in humans (Brandt 1995). Due to these restrictions, engineers began to look for other fibres as a replacement for asbestos. In the 1960s and 1970s, alternative fibres were found which could be used in concrete applications such as steel, glass, carbon, and polypropylene (ACI 544 1996).

Nowadays, fibre reinforced concrete (FRC) has been widely investigated, developed, and applied everywhere in the world (ACI 544 1996).

2.2 Fibre reinforced concrete (FRC)

In FRC, fibres are added not to increase the strength of the structural concrete (even though there is a little improvement) but mainly to control cracking,

especially at the post cracking stage, by bridging the cracks (Mindess, Young and Darwin 2003). Furthermore, fibre is added to concrete to improve the toughness, strength (high performance fibre), dynamic resistance, and cracking resistance of the cement composites (Schlangen *et al.* 2010). It is also confirmed by Neville and Brooks (2010) that the tensile strength and toughness of concrete is improved as a result of reinforcement with random dispersed fibre. Besides the enhancement in the tensile strength, the crack opening can be more controlled and the matrix stresses at the crack tip can be reduced (Bayer and Richter 2010). Despite all the features that are introduced by FRC, it must be understood that fibre reinforcement is not a substitute for conventional reinforcement (Bentur and Mindess 2006).

2.2.1 FRC behaviour

As mentioned above, the principle of using fibres to reinforce concrete is to bridge the cracks that occur in the matrix at the post cracking stage. Therefore, the fibres may increase the strength of the composite after cracking, which is called strain hardening, also, which is more important, they increase the toughness of the composite, even if the stress-strain curve is descending after first cracking (strain softening). In order to achieve the strain hardening behaviour, the volume fraction of the fibre (V_f) should be more than the critical volume fraction ($V_{f,crit}$) to provide sufficient fibres that can resist tensile stresses (Bentur and Mindess 2006).

Fibre reinforced concrete (FRC) behaviour can be classified based on the post tension behaviour into strain-softening or strain-hardening, as shown in Figure 2-1 (Naaman 2007). From the figure, it can be seen that the behaviour of strain-softening of conventional FRC shows a stress decreasing after initial cracking with increasing in the strain at single crack. While at strain-hardening, the stress continuously increases after the first crack, with increasing ductility, which produces multiple cracking. The stress-strain behaviour of strain-hardening can be classified into three stages. The first stage is elastic behaviour (I), characterised by a steep slope and a composite which is not cracked (see Figure 2-1b). In addition, the type of fibre material has no effect

on the stiffness at this stage (non-cracked composite). The second stage begins after the first crack has occurred and is followed by the development of multiple cracking (II), until there are no more cracks. Then, in the third stage, the loading resistance drops (III). No more cracks develop at this stage and only one of the existing cracks widens with the increasing strain while the other cracks unload, therefore, becoming smaller in width. Strain-hardening can be achieved by adding a reasonable quantity of modern fibre to create high performance fibre reinforced concrete (HPFRC) (Bentur and Mindess 2006).

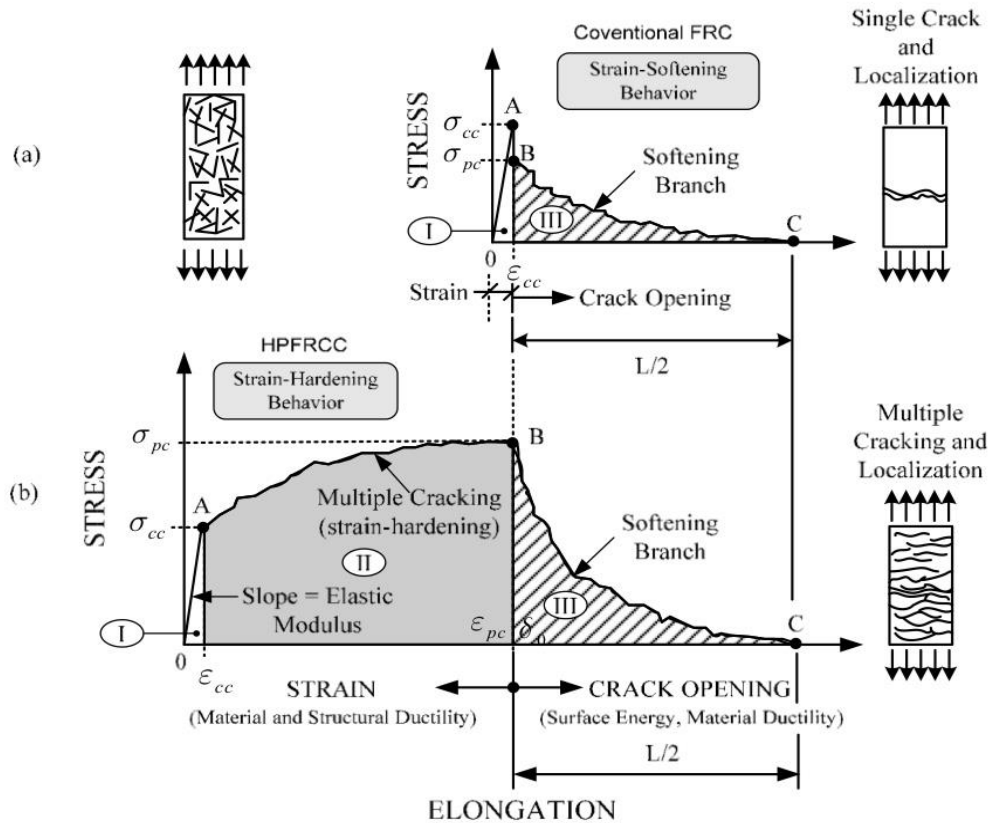


Figure 2-1 Stress-strain behaviour of FRC: a) Strain-softening; b) Strain-hardening (Naaman 2007).

2.2.2 Fibre-matrix interaction

The matrix and fibre are individually considered as a brittle material; however, fibres are less brittle than the matrix. Therefore, a ductile behaviour can be achieved through multiple cracking. The properties of the fibre and matrix are

easy to obtain while the difficulty lies in determining the behaviour of the fibre-matrix interaction (Schlangen *et al.* 2010). The improvement in the mechanical properties of FRC mainly depends upon the fibre-matrix interactions. Such interactions are significantly affected by the bond between the matrix and the fibre. Kabele *et al.* (2006) and Soranakom and Mobasher (2009) stated that the fibre-matrix interfacial bond is the most significant factor controlling meso-mechanical behaviour, for example multiple cracking. The bond and frictional resistance are the main criteria which describe the fibre-matrix interface (Kruger, Reinhardt and Fichtlscherer 2001). However, the bond cannot be directly calculated from the characteristics of the single filaments. Therefore, careful consideration of this point is crucial as the post behaviour mainly depends on the fibre-matrix bond. In an uncracked composite, the shear bond transfers the load from the matrix into the fibre, however, after cracking the load carried by the fibres that bridge the cracks is transferred back into the uncracked matrix through the shear bond (Bartos 1981).

The properties of the area surrounding the fibres play an important role in fibre-matrix interaction. This area is called the transition zone and the paste in this area is significantly different from the bulk paste; moreover, the transition zone may differ with time (Bentur and Mindess 2006). Furthermore, Majumdar (1974) concluded that the interface properties of glass reinforced concrete change with time due to two causes; one is a chemical attack and the second is the change in the physical properties of the fibre. In addition to changes in the fibre-matrix interface, Zhu and Bartos (1997) realised that aging affects the microstructure of the fibre-matrix interface and fibre-fibre interface. However, the strong bond between the fibre and matrix of fibre reinforced concrete may lead to undesirable brittleness failure (Bartos 1981). For these reasons, the FRC interface is complicated due to the change in the bond strength over time, especially in multifilament FRC, because not all filaments are certain to be surrounded by the matrix, whilst the interface of monofilaments, such as steel fibre, is similar to the interface between clean rebar and concrete in normal reinforced concrete (Purnell 2010a).

There are three models for stress transfer: in the first it is assumed that the fibre-matrix interface is at elastic continuity (Greszczuk 1969); in the second, the frictional shear transfers the stress between matrix and fibre (Aveston, Cooper and Kelly 1971); and the third is a combination between the first two models (Laws, Lawrence and Nurse 1971). Fibre-matrix stress transfer behaviour was clarified by Mobasher and Li (1996), Figure 2-2. The figure shows four stages of fibre pulling out stresses which are transferred by adhesional strength (τ_{au}) until peak load (first two stages). Then, the transfer stresses are governed by frictional resistant strength (τ_{fu}) until the fibre is completely debonded from the matrix. Both of them (adhesional and frictional strength) can be calculated using the shear strength approach (Peled and Bentur 2003).

$$\tau = \frac{P}{2\pi r l} \quad (2.1)$$

where

τ is the interface bond strength.

P is the pull out force.

r is the pulled yarn radius.

l is the embedded length.

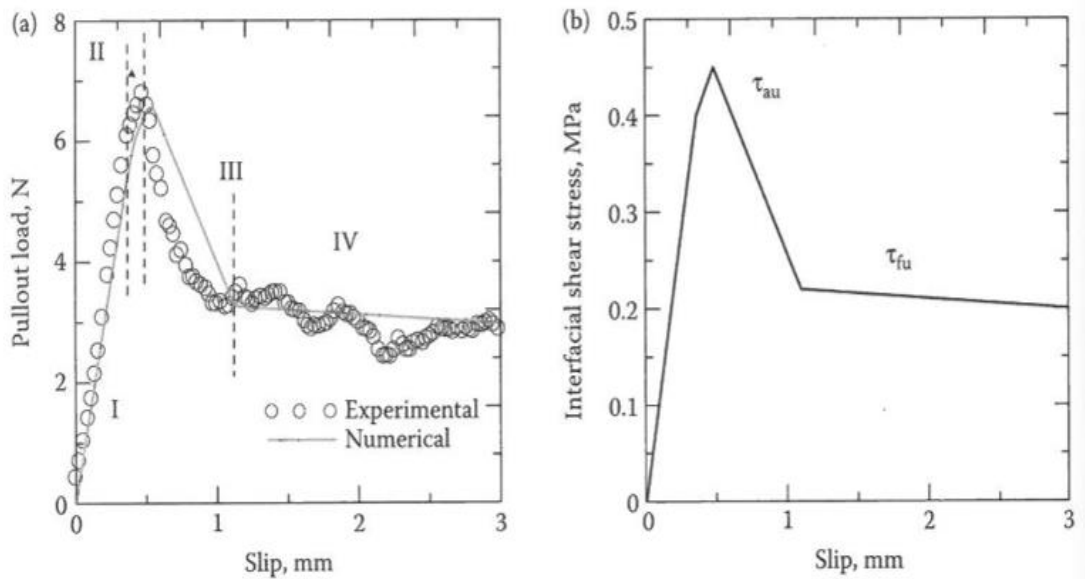


Figure 2-2 Fibre pull out test results of a sample cured for 3 days and fibre embedded length 20 mm (Mobasher and Li 1996).

2.2.3 FRC flexural moment

Hannant (2003) experimentally noticed differences between post cracking flexural strength and the uniaxial tensile strength of fibre reinforced concrete (FRC) which increases the need for special understanding of flexure. The flexural strength at post cracking is around twice the tensile strength. Figure 2-3 shows the stress and strain distribution of a cracked fibre reinforced concrete beam. It can be seen in Figure 2-3(c) that the fibres at the crack section are bridging the cracks. However, the assumption of an equivalent composite stress block (Figure 2-3(d)) is made in order to calculate the approximate stresses as the exact stresses are difficult to compute. There are five factors which influence the shape of the stress block, namely crack width, fibre volume fraction, bond strength, orientation and length efficiency. Kwan, Ramli and Cheah (2014) found a direct relationship between fibre volume fraction and flexural strength.

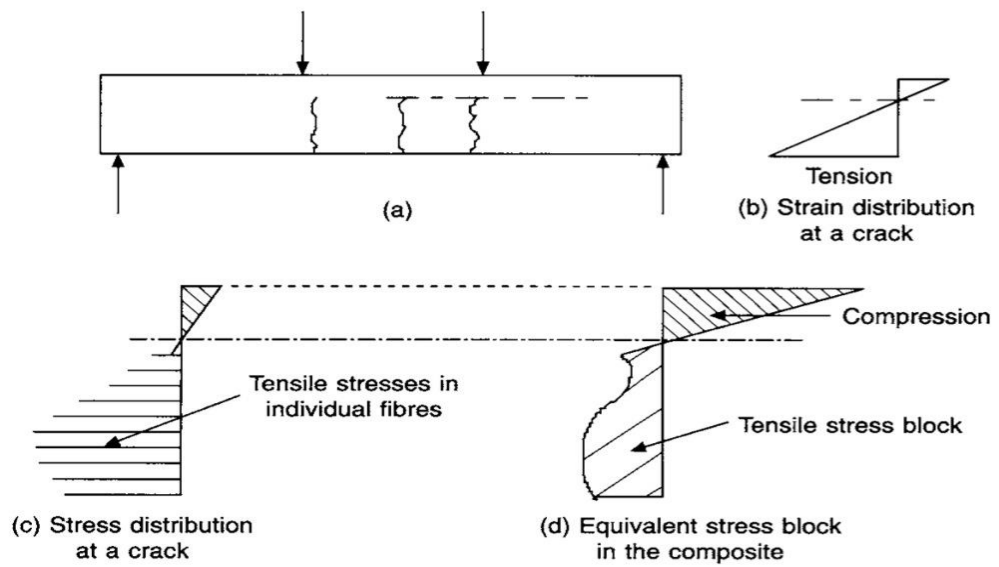


Figure 2-3 Stresses and strains of a cracked fibre reinforced concrete beam (Hannant 2003).

Figure 2-4 shows the stress blocks of FRC before and after cracking. The resisting moment of the two stress blocks can be calculated as follows (width is unity):

$$M = \frac{1}{6} \sigma_{fl} D^2 \quad (2.2) \text{ for Figure 2.4(a)}$$

$$M = \frac{13}{32} \sigma_{cu} D^2 \quad (2.3) \text{ for Figure 2.4(b)}$$

where,

D is the beam height;

σ_{fl} is the flexural tensile stress at the un-cracked section;

σ_{cu} is the flexural tensile stress at the cracked section.

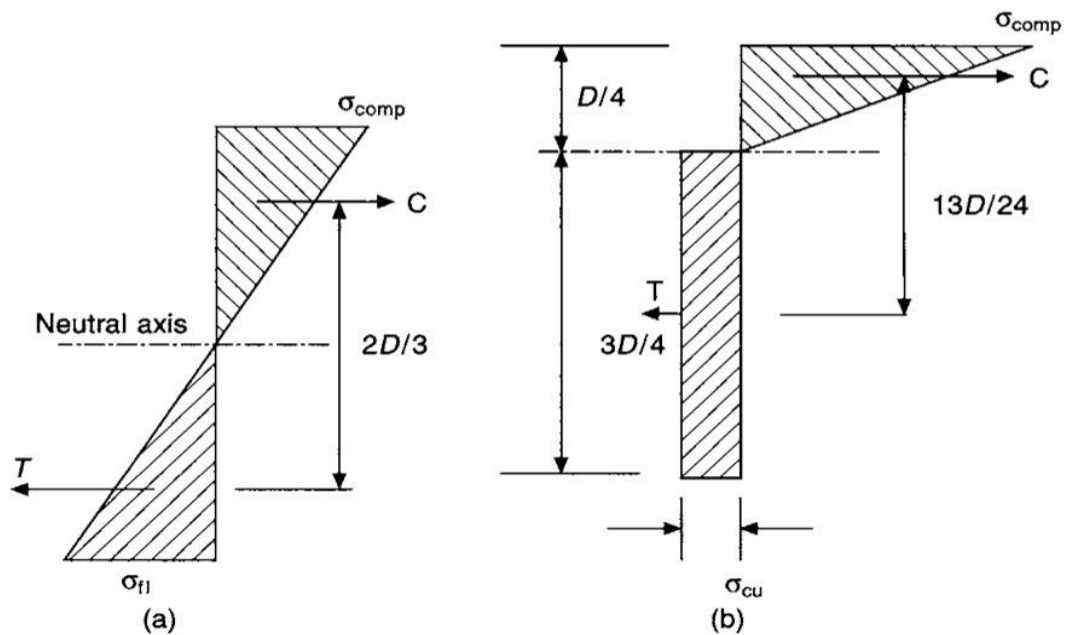


Figure 2-4 a) Stress block at elastic flexural in tension and compression. b) Stress block at elastic in compression and plastic in tension (Hannant 2003).

2.2.4 Efficiency factors of fibre reinforced concrete

The efficiency factor is defined by Laws (1971) as a parameter describing the degree to which effective exploitation of fibre strength and stiffness in a fibre reinforced matrix is achieved. Bentur and Mindess (2006) stated that there are two measurements for determining the efficiency of fibre reinforcement in a matrix, as follows: how much the increase in the strength, and how much the improvement in the toughness. However, there are a number of factors that influence the efficiency of fibre which cannot be ignored, such as fibre length, orientation, and bond. Therefore, the magnitude of the tensile stresses that are transferred from the matrix to the fibre determine the efficiency of the fibre.

The efficiency factor should be applied to the calculation of composite stress because of the variation in the composite properties. Efficiency factor (η) is a value between 0 and 1 ($0 \leq \eta \leq 1$). This value represents the efficiency effect of fibre length, fibre orientation, and bond strength, as follows:

$$\eta = \eta_l \eta_o \eta_\tau \quad (2.4)$$

where,

η_l is the length efficiency factor, see Figure 2-5.

η_o is the orientation efficiency factor, see Figure 2-5.

η_τ is the bond efficiency factor.

The bond strength of the cement composite is affected by the length and diameter. Therefore, the critical length of fibre determines the minimum fibre length which is enough to mobilise its ultimate tensile strength (Swamy 1975). Figure 2-6 shows the two types of failure based on the length of fibre. The length efficiency factor of continuous fibre (η_l) is 1 (Purnell 2010c).

AR-glass and carbon fibre structures are sensitive to the transverse and bending load (Hegger *et al.* 2006b). Therefore, the position of the fibre reinforcement relative to the load direction or the crack edges has to be taken into consideration. The fibre orientation has an influence on the composite properties (Swamy 1975), which is also concluded by Mashima, Hannant and Keer (1990). Their conclusion is that the first cracking stress and the ultimate composite stress are not just affected by the fibre properties but also by the orientation of the fibre. The ultimate strength of the composite reduces when the fibre angle increases. However, it is very difficult to understand the behaviour of inclined fibre reinforcement (Hegger and Voss 2004).

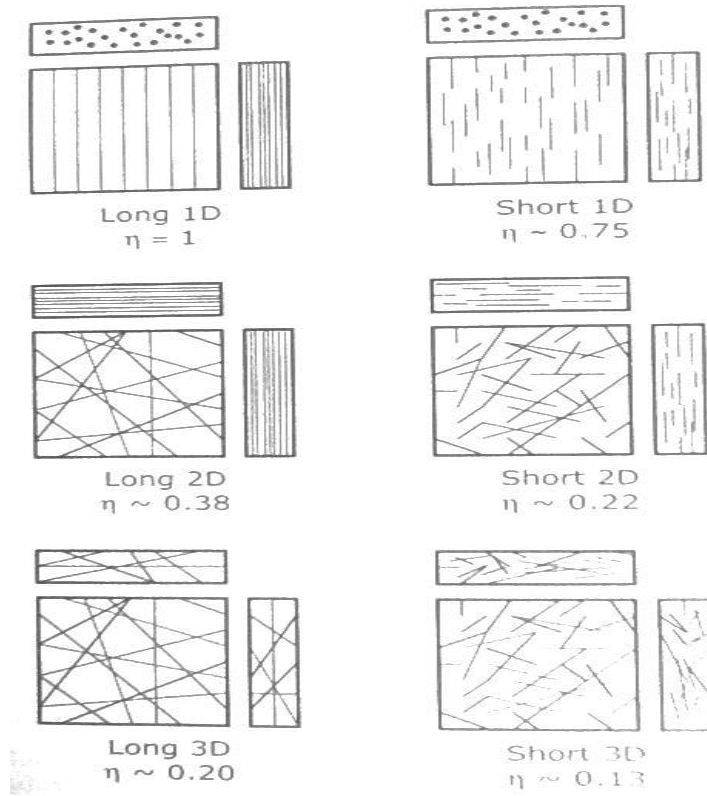


Figure 2-5 Length and orientation efficiency factor (Purnell 2010c).

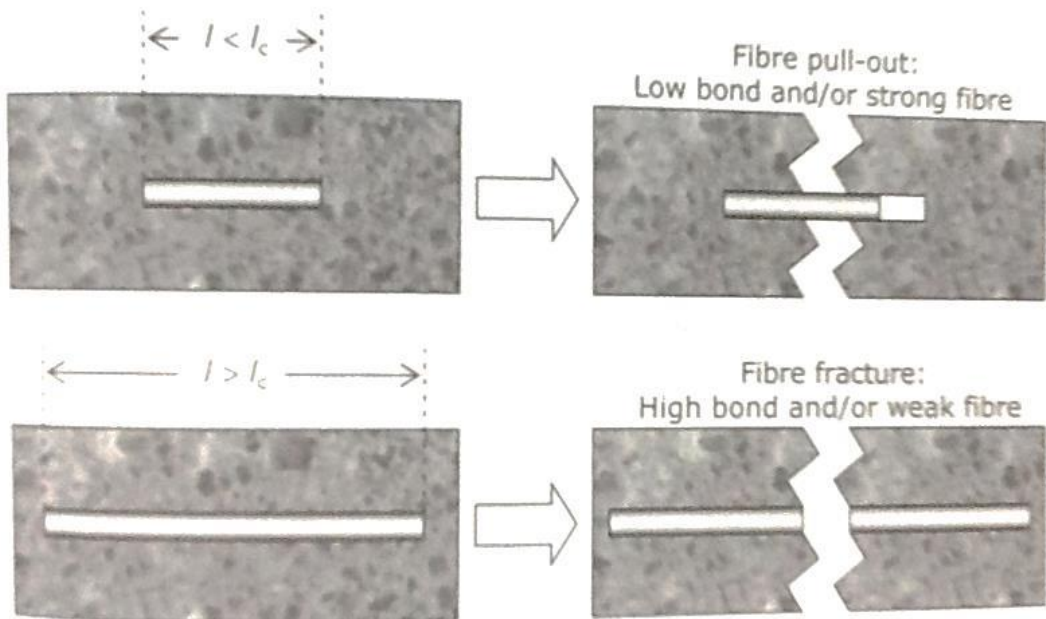


Figure 2-6 Two types of fibre failure (Purnell 2010c).

2.2.5 Mechanics of FRC

Figure 2-7 shows Aveston, Cooper and Kelly (1971) model for fibre reinforced concrete. From the figure, the behaviour can be divided into three regions. First, the elastic region (uncracked) which is characterised by a steep slope. In this region, the load is mostly carried by the matrix which can be represented by the following equation:

$$\sigma_c = \sigma_m V_m + \sigma_f \eta V_f \quad (2.5)$$

where,

σ_c is the composite stress.

σ_m is the matrix stress, $E_m \varepsilon_m$.

σ_f is fibre stress which at this stage is $= E_f \varepsilon_m$.

ε_m is matrix strain;

E_m is the modulus of elasticity of the matrix;

E_f is the modulus of elasticity of the fibre;

V_f is the volume fraction of fibre;

V_m is the volume fraction of the matrix;

η is the efficiency factor ($0 \leq \eta \leq 1$) which accounts for the variation in composite properties with fibre architecture, Eq. 2.4.

It must be said that these equations apply to the case of the one dimensional direction of the fibre.

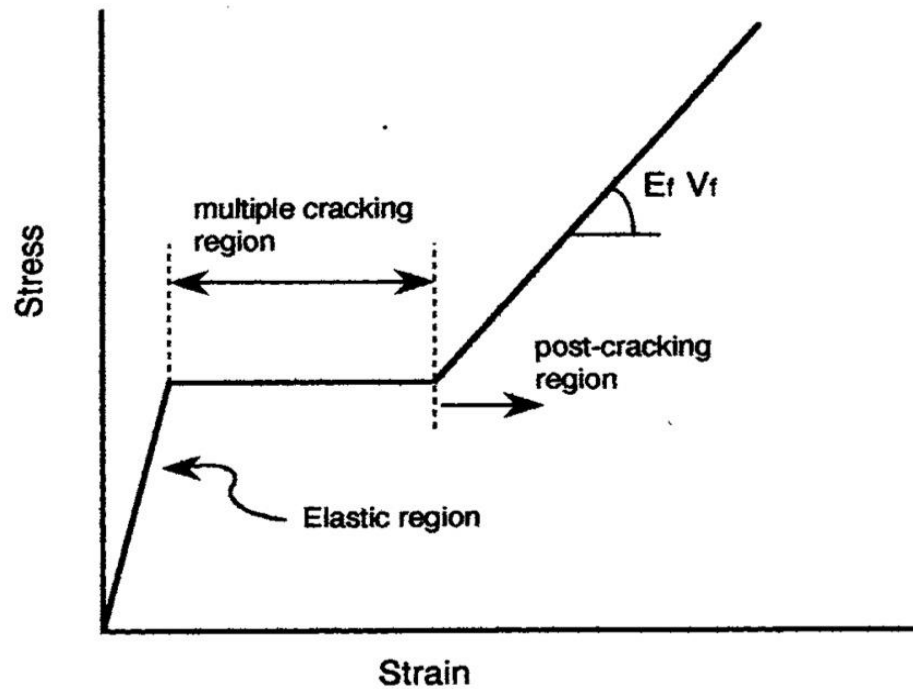


Figure 2-7 Stress-strain model for FRC (Aveston, Cooper and Kelly 1971).

The first crack occurs when the strain of the composite becomes greater than the ultimate matrix strain ε_{mu} . Thus, the composite does not fail if the ultimate load of the fibre is more than the ultimate load of the composite ($\sigma_{cu} > \sigma_c$).

$$\sigma_{fu}\eta V_f > E_m \varepsilon_{mu} V_m + E_f \varepsilon_{mu} \eta V_f \quad (2.6)$$

Where;

ε_{mu} is the ultimate strain of matrix;

σ_{fu} is the ultimate strength of the fibre.

After the cracking point, the post cracking behaviour depends on the critical volume fraction (V_{fcrit}). As a result of the zero stress that can be carried by the matrix at the cracks, the volume fraction of fibre is drawn from Eq. 2.5, as follows:

At cracked section:

$$\sigma_m = 0$$

The quantity of fibres to resist the load is:

$$\sigma_f = \sigma_{fu}$$

Therefore,

$$V_{fcrit} = \frac{\sigma_c}{\eta\sigma_{fu}} \quad (2.7)$$

Normally, the composite stress is similar to matrix stress before cracking ($\sigma_c \approx \sigma_{mu}$), thus:

$$V_{fcrit} = \frac{\sigma_{mu}}{\eta\sigma_{fu}} \quad (2.8)$$

Therefore, if $\eta V_f \gg V_{fcrit}$, and as a result of the increasing the applying load, the multiple cracking region forms. The mechanism of this region is that the stress on the fibres at the first crack is transferred back into the matrix and, with an increase in the applied load, another matrix crack forms until the matrix is full of parallel spaced cracks.

In cases where the volume fraction is much greater than the critical volume fraction, the post cracking region forms once no further cracking occurs. In this region, the additional load is completely carried by the fibres which results in pull out of fibres until the composite fails. Therefore, the ultimate composite stress is:

$$\sigma_{cu} = \eta V_f \sigma_{fu} \quad (2.9)$$

where;

σ_{cu} is the ultimate composite strength.

However, this equation is considered to provide an over estimation of the ultimate composite stress because of the damage that occurred in the fibre during the loading (Purnell 2010b).

On the other hand, in the case of $\eta V_f < V_{f_{crit}}$, the reinforced member is unable to provide multiple cracking and post cracking behaviour. However, it can be of benefit because it improves the toughness because of post tension behaviour as it is shown in Figure 2-1a. However, the behaviour at this stage depends on the fibre length in comparison to the critical length (see Figure 2-6). If fibre length is greater than the fibre critical length, the fibre will be broken, thus, there is no improvement in the toughness, while at fibre lengths similar to or lower than the critical length, the ability to produce post peak tension behaviour is high because of the required strength to pull the fibres out of the matrix.

2.3 Textile reinforced concrete (TRC)

The aerospace and automobile industries have been exploring textile materials for decades. Ko (1993) stated that the excellent characteristics of textile reinforcement, such as its light weight, high strength, flexibility, and toughness, have made it attractive to the Boeing Aircraft Company for producing plane wings since the 1920s. This material opened the door to a variety of construction designs that can be effectively applied by using composites. The high cost, in terms of money and time, incurred by the corrosion of steel reinforced concrete has forced engineers to study different kinds of reinforcement that can perform similarly to steel, and a variety of fibres has therefore been adopted. However, they were still only applied as a secondary form of reinforcement, until textile materials were developed for use in concrete. The main advantage of textile reinforcement over fibres is that they can be placed at the locations that are subjected to tensile stresses. At the beginning of this millennium, researchers began to work towards a fully utilization of the fibre thus the term textile reinforced concrete (TRC) began to

be used. Mid 2002, RILEM (International Union of Laboratories and Experts in Construction Materials, Systems and Structures) established the TC 201-TRC committee to investigate the various issues related to textile properties under different conditions (Reinhardt *et al.* 2006b).

Fibre reinforced concrete is dispersed randomly over concrete members which means there is wastage of the fibre; for instance, the fibres allocated at compression areas are not fully utilized. Therefore, TRC is expected to perform better than FRC as the major difference between FRC and TRC is the behaviour under tension (Mumenya, Tait and Alexander 2011) because textile reinforcement can be positioned where needed. Textile reinforced concrete (TRC) has been investigated in the last decade by a number of studies in terms of strength, durability, bond, behaviour, modelling and design method. It is considered to be a new composite material that could be used in the building and construction industry (Brockmann and Brameshuber 2005) as the high strength of textile reinforced concrete can carry high tensile loads, similar to steel reinforced concrete (Hinzen and Brameshuber 2009). Researchers concluded that this material can considerably improve the mechanical properties of cement matrices (Cohen *et al.* 2006). However, there are some areas of uncertainty with regard to textile reinforcement, as listed by Hegger *et al.* (2006b). These are: unclear filament properties such as filament diameter, - flaws in filament production, - bond properties between filaments themselves and between matrix and filaments, - filament adjustment, - fibre orientation.

The following sections study the components of textile reinforced concrete, behaviour of textile reinforced concrete, bond, and design method.

2.3.1 Cementitious matrix

The composite material normally consists of matrix and reinforcement as both the fibre and matrix keep their own characteristics, however, they affect the final composite properties (Schwartz 1997). There is a variety of materials that can be used as the matrix, including polymers, metals, and ceramics. In the

last decades cementitious matrices have dominated the civil engineering industry, as they are cheap and have properties such as high strength under compression. Cementitious matrices can be classified into two kinds; one is a cement matrix which consists only of cement, sand, and water, and the second is a concrete matrix which is composed of cement, sand, coarse aggregate, and water (Bentur and Mindess 2006). Therefore, the type of mixture that is used in TRC is of great importance because of the penetration of textile reinforcement which may cause a reduction in efficiency if it is not well penetrated, thus, the tensile strength of TRC is decreased in comparison with the tensile strength of textile reinforcement alone (Dolatabadi *et al.* 2010). The composite behaviour can be improved, if the matrix quality is improved (Peled, Bentur and Yankelevsky 1999). On the other hand, Keil, Cuypers and Wastiels (2008) claimed that the effect of the matrix mix proportions on the composite properties is small. A particulate matrix which is around 10 μm cannot penetrate inside the filaments because this is different from a viscous fluid polymer matrix which impregnates the gaps between the filaments easily (Bentur and Mindess 2006).

2.3.1.1 Fine grained concrete

Fine grained concrete is used to improve the bond between the rovings (continuous strands of parallel filaments) and the matrix by increasing the probability of penetration of concrete between filaments. The mixture needs to be able to penetrate the rovings and filaments of the textile reinforcement (Peled *et al.* 2008; Cohen *et al.* 2006). The matrix penetration is influenced by several factors; the geometry of the yarn, cement particle size, and capillary force (Dolatabadi *et al.* 2010). Therefore, the maximum size of fine aggregate should be less than 2mm, and thus, the mix can be considered as a mortar. Unlike fibres, textile reinforcement needs full concrete penetration to ensure a high bonding (Brameshuber *et al.* 2006). The main differences are: first, the primary use of textiles in comparison to fibres, as it is used as a secondary reinforcement; and second, the fibres are normally loose, thus, the mixture can penetrate them easily while a textile is tight and stitched. In addition to the aggregate size, the mix must be workable and at the same time consistent.

Accordingly, cementitious replacements and plasticisers may be needed such as fly ash and super-plasticisers. The use of the replacement materials is not only to improve the flow ability but also to improve the mechanical properties and durability (Brockmann 2005). In addition to that, the capacity of composite is affected by the mixture proportions, aggregate size, and sand content (Swamy and Fattuhi 1974). Table 2-1 shows the different types of mixes that have been considered by researchers.

Table 2-1 Matrix components (Brameshuber *et al.* 2006).

Materials		Mineral based matrices				
		PZ-0899-01 SFB 532	FA-1200-01 SFB 532	RP-03-2E SFB 532	Alphadur® SFB 532	MF-02-101 SFB 532
Cement content	kg/m ³	490	210	980	-	441
Cement type	-	CEM I 52.5	CEM I 52.5	CEM I 52.5	-	CEM I 52.5
Ready made mixture	kg/m ³	-			2400 ¹⁾	-
Fly ash f		175	455	210	-	210
Silica fume s		35	35	210	-	-
Metakaolin m		-	-	-	-	49
Binder (c+f+s+m)		700	700	1400	2400	700
Plasticiser	% by mass of binder	1.5	0.9	2.5	0.6	2.0
Siliceous fines 0 - 0.125 mm	kg/m ³	500	470	118	-	500
Siliceous sand 0.2 - 0.6 mm		715	670	168	-	715
Water		280	280	350	228	280
w/c	-	0.57	1.33	0.36	n.m. ²⁾	0.63
w/b = w / (c+f+s)	-	0.40	0.40	0.25	0.10	0.40

¹⁾ based on blast furnace slag cement

²⁾ n.m. – not mentioned

2.3.2 Textile reinforcement

These materials (matrices) are unable to resist the tensile stresses when a load is applied which causes a brittle failure. Ductile materials have been used to reinforce these kinds of matrix to ensure that they have enough strength and ductility. Figure 2-8 shows various types of fibres.

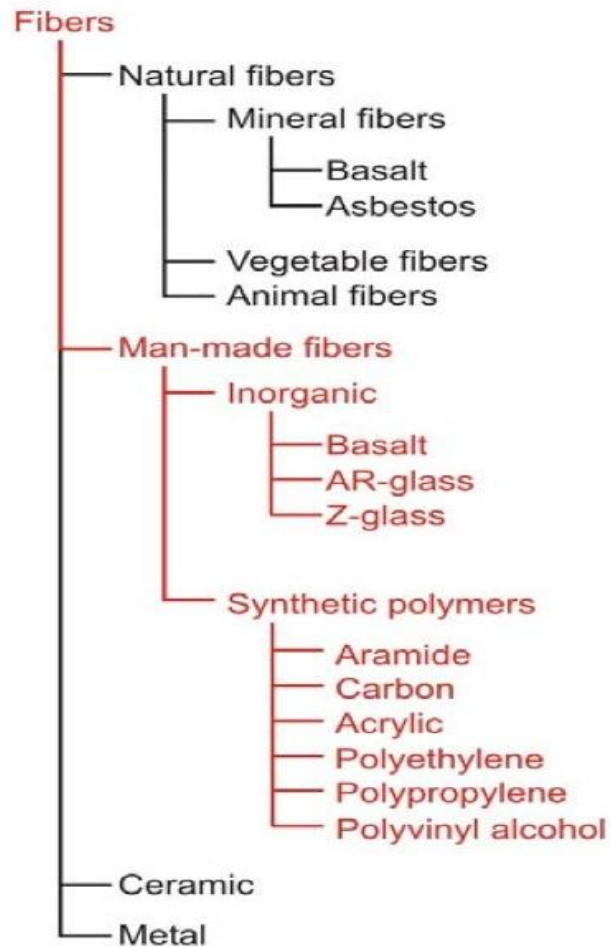


Figure 2-8 Various kinds of fibres (ITP, TU Dresden).

Before moving on to talk about textile reinforcement, it is necessary to clarify some of the terminology (Aldea, Gries and Roye 2006):

Textile: applied to woven fabric, filaments to use as yarns, yarns, and garments.

Fabric: fibres and/or yarns assembled by weaving, knitting, and braiding.

Roving: continuous strands of parallel filaments.

Yarn: a number of filaments laid together without a twist; a number of filaments laid together with a degree of twist; a single filament with or without a twist.

Strand: a single fibre, filament.

Tow: continuous fibre filaments without definite twist.

Filament: a fibre of an indefinite length; an ordered assemblage of textile fibres.

Tex: a unit for expressing linear density.

Warp (0 direction): a set of yarns in all woven fabrics that is interwoven with the weft. Normally, the warp is laid down in the loading direction, which is also called the 0 direction.

Weft (90) direction: in this study, a set of yarns interwoven with the warp. Normally, the weft is in a direction across with loading direction, which is also called the 90 direction.

Textile material normally consists of a two-dimensional bi-axial textile, and each direction has a number of rovings (warps/wefts). These rovings are a bundle of filaments, also known as multifilaments, and each roving consists of hundreds of single filaments, indeed up to thousands of filaments, which are expressed by 'k'. Figure 2-9 illustrates different types of two dimensional textile reinforcements that are normally used to reinforce concrete with different numbers of filaments for glass, carbon, and glass-carbon textile. Textile fibre can take many forms such as woven, braided, knitted, or stitched (Mobasher 2011). Therefore, the packing density of a roving cross section

varies and, as Dolatabadi *et al.* (2010) found, matrix penetration is increased at low packing density. The packing density decreases when the stitch length increases and the knitting tension decreases. However, there are three levels on which the textile reinforcement should be considered,, one has to do with the mechanical properties of the individual filaments, the second concerns the roving geometry, and the third involves the fabric structure (Bentur and Mindess 2006).

Textile surfaces are very smooth. Therefore, Gray and Johnston (1987) concluded that the fibre texture may affect the post crack properties of the composite. An investigation into the effect of textile geometry on cement penetration is needed (Dolatabadi *et al.* 2010).

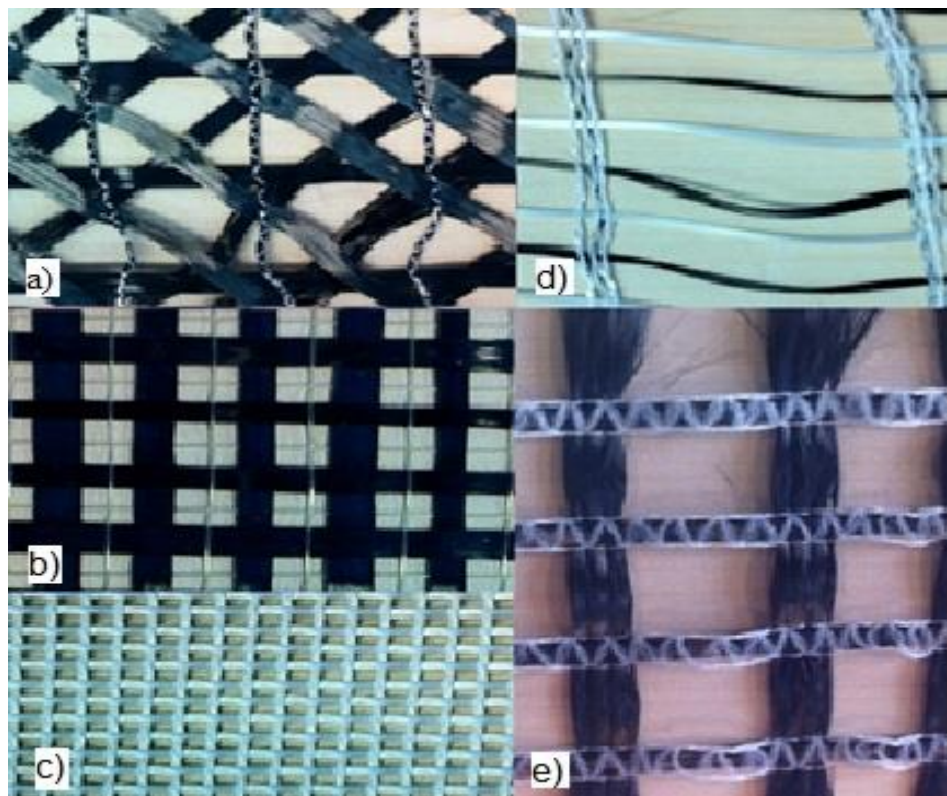


Figure 2-9 Different types of woven textile, a) Multi-axial carbon, b and e) Biaxial carbon, c) Biaxial glass, d) Glass-carbon fabric.

2.3.3 Textile properties

The properties of textile reinforcement are what distinguish it from the other type of reinforcements in connection with tensile strength, modulus of elasticity, stiffness, stability, and utilization. Figure 2-10 shows the properties of different types of textile materials. It can be seen that the carbon properties are impressive. The tensile strength and the modulus of elasticity of carbon are almost double those of glass. Therefore, after cracking occurs, the stiffness of two layers of carbon textile reinforced concrete is three times greater than two layers of AR-glass textile reinforced concrete due to the high modulus of elasticity of the carbon, as shown in Figure 2-11 (Hegger *et al.* 2006b). Both AR-glass and carbon textile behaviour are linear until they reach the ultimate load as there is no plasticity (Yin, Xu and Wang 2015). Tensile tests were carried out by Jesse and Curbach (2003) on 10 commercial rovings of AR glass from different suppliers. The results showed that the tensile strengths of single filaments were close to each other at 2000 MPa, while the strands' tensile strengths were much lower than the filaments' tensile strength with high variation which ranged between 444-1476 MPa.

Also, Figure 2-10 illustrates that the tensile strength of filaments is always greater than the tensile strength of yarn, as will be discussed in section 2.3.5.1.

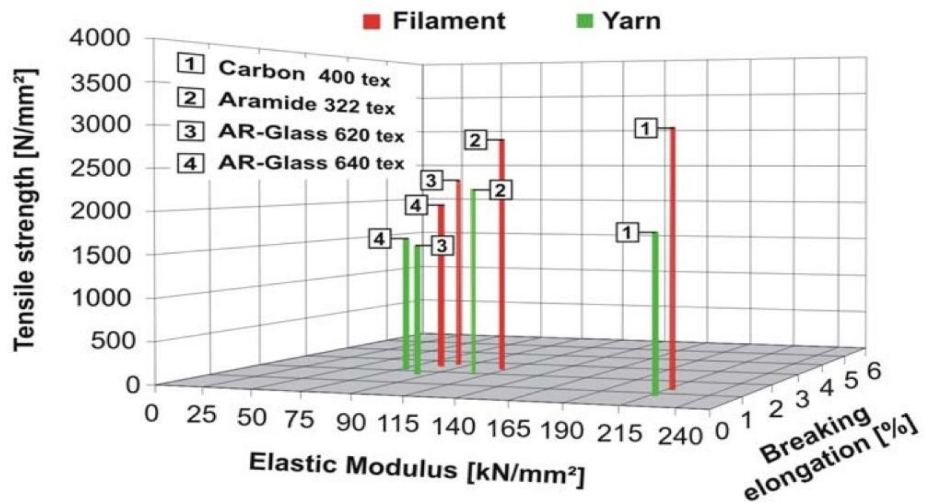


Figure 2-10 Mechanical properties of various textile materials (ITP, TU Dresden).

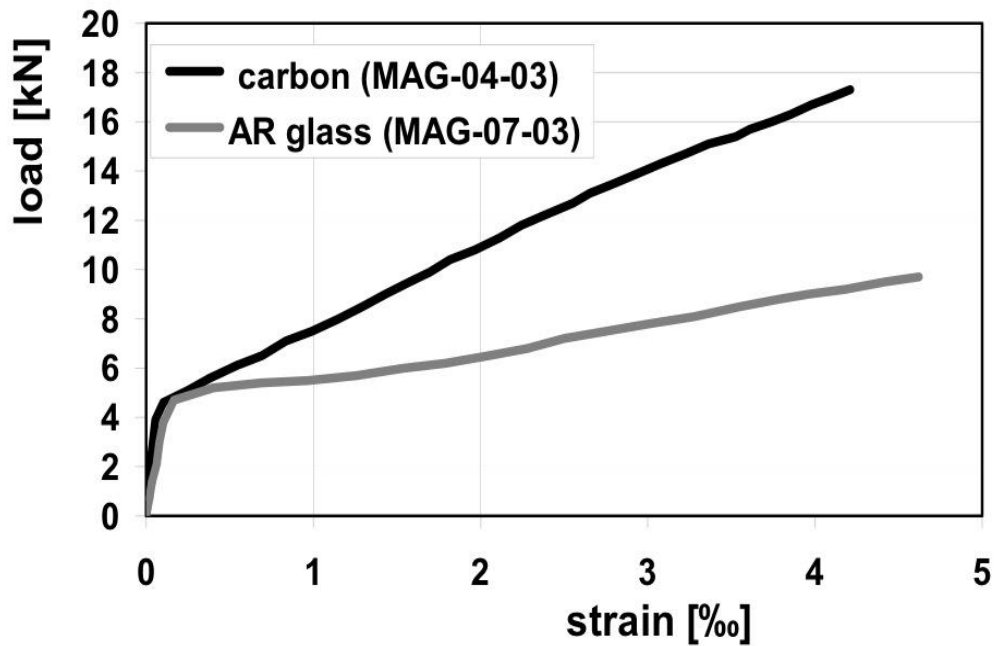


Figure 2-11 Load-strain of two layers of carbon and glass textile reinforced concrete, respectively (Hegger *et al.* 2006b).

Durability in civil engineering is a real issue that has to be seriously taken into account. Deterioration due to corrosion in steel reinforced concrete is one of the disadvantages of applying steel reinforcement. Unlike steel reinforcement, TRC has features which give it advantages over steel reinforcement. According to Hartig *et al.* (2008), textile materials (AR-glass or carbon) provide good resistance to the alkaline environment of concrete. This does not mean that textile reinforcement is completely unaffected by environmental conditions but it is infinitely better than steel reinforcement. Raupach (2002) found a reduction in ultimate load and strain due to storage in warm water. Moreover, Butler *et al.* (2009) found losses in durability with increasing age depending on the concentration of the alkalinity in the pore solution. Furthermore, Kabele *et al.* (2006) believed that the fibre-matrix interaction is harmed by chemical exposure. Understanding the deterioration which was resulted from the durability, it helps to produce a proper design of structural member reinforced by textile reinforcement (Butler, Mechtcherine and Hempel 2010).

2.3.4 Textile geometry

The fibre-matrix interaction is significantly influenced by the fabric geometry; for example, woven, knitted, or crimped. Therefore, it can be said that the main parameters in the geometrical characteristics are the rovings and how these rovings are combined together. The large variety of textiles allows for a greater flexibility of properties, which means that they can be used in many applications (Gries *et al.* 2006). However, Peled and Bentur (2000) stated that the fabric geometry cannot be seen simply as a means to hold the rovings together, it can improve bonding and achieve strain hardening even if the roving modulus is low. The layout and geometry of textile reinforcement can improve positively or negatively on the bonding, and thus, on the composite performance. Therefore, changing the geometry may help to produce the required behaviour, such as strain hardening of low modulus fibre composites. Peled and Bentur examined three different geometries (woven fabrics, weft insertion knitted fabrics, and short weft knitted fabrics, see Figure 2-12). It is found that the woven fabric may improve the efficiency factor, which is

explained by Peled, Bentur and Yankelevsky (1999). This is as a result of the crimped geometry which led to the improvement in the bonding due to anchorage of the fibre to the cement matrix, see the yarn shape at woven fabric in Figure 2-12, of woven fabric. While the weft insertion knitted fabric shows lower efficiency factor which attributed to the weak bond of knitted fabric. Peled, Bentur and Yankelevsky (1998) added that dividing the rovings of a fabric into small numbers of filament bundles is expected to produce better bonds as a result of penetration improvement. In addition to this, Hegger *et al.* (2006b) stated that the type of weave can significantly decrease composite strength and increase crack spacing. The reinforcement efficiency may be affected by the crimped geometry as a result of stresses that are produced in the yarns that are not parallel to the loading direction (Aveston, Cooper and Kelly 1971). A strong anchorage occurs due to the complexity of the geometrical shape of fabric (not straight rovings) which leads to an enhancement in the behaviour of the composite (Hegger *et al.* 2006b). Other types of fabric were studied by Peled and Bentur (1998), who found that knitted fabric reinforcement has higher efficiency than straight rovings and that woven fabric efficiency is better than that of knitted fabric and straight rovings. This is attributed to the crimped geometry of rovings in the woven fabric. The weft rovings in weave fabric can work as a direct anchorage to avoid warp slipping. Thus, the ultimate load of fabric at different weft spacings is almost the same (Colombo *et al.* 2013).

Therefore, it can be said that the more complex the geometry, the greater the bond that can be achieved, thus strain hardening behaviour of low modulus rovings can be obtained (Peled and Bentur 2000).

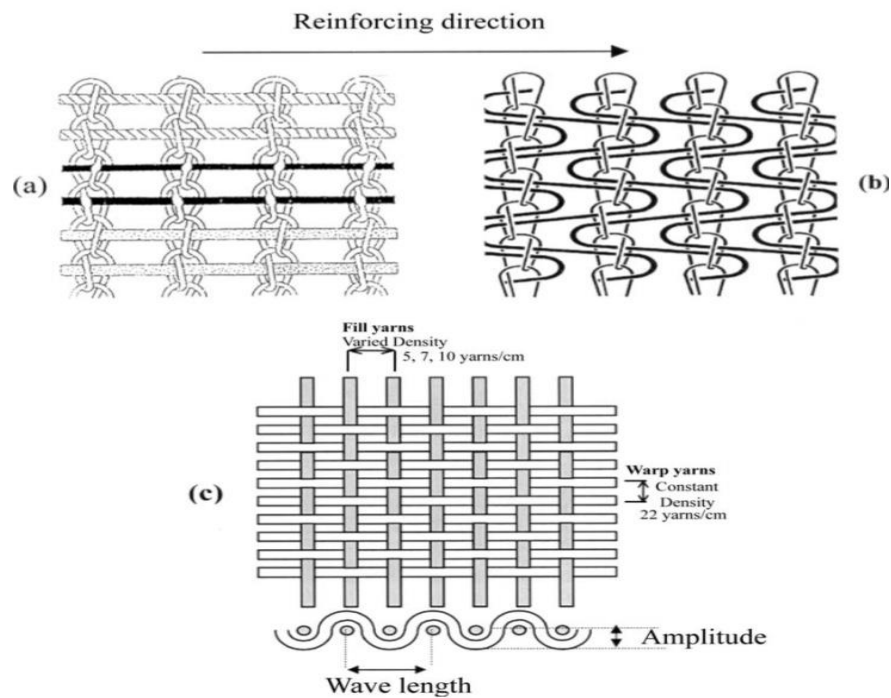


Figure 2-12 Different fabric structures: a) weft insertion knit fabric, b) short weft knit fabric, and c) woven fabric (Peled and Bentur 2000).

2.3.5 Textile reinforced concrete behaviour

It is well known that adding fibre to cement or concrete changes the behaviour of concrete and the failure mode from brittle to more ductile by bridging cracks. In this section, the change in the behaviour of plain concrete due to the use of textile reinforcement to reinforce concrete is studied. The behaviour of textile reinforced concrete (TRC) has so far not been fully investigated (Hegger *et al.* 2006b). Generally, TRC stress-strain behaviour is similar to that of steel reinforced concrete; however, there is no yield in the textile reinforcement in comparison to the steel reinforcement which means that there are no clear signs that failure is imminent (Häußler-Combe and Hartig 2007). In normal FRC the fibres are randomly dispersed in the concrete mix irrespective of where they are most needed in the structural members. On the other hand, for TRC, the textile reinforcement is placed in the required location to resist tensile loading, as shown in Figure 1-5

The main difference between TRC and fibre reinforced cementitious composite (FRC) is the tension behaviour after cracking occurs. The stresses are immediately carried by the fibres or the textile after the first crack. However, in the case of fibre reinforced concrete, a localized crack occurs, while in the case of textile concrete (TRC) the bridging cracks enable the concrete to continue to carry the stress, which leads to a form of multi-cracking until the stress is completely carried by the textile reinforcement (Mumenya, Tait and Alexander 2011).

The load bearing behaviour of textile reinforced concrete is significantly affected by the bond effectiveness, mechanical properties, type of material, amount and orientation of textile reinforcement (Voss 2006). However, textile reinforced concrete is still relatively new and there is little information available (Mumenya, Tait and Alexander 2011).

2.3.5.1 TRC tensile strength

The ultimate tensile strength is not activated due to bonding mechanism between strand and matrix (Banholzer 2006), which is explained in section 2.3.5.2. Therefore, the tensile test on the rovings cannot predict the load-bearing capacity of the composite (Hegger *et al.* 2006b). It can be said that the composite tensile strength is lower than the filament tensile strength by around 50% (Jesse and Curbach 2003). Figure 2-13 compares between different forms of textiles. The figure shows how the different forms of textile (filament, roving, and textile) vary in capacity and the capacity of textile reinforced concrete. The explanation of these differences is not fully understandable because of the complexity of the mechanism of multifilament failure. The ultimate load of a single filament in the composite depends on different factors. These variations between TRC composite and filaments and between filament and roving can be listed as follows (Hegger *et al.* 2006b):

- Uncertainty about filament properties.
- Flaws in some filaments may occur during the production process.

- Bond properties between filaments themselves and between roving and matrix.
- Fibre orientation.

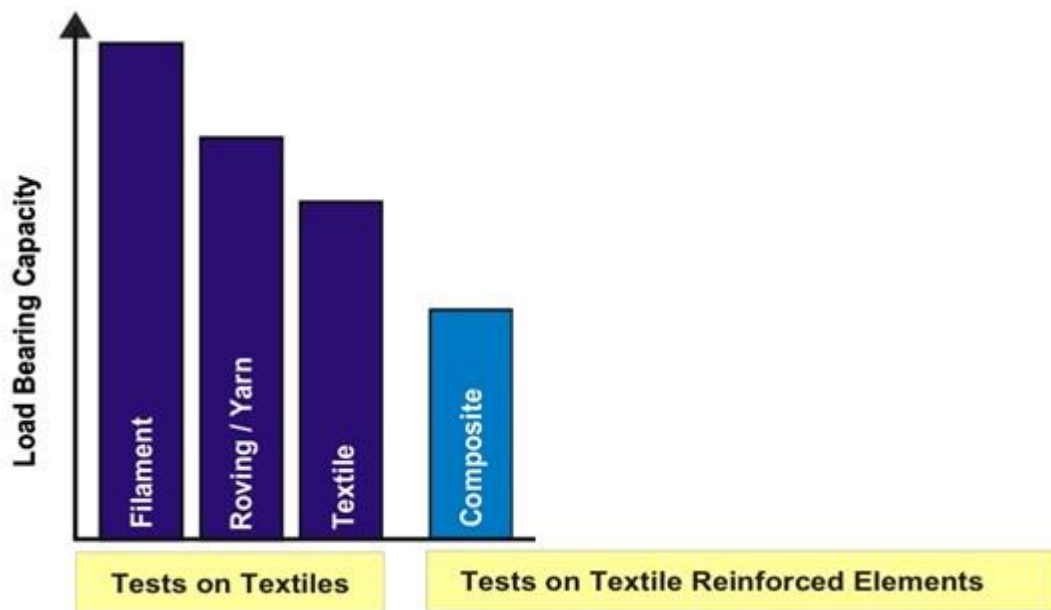


Figure 2-13 Load bearing capacity of different forms of textile, such as filaments and roving (Hegger *et al.* 2006c).

2.3.5.2 Textile pull out

As a result of the complexity of textile reinforcement, there is, as yet, no pull out test for measuring the bond between the textile and matrix, which might help us to obtain a better understanding of interfacial relations. The difficulty of the relationship between textile reinforcement and concrete can be accounted for the bond mechanism, which is as follows; the external filaments are well bonded to the matrix, which leads to fracture during the test, while the internal filaments undergo pull-out (Bentur and Mindess 2006). Therefore, the

external filaments strongly resist sliding in comparison to the interior filaments (Zhu and Bartos 1997). Four AR-glass strand specimens were prepared, as shown in Figure 2-14, and tested by Banholzer (2006). The pull-out behaviour of these specimens is shown in Figure 2-15. To look more closely, Banholzer investigated the active filaments (not fractured) during the pull out test. Figure 2-16 shows the number of filaments that remained intact during the test. It can be said that not all of the filaments at peak load are broken, as some of them are still active, and their number dramatically decreases with displacement. At the end of loading, a few hundred filaments pull out of the roving without failure. Also, if the fabrics are in contact with each other, that leads to a decrease in the area of the matrix-fibre interface which causes a sliding in the fibre (Colombo *et al.* 2013). Figure 2-17 was created based upon this information, and provides a schematic description of the roving failure mechanism. Based on this concept Hegger, Bruckermann and Chudoba (2004) developed a ring model to analyse the bond from outside to inside as shown in Figure 2-18. This model assumes that the roving is idealized as layers and that the bond decreases with distance from the core filaments. The percentage of filaments which are activated at the peak load of the pull out test is 65% while the rest are activated in the post peak zone (Hegger, Bruckermann and Chudoba 2004).

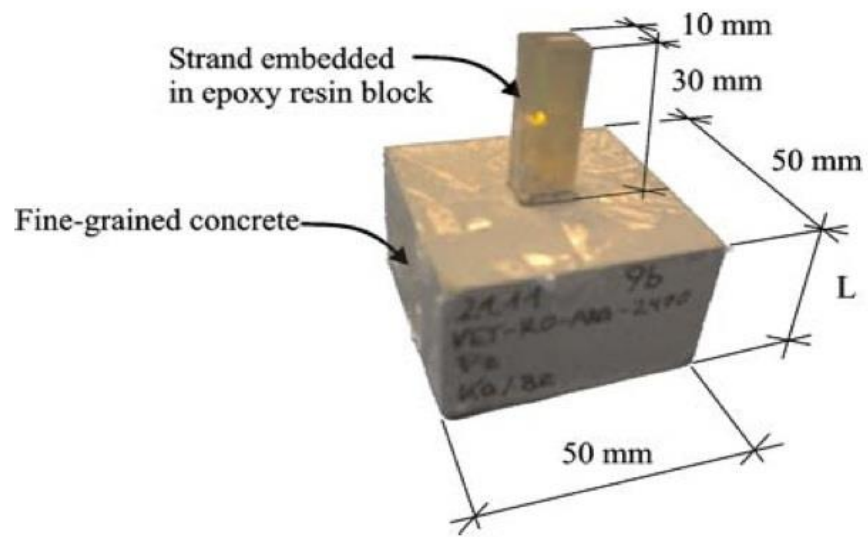


Figure 2-14 Specimen for the one sided strand pull out test (Banholzer 2006).

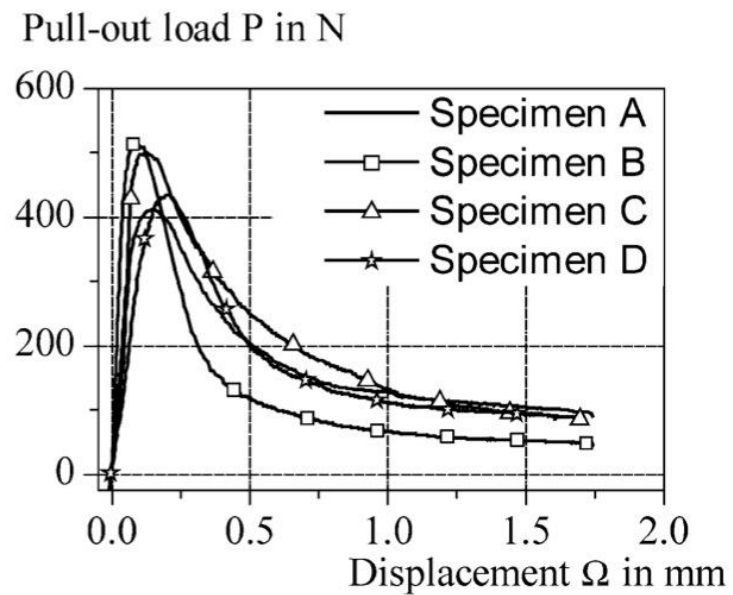


Figure 2-15 Specimen responses to pull out test (Banholzer 2006).

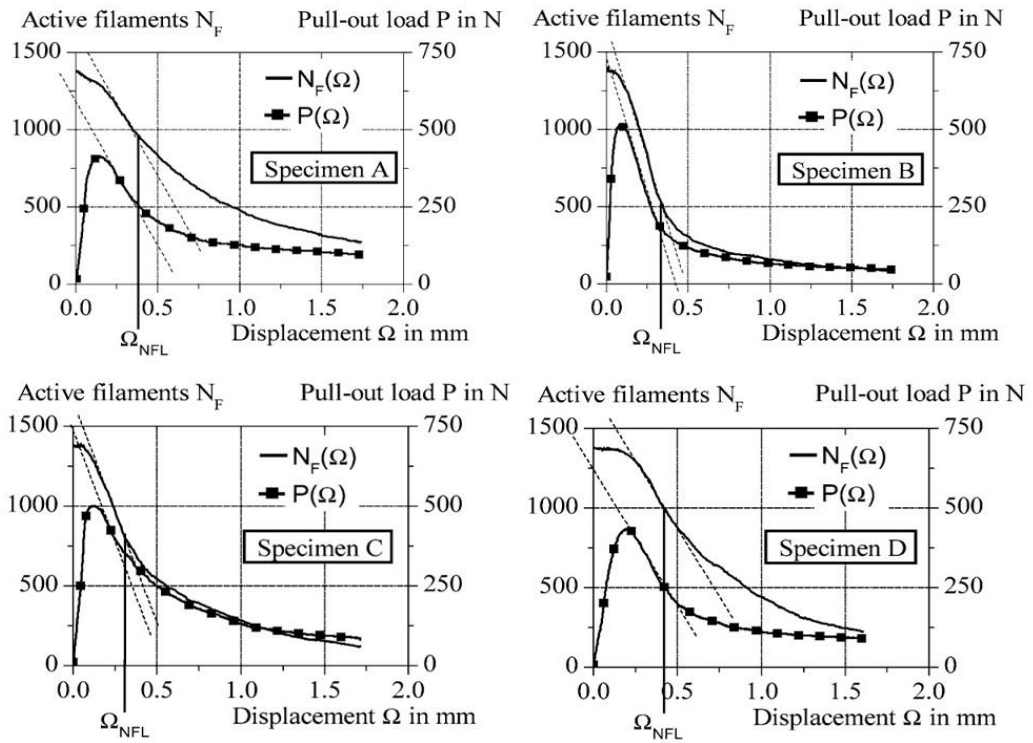


Figure 2-16 Active filament versus displacement diagram $N_F(\Omega)$ and pull out load versus displacement $P(\Omega)$ for specimens A to D (Banholzer 2006).

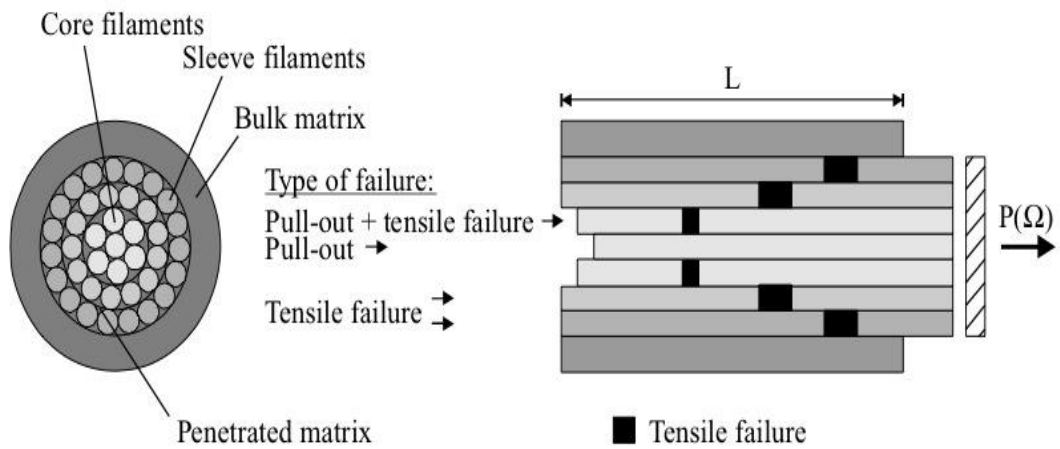


Figure 2-17 Failure mechanism of a strand embedded in a cement based matrix under a pull out load (Banholzer 2006).

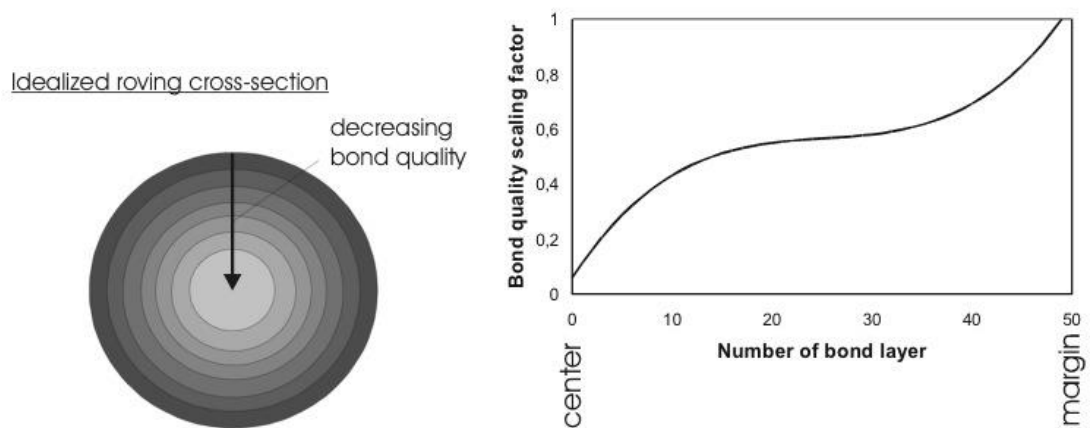


Figure 2-18 Bond layer model (Hegger, Bruckermann and Chudoba 2004).

Therefore, the pull out behaviour of a roving is controlled by the strong bond of the outer filaments and the slippage of the inner filaments (Majumdar 1974; Banholzer 2006). The inner and outer filaments are affected by the matrix penetration and, in the case of a cement matrix, the quality of penetration is uncertain due to the difficulty of measuring the extent to which the cement penetrates the filaments and the quality of the hydration products. This leads to the breakage of the filaments layer after layer beginning from the outer and moving to the inner ones (Banholzer 2006).

The main phenomenon in continuous fibres is the slippage inside the fibres. At the tensile load and due to the direct contact between the cement and the outer fibre at the surface, slippage occurs which causes uneven stress distribution in the fibre cross section. This phenomenon is expected to influence the mechanical behaviour of composites (Ohno and Hannant 1994). However, Zhu and Bartos (1997) reported that, the slip between inner and outer filaments is significantly reduced with time due to the precipitation of hydration products.

2.3.5.3 Stress-strain behaviour of TRC

The behaviour of a single filament of AR-glass and carbon is elastic until failure, while for yarn fibre, the failure behaviour is different and complicated to understand (Hartig *et al.* 2012). The failure behaviour of a composite is significantly affected by the mechanical properties of textile reinforcement.

The curve of stress-strain behaviour of textile reinforced concrete (TRC) under uniaxial loading is shown in Figure 2-19. It can be seen that the behaviour can be divided into three stages, as in the figure, which is similar to the stress-strain curve that was predicted by Aveston, Cooper and Kelly (1971). Therefore, the composite stresses at these different stages are similar to those of FRC which was discussed previously (see section 2.2.4), as follows (Purnell 2010b):

Before matrix cracks:
$$\sigma_c = \sigma_m V_m + \sigma_f \eta V_f \quad (2.5)$$

$$\sigma_c = \sigma_m (1 - V_f) + \sigma_f \eta V_f$$

Where σ_c is the composite stress.

σ_m and σ_f are the matrix and fibre stresses, respectively.

V_m and V_f are the matrix and fibre volume fractions, respectively.

η is the efficiency factor.

Post cracking stress:
$$\sigma_{cu} = \sigma_{fu} \eta V_f \quad (2.10)$$

Where σ_{cu} is the ultimate composite strength.

σ_{fu} is the ultimate fibre strength.

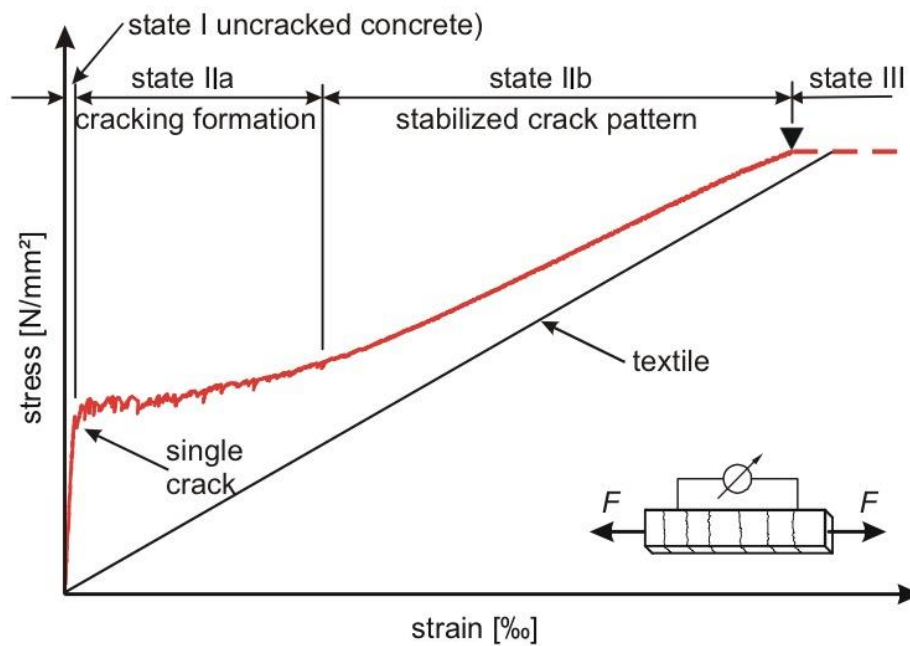


Figure 2-19 Stress-strain behaviour of textile reinforced concrete under uniaxial loading (Hegger *et al.* 2006c).

2.3.5.4 Cracking

Similar to other composite materials, the cracks appear in the tension zone of the concrete section due to the low resistance to tensile stress of the concrete matrix. At the uncracked stage, the textile reinforced concrete behaviour depends mainly on modules of elasticity of the concrete, while in the cracked section the load is completely carried by the reinforcement, which in this case are the filaments. Understanding the cracking process helps us to critically evaluate the load bearing capacity, deformation behaviour, and to design serviceability. From Figure 2-19, it can be seen that the cracks begin when the concrete reaches the ultimate tensile strength which means that they cannot carry any more tensile load. Therefore, the multiple cracks begin to form when there is enough bonding between fibre and matrix and sufficient quantity of reinforcement (Mashima, Hannant and Keer 1990), also, the stiffness of the fabric cement is high enough to prevent the new cracks from widening, therefore, more cracks are initiated due to transfer of the stress from fibre to concrete (Mobasher and Li 1996). This continues, with increasing loading, until no more cracks occur. Then, the textile reinforcement is strained

up to the ultimate strength of rovings (Hegger *et al.* 2006b). The increase in the volume fraction results in a decrease in the crack spacing (Colombo *et al.* 2013). In agreement with Swamy and Colombo, Bentur and Mindess (2006) stated that first crack strength can be increased as a result of increasing volume fraction. The crack spacing is not influenced by the fibre material, however, the average crack width of glass reinforced concrete is almost double that of carbon reinforced concrete (Hegger *et al.* 2006b). Also, the increase in the fabric and crimped geometry density reduce the crack spacing (Peled, Bentur and Yankelevsky 1999) which can be accounted for the increase in the volume fraction of textile reinforcement. An increase in the number of cracks indicates an improvement in the bond (Peled, Bentur and Yankelevsky 1999).

The number and widths of cracks are influenced by different parameters. The volume fraction of the fibre determines the number of initial cracks (Hegger *et al.* 2006b). Moreover, Colombo *et al.* (2013) found that the cracking properties are influenced by the loading rate, sample moisture, aging, and the bonding strength of the fibre-matrix interface. The outer bond of AR-glass roving plays a role in cracking spacing while the inner bond affects the failure process because it contributes to the stress in the post cracking stage (Rypl *et al.* 2009).

The cracking mechanism is difficult to understand (Mumenya, Tait and Alexander 2011). Therefore, understanding stress-strain behaviour and crack development as a function of loadings helps to produce a proper design for textile reinforced concrete (Hegger *et al.* 2006b).

2.3.6 Bending moment behaviour of TRC

The behaviour of a reinforced concrete beam when bent is normally explored with regard to load and deflection rather than stress and strain (Johnston 2000). As expected, the behaviour of a textile reinforced concrete beam, when bent, is a little different to that of a steel reinforced concrete beam, because it involves reinforcement that has different properties from steel. It is also

different between the textile fabrics themselves such as woven, weft insertion knit, straight roving.. etc. Swamy and Hussin (1989) stated that the use of woven fabric leads to improvement in the flexural behaviour. Moreover, Peled and Bentur (2003) found the behaviour of flexural prisms ($13\text{ mm} \times 20\text{ mm} \times 110\text{ mm}$) reinforced by crimped structure textile is better than woven fabric, and the woven structure textile is better than the straight roving, all at the same volume fraction, as shown in Figure 2-20. This good behaviour in crimped geometry can be accounted for by bonding as they found that crimped yarn contributed significantly to the bond due to the anchoring effect. It can be seen that the flexural strength of woven fabric is almost double that of straight yarn. In the same way, the perpendicular rovings may influence the flexural strength of different composites, as in Figure 2-21. The increase in the density of weft rovings leads to an increase in the flexural strength of woven fabric while in the knitted weft insertion the flexural strength decreases.

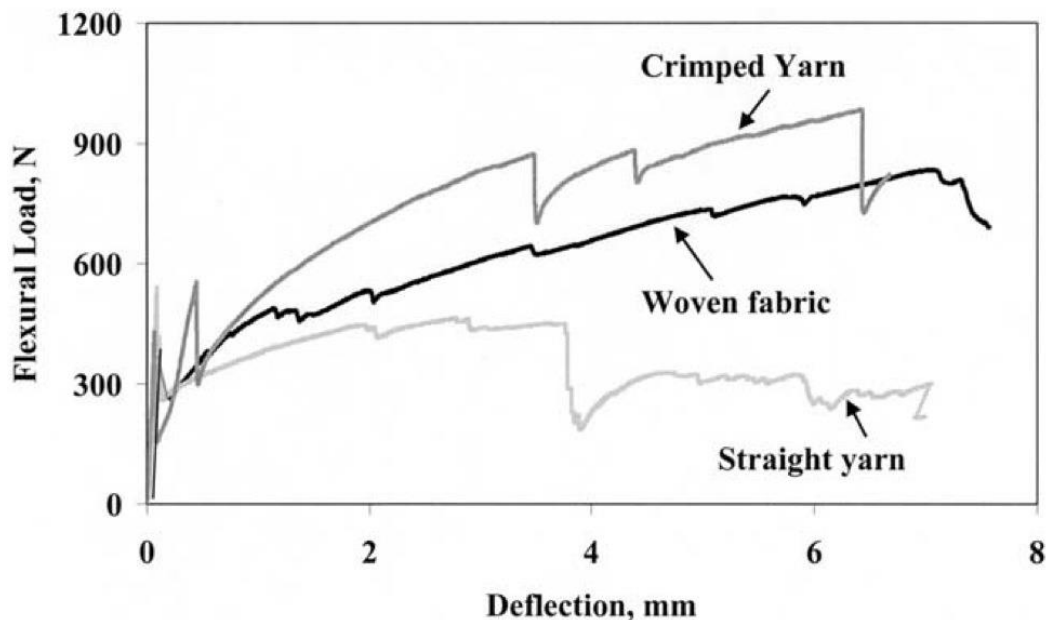


Figure 2-20 Flexural behaviour of different geometries of PE at $V_f = 5.7\%$ (Peled and Bentur 2003).

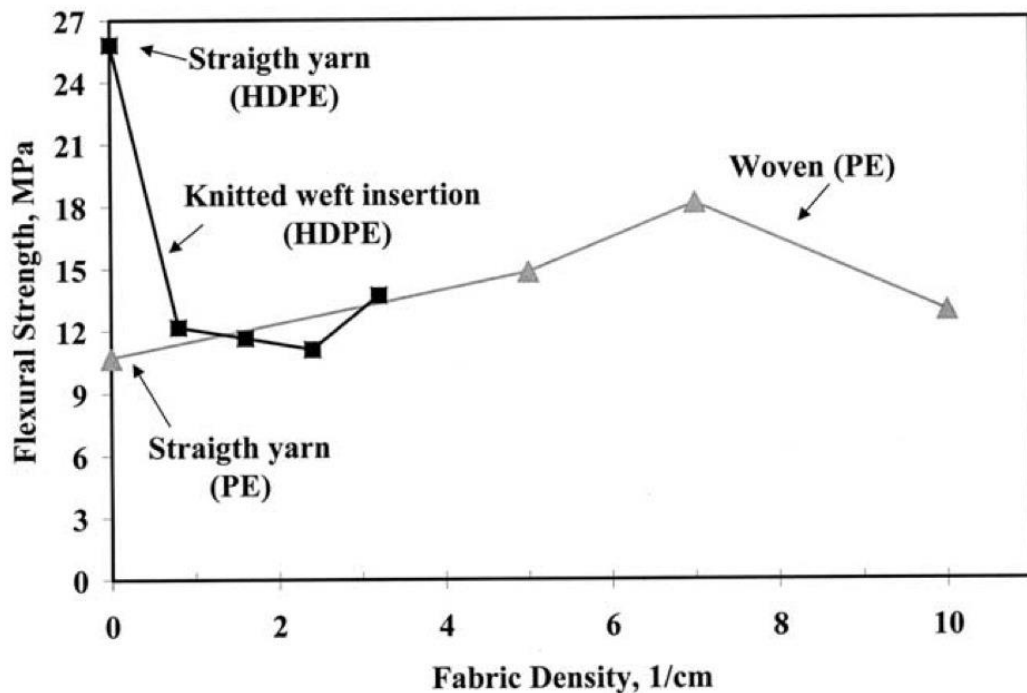


Figure 2-21 Influence of the density of weft rovings on flexural strength (Peled and Bentur 2003).

2.3.7 Efficiency of textile reinforced concrete (TRC)

Textile reinforced concrete is expected to be more efficient than FRC because of the textile reinforcement located in the loading direction which means better utilization of the reinforcement. Bentur and Mindess (2006) state that the short fibres which are angled with respect to the loading direction have lower efficiency than the continuous fibres which are parallel to the loading direction. To achieve 90% of fibre efficiency, the fibre length has to be more than 5 times the critical length, and up to 10 times, which is obviously achieved with respect to TRC. However, the tensile strength of the filaments is not fully used in TRC due to the decrease in the bond from the outer filaments towards the inner filaments of the roving (Voss 2006; Voss *et al.* 2006b). In order to improve the efficiency, knitted fabrics are used with small diameters as it is observed that the yarn diameter and the size of the opening loop of knitted yarns have a noticeable effect on the efficiency of textile reinforcement; when the diameter decreases and the loop size increases, the performance and the bond are

improved which can be attributed to the penetration of concrete to the filaments (Cohen *et al.* 2006). This is also confirmed by Dolatabadi *et al.* (2010) to obtain high efficiency, an adequate bond between all fibres in the roving and cement matrix has to exist. Also, it needs to be said that the type and properties of reinforcement and the geometry could positively or negatively influence the efficiency. The value of efficiency in flexural behaviour is high for crimped structure textiles due to the good bonding induced (Peled and Bentur 2003). In addition to the bond, the orientation of the TRC plays a vital role in the efficiency factor (Voss 2006; Hegger *et al.* 2006c). Flaws in the filaments lead to a noticeable reduction in stiffness and strength (Vorechovský, Jerábek and Chudoba 2006). It is also confirmed by Häußler-Combe and Hartig (2007) that the reduction in the stiffness of a TRC is attributable to the early failure of filaments. Because of all of the above, and also due to production processes, some filaments are broken, alignments change, and there are changes in fibre orientation, therefore, it is necessary to consider efficiency factors when accounting for the variations in the composite properties of TRCs.

2.3.8 Bond

It can be confidently said that the bond is one of the most significant factors affecting the overall performance in textile reinforced concrete (Williams Portal, Lundgren and Malaga 2014). It plays a vital role in determining the load bearing capacity and the behaviour of structural members reinforced by textiles. Shi-lang and He (2006) reported that textile reinforced concrete has been used for a while; however, the basic mechanical properties, such as bond and load bearing capacity, are not well understood. Shi-lang and He (2006) and Graf *et al.* (2007) found that, unlike steel bars, the cross section of the roving is inhomogeneous along the textile reinforcement while a steel reinforcement is the same over the whole of the steel bar. Accordingly, the bond behaviour in ordinary RC and TRC is completely different. Also, the tensile stress-strain behaviour of continuous fibre is complicated due to the bonding mechanism as the shear strengths at the fibre-cement interface and

within the bundles of fibre themselves are markedly different (Ohno and Hannant 1994) which adds further complexity to the bond behaviour.

Figure 2-22 and Figure 2-23 show the outer and inner filaments and that the matrix does not fully penetrate the inner filaments. The type of stitching should be mentioned here as it may affect the concrete penetration and the friction between the filaments (Hanisch *et al.* 2006). Furthermore, increasing numbers of filaments may lead to a decrease in the fabric bond (Bentur and Mindess 2006). Due to the effect of penetration, some adjustments (for example, using silica fume) could be made to study how the behaviour of textile reinforcement in concrete is changed (Banholzer 2006) because of the expected change in the bond. In addition to the factors that affect the bond, different fibre diameters have influenced the test results due to their influence on the bond. Also, the bond cannot be understood by knowing single roving bond as the geometry of the fabric has an influence on the fabric bond (Bentur and Mindess 2006). Figure 2-24 shows the bond structure of a woven textile embedded in a cement matrix. In addition, the bond behaviour could be affected by the binding and the cross section of the roving and the fibre material. The water/cement ratio has an effect on the bond strength as well, as it changes the porosity of the matrix (Majumdar 1974). Moreover, aging is crucial as it may change the failure mode because of filling the gaps that in the transition zone. At early age of hydration, a lot of porous are in the transition zone which they have been densified with time and that leads to change in the failure pattern (Stucke and Majumdar 1976).

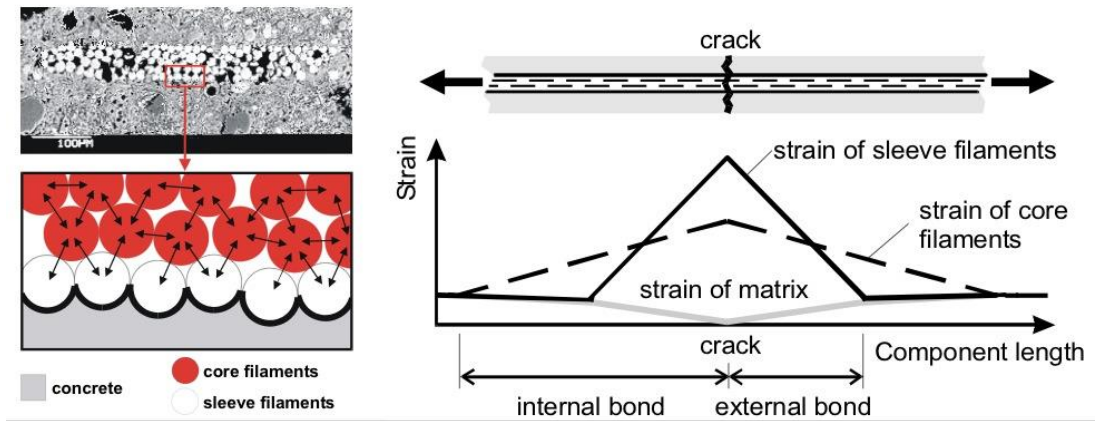


Figure 2-22 The internal strain in the roving (Jesse *et al.* 2008).

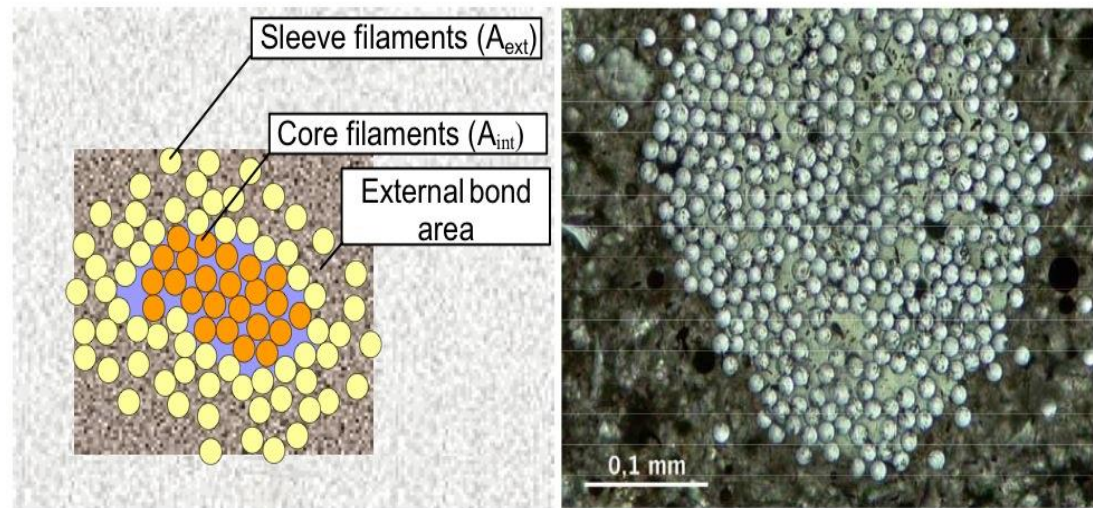


Figure 2-23 Inner and outer bond (Reinhardt *et al.* 2006b).

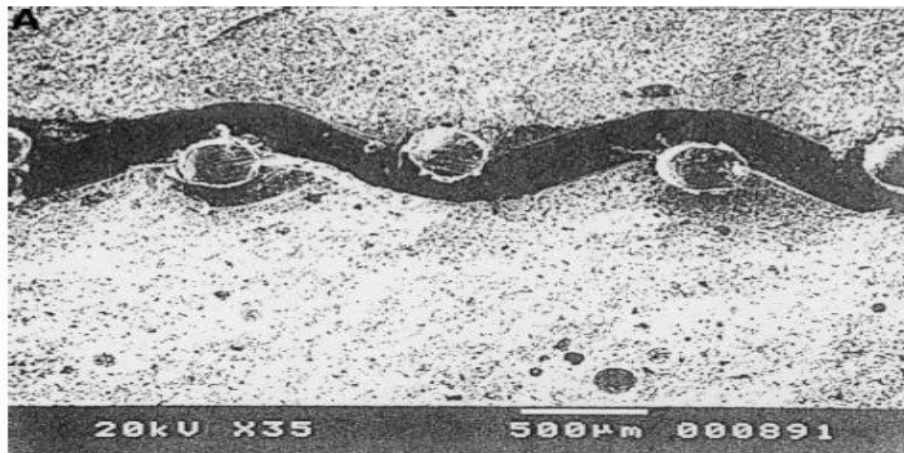


Figure 2-24 Woven fabric embedded in cement matrix (Peled, Bentur and Yankelevsky 1998).

Purnell (2010a) reported typical bond strength (τ) of multifilament carbon and glass fibres as 0.6 MPa for carbon, and $0.5\text{-}1 \text{ MPa}$ for fresh and aged glass fibre reinforced concrete. However, these values are not accurate enough because of the difficulty of understanding the interaction between filaments and matrix – at the very least, the contact perimeter is not known.

2.4 Design method

The increased use of TRCs in the last decade has led to a real need to develop new methods of designing structural elements which satisfy requirements, but according to Hegger *et al.* (2006c), no design method for TRCs is yet available. As a result of this, the applications of TRCs are still limited, and there is a clear need for experimentation (Freitag *et al.* 2006). Data base and design methodologies need to be developed with the aim of exploiting the advantages of textile reinforcement (Ko 1993), although tests have been carried out by many researchers to investigate textile reinforced concrete, the mechanisms are still not understood in detail (Hegger *et al.* 2006c).

Designing the ultimate load for textile reinforced concrete differs from the method used for short fibre reinforced concrete. This is a result of the way that fibres fail, namely, pulling out for short fibres, and broken fibres in textiles

(Hegger *et al.* 2006b). Because of this, one of the main requirements of a successful application is the design method (Voss *et al.* 2006b; Hegger *et al.* 2006c), although the design process is still uncertain (Hegger *et al.* 2006b). Continuous fibre reinforcements are fundamentally similar to conventional reinforced concrete (Swamy and Mangat 1974). However, according to Voss (2006), unlike steel reinforced concrete, TRCs' behaviour is different because of the differences in the bond characteristic and the material properties of the textile. However, tensile, shear and moment of steel reinforced concrete models could be adjusted to be used in textile reinforced concrete by analogy. The flexural capacity of textile reinforced concrete depends on the load-bearing capacity of the textile reinforcement. Therefore, by knowing the tensile strength of the textile, the flexural capacity can be determined by analogy to steel reinforced concrete (Hegger *et al.* 2006b).

For a design purpose that complies with all the requirements, a number of parameters have to be measured. Knowing the first crack and ultimate flexural strength is certainly useful for design and can be determined from the load-deflection behaviour (Swamy and Mangat 1974). More considerations have been taken into account as a result of the inhomogeneous cross sections of the rovings (Voss 2006). The amount of material, and the orientation of the textile reinforcement have to be taken into consideration when developing a design method for TRCs.

2.4.1 Flexural design of TRC

As discussed earlier, concrete/cement matrices cannot bear high tensile stresses. Therefore, materials with high tensile strength are used to resist such stresses. Normally, beam flexure is measured by load-deflection rather than stress-strain. In the following sections, the design methods of previous researchers will be presented.

2.4.1.1 Papanicolaou's method

Papanicolaou and Papantoniou (2010) investigated the behaviour of 22 beams with dimensions of $150\text{ mm} \times 100\text{ mm} \times 1500\text{ mm}$. The beams were reinforced with steel and textiles, as shown in Figure 2-25. A four point bending test was used to perform the test. Some assumptions were made to simplify the flexural calculations, as follows: plane cross sections before bending remain plane after bending, tension contribution of concrete is negligible, there is uniform stress distribution across each rovings' cross section; there is a perfect bond between concrete and textile reinforcement.

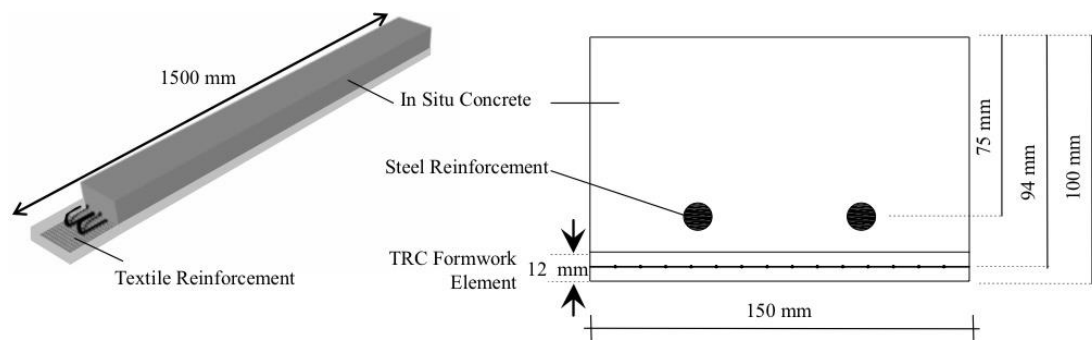


Figure 2-25 Beam details.

To obtain better predictions of the flexural capacities of the beams some adjustments were made:

- The carbon and glass ultimate tensile strength were substituted by effective tensile strength. This is because of the progressive fibre damage at the crack edges. It is represented by reduction factor k_r , as follows:

$$k_r = 0.65 \text{ for carbon}$$

$$k_r = 0.75 \text{ for glass}$$

thus, the effective tensile strength (f_{eff}) is:

$$f_{eff} = 0.65f_u \text{ for carbon.}$$

$$f_{eff} = 0.75f_u \text{ for glass.}$$

where, f_u is the ultimate tensile strength of an individual filament.

- Coating effect was considered; k_b expresses the textile area in good contact with the matrix, k_s expresses the strain lag which accounts for the differentiation in strain between the inner and outer filaments.

k_b and $k_s = 1$ for impregnated textile.

$k_b = 0.25$ and $k_s = 0.4$ for uncoated textile, which means that only a quarter of the textile reinforcement area is in a perfect bond with the matrix. However, Papanicolaou stated that more experimental investigation was needed. These variations are shown in Figure 2-26.

Papanicolaou used the tensile strength of the filament in the design method calculation. This strength is confirmed to be higher than the roving tensile strength, therefore, it may lead to inaccurate calculations. In addition, the effect of the bond was taken into account by considering the area in contact with matrix k_b , however, this is believed to be quite conservative.

In addition, there is no obvious methodology used to design the TRC beam.

Therefore, the approach used by Papanicolaou to design a TRC beam may greatly underestimate the composite capacity of the beam, and the methodology is uncertain.

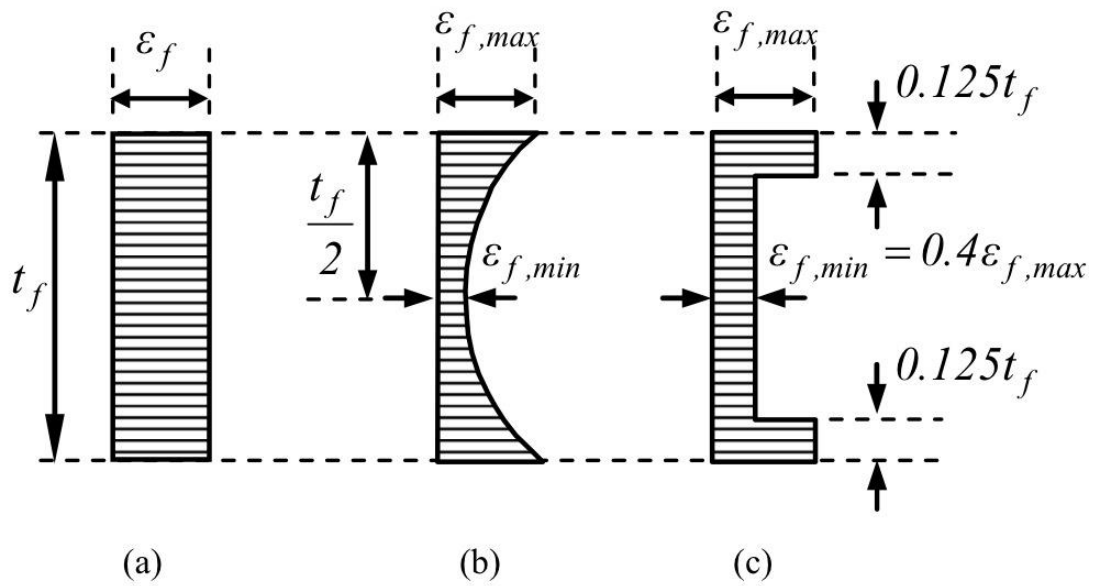


Figure 2-26 Strain profile of the cross section of the roving (Papanicolaou and Papantoniou 2010): a) strain distribution in a coated roving; b) uncoated roving; c) simplification of strain distribution in an uncoated roving.

2.4.1.2 Voss's method

Voss *et al.* (2006a) and Hegger and Voss (2008) investigated I section beams with dimensions 110 mm flange width x 120 mm high x 1000 mm length. A four point bending test was carried out as shown in Figure 2-27.

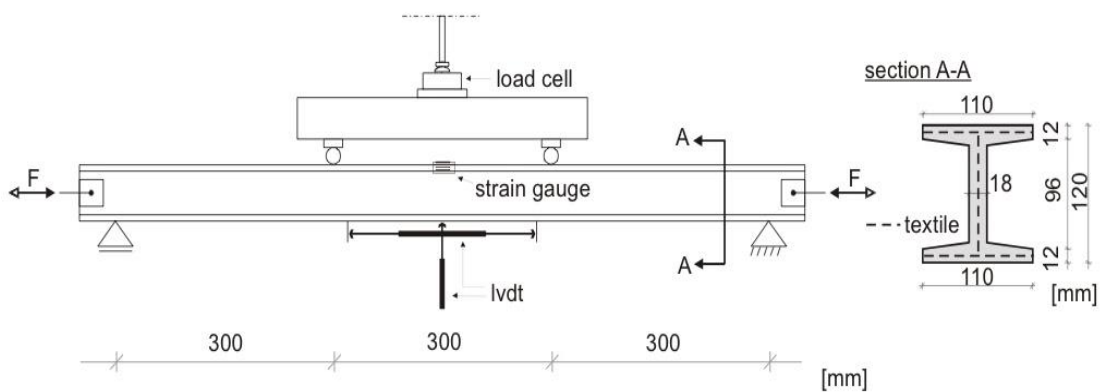


Figure 2-27 Beam details.

The tensile strength of TRC (F_{ctu}) can be calculated after considering factors that affect the value of tensile strength of textile reinforcement.

The efficiency is governed by the bond between the matrix and textile which is affected by the filament diameter, type of interlacing, and the roving thickness. As a result, the roving geometry and the penetration are affected. For six single tests Voss and Hegger found that the efficiency factor (k_1) of glass fabric is 0.42 and for carbon is 0.20-0.25.

Figure 2-28 demonstrated that the direction of the textile reinforcement could change at the crack edges which results in across stresses are added on the longitudinal reinforcement. The ratio $k_{0,\alpha}$ represents the load bearing capacity in the sloped textile reinforcement relative to the load bearing capacity in the longitudinal textile reinforcement. It can be assumed that the tensile strength of textile reinforcement decreases linearly as the angle (α) increases between the direction of the tensile load and the alignment of the rovings.

Therefore, the tensile strength of TRC can be calculated as follows:

$$F_{ctu} = A_t f_t k_1 k_{0,\alpha} k_2 \quad (2.11)$$

where, A_t is the cross sectional area of textile reinforcement.

f_t is the tensile strength of the filament.

k_1 is the efficiency factor: $k_1 = \frac{\sigma_{fu}}{f_{filament}}$

$k_{0,\alpha}$ is the factor for orientation of the reinforcement: $k_{0,\alpha} = 1 - \frac{\alpha}{90^\circ}$

k_2 is the biaxial load factor: $k_2 = 1 - 22 \frac{\sigma_{c,lateral}}{\sigma_{fu}} \leq 1.0$

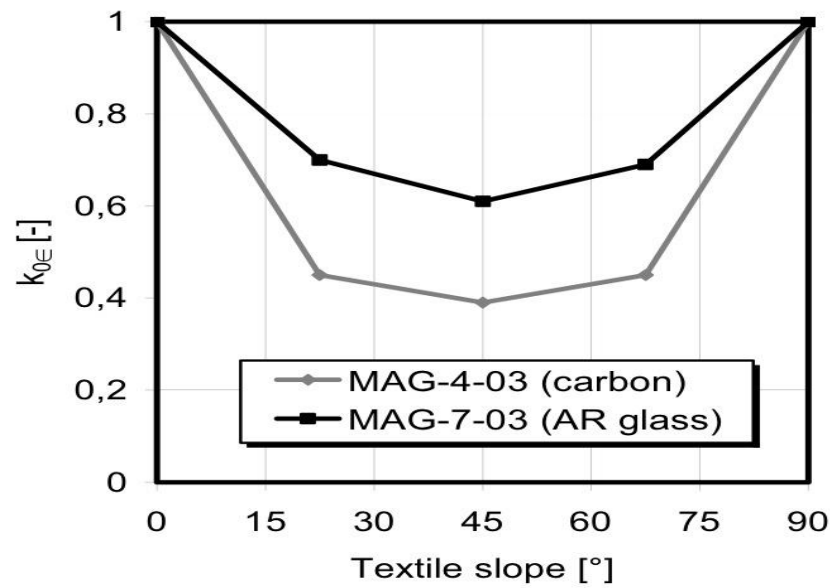


Figure 2-28 Influence of the change in textile direction on load bearing capacity (Hegger and Voss 2004).

In order to calculate the flexural bearing capacity, the transversal effect on the reinforcement was taken into account. Figure 2-29 shows the ratio between the ultimate flexural load and the tensile load. The increase in the flexural strength of carbon reinforced concrete is due to the large deflection carbon TRC can exhibit, therefore, increasing the curvature. This leads to stresses acting on roving which means better bond performance of the filaments. The factor is used to express the effect of transversal stresses as follows:

$$k_{fl,p} = 0.90 \text{ in the case of glass TRC.}$$

$$k_{fl,p} = 1 + 40 \frac{A_t}{A_c} \text{ in the case of carbon TRC.}$$

where $k_{fl,p}$ is the factor for bending loading.

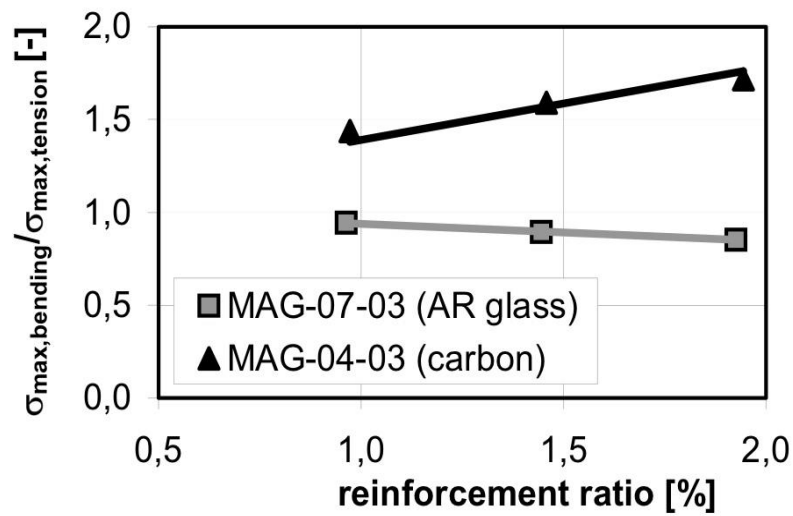


Figure 2-29 Ratio between ultimate tensile strength under bending moment and tensile loading (Voss *et al.* 2006a).

Knowing the tensile strength of reinforcement F_{ctu} and the inner lever arm z , the bending capacity of the TRC beam is:

$$M_u = k_{fl,p} F_{ctu} z \quad (2.12)$$

The bending capacity of the carbon textile reinforced concrete beam is:

$$M_u = \left(1 + 40 \frac{A_t}{A_c}\right) A_t f_t k_1 k_{0,\alpha} k_2 z$$

F_{ctu} is the tensile strength of the textile reinforced concrete.

z is the internal lever arm ($\approx 90\%$ of the static effective height).

Based on this equation and in the case of the carbon TRC beam in 0° direction and with no lateral stress, the only factor to be considered is the efficiency factor (k_l). The different factors are:

$$k_1 = 0.25$$

$$k_{0,\alpha} = 1$$

$$k_2 = 1$$

$$k_{fL,p} = 1 + 40 \frac{A_t}{A_c} > 1$$

The result of multiplying these factors is ~ 0.25 . Therefore, it can be said that only around 25% of TRC bending capacity is exploited. In this design methodology, there are several things which are worthy of note. The efficiency factor (k_1) is in fact not the efficiency factor; it could be said to be the practical tensile strength of the roving. Also, it is considered to be between 0.20 and 0.25 for carbon which is conservative. The use of single filament tensile strength f_t is not accurate as it is mentioned in the literature that the tensile strength of the roving is lower than the single filament tensile strength. Moreover, the total area of textile reinforcement is not all activated due to the bond issue, thus, using total area is imprecise without considering the effect of the bond. As a result of not taking into account the bond effect, the bending moment capacity is overestimated (Alrshoudi and Purnell 2015). Also, assuming the effective depth by 90% from beam height consider a simplifying of calculation in this early stage of design methodology investigation. This assumption seems to avoid taking into account the concrete strain as it may not reach the ultimate, while this equation is based on the ultimate strain of concrete.

2.5 TRC manufacturing methods

Manufacturing textile reinforced concrete TRC is the way of combining the matrix and textile reinforcement together in order to produce TRC. There are various techniques that can be used to produce textile reinforced concrete. Moreover, method used to produce textile reinforced concrete may have a significant influence on the bond. Figure 2-30 shows the penetration of two different processing methods. It can be clearly seen that the pultrusion method produces a high penetration in comparison with the casting one. Besides that,

Colombo *et al.* (2013) stated that a good bond between concrete and fabric reinforcement can be achieved by improving the mixture workability in order to make it flow through the fabric.

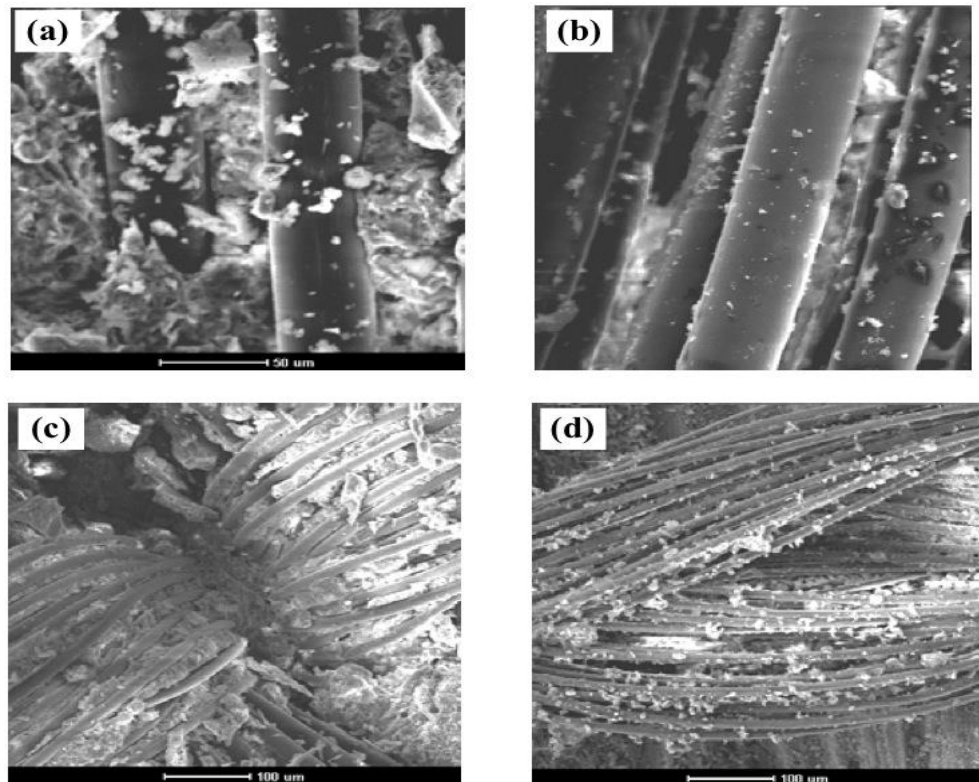


Figure 2-30 Cement penetration of two methods of processing: a) and c) pultrusion, and b) and d) casting (Reinhardt *et al.* 2006a).

2.5.1 Hand lay-up

This is also called contact moulding or the hand laminating technique. It is considered to be one of the oldest and simplest methods of composite fabrication. The method gives more control over textile placement than the spray method and is suitable for large components and complex shapes, however, it requires more labour. The production steps are as follows:

- 1- Mould preparation.
- 2- Casting concrete cover.

- 3- Hand lay-up.
- 4- Finishing.

2.5.2 Pultrusion

Pultrusion is a continuous process for producing fabric-cement laminate composite. It can be used to produce fabric-cement sheets with different widths, lengths, and thicknesses. The production processes are as follows:

- 1- Fabric passed through cement slurry.
- 2- Paste consolidated in the openings fabric through a set of rollers.
- 3- Excessive paste removed.
- 4- Composite laminates formed.
- 5- Additional limited pressure on the laminates to improve penetration.

2.5.3 Filament winding

Filament winding is used to produce thin reinforced composite. The production processes are as follows:

- 1- Fabric passed round steel bars.
- 2- Wetting the fabrics.
- 3- Fabric passed through cement bath.
- 4- Fabric passed through steel bars to be drained off.
- 5- Fabric entered cement impregnation tube.
- 6- At the tube exit, sliding table moves transverse to the fibre direction.

2.5.4 Module process

The module process is designed to produce textile reinforced elements at low capacity with more flexibility in product choice.

There are also other techniques that can be used to produce textile reinforced concrete, such as extrusion and wellcrete.

2.6 TRC applications

The main advantage of textile reinforcement is corrosion resistance. The cover thickness of concrete members can be reduced up to 10 mm which allows us to produce thin walled structural elements (Hegger *et al.* 2006a). Also, the density, the yarn distance, and the orientation of filaments can be located based on the acting stresses which provide more architectural flexibility and high utilization of textile reinforcement. The reduction in the fibre reinforcement is up to 80% in comparison with conventional glass fibre reinforced concrete which represents an effective exploitation of fibre (Butler, Lieboldt and Mechtcherine 2009). The following sections present various applications around the world of textile reinforced concrete.

2.6.1 Façade panels

As a result of using textile instead of steel reinforcement, it is possible to design innovative architecture. Moreover, using textile reinforcement is economical because it attracts savings in material, transport, and anchorage costs (Hegger, Horstmann and Zell 2008). Figure 2-31 illustrates a range of buildings clad with TRC façade panels, produced by the Fydro company from the Netherlands.

2.6.2 Decentralised wastewater treatment plants

This application is common in Germany which has many decentralised wastewater treatment plants. They must be cost effective and durable, so textile reinforcement is applied to reinforced concrete tanks. Figure 2-32 shows decentralised wastewater treatment plants made of textile reinforced concrete. The wall thickness is 40 mm which is half the thickness of a steel reinforced concrete tank.



a) School centre, Dusseldorf, Germany



b) Office building, Dortmund, Germany



c) Office building, Arnhem, Netherlands

Figure 2-31 TRC façade panels on various buildings.



Figure 2-32 TRC for decentralised wastewater treatment plants (ibac, IMB RWTH Aachen University + Fa.Mall).

2.6.3 Integrated formwork

Figure 2-33 shows textile reinforced concrete formwork integrated with steel reinforced concrete floors. It was developed, with Stuttgart University, at Aachen RWTH University.

2.6.4 Various applications

The ease of installing the textiles helps to produce different structures strengthened by textile reinforcement. Figure 2-34 demonstrates the variety of such applications.

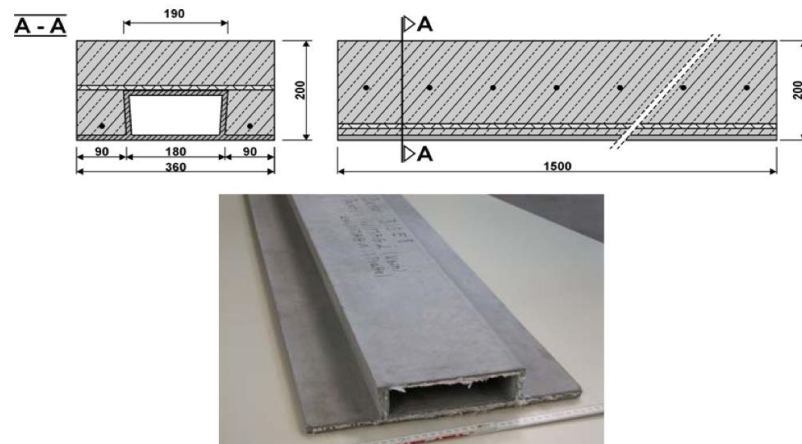


Figure 2-33 TRC formwork elements integrated with steel reinforced concrete floors.



Figure 2-34 Various applications of TRC by a) Prull (1995), b) Lieboldt *et al.* (2005), c) RWTH Aachen Germany.

2.7 Conclusion

In this chapter some physical and mechanical properties of FRC and TRC have been reviewed. It can be seen that there is a determination to develop composite materials with excellent properties to overcome weaknesses in conventional reinforced concrete, such as corrosion. The properties of textile reinforcement, including its high tensile strength, high modulus of elasticity, chemical resistance and low weight, make it attractive. However, there is an obvious lack of data concerning textile reinforced concrete in general and textile reinforced concrete design methods in particular. The successful application depends on the existence of a proper design method which takes all of the structural variables into consideration.

The main conclusions that can be drawn from the literature are as follows:

- Fibres are dispersed randomly in concrete section, therefore, they are not fully used. Nevertheless, fibres are used in FRC to control cracks and improve toughness not to increase the strength of concrete members.
- Textile reinforcement can be positioned where needed, thus, the fibres are effectively used. Therefore, it can be utilized in RC members as a main reinforcement. Also, it can be formed with a variety of geometries and layouts, for example, woven fabric, knitted, or crimped. Textile reinforcement has excellent mechanical and chemical properties, corrosion resistance, low weight, and is easy to install, and it can be applied in a variety of applications with reduced concrete cover, such as in façade panels, concrete pipes, and frameworks.
- For better bonding, a matrix of fine grained concrete is preferred to improve the penetration. The textile-matrix interaction is complicated because of the type of bond between matrix and textile. Due to the multifilament roving, the matrix is in direct contact with the outer filament while contact with the inner filaments depends on the penetration of the matrix and cement hydration. Therefore, bonding is crucial in TRC. As a result, the bond behaviour of textile reinforced

concrete is different from the bond behaviour of steel reinforced concrete. This can be attributed to the inhomogeneity of the roving area along the textile reinforcement in comparison with steel bars.

- Filament tensile strength is higher than roving tensile strength, and the latter is higher than composite tensile strength. The reason behind this is not completely understood.
- As yet, there is no textile mechanical standard test. Therefore, there is a need for more experimentation on TRC.
- For various reasons (flaws introduced by textile reinforcement production processes; changes in orientation; complexity of the bond; the difficulty of accurately measuring the mechanical properties of textile reinforcement; fibre diameter, loop size, and geometry) it is necessary to use efficiency factors in TRC design.
- TRC can be produced by different manufacturing methods, including hand lay-up, pultrusion, filament winding, and the module process.

However, there are many areas with regard to textile reinforced concrete which have not yet been fully investigated and understood. Therefore, this study will look at some of those unexplored areas and study some of the issues that have not been completely covered:

- To the author's knowledge, no study has investigated carbon textile reinforcement as a main and only reinforcement in rectangular concrete beam at large size beam.
- Study of a textile reinforced concrete beam with different layouts and geometries, to achieve a comprehensive understanding of carbon TRC flexural behaviour, and to help introduce a design method for TRC.
- The bond efficiency factor of carbon TRC is still not fully investigated. Voss found a value of the efficiency factor for carbon textile reinforced concrete, however, it was based on the tensile strength of the filament. Therefore, it needs to be determined experimentally based on the roving tensile strength in order to account for the reduction in TRC performance because of the bond.

- Comparison of TRC beams with steel reinforced concrete beams is essential in order to develop a deep understanding of TRC behaviour. However, to the author's knowledge, no experimental investigation has been conducted to compare carbon textile reinforced concrete beam behaviour with that of steel reinforced concrete beams.
- Developing a design method that is able to determine the required quantity of textile reinforcement will facilitate the application of TRC. Therefore, this study will investigate the design methodology that could be used to design carbon textile reinforced rectangular concrete beams.
- In general, there is an obvious lack of experimental investigation into TRC beams. Therefore, this study will support and increase the database of textile reinforced concrete to provide a better understanding of TRC performance.

CHAPTER 3

MATERIALS AND METHOD

3.1 Introduction

In this chapter the experimental works are described in terms of the equipment, materials and their properties, mix designs, curing and tests used in the research. All the tests were conducted in the George Earle lab of the Civil Engineering School in the University of Leeds.

3.2 Materials

The properties of the materials that have been used in this project are presented in this section.

3.2.1 Cement

The cement matrix used throughout the all this project was ordinary Portland cement CEM I. The supplier was Castle Cement Ltd in the United Kingdom and the cement complies with the requirement of BS EN 197-1. The bags come with water-proof air-tight packaging to protect the cement and prevent it from deterioration. Table 3-1 shows manufacturer data sheet of the chemical components and physical properties of the cement used in this study.

Table 3-1 Manufacturer data sheet of chemical compositions and physical properties of OPC.

Oxide composition	% by weight
CaO	63.63
SiO ₂	21.03
Al ₂ O ₃	4.73
SO ₃	3.0
Fe ₂ O ₃	2.93
MgO	2.67
K ₂ O	0.65
Na ₂ O	0.30
Compound composition	% by weight
C ₃ S	51.33
C ₂ S	21.14
C ₄ AF	8.86
C ₃ A	7.49
Physical properties	
Specific surface area	0.341 m ² /g
Specific gravity	g/cm ²

3.2.2 Fly ash

Fly ash was used with fine grained concrete at small scale beams in order to increase the bond of textile reinforced concrete. Moreover, it is used to enhance the mixture workability. Brameshuber *et al.* (2006) stated it is found that the presence of fly ash also results in improved penetration and thus good bond. The fly ash used was Castle BS EN 450 which was supplied by Castle Cement Ltd in the United Kingdom. It complies with the requirements of BS EN450 : 1995. Table 3-2 shows manufacturer data sheet of the chemical compounds and physical properties of fly ash used in this study.

Table 3-2 Manufacturer data sheet of chemical compounds and physical properties.

Chemical compounds	Average % by weight
SiO ₂	50
Al ₂ O ₃	30
Fe ₂ O ₃	7
CaO	3
MgO	1
K ₂ O	3
Na ₂ O	1
TiO ₂	1
SO ₃	0.5
Cl	0.1
Total alkaline (Na ₂ Oaq)	Less than 5
Loss on ignition	Less than 7
Fineness (residue on 45 microns)	Less than 40
Physical properties	
Physical state	Particulate
Mean particle size	5-50 microns
pH	pH of wet Fly Ash 9-10
Density	2000 – 2200 kg/m ³

3.2.3 Silica fume

Silica fume used in this study was ElkemMicrosilica Grade 920E. This product was supplied by Elkem Materials and conformed to the requirements of EN 13263. It is used to improve the mechanical strength of concrete and also to enhance the interface between paste and adjacent materials (Köksal *et al.* 2008). Accordingly, the cement-textile interaction is improved. Table 3-3 shows the manufacturer data sheet of chemical compounds and physical properties.

Table 3-3 Manufacturer data sheet of the chemical compounds and physical properties

Chemical compound	% by weight
SiO ₂	> 85
SO ₃	< 2
Cl	< 0.3
Free CaO	< 1.0
Free Si	< 0.4
Loss on Ignition LOI	< 4
Physical properties	
Colour	Grey
Odour	Odourless
Melting point (°C)	1550 - 1570
Specific gravity	2.2 - 2.3
Bulk density (kg/m ³)	150 – 700
Specific surface (m ² /g)	15 – 30
Particle size, mean (µm)	≈0.15

3.2.4 Fine aggregate

The role of fine aggregate in textile reinforced concrete is highly important as in many cases it is the only aggregate used i.e. without coarse aggregate. The supplier of fine aggregate was Tarmac Roadstone Ltd. and the grading complied with BS 882: 1992, zone M. The sieve analyses carried out at the lab showed that 80% of aggregate is 2 mm or less. The sieve analysis results are shown in Table 3-4.

Table 3-4 Sieve analyses results of fine aggregate

BS sieve size	Weight retained	Cumulative percentage retained (%)	Cumulative percentage passing (%)	BS 882 grading zone M
> 2.36 mm	19	3.8	100	-
2.36	80	19.8	80.2	65 – 100
1.18	44	28.6	71.4	45 – 100
600 µm	62	41	59	25 – 80
300 µm	167	74.4	25.6	5 – 48
150 µm	99	94.2	5.8	-
Pan	29	100	0	-
Total	500			

3.2.5 Coarse aggregate

The supplier of the coarse aggregate with maximum size 10 mm was Tarmac Roadstone Ltd. It was uncrushed quartzitic aggregate with irregular shape and smooth surface. The sieve analyses results of coarse aggregate carried out at the lab are shown in Table 3-5. The grading complied with the requirement of BS 882: 1992.

Table 3-5 Sieve analysis results of coarse aggregate 10 mm.

BS sieve size	Cumulative percentage Passing (%)	BS 882 grading
> 10 mm	100	100 - 100
10	96	85 – 99
8	76	–
6.3	47	–
5	14	–
4	4	0 - 20
2.8	2	-
2	2	0 - 5
1	2	-
500 µm	2	-
250 µm	2	-
125 µm	2	-
63 µm	1.5	0.0 – 1.5

3.2.6 Water

The water used throughout the project was tap water. Neville (1995) reported that there is no clear standard for the quality of mixing water, however, it should be clean water and not include too much organic or inorganic substances.

3.2.7 Superplasticisers

Superplasticiser (SP), otherwise known as high range water-reducing admixture, was used to improve the workability of the concrete mixture and reduce the water/cement ratio. Mix cohesion was not changed and there was no excessive bleeding or segregation. In this study, Sika[®]ViscoCrete 25MP was provided by Sika. This product meets the requirements of BS EN 934-2.

The technical data provided from manufacturer of superplasticisers is shown in Table 3-6.

Table 3-6 Technical data of Sika®ViscoCrete 25MP.

Chemical base	Modified polycarboxylate
Density	1.06 kg/l (at +20°C)
pH value	4.5±0.5
Freezing point	+1°C
Total chloride ion content	< 0.1% (chloride free)
Air entrainment	Negligible, normally a minimal increase
Effect on setting	Slight extension to normal setting
Effect of overdosing	Increased workability and segregation
Service temperature	1°C to + 35°C suitable
Alkali content	0.5% maximum

Based on the manufacturer data sheet, the dosage percentage is from 0.2% to 0.8% by weight of cement for medium workability and from 1.0% to 2.0% by weight of cement for special applications such as self-compacting of ultra-high strength.

3.2.8 Reinforcement

Two types of reinforcement were used in this study. One is the steel reinforcement and the second is textile reinforcement.

3.2.8.1 Steel reinforcement

The diameter of deformed steel rebar was 8 mm . It was supplied by Barret Steel Limited. The mechanical properties from the Manufacturer data sheet is yield strength $f_y = 500\text{ MPa}$ and yield strain is $\epsilon_y = 0.0025$.

3.2.8.2 Textile reinforcement

Four different types of textile reinforcement were used in this study. Two types of textile reinforcement with different looping sizes and two types of tows with different number of filaments were all investigated. All these reinforcements were carbon fibre supplied by FormaxMultiaxial Reinforcements. Figure 3-1 shows the types of carbon textile reinforcement that were used to reinforce beams. Manufacturer data sheets for all the types of textile reinforcement are shown in Table 3-7, Table 3-8, Table 3-9, and

Table 3-10. C50k, 260, 0/90 stands for carbon (C), 50 thousands of filaments per roving (50k), 260g per square meter, and bi-directional textile (warp (0) and weft (90) or 0/90). The nominal tensile strength of single filaments and the modulus of elasticity of the all various carbon reinforcements was 4000 MPa and 235000 MPa, respectively as reported by the manufacturer, however, experimental tensile test were carried out to establish the engineering properties, see section 3.5.2. Table 3-7 shows the properties of first carbon textile reinforcement (C50k, 260, 0/90). Figure 3-2 and Figure 3-3 shows the structural layout of the carbon textile reinforcements (C50k, 260, 0/90).

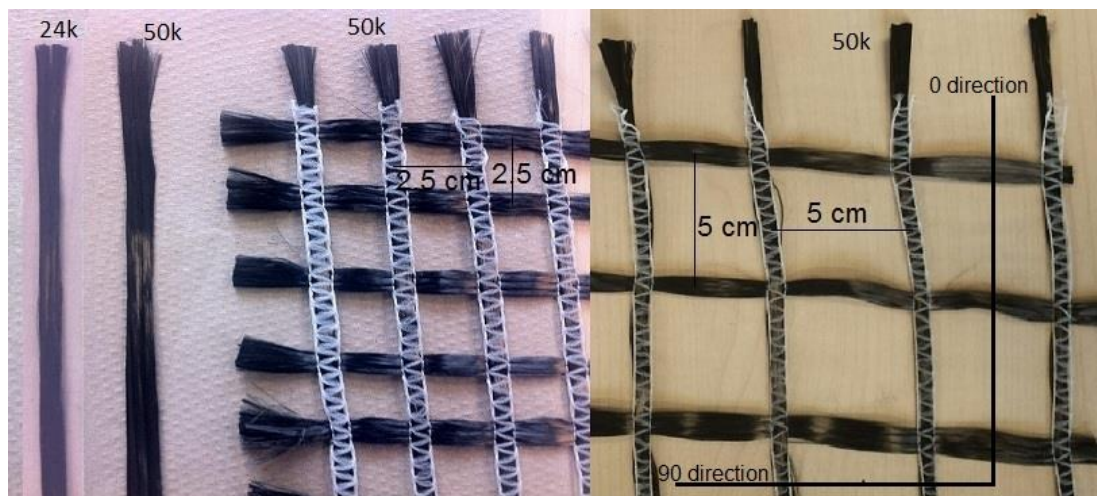


Figure 3-1 Different types of carbon reinforcements.

Table 3-7 25 mm carbon textile properties of biaxial reinforcement (C50k, 260, 0/90).

Properties	Bi-directional, 50k
filament diameter, μm	7.0
Number of filaments, k	50
Fabric weight, g/m ²	260
mesh spacing, mm	25
Tensile strength, f_t (MPa)	4000
Modulus, E_f (MPa)	235000

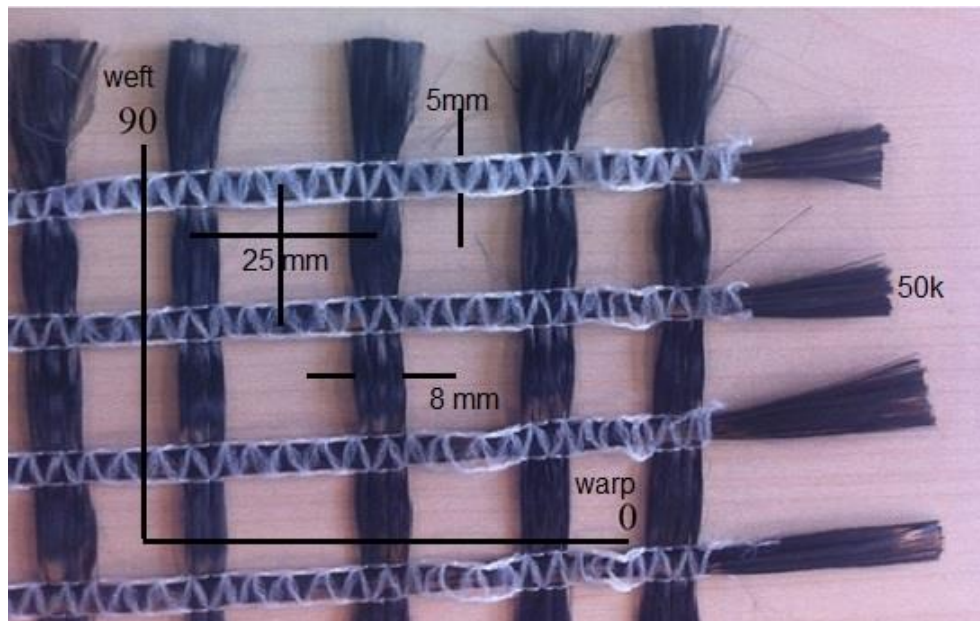


Figure 3-2 Layout of biaxial carbon textile reinforcement with 2.5 cm looping size.

Table 3-8 50 mm roving (warp and weft) spacing of carbon textile properties of biaxial reinforcement (C50k, 150, 0/90).

Properties	Bi-directional, 50k
filament diameter, μm	7.0
Number of filaments, k	50
Fabric weight, g/m ²	150
mesh spacing, mm	50
Tensile strength, f_t (Mpa)	4000
Modulus, E_f (Mpa)	235000

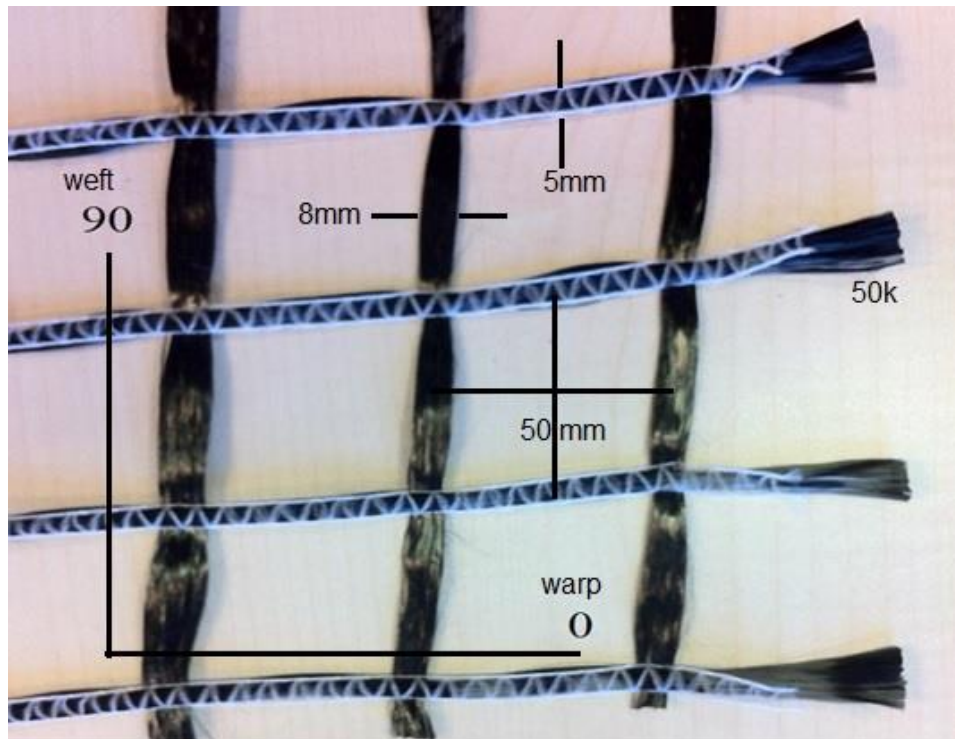


Figure 3-3 Layout of biaxial carbon textile reinforcement with 5 cm looping size.

Table 3-9 Carbon textile properties of tow (uniaxial) reinforcement (C24k).



	Properties	Uni-directional, 24k
	Filament diameter, μm	7
	Number of filaments, k	24
	Fabric weight, g/m²	63
	Fabric spacing	-
	Tensile strength, f_f (Mpa)	4000
	Modulus, E_f (Mpa)	235000

Table 3-10 Carbon textile properties of tow (uniaxial) reinforcement (C50k).

	Properties	Uni-directional, 50k
	Filament diameter, μm	7
	Number of filaments, k	50
	Fabric weight, g/m²	130
	Fabric spacing	-
	Tensile strength, f_f (Mpa)	4000
	Modulus, E_f (Mpa)	235000

3.3 Preliminary work

In order to cast a proper mixture that will be combined with textile reinforcement to produce TRC, trial mixes have been done to obtain the optimum mix which achieves the desire workability and cohesion.

3.3.1 Trial mixes

To obtain a reliable concrete mix, a number of trial mixes were cast in order to provide suitable penetration, workability, no bleeding, no segregation and consistency. Slump and the flow table tests were applied with reference to BS EN 12350-2 and BS EN 12350-5, respectively. There were two types of concrete mix cast; fine grained concrete used for the small scale beams (see section 3.4) and normal concrete used for large scale beams (see section 3.4). As there is no standard yet to follow in designing fine grained concrete which is compatible with textile reinforcement, the mix that was designed by SFB 532 at Aachen University in Germany (Brameshuber *et al.* 2006) (with some adjustment) was used. Table 3-11 shows the adjusted design of mix proportions of SFB 532 institute. The fine aggregate in SFB 532 was classified to two parts, one is from 0 to 0.125 mm and the second is from 0.2 to 0.6 mm, while, in this mixture the maximum fine aggregate size was 2.4 mm. The mixture was highly saturated, bleeding, sandy, segregated, and collapsed. The average compressive strength was 60 MPa. Therefore, the proportions percentage was adjusted to find a more suitable mixture. Table 3-12 shows the different mix proportions and their properties of fine concrete. It can be seen when the binder percentage was high, the mixture properties were not preferable (i.e. highly bleeding and segregated). However, at low percentage of binder, ~ 25%, the properties of the mixture was acceptable and the workability was good.

Table 3-11 Matrix compositions.

Cement, kg/m³	490
Fly ash, kg/m³	175
Silica fume, kg/m³	35
Total binder kg/m³	700
Super Plasticiser (1.50%), Litre	10.5
Sand, kg/m³	1215
w/c	0.40
Water, kg/m³	280
Total, kg/m³	2195

Table 3-13 shows the different mixes proportions and associated properties for normal concrete. The mixes were designed according to ACI 211.

3.4 Casting and curing

There were two groups of moulds cast; small scale beams with dimensions *100 mm x 100 mm x 500 mm* and large scale beams with dimensions *120 mm x 200 mm x 2600 mm*. The mix was cast up to the required cover of each studied beam. Then, the textile reinforcements were laid in the required layout for each beam. After that, the concrete mix was poured again until the top of the beam mould was reached.

After casting, the prisms were left covered by plastic for 24 hrs then de-moulded and moved to a curing room to complete 28 days at 20 ± 2 °C and 100% relative humidity.

Table 3-12 Properties of different mixes at preliminary stage of fine concrete.

Concrete Mixture	Type	Mix1 (kg/m ³)	Percentage %	Mix2 (kg/m ³)	Percentage %	Mix3 (kg/m ³)	Percentage %
Cement	OPC	600	75	250	69	265	73
Fly ash	EN 450	160	20	92	25	100	27
Silica fume	Grade 920-D	40	5	20	6	0	0
Total binder		800	37	362	23	365	23
SuperPlasticiser (SP), Litre	ViscoCrete 25 MP	(1%) 8		(0.8%) 2.9		(2%) 7.3	
Sand		1070	49	1040	65	1040	67
w/c ratio		0.38		0.53		0.42	
Water	Tap water	304	14	192	12	153	10
Total		2174	100	1594	100	1558	100
Flow table test(cm)		flowing		27		25	
Comment		* highly segregated * highly bleeding * sticky		* cohesive * consistency		* cohesive * consistency	
Compressive strength (MPa)		57		40		53	

Table 3-13 Properties of different mixes at preliminary stage of normal concrete.

Concrete Mixture	Type	Mix1 (kg/m ³)	Mix2 (kg/m ³)
Cement	OPC	504	504
CA 3/8"(10 mm)		1108	1108
Sand		683	683
water		159	177
w/c		0.32	0.35
SuperPlasticiser (SP), Litre	ViscoCrete 25 MP	(1.5%) 7.7	(1.5%) 7
Slump test (cm)		50	110
Comment		* not enough workability * stiff	* good workability * good consistency
Compressive strength (MPa)		95	94

3.5 Mechanical Testing

Various tests have been done to obtain the mechanical properties of this composite material including some related to textile reinforcement such as tensile test; some related to the concrete matrix such as compression test; and the rest related to the textile and concrete together as a composite such as pull-out test and flexural test.

3.5.1 Compression test

After 28 days of curing, compression tests were carried out to obtain the compressive strength of the concrete matrix. Three cubes ($100 \times 100 \times 100$

mm^3) of each mix were tested by ToniPACT 3000 testing machine in 3000 kN capacity. Figure 3-4 shows the compression test setup. The test was performed to comply with BS EN 12390.



Figure 3-4 Compression test setup.

3.5.2 Tensile test

The tensile behaviour of textile and steel reinforcement was measured. The tensile strength of textile is provided by the manufacturer (sec. 3.2.8.2), however, this strength represents one single filament. The tensile strength of a single filament is higher than that of multi-filaments (Gries *et al.* 2006). As the textile reinforcement is used in bundles, rovings or woven patterns, obtaining the tensile strength of the multi-filaments roving is necessary. Thus, ten samples of carbon tow were tested which the strands consisted of 50k of filaments.

The total length of the tested roving was 33.5 cm and the last 8 cm of each edge was encased in resin to form a grip that could be held in the jaws of the testing machine. Figure 3-5 shows the setup of how the sample was prepared.

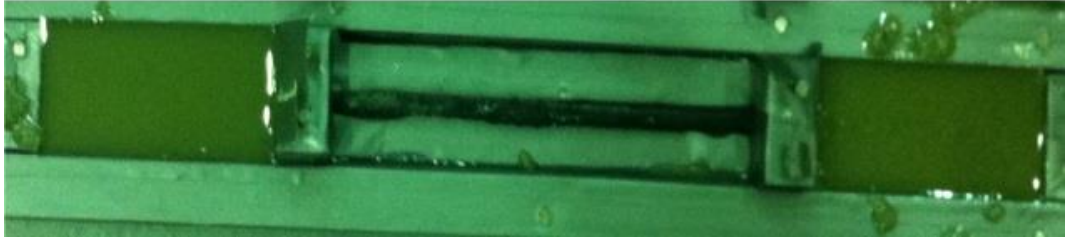


Figure 3-5 Textile roving preparation before test.

The rovings were tested on a tensile testing machine, (Instron –TVL) with 300 kN capacity, as it is shown in Figure 3-6. The clear distance between the two holders was 17.5 cm. The stroke rate was 1 mm/min.



Figure 3-6 The setup of tensile test of carbon roving.

Also, the tensile strength of steel reinforcement was obtained. The steel rebar was tested on a tensile testing machine (Instron 8500). The test was carried out to comply with BS 4449:2005. Figure 3-7 shows the tensile test setup of steel reinforcement.



Figure 3-7 Tensile test setup of steel rebar.

3.5.3 Pull out test

The pull-out test was carried out to investigate the bond properties between textile reinforcement and mixture. The total length of roving is *400 mm*, the both ends of roving were cast into a concrete mould embedded to a *50 mm*

depth. Figure 3-8 shows the set-up of the pull out test. The tests were performed on an Instron machine with loading rate at 1mm/min.

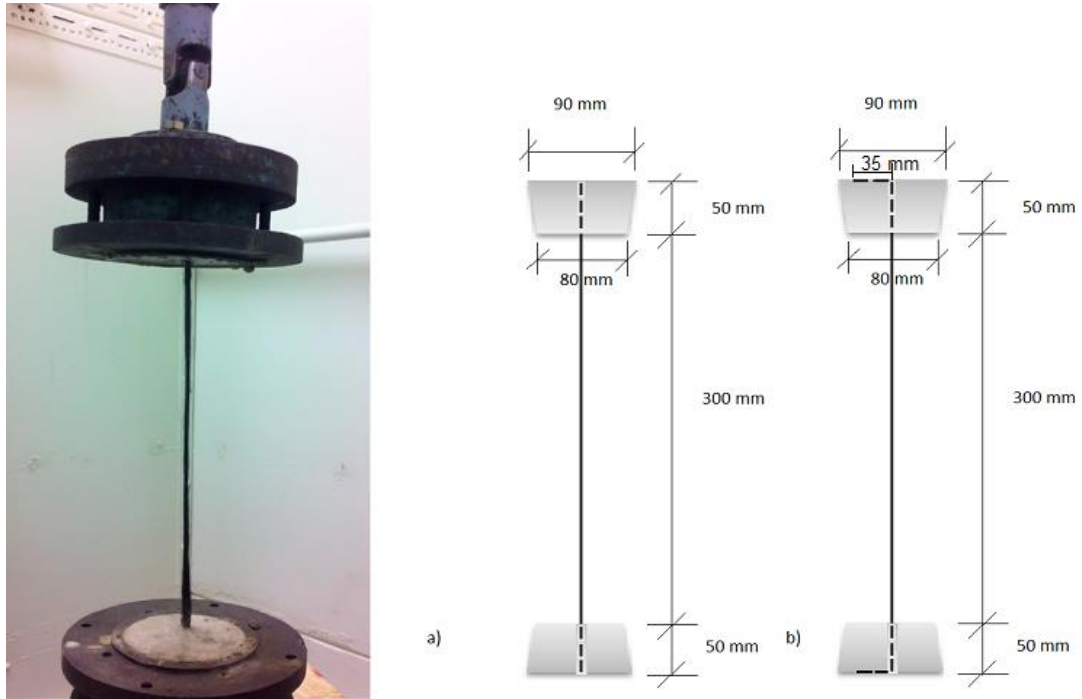


Figure 3-8 Pull-out test set-up a) straight edge b) anchored edge.

3.5.4 Flexural test

The main test in this study is the flexural test which measured the capacity of beam in terms of flexural strength and ductility. The behaviour and toughness of different reinforcement layouts in textile reinforced concrete beam were assessed. Four point bending tests were carried out to investigate the flexural properties of 76TRC beams. These beams are divided into two groups; first is small scale beams ($100 \times 100 \times 500 \text{ mm}^3$) and the second is large scale beams ($120 \times 200 \times 2600 \text{ mm}^3$). The number of small scale beams was 64 while the large beam group was 12 beams. An LVDT was installed at the middle of span at each beam to measure the deflection. A ToniPACT 3000 testing machine with 150 kN capacity performed the test at loading rate of 0.1 kN/sec (for small prisms) while for large scale beam hydraulic rams and custom loading frames were used at the same loading rate. Crack spacing

and crack width were measured for some beams. Figure 3-9 and Figure 3-10 show the four point bending test setup for small and large scale beams. A digital data acquisition system was connected to record the load versus deflection. The resolution of loading was 0.01 kN and 0.001 mm of deflection. In order to help spot the first crack, the two sides of the beams between the loading points were painted white. Also, between the two loading points, Demecs strain gauges were installed on both sides of selected beams to measure surface strain. The horizontal and vertical spacing between Demecs are shown in Figure 3-11. An Optical microscope was used to measure the crack width at the bottom of the concrete side. Figure 3-12 shows the Optical microscope device.

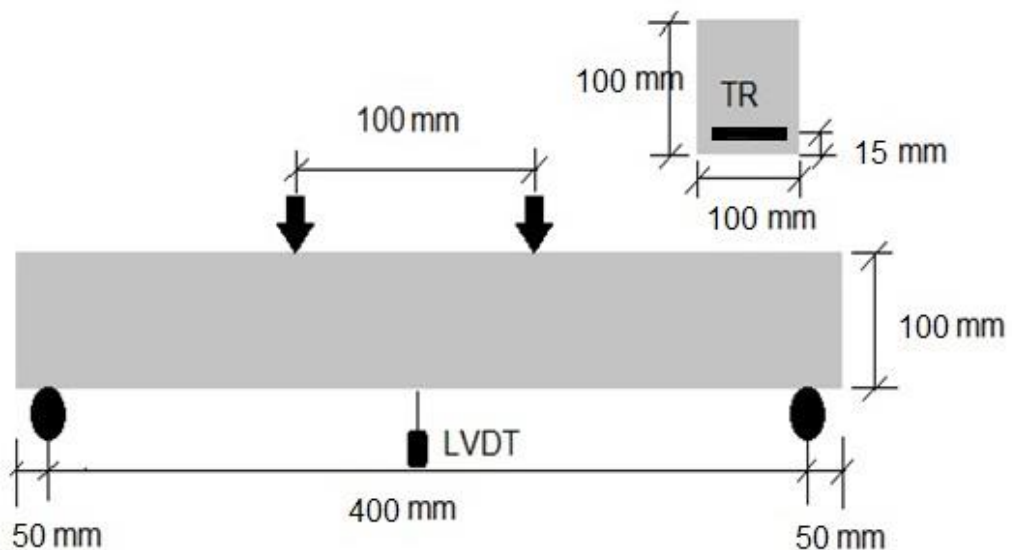


Figure 3-9 Set-up of four point bending test of small scale beam.

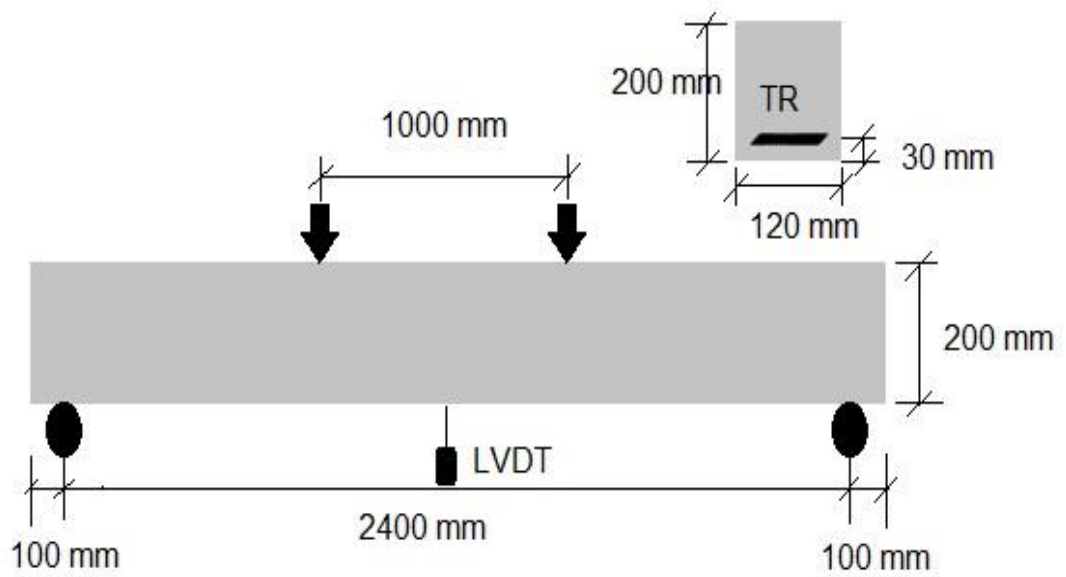


Figure 3-10 Experimental set-up of four point bending test of large scale beam.

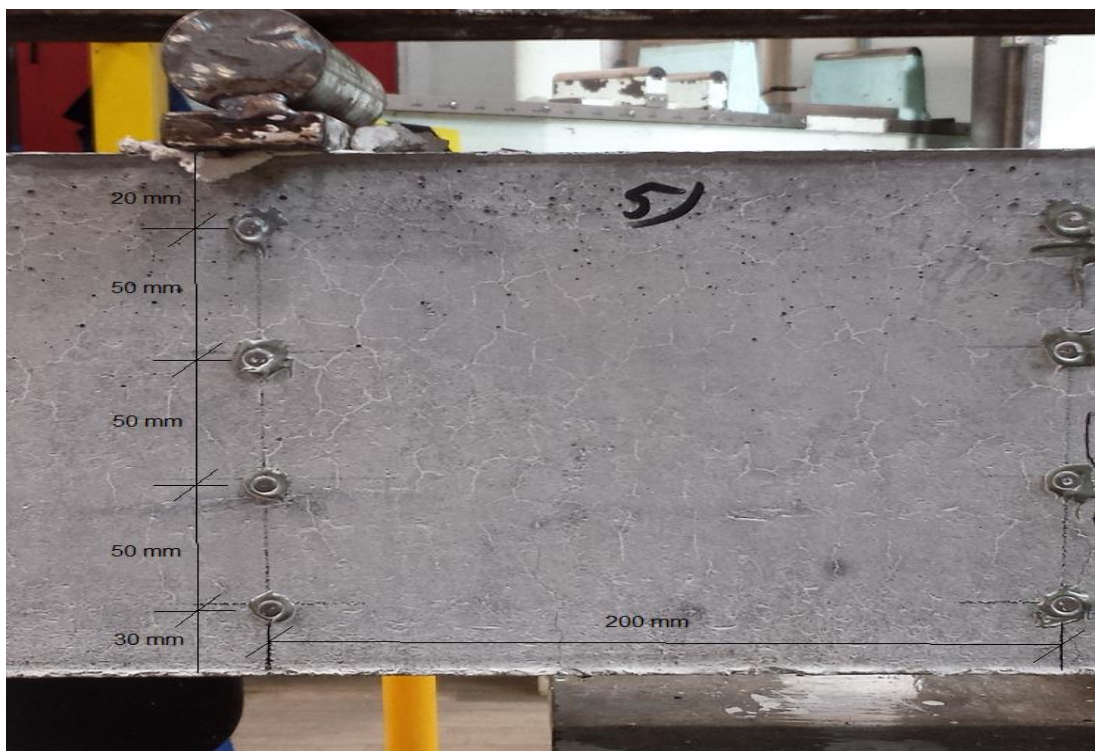


Figure 3-11 Demecs setup.

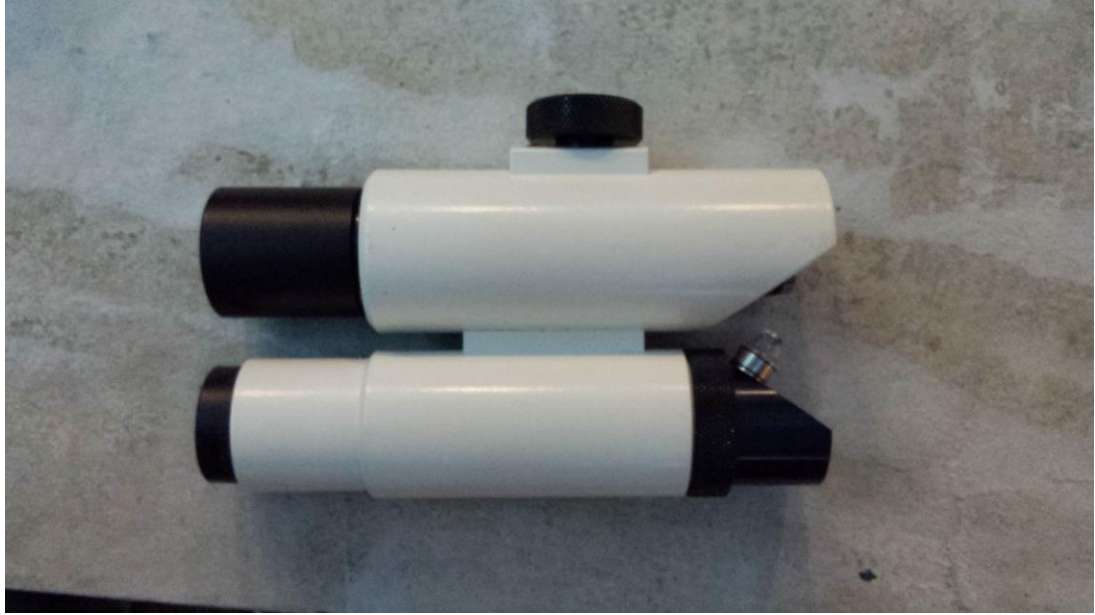


Figure 3-12 Optical microscope.

3.6 Experimental programme

To summarise the experimental work the charts in Figure 3-13 and Figure 3-14 help illustrate the programme. From the figures, it can be seen that the number of beams are 64 and 12 beams for small scale and large scale beams, respectively. The small scale beams were divided into five categories based on the type of reinforcement: woven fabric (two-dimensional/bi-axial direction), one dimensional direction (uni-axial direction), chopped fibre, plain concrete, and steel reinforcement (control). Each category was subdivided into a number of groups. Two identical beams were cast of each particular beam. Large beams were categorised into three groups based on the type of reinforcement. They are woven fabric (two-dimensional direction or bi-axial direction), one dimensional direction (uni-axial direction), and steel reinforcement (control). Crack spacing and crack width were measured in some of these large beams in order to have a fuller understanding of textile reinforced concrete behaviour.

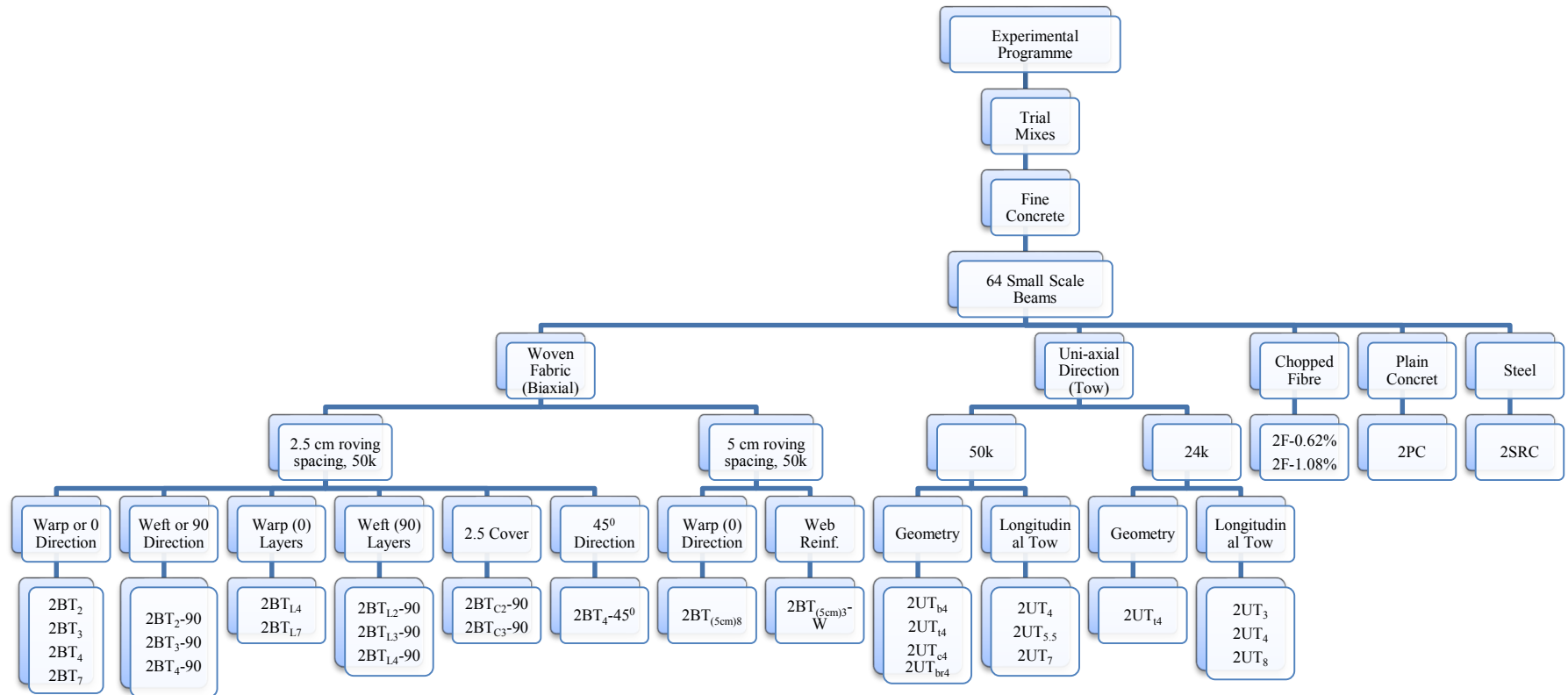


Figure 3-13 Experimental programme for small scale beams.

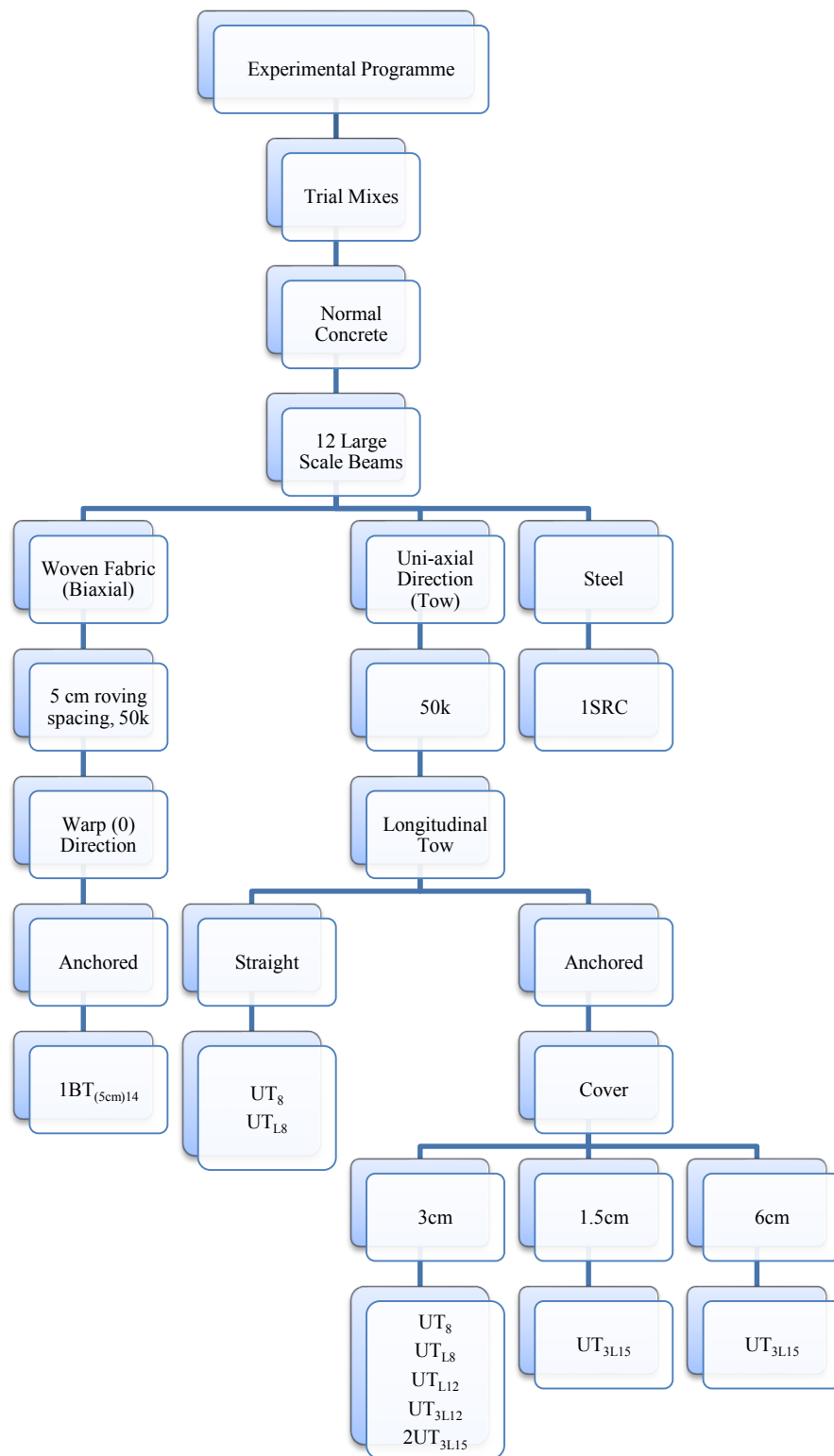


Figure 3-14 Experimental programme for large scale beams.

3.6.1 Notation

Before explaining the meaning of the notations used to describe the type and layouts of applied reinforcement, some words need to be defined:

Warp (0direction): a set of yarn in all woven fabrics is interwoven with weft. Normally, warp is put in loading direction, which is also called 0direction.

Weft (90) direction: in this study, it is a set of yarn interwoven with warp. Normally, weft is in a direction across with loading direction, which is also called 90direction.

T_n : stands for textile reinforcement, and n is the number of textile layers. The number of warps in each layer should be considered 4 in all beams and the spacing between warps is *2.5 cm* unless detailed otherwise. Figure 3-15 shows the default of reinforcement details for small scale beams.

3.6.1.1 Small scale beams

3.6.1.1.1 Biaxial textile

It is a woven fabric and there were two different layouts used, one is *2.5 cm* and the second is *5 cm* the spacing between warps. The majority of beams were casted by using *2.5 cm* as reinforcement.

Biaxial textile at *2.5 cm* was divided into 6 groups based on the layouts of reinforcement:

- Warp (0 direction)

BT_2 , BT_3 , BT_4 , and BT_7 stands for 2, 3, 4, and 7 layers of fabric over each other, respectively, in warp direction of bi-directional textile (woven fabric) which means the warpsroving is resisting the load, see Figure 3-15a.

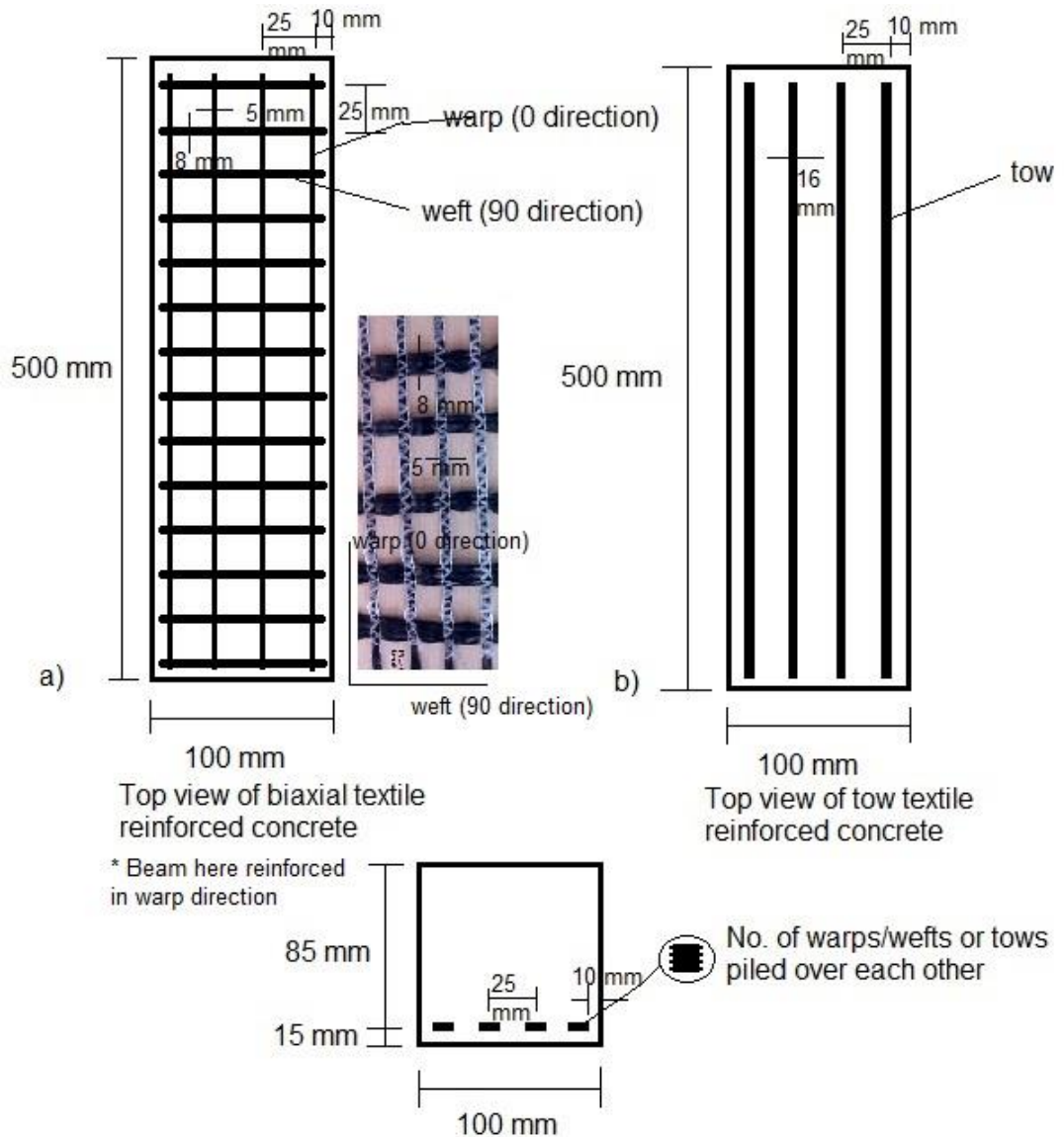


Figure 3-15 Basic reinforcement details of small scale beam; a) biaxial textile reinforced concrete. b) tow textile reinforced concrete.

- Weft (90° direction)

BT₂-90, BT₃-90, and BT₄-90 stands for 2, 3, and 4 layers of fabric over each other, respectively, in weft direction of bi-directional textile (woven fabric). The beams here were reinforced in weft direction which means the applied load will be resisted by wefts rovings while the warps fibre is perpendicular on the loading direction, see Figure 3-16.

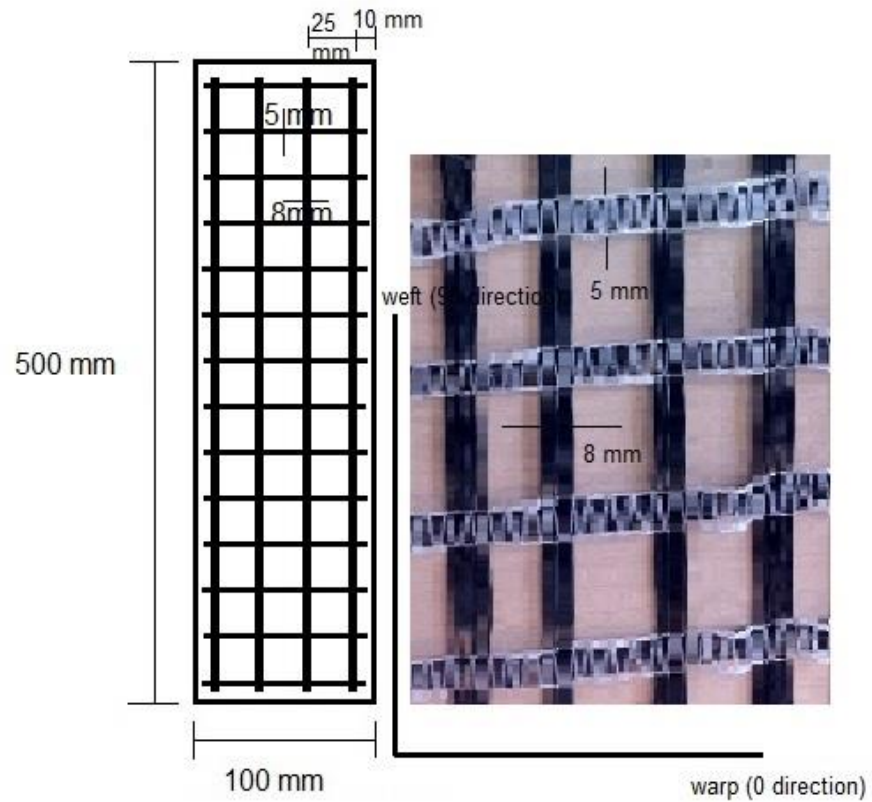


Figure 3-16 Top view of weft direction of textile reinforced concrete.

- Warp (0°) in layers

BT_{L4}, and BT_{L7} stands for 4 and 7 layers of fabric and are divided into two separated layers with 15 mm spacing. Each layer has the half of whole textile reinforcement number (for example $4/2=2$ biaxial textile/layer), see Figure 3-17.

- Weft (90°) in layers

BT_{L2-90}, BT_{L3-90}, and BT_{L4-90} stands for 2, 3 and 4 layers of fabric and are divided into two layers with 15 mm spacing. Each layer has the half of whole textile reinforcement number (for example 4 layers of fabric/2 layers=2 textile in weft direction/layer). Figure 3-17 shows the two layers locations.

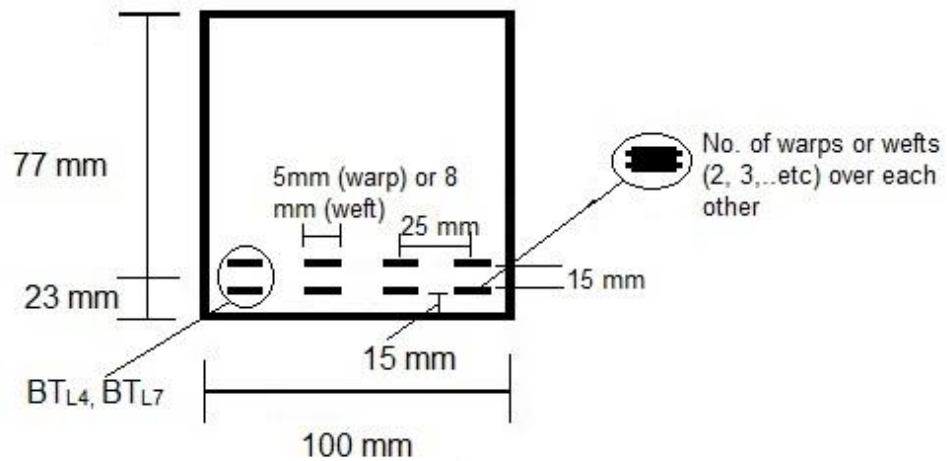


Figure 3-17 Biaxial textile reinforcement reinforced concrete in two separated layers of warp or weft direction.

- 2.5 cm cover

BT_{C2-90} and BT_{C3-90} stands for 2 and 3 layers of fabric over each other, respectively, in weft direction of bi-directional textile (woven fabric) and the cover thickness is 25 mm. Figure 3-18 shows the concrete cover 25 mm.

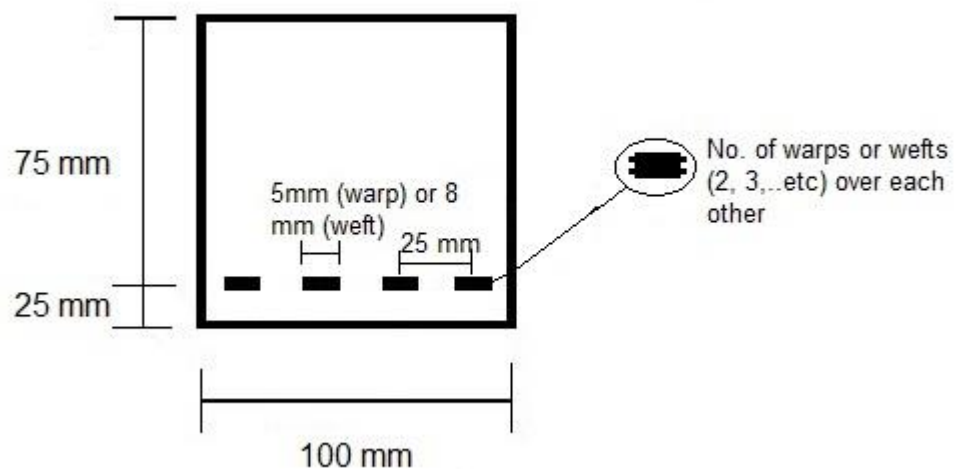


Figure 3-18 25 mm cover thickness.

- 45° direction

BT_{4-45°} stands for 4 layers of fabric over each other and orientated at 45° direction of bi-directional textile (woven fabric).

Biaxial textile (woven fabric) at 5 cm was divided into 2 groups:

- Warp (0°) direction

BT_{(5cm)8} stands for 8 layers of fabric over each other with 5 cm spacing between warps. The textile laid down in warp direction of bi-directional textile (woven fabric). The number of warps in each layer here is 2. Figure 3-19 shows textile with 5 cm warps spacing reinforced concrete.

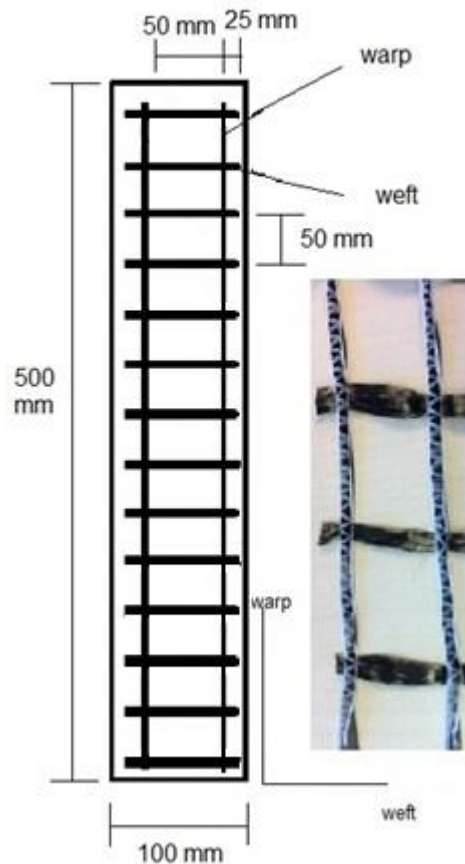


Figure 3-19 Top view of 5 cm woven fabric of textile reinforced concrete.

- Web reinforced beam

BT_{(5cm)3-W} stands for 3 layers of fabric over each other with 5 cm spacing between warps. The textile laid down in warp direction of bi-directional textile (woven fabric). The beams here were reinforced in the vertical side (shear reinforcement). Figure 3-20 shows the textile reinforcement were used in vertical sides.

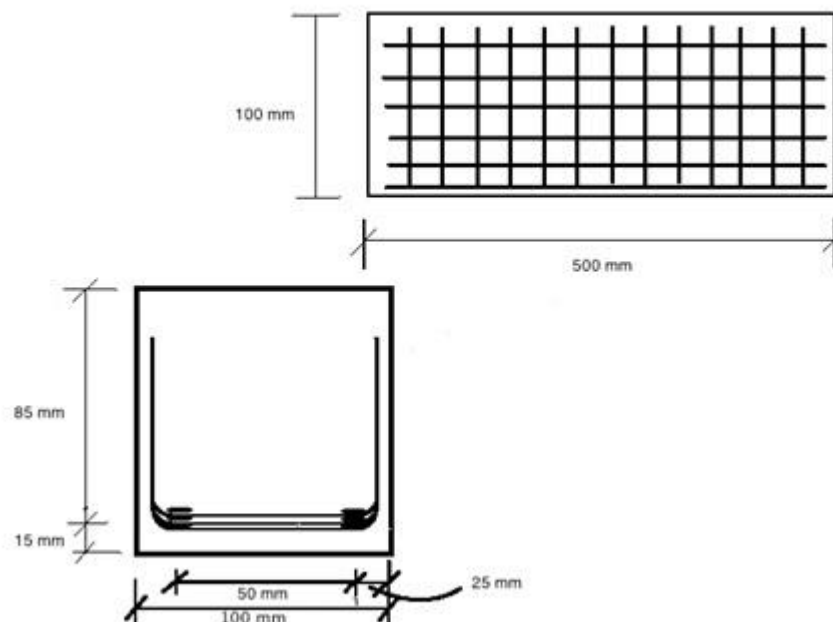


Figure 3-20 Cross section and side view of web reinforcement.

3.6.1.1.2 Tow textile (uni-axial textile)

There were two types of tow textile (uni-axial textile reinforcement) used. First is with 50k filaments (50 thousands of filaments) in one tow, and the second is with 24k filaments in one tow. The number of tows in each layer is 4 with spacing between tows is ~ 2.5 cm in each layer, see Figure 3-15b.

Uni-axial reinforcement with 50k divided into 2 groups:

- Geometry

UT_{b4}, UT_{t4}, UT_{c4}, and UT_{br4} stands for 4 layers of tows bundled, twisted, crimped and braided textile, respectively, and piled over each other in uni-axial direction (one dimensional textile reinforcement). Figure 3-21 shows different geometry layout of tows.



Figure 3-21 Different patterns of tows.

- Longitudinal tows

UT₄, UT_{5.5}, and UT₇ stands for 4, 5.5, and 7 layers of tows, respectively, piled over each other and simply laid down straight in uni-axial direction (one dimensional textile reinforcement), see Figure 3-22.



Figure 3-22 Longitudinal tows reinforced concrete beam.

Uni-axial reinforcement with $24k$ divided into 2 groups:

- Geometry

UT_{t4} stands for 4 layers of tows twisted and piled over each other in uni-axial direction (one dimensional textile reinforcement).

- Longitudinal tows

UT_3 , UT_4 , and UT_8 stands for 3, 4, and 8 layers of tows, respectively, piled over each other and simply laid down straight in uni-axial direction (one dimensional textile reinforcement).

3.6.1.1.3 Chopped fibre

Short carbon fibres with length $4-5\text{ cm}$ in order to reinforce concrete beams.

F-0.62% and F-1.08% stands for 0.62% and 1.08% fibre volume fraction of short fibres reinforced beams, respectively.

3.6.1.1.4 Plain concrete

The concrete beam was not reinforced, only concrete.

PC stands for unreinforced concrete beam.

3.6.1.1.5 Steel

Beams here reinforced with one $\varnothing 8$ bar steel reinforcement. This quantity of reinforcement area was chosen in order to experimentally compare the load-deflection behaviour of steel reinforced concrete beam with the textile reinforced concrete beam at the same area and also at the different areas. In addition to that TRC beam moment capacity and cracks behaviour compared with SRC beam

SRC stands for steel reinforced concrete beam.

3.6.1.2 Large scale beams

For large scale beams, the same idea was used to describe samples. However, the number of warps (in biaxial textile) is 3 while in tows textile (in uni-axial textile) in each layer was varied between 3 and 4, and the cover spacing is 3 cm otherwise, it will be mentioned. Figure 3-23 shows the default of reinforcement details of large scale beam.

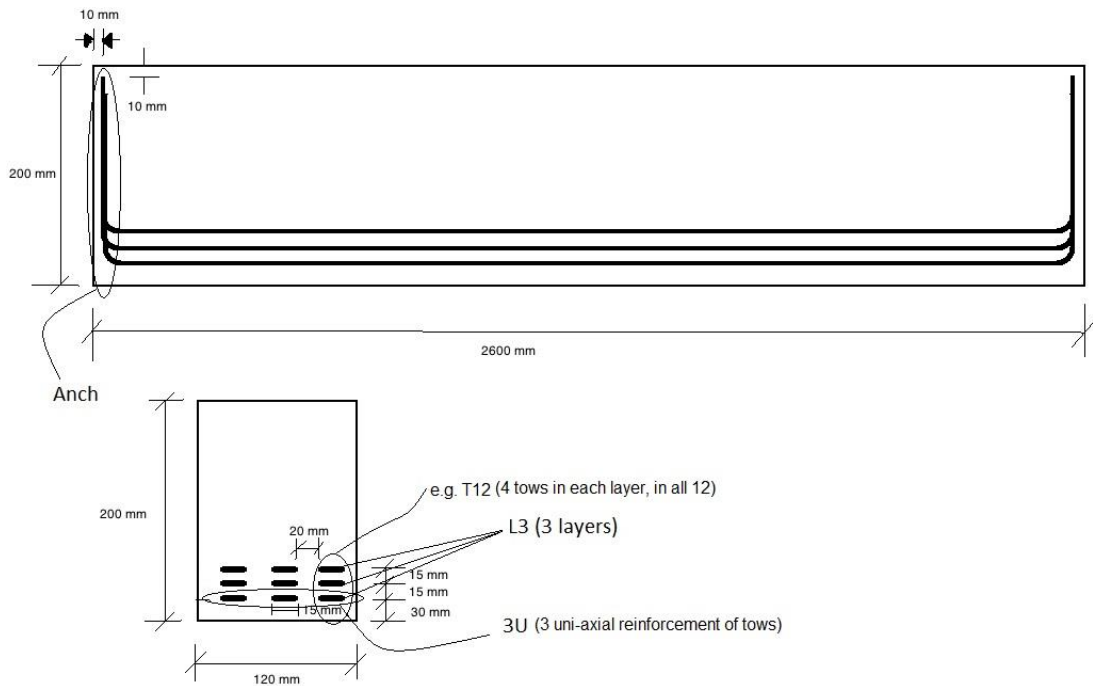


Figure 3-23 Beam reinforcement detail of large scale beam.

3.6.1.2.1 Woven fabric

There was one layout used which was 5 cm the spacing between warps. In each layer, the number of warps is 3.

- Warp (0^0) direction

BT_(5cm)14-Anch-2.6 stands for 14 layers of fabric over each other with 5 cm spacing between warps. The textile laid down in warp direction of bi-directional textile (woven fabric), see Figure 3-24. The reinforcement was anchored before 10 mm from the both ends of 2.6 m beam. It is done by tying the anchored textile to the crossed bar placed on the top of mould to hold the reinforcement. This can be considered an advantage of textile reinforcement due to the simplicity and easiness of forming the textile inside the mould.

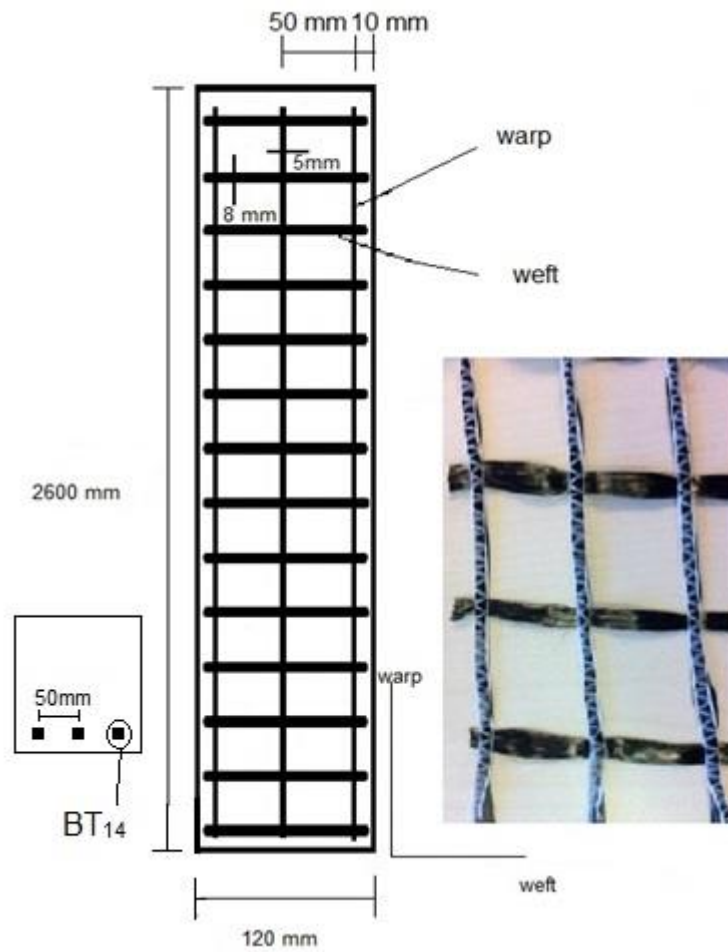


Figure 3-24 Top view of biaxial textile reinforced concrete beam.

3.6.1.2.2 Tow textile (Uni-axial direction)

There was one type of tow textile (uni-axial textile reinforcement) used which was *50k*. However, the end of reinforcement was kept straight or anchored. Moreover, all the reinforcement was divided into 3 layers (for example 15 tows/3 layers = 5 tows/layer) and the horizontal spacing between tows in each layer tried to be kept *2 cm*, otherwise, it will be mentioned.

- Straight end

4UT₈-S-2.6 stands for 8 tows piled over each other. The number of uni-axial reinforcement in each layer was 4 (4U) and the reinforcement edge was straight (S) at the both ends of 2.6 m beam, see Figure 3-25a.

4UT₈-S-L-2.6 stands for 8 tows divided into 2 layers (L). The number of uni-axial reinforcement in each layer was 4 (4U) and the reinforcement edge was straight (S) at the both ends of 2.6 m beam, see Figure 3-25b.

- Anchored

4UT_{8 or 12}-Anch-2.6 stands for 8 or 12 tows piled over each other. The number of uni-axial reinforcement in each layer was 4 (4U) and the reinforcement edge was anchored (Anch) at the both ends of 2.6 m beam. It is similar to Figure 3-25a apart from the edge is here anchored.

4UT₈-Anch-L-2.6 stands for 8 tows divided into 2 layers (L). The number of uni-axial reinforcement in each layer was 4 (4U) and the reinforcement edge was anchored (Anch) at the both ends of 2.6 m beam. It is similar to Figure 3-25b apart from the edge is here anchored.

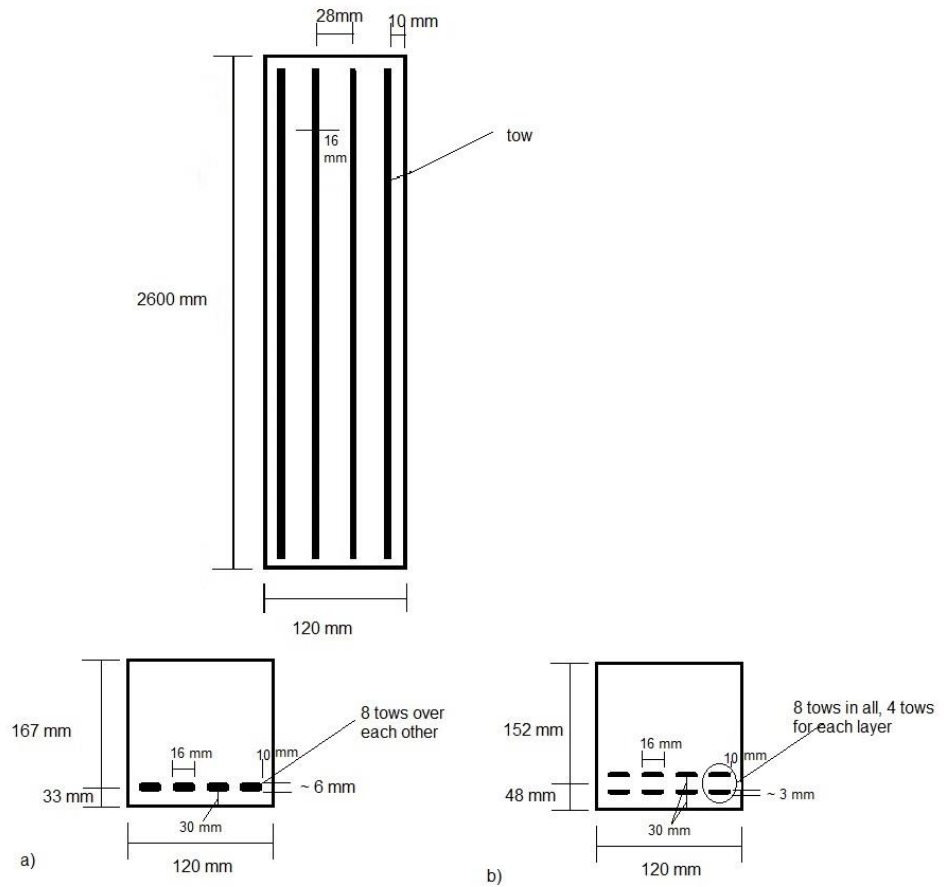


Figure 3-25 Uniaxial textile reinforcement; a) 4UT₈-S-2.6, b) 4UT₈-S-L-2.6.

3UT₁₂ or 15-Anch-L₃-2.6 stands for 12 or 15 tows divided into 3 layers (L₃). The number of uni-axial reinforcement in each layer was 3 (3U) and the reinforcement edge was anchored (Anch) at the both ends of 2.6 m beam, see Figure 3-26a.

- Cover (1.5 cm and 6 cm)

3UT₁₅-Anch-L₃-2.6-C₁₅ or 60 stands for 12 or 15 tows divided into 3 layers (L₃). The number of uni-axial reinforcement in each layer was 3 (3U) and the reinforcement edge was anchored (Anch) at the both ends of 2.6 m beam. The cover thickness was 15 mm (see Figure 3-26b) or 60 mm.

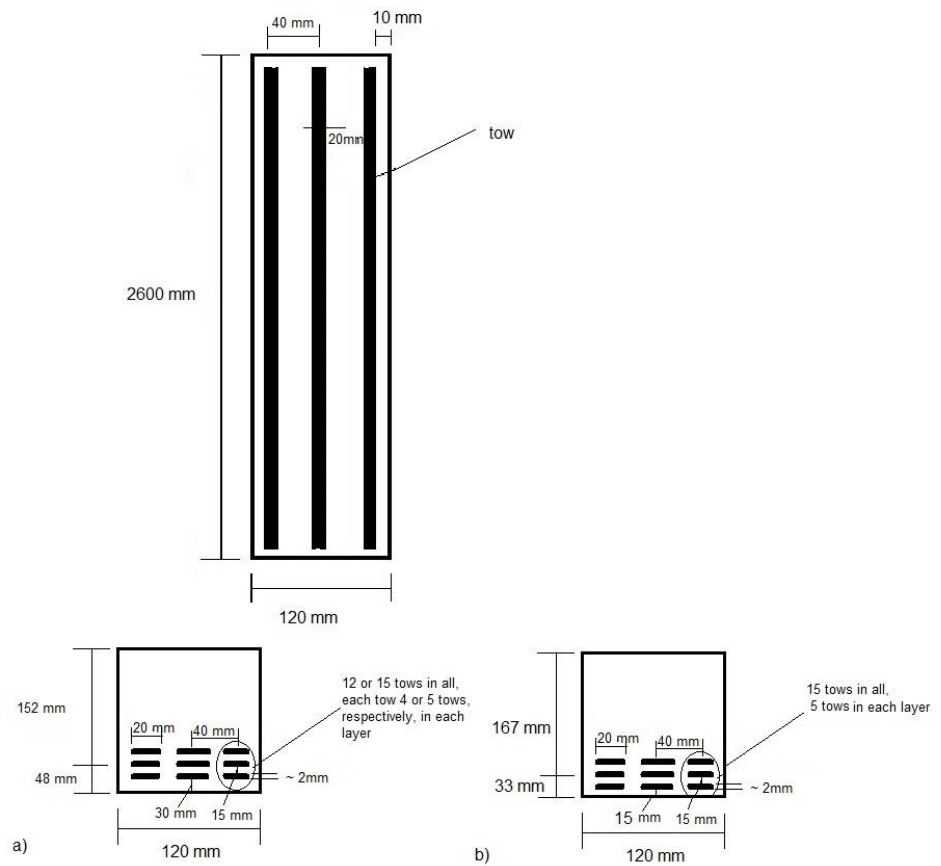


Figure 3-26 Uniaxial textile reinforced concrete at different layouts; a) 3UT₁₂ or 15-Anch-L₃-2.6, b) 3UT₁₅-Anch-L₃-2.6-C₁₅

3.6.1.2.3 Steel

Beam here reinforced with steel reinforcement. Figure 3-27 demonstrates the steel reinforcement details.

SRC stands for steel reinforced concrete beam.

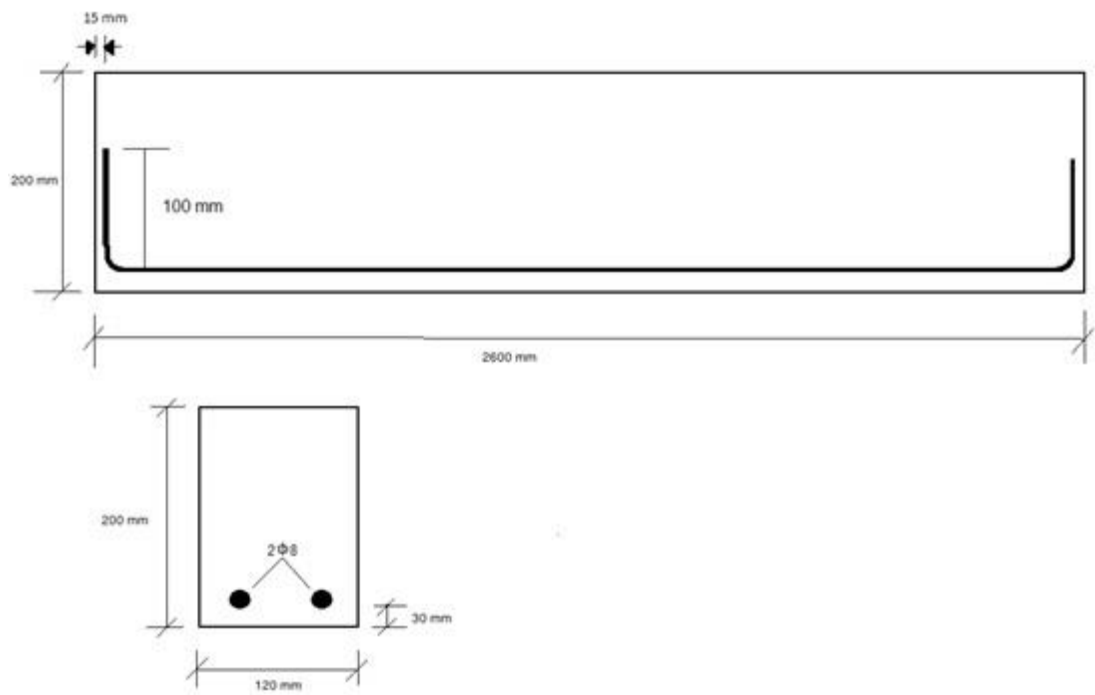


Figure 3-27 Steel reinforcement details.

CHAPTER 4

RESULTS

4.1 Introduction

In this chapter, the whole of the experimental results are presented. The following sections show: the results of tensile tests at variety of textile layouts; pull out tests of rovings; four point bending test of carbon textile reinforced concrete beams; plain concrete; and steel reinforced concrete.

4.2 Tensile testing of reinforcement

Tensile test was conducted in order to obtain the tensile behaviour of carbon roving and steel rebar. The average of ultimate tensile strength of carbon roving (f_{fu}) was 1550 MPa with standard deviation 60 MPa while the average of ultimate tensile strain (ϵ_{fu}) was 0.02 . It is apparent that all the tensile strength result is lower than single filament strength as reported by the manufacturer (4000 MPa). This findings is in agreement with results of (Hegger *et al.* 2006c) which showed the same conclusion. Therefore, the tensile strength of single filament must not be used to represent the textile strength in composite. The reduction in the tensile strength of multi-filaments in compare with single filament can be accounted for the eccentric loading which caused part of filaments were stressed or elongated more than other filaments, therefore, immature failure occurred. Figure 4-1 shows the tensile stress-strain behaviour of carbon roving consisted of $50k$ filaments. It can be seen that the behaviour is elastic up to the failure and unlike steel reinforcement there is no yield plateau. Figure 4-2 shows the tensile stress-strain behaviour of 8 mm steel rebar. It can be seen that the behaviour is elastic until the yield strength (f_y) of 8 mm steel rebar at 520 MPa and yield strain (ϵ_y) 0.00255 . Then, it is exhibited high deformation at nearly the same load.

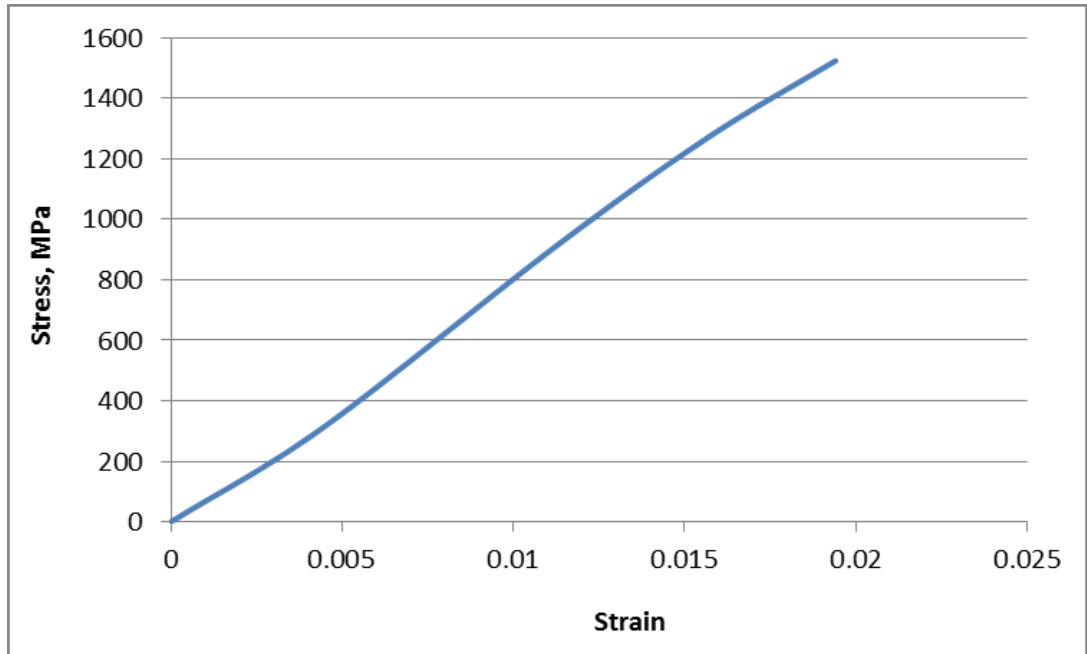


Figure 4-1 Tensile stress-strain behaviour of carbon tow, 50k.

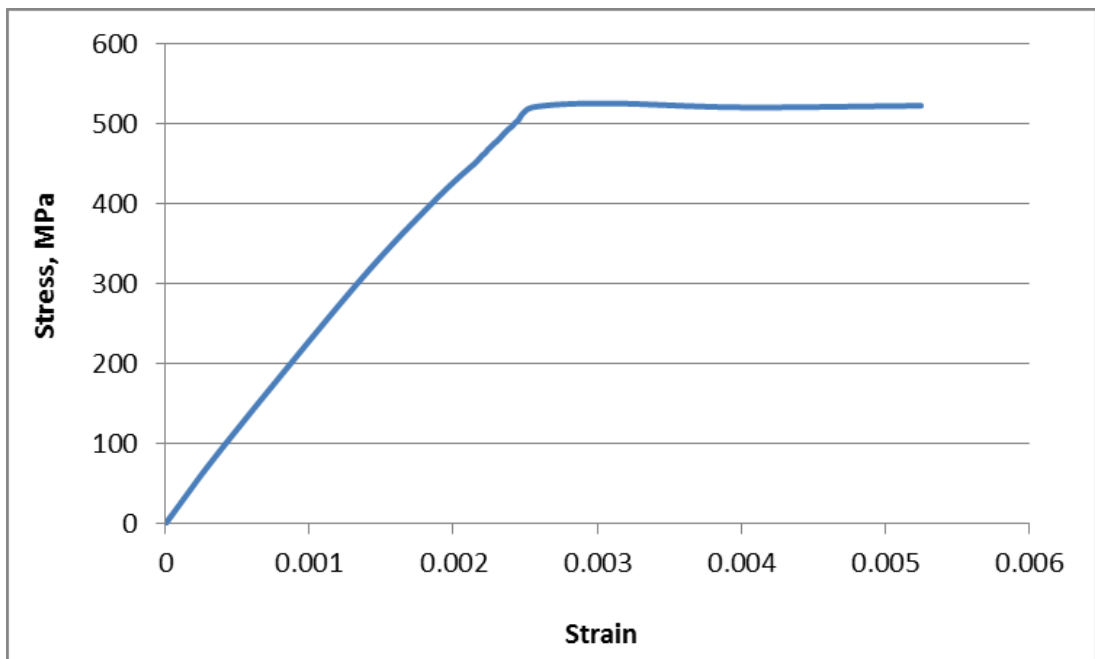


Figure 4-2 Tensile stress-strain behaviour of 8 mm steel rebar.

4.3 Pull out test

Textile pull out testing was tried to be carried out in comply with BS EN 10080:2005. Pull out test was conducted on two different layouts. First one, the tow at the edge was straight, while, the second is the edge of tow is anchored, Figure 3.8. The average pull out strength of three samples of straight tow is 0.08 kN Therefore, the bond strength (τ) can be calculated from this equation:

$$\tau = \frac{P}{2\pi rl} \quad 2.1$$

It is assumed that the multifilament bundle is a single reinforcing unit with no voids between filaments, thus, the diameter is the whole bundle (Peled, Zaguri and Marom 2008). Therefore, in order to determine the equivalent tow radius, the tow's area is calculated:

The tow's thickness is 0.5 mm and the width is 16 mm , thus, the area is 8 mm^2 . From this area, the equivalent circle radius is computed which is 1.6 mm . Thus, the bond strength of straight edge tow is 0.16 MPa (l is 50 mm). In order to increase the pull out strength the anchored edge tow is applied, therefore, the pull out strength improved to 0.80 kN (l is 85 mm), see section 3.5.3.

However, measuring the exact pull out strength was difficult due to many reasons. First the carbon textile surface is slippery which makes it impossible to hold it in the normal jaw. The carbon filaments slipped at the grab location during the loading which resulted in false readings. Second, the carbon textile is sensitive to any change in the test setup such as textile verticality during the test. Therefore, an adjustment made to the test setup to help to hold the textile during the test. Both ends of a carbon roving were cast in concrete to provide edges that could be held by the jaw. However, while the machine was pulling the carbon roving, the inner filaments were easily slipped in case of straight edge, while at the anchored edge the inner filaments slipped as well but at

higher pull out strength. However, it can be said it is better to have only one side is embedded while the other side is gripped tightly by epoxy or special jaw. This helps to measure the pull out strength more accurately because of pull out of textile and the slip of inner filaments will be from one side instead of two sides, therefore, the behaviour could be measured more accurately. From the results, the bond strength result is 0.16 MPa and when textile anchored at the bottom of concrete the strength is needed to pull out the inner filaments increased to 0.94 MPa .

4.4 Four point bending test

Four point bending was carried out to test seventy six beams with different reinforcement layouts, geometries, numbers of filaments, and beam sizes in order to investigate the flexural behaviour of TRC such as load-deflection behaviour, failure mode, crack spacing, and crack width. The following sections present the results of two different categories; first, small scale beams and secondly, large scale beams. Each category is classified into groups as described in ([sections 3.6.1.1](#) and [3.6.1.2](#)).

4.4.1 Small scale beams

The dimensions of the beams in this category are $100 \times 100 \times 500$, all the dimensions in *mm*. All the codes and reinforcement details are explained in the experimental programme chapter ([section 3.6.1](#)). The groups are classified based on the type of reinforcement; woven fabric, uni-axial reinforcement, chopped fibre, plain concrete, and steel. Some of these groups are also divided into subgroups.

4.4.1.1 Plain concrete

The beams in this group were not reinforced in order to obtain some of the concrete properties. Table 4.1 presents the results of plain concrete tested by four point bending. From the table, the average cracking load (which is the ultimate load of non-reinforced concrete) is at 12.9 kN and the average

ultimate deflection of this non-reinforced concrete is 0.19 mm . Figure 4-3 shows the unreinforced concrete behaviour.

Table 4.1 The results of plain concrete.

Reinforcement	Ultimate Load, kN		Average	Deflection, mm		Average	Failure Mode
	Sample1	Sample 2		Sample1	Sample2		
Concrete	13.3	12.6	12.9	0.2	0.19	0.19	Brittle

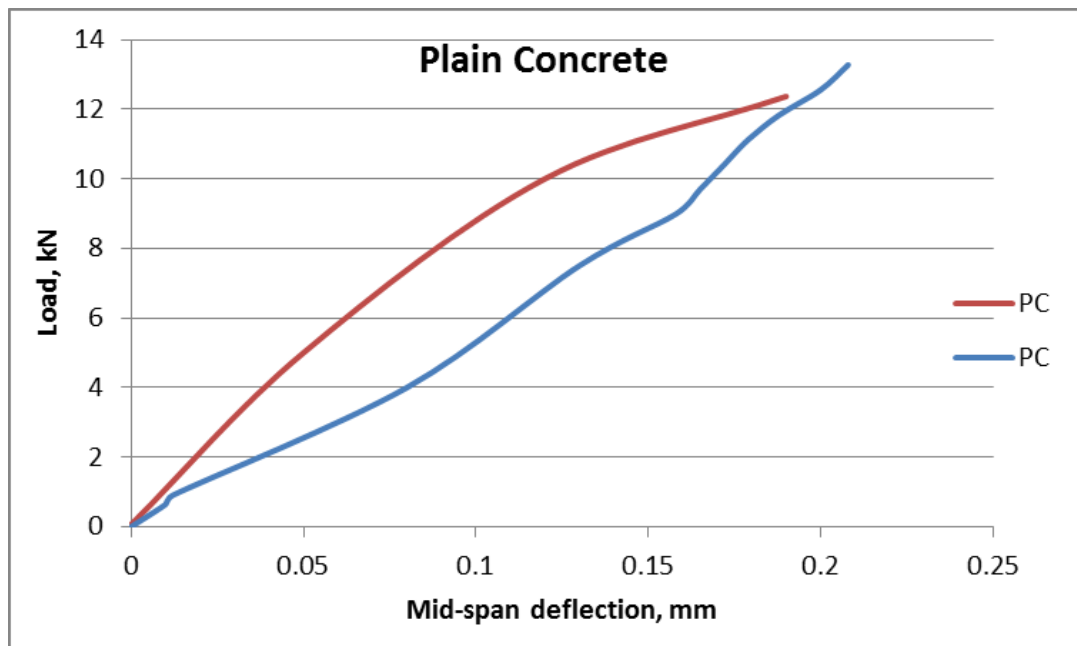


Figure 4-3 Load-Deflection behaviour at mid-span of plain concrete beam.

4.4.1.2 Biaxial textile (woven fabric)

Two types of fabrics were used; the same number of filaments per roving but the warps spacing is different. First is with *2.5 cm* warps spacing and the second is with *5 cm* spacing. Table 4.2 presents the results of beams reinforced by variety lay outs of *2.5 cm* woven fabric. Table 4.3 presents the results of beams reinforced by variety lay outs of *5 cm* woven fabric. As Table 4.3 shows the increase of the textile reinforcement quantity leads to an improve in the beam capacity in terms of flexural strength and deflection. Figure 4-4 shows the behaviour of different numbers of *2.5 cm* woven fabric at warp direction reinforced concrete beams at different volume of fraction (%). Figure 4-5 demonstrates the cracks pattern of BT_{7,50k}. Figure 4-6 to Figure 4-18 shows the behaviour and cracks patterns of different geometries and lay outs of woven fabric. The further discussion about the effect of different parameters will be investigated in the next chapter (Chapter 5).

Table 4.2 The results of 2.5 cm textile reinforced concrete beams at different lay outs.

	Reinforcement	Effective Area, mm ²	V _f , %	Ultimate Load, kN		Average	Deflection, mm		Average
				Sample1	Sample2		Sample1	Sample2	
Warp or 0 Direction	BT₂, 50k	15.4	0.37	14.2	14.2	14.2	0.18	0.17	0.18
	BT₃, 50k	23.1	0.46	15.14	15.2	15.2	0.22	0.25	0.24
	BT₄, 50k	30.8	0.62	26.0	23.15	24.6	1.6	2.0	1.8
	BT₇, 50k	53.9	1.08	31.31	28.1	29.7	1.9	3.1	2.6
Weft or 90 Direction	BT₂-90, 50k	15.4	0.29	16.73	14.0	15.4	0.6	1.0	0.8
	BT₃-90, 50k	23.1	0.46	18.6	15.0	16.9	0.96	0.17	0.6
	BT₄-90, 50k	30.8	0.62	23.5	24.6	24.0	1.4	1.64	1.5
Warp (0) Layers	BT₄-L, 50k	30.8	0.62	24.2	24.2	24.2	3.2	3.3	3.25
	BT₇-L, 50k	53.9	1.08	21.1	23.2	22.2	2.0	2.0	2.0

Table 4.2 Continued

	Reinforcement	Effective Area, mm ²	V _f , %	Ultimate Load, kN		Average	Deflection, mm		Average
				Sample1	Sample2		Sample1	Sample2	
Weft (90) Layers	BT ₂ -90-L, 50k	15.4	0.29	13.6	14.1	13.85	0.52	0.5	0.51
	BT ₃ -90-L, 50k	23.1	0.46	22.5	26.2	24.35	1.2	1.8	1.5
	BT ₄ -90-L, 50k	30.8	0.62	34.4	32.7	33.5	2.1	1.8	2.0
2.5 Cover	BT ₂ -90-C, 50k	15.4	0.29	13.6	15.1	14.4	0.13	0.15	0.14
	BT ₃ -90-C, 50k	23.1	0.46	14.01	18.55	16.3	1.8	1.8	1.8
45 Direction	BT ₄ -+45/-45, 50k	-	0.74	16.0	14.7	15.3	0.22	0.23	0.23

Table 4.3 The results of 5 cm textile reinforced concrete beams at different lay outs.

	Reinforcement	Effective Area, mm ²	V _f , %	Ultimate Load, kN		Average	Deflection, mm		Average
				Sample1	Sample2		Sample1	Sample2	
Warp or 0 Direction	BT _{(5cm)8} , 50k	30.8	0.62	20.8	15.72	18.3	3.9	4.5	4.2
Web Reinforcement	BT _{(5cm)3-W} , 50k	11.5	0.46	14.44	13.8	14.1	2.8	2.9	2.85

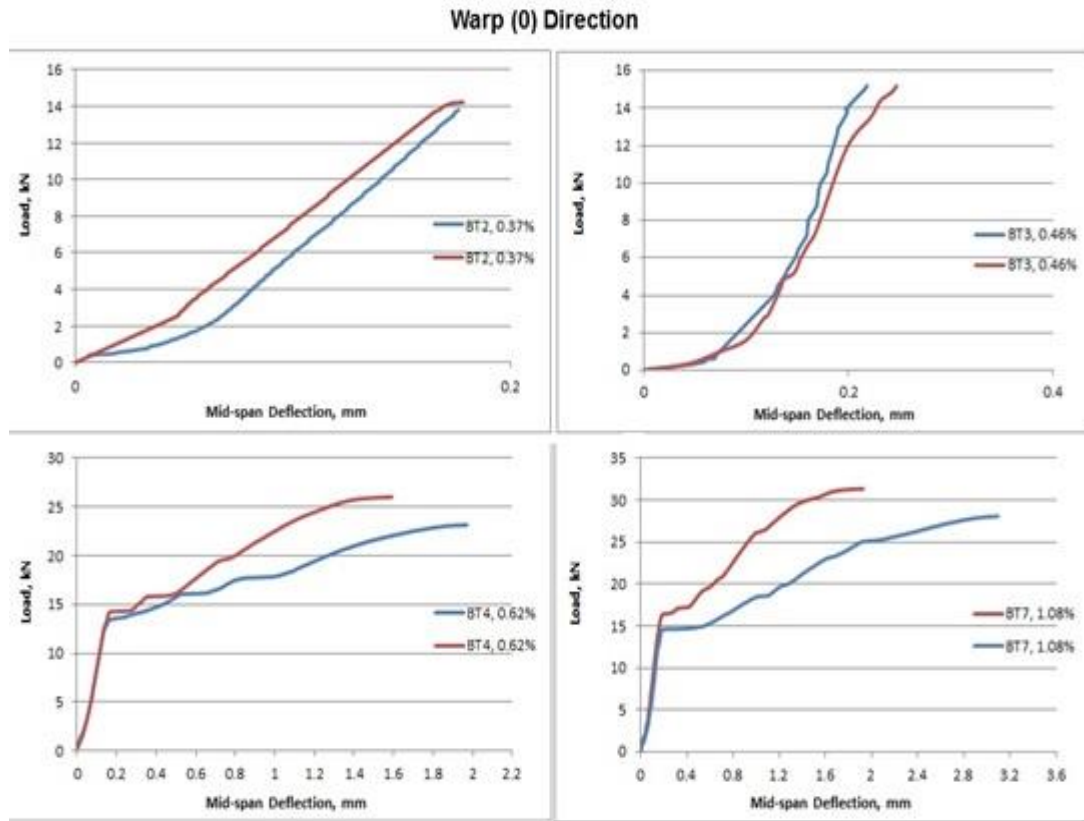


Figure 4-4 Load-Deflection behaviour at mid-span of woven fabric (2.5 cm) at warp direction reinforced beams.



Figure 4-5 Cracks pattern of beam reinforced by BT₇,50k.

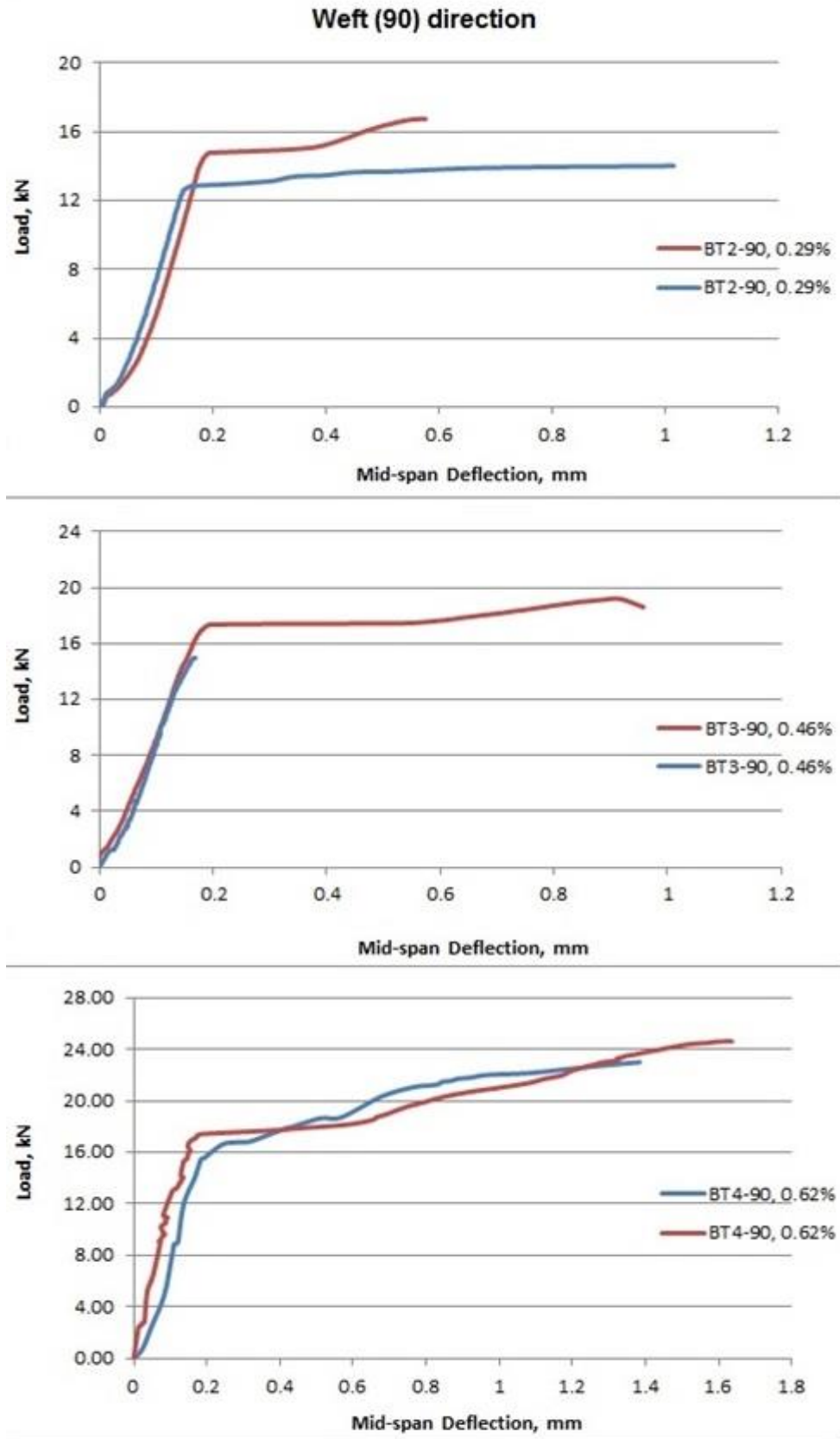


Figure 4-6 Load-Deflection behaviour at mid-span of woven fabric (2.5 cm) at weft direction reinforced beams.



Figure 4-7 Cracks pattern of beam reinforced by BT₄-90,50k.

Layering warp (0) direction

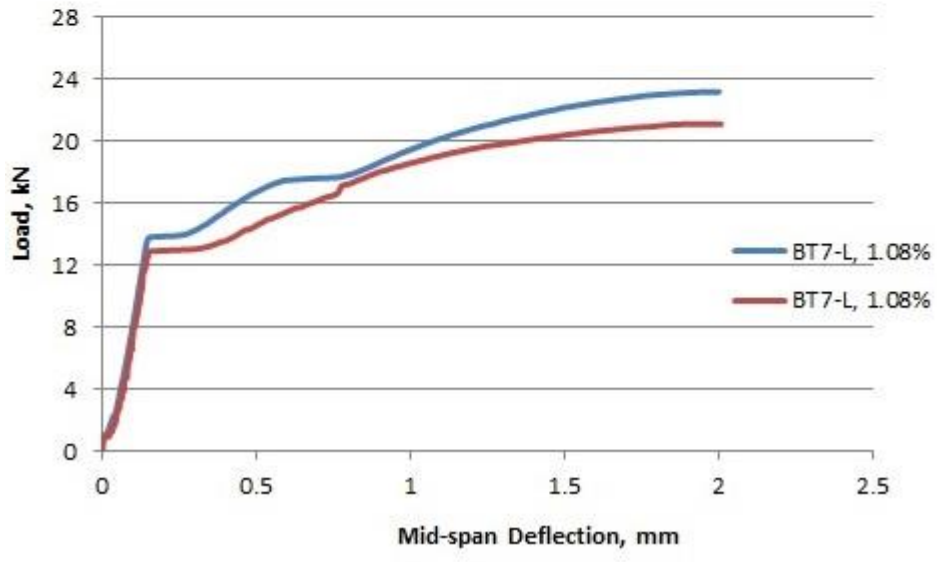
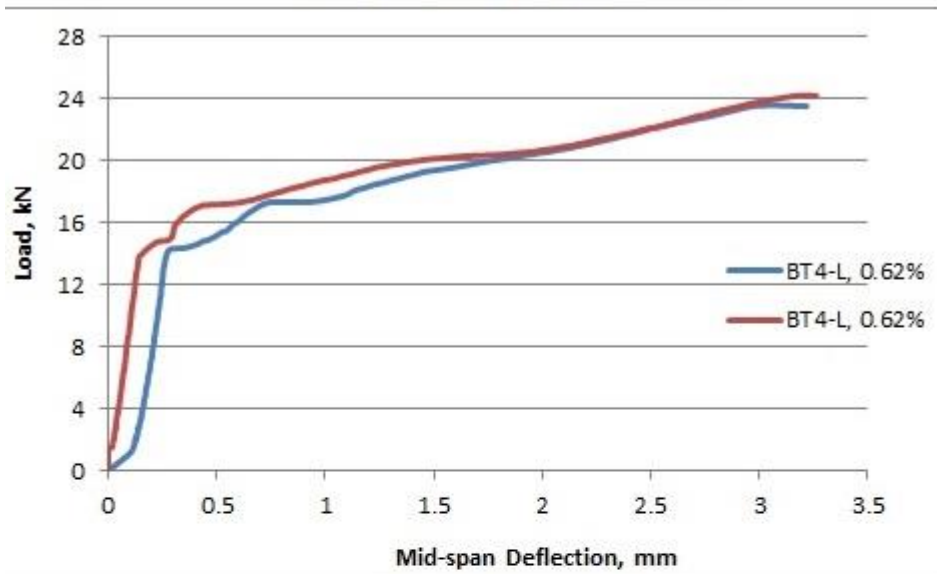


Figure 4-8 Load-Deflection behaviour at mid-span of different layers of woven fabric (2.5 cm) at warp direction reinforced beams.



Figure 4-9 Cracks pattern of beam reinforced by BT₇-L,50k.

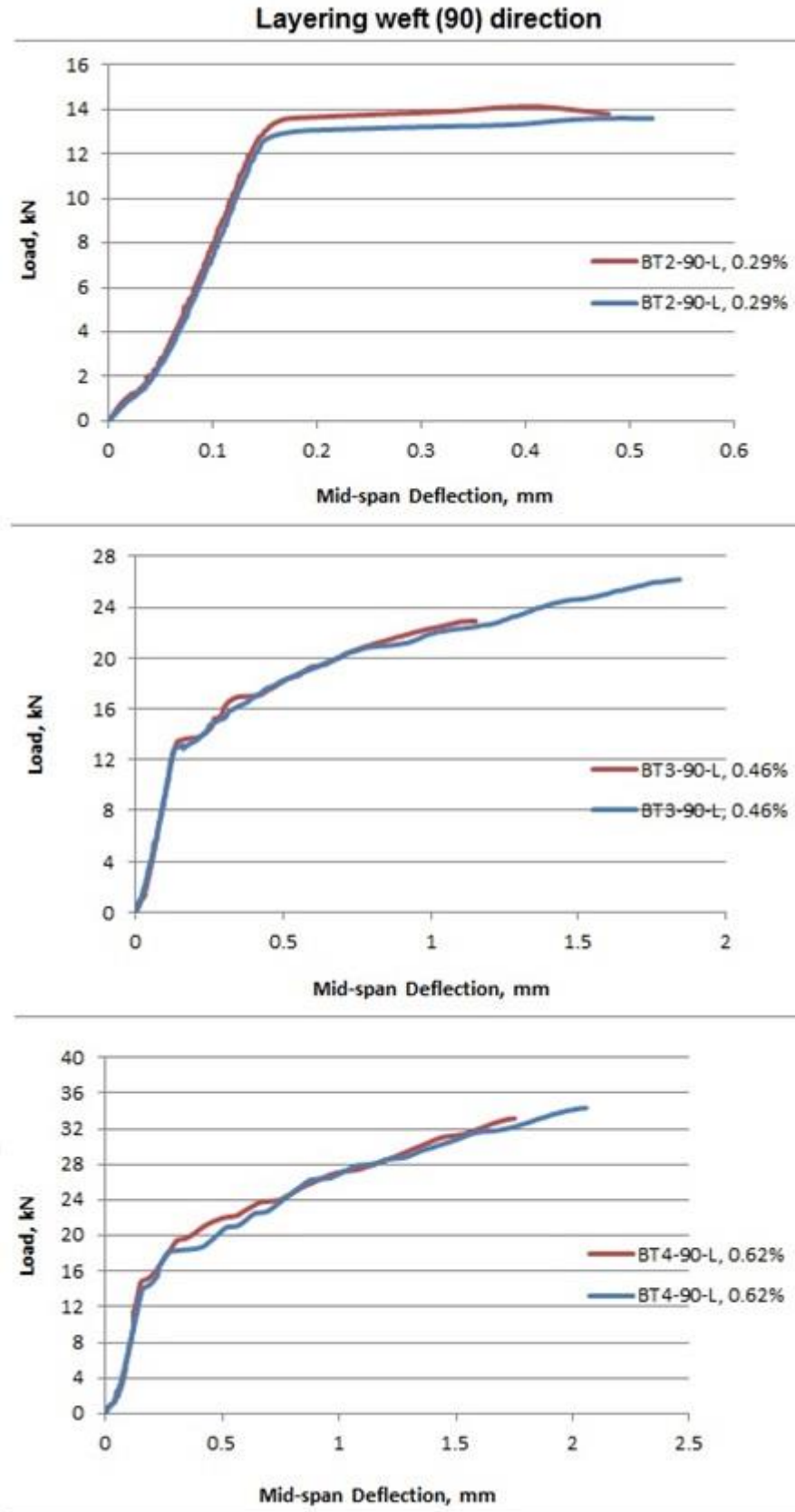


Figure 4-10 Load-Deflection behaviour at mid-span of different layers of woven fabric (2.5 cm) at weft direction reinforced beams.

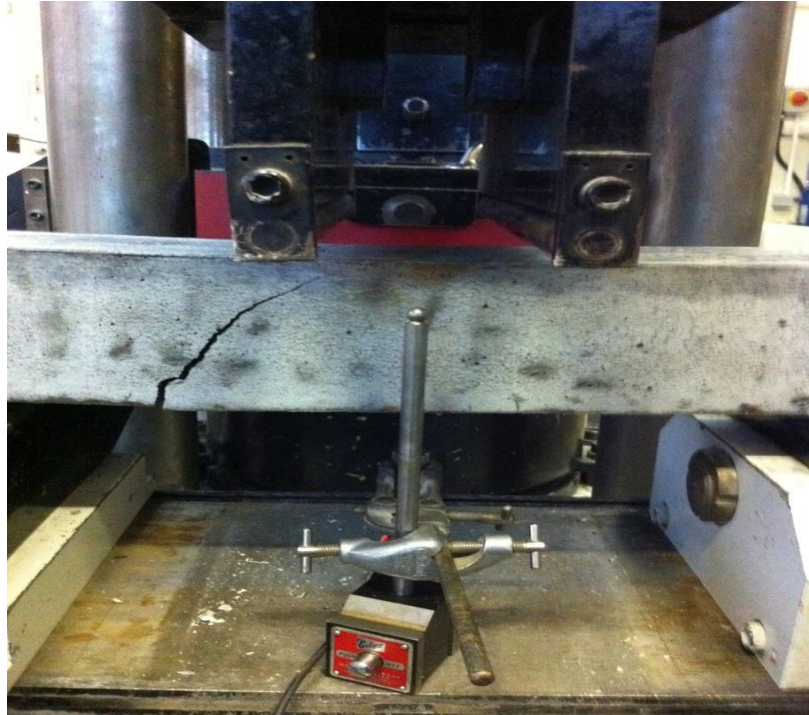


Figure 4-11 Cracks pattern of beam reinforced by BT4-90-L,50k.

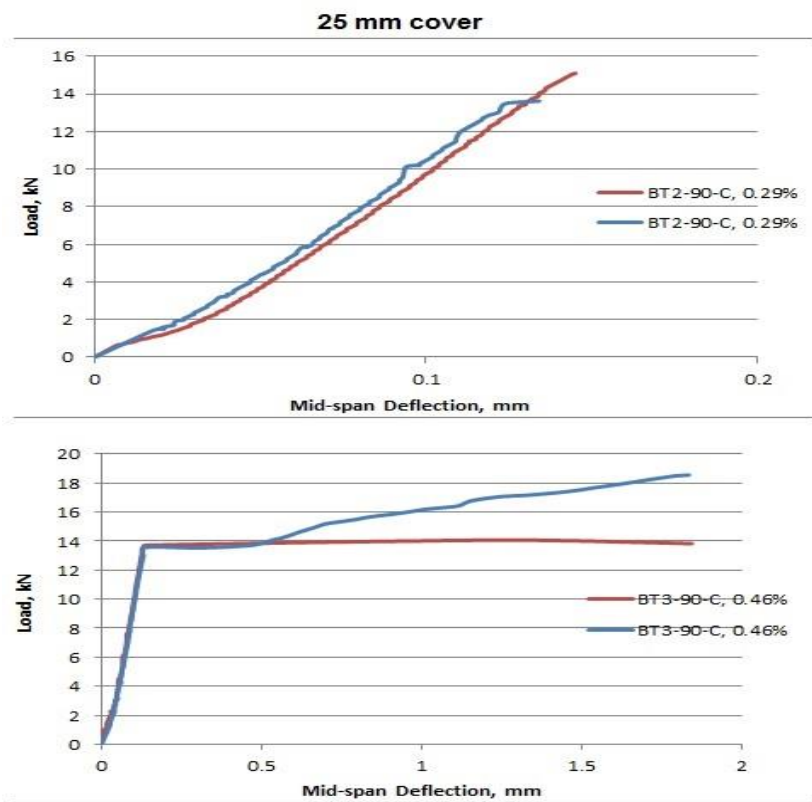


Figure 4-12 Load-Deflection behaviour at mid-span of woven fabric (2.5 cm) at weft direction reinforced beams with 2.5 cm cover.



Figure 4-13 Cracks pattern of beam reinforced by BT₃-90-C,50k.

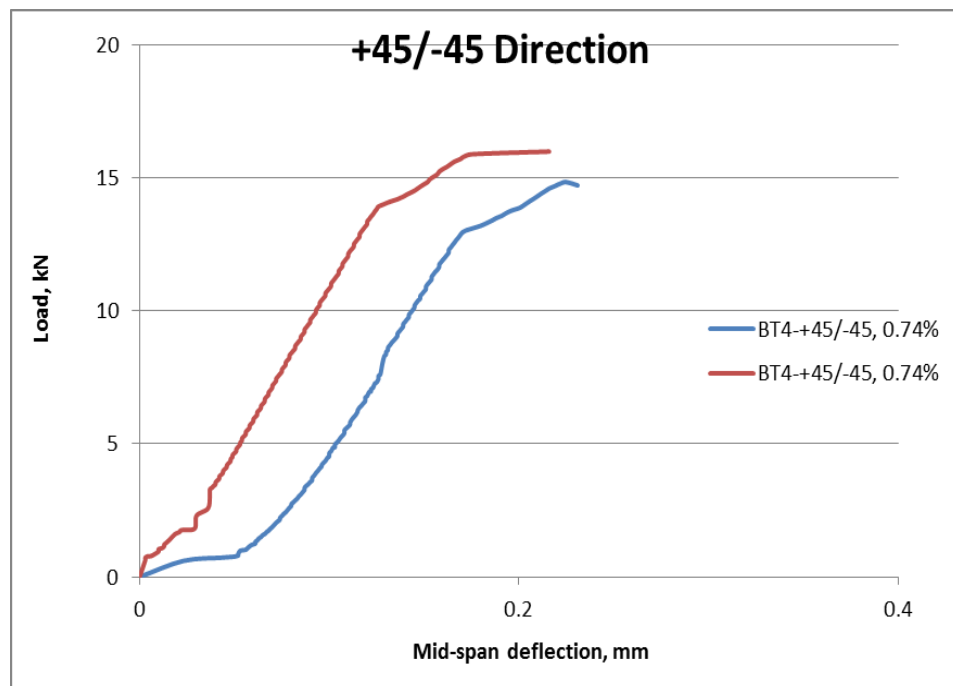


Figure 4-14 Load-Deflection behaviour at mid-span of woven fabric (2.5 cm) at ± 45 direction reinforced beams.

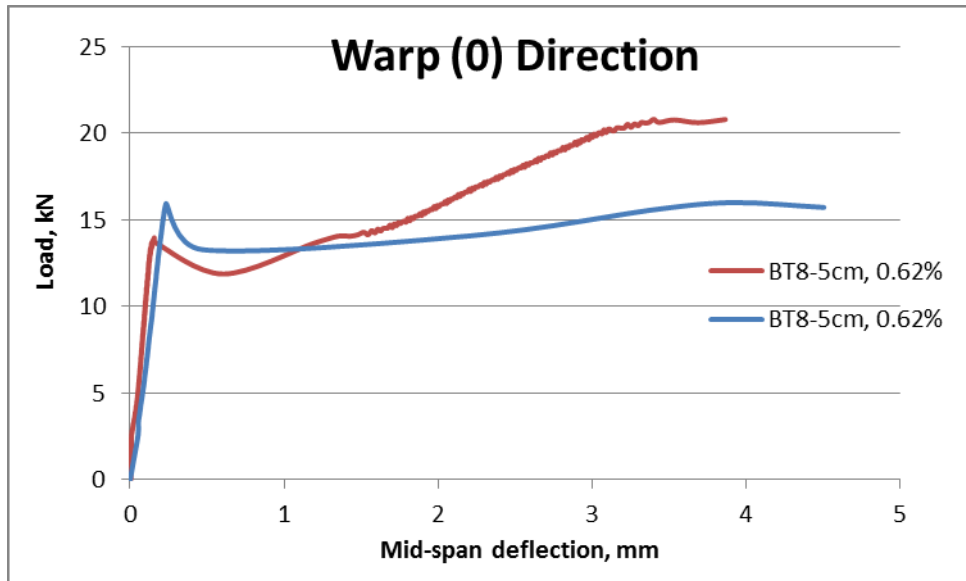


Figure 4-15 Load-Deflection behaviour at mid-span of woven fabric (5 cm) at warp direction reinforced beams.

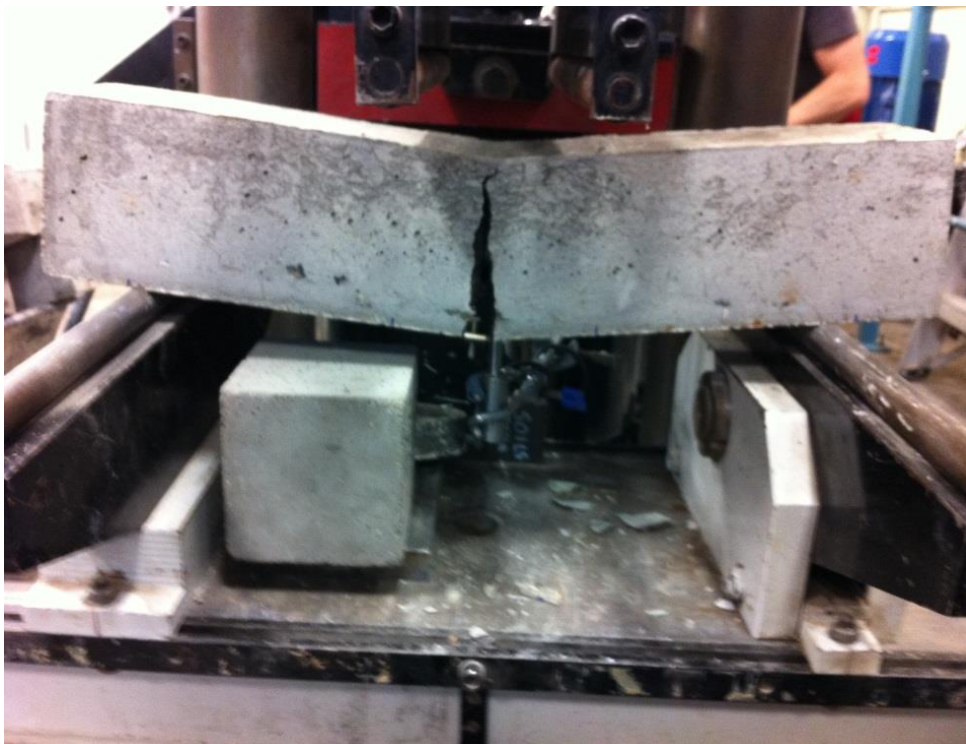


Figure 4-16 Cracks pattern of beam reinforced by BT₈ -5cm,50k.

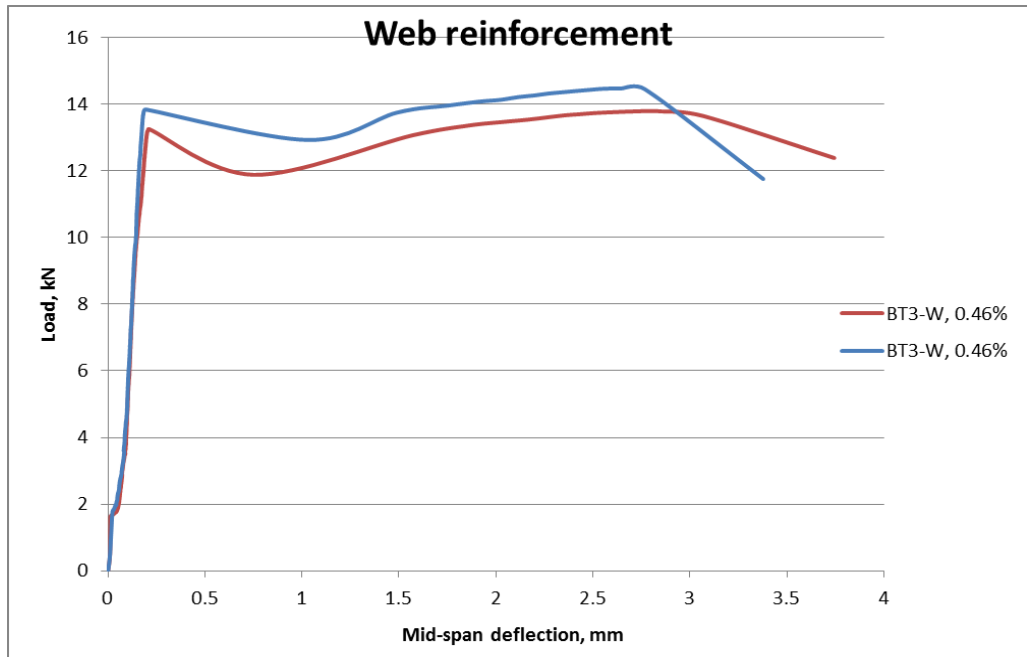


Figure 4-17 Load-Deflection behaviour at mid-span of web woven fabric (5 cm) at warp direction reinforced beams.



Figure 4-18 Cracks pattern of beam reinforced by BT₃-W, 50k.

4.4.1.3 Tow textile (uni-axial textile)

Beams were reinforced by two types of uni-directional tow; one is with *50k* of filaments and another is with *24k* of filaments. Each type was applied with different geometries and lay outs. Table 4.4 presents the results of uni-axial tow (*50k*) reinforced beams with different geometries. Table 4.5 presents the results of uni-axial tow but consisted of *24k* filaments reinforced beams with different geometries. It can be seen from Table 4.4 and Table 4.5, the flexural load and deflection improve as a result of adding more reinforcement. Also, the change in the textile geometry leads to change in the capacity, although, the effective area is the same. Figure 4-19 to Figure 4-24 shows the behaviour and cracks patterns of different geometries and lay outs of uni-axial reinforcement.

Table 4.4 The results of uni-axial roving with 50k filaments reinforced beams.

	Reinforcement	Effective Area, mm ²	Vf, %	Ultimate Load, kN		Average	Deflection, mm		Average
				Sample1	Sample2		Sample1	Sample2	
Geometry	UT_{b4}, 50k	30.8	0.31	32.0	33.4	32.7	3.1	2.9	3.0
	UT_{br4}, 50k	30.8	0.31	23.8	23.8	23.8	2.85	2.3	2.6
	UT_{c4}, 50k	30.8	0.31	20.5	20.1	20.3	2.2	2.5	2.4
	UT_{t4}, 50k	30.8	0.31	13.5	14.0	13.8	0.12	0.13	0.13
Longitudinal Tow	UT₄, 50k	30.8	0.31	26.5	28.5	27.5	1.9	1.8	1.9
	UT_{5.5}, 50k	42.3	0.51	30.8	31.8	31.3	2.1	2.0	2.1
	UT₇, 50k	53.8	0.54	32.9	32.8	32.9	2.2	2.0	2.1

Table 4.5 The results of uni-axial roving with 24k filaments reinforced beams.

	Reinforcement	Effective Area, mm ²	Vf, %	Ultimate Load, kN		Average	Deflection, mm		Average
				Sample1	Sample2		Sample1	Sample2	
Geometry	UT₄, 24k	14.8	0.15	14.2	13.7	14.0	0.16	0.13	0.15
Longitudinal Tow	UT₃, 24k	11.1	0.13	13.3	13.3	13.3	0.18	0.17	0.18
	UT₄, 24k	14.8	0.15	14.7	14.7	14.7	0.45	0.26	0.35
	UT₈, 24k	29.5	0.29	20.4	24.0	22.2	1.5	1.5	1.5

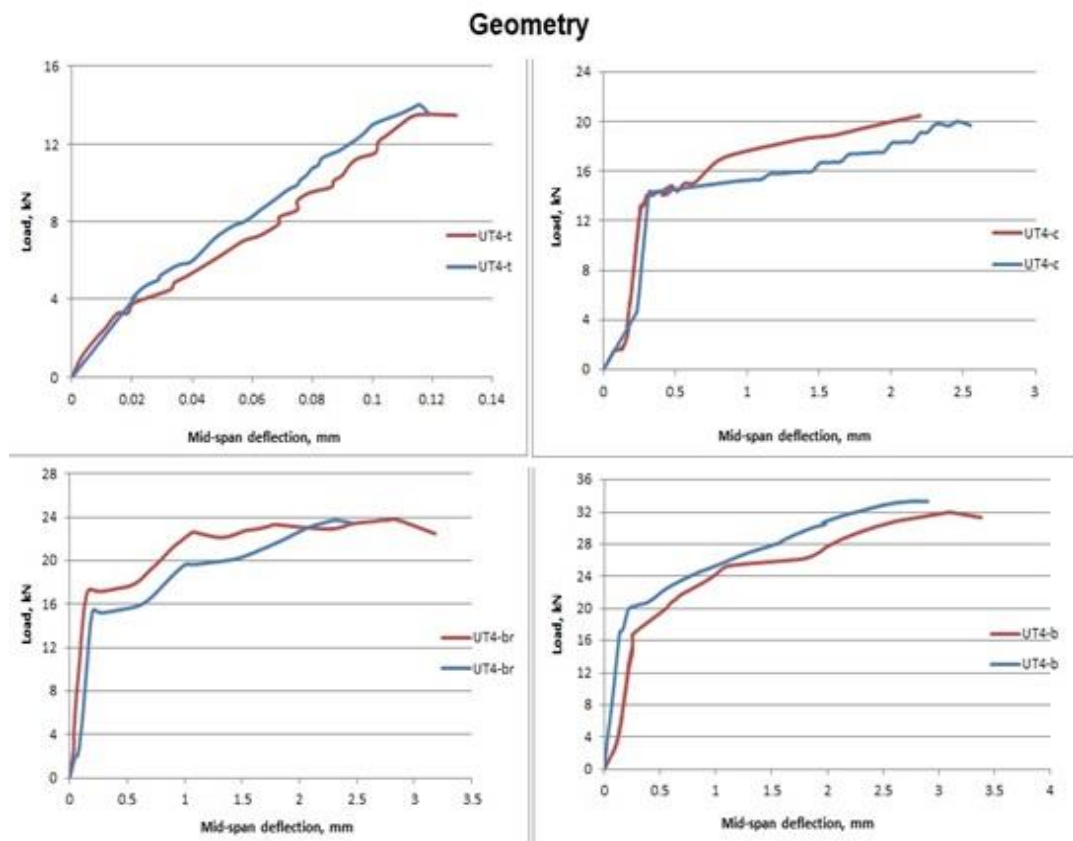


Figure 4-19 Load-Deflection behaviour at mid-span of uni-axial tow at the same volume fraction (0.31%) with different geometries.



Figure 4-20 Cracks pattern of beam reinforced by UT_{b4},50k.

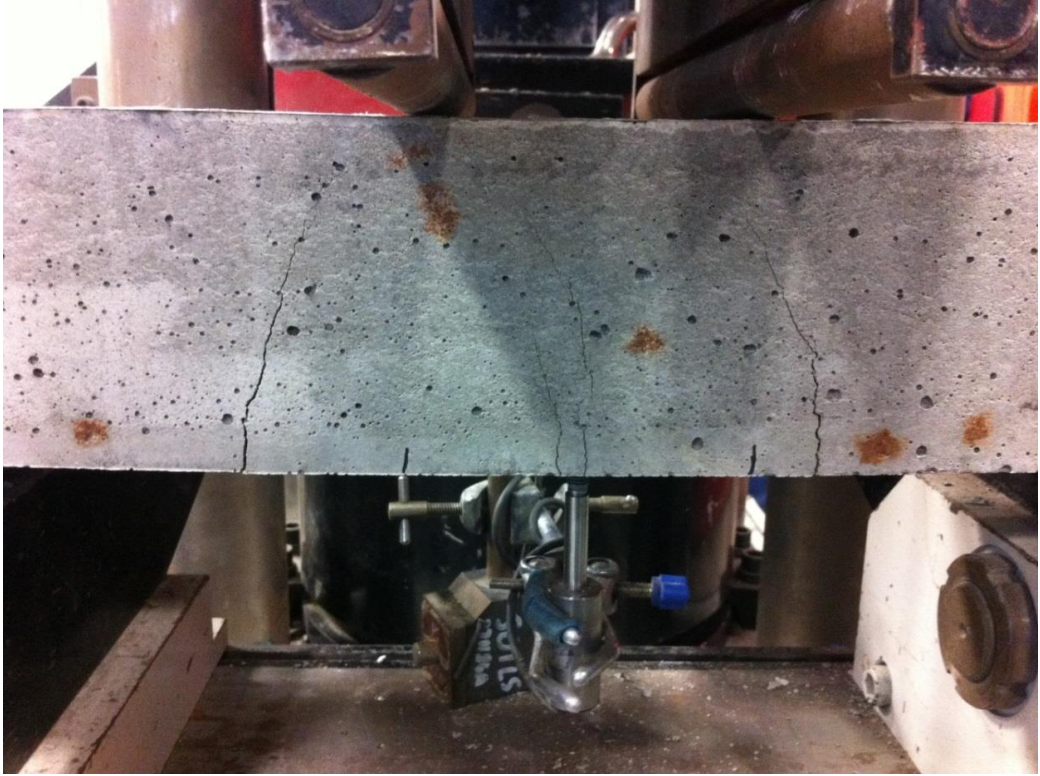


Figure 4-21 Cracks pattern of beam reinforced by $UT_{br4,50k}$.

Longitudinal Tow

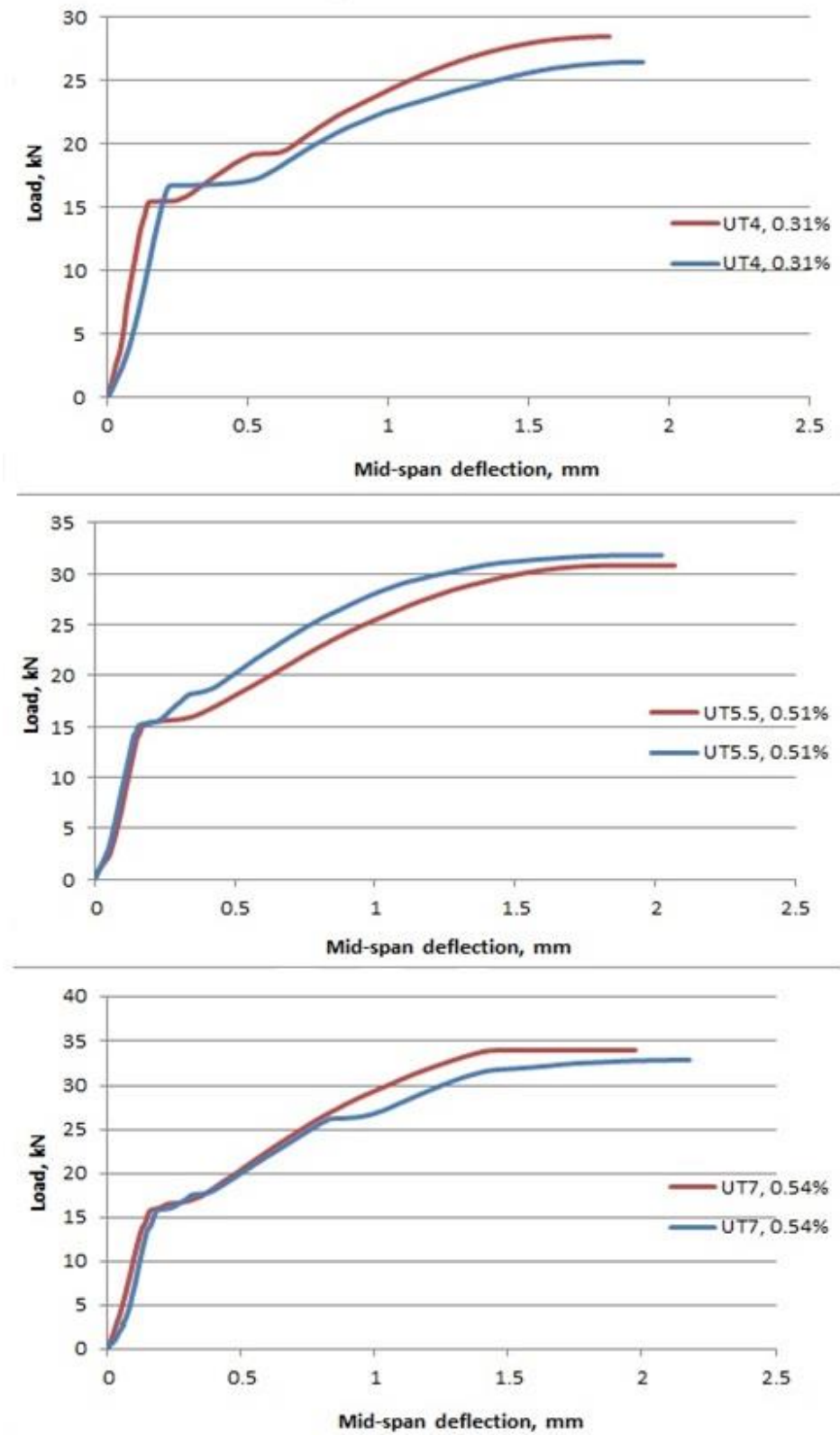


Figure 4-22 Load-Deflection behaviour at mid-span of uni-axial tow at different quantity of fibre.

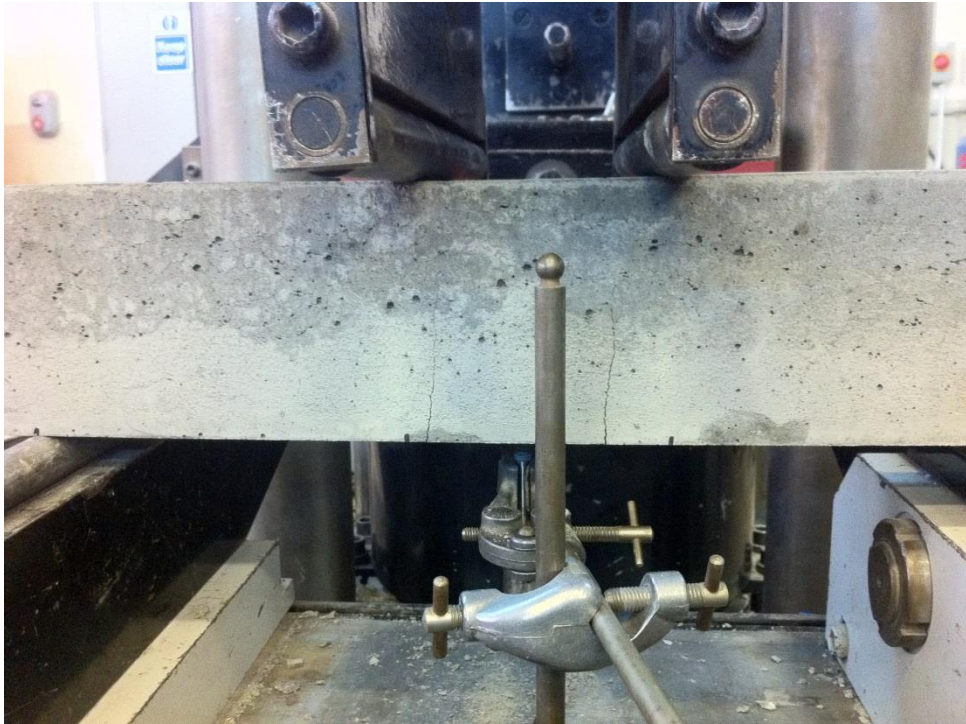


Figure 4-23 Cracks pattern of beam reinforced by UT₄,50k.



Figure 4-24 Cracks pattern of beam reinforced by UT₇,50k.

4.4.1.4 Chopped fibre

Short fibres were used to reinforce concrete beams in order to investigate the behaviour and compare it with continuous fibres. Table 4.6 presents the results of four beams reinforced by different volume fraction of fibre. The results in Table 4.6 show that the ductility in the chopped fibre is significantly lower than textile reinforcement. Also, the same is occurred for the flexural capacity as it is dropped in comparison with TRC. Figure 4-25 shows the behaviour of chopped fibre at different volume fraction of fibre. Cracks pattern is shown in Figure 4-26.

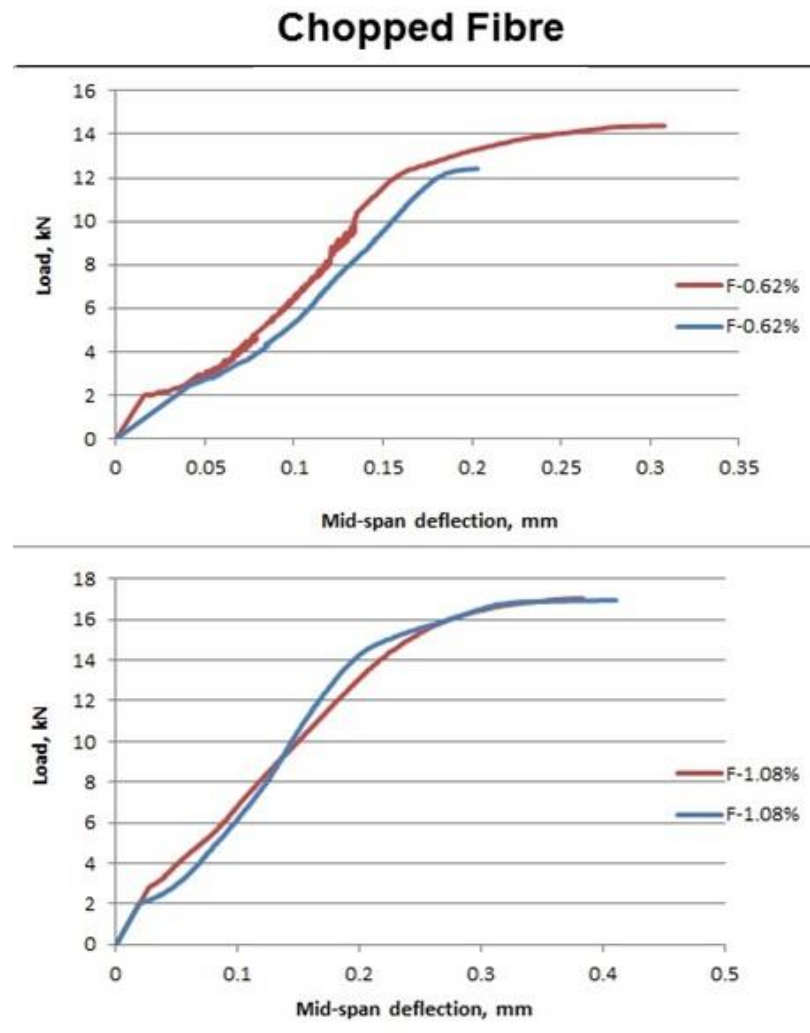


Figure 4-25 Load-Deflection behaviour at mid-span of short fibre at different quantity.



Figure 4-26 Cracks pattern of beam reinforced by short fibres T-1.08%,50k.

4.4.1.5 Steel

Two beams were reinforced by steel reinforcement. The steel reinforcement area was chosen to be nearly similar to the maximum textile reinforcement cross sectional area used in this study. Therefore, it can be compared TRC beam behaviour with SRC beam behaviour. Also, the design concept of textile reinforced concrete beam will be derived from steel reinforced concrete beam design. Accordingly, the results will be used as control of TRC. Table 4.7 presents the results of steel reinforced concrete beams. Steel reinforced beam exhibits high ductility as it is presented in Table 4.7. The average deflection is 6.4 mm and the average ultimate load is 31.4 kN . Figure 4-27 shows the behaviour of steel reinforced concrete beam. Figure 4-28 demonstrates the crack pattern of steel reinforced concrete.

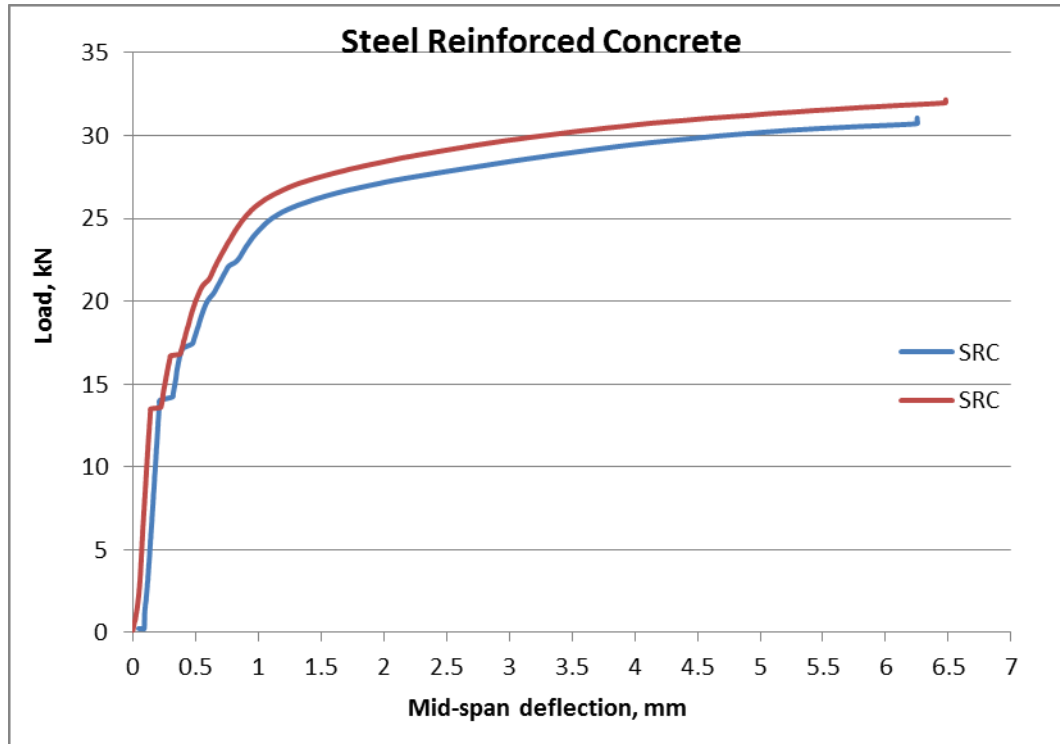


Figure 4-27 Load-Deflection behaviour at mid-span of steel reinforced concrete beam.



Figure 4-28 Cracks pattern of beam reinforced by steel.

Table 4.6 The results of chopped fibre reinforced concrete beams.

Reinforcement	Effective Area, mm ²	V _f , %	Ultimate Load, kN		Average	Deflection, mm		Average
			Sample1	Sample2		Sample1	Sample2	
F-0.62%, 50k	-	0.62	14.4	12.4	13.4	0.31	0.2	0.25
F-1.08%, 50k	-	1.08	17.0	17.0	17.0	0.41	0.37	0.39

Table 4.7 The results of steel reinforced concrete beams.

Reinforcement	Area, mm ²	V _f , %	Ultimate Load, kN		Average	Deflection, mm		Average
			Sample1	Sample2		Sample1	Sample2	
SRC	50.2	0.50	30.7	32.0	31.4	6.2	6.5	6.4

4.4.2 Large scale beams

TRC exhibited a good performance in the small scale beams in comparison with steel reinforced concrete in terms of ultimate flexural load and the ductility which gave the foundation to scale up to the long span beams. Twelve beams with $120 \times 200 \times 2600$ (all dimensions in *mm*) were tested. The beams were categorised based on the type of reinforcement as follows; woven fabric, uni-axial direction, and steel reinforcement. Some category was classified into groups based on the lay-out and geometry of reinforcement. The following section presents the results of the tested beams.

4.4.2.1 Biaxial textile (woven fabric)

Beams were reinforced by bi-axial direction textile with 5 cm spacing between warps. The number of biaxial textile fabric was 14 piled over each other. Each fabric consisted of 3 warps. The results are presented in Table 4.8. The load-deflection curve is shown in Figure 4-29. In Figure 4-30 the cracks formation is demonstrated.

Table 4.8 Fabric reinforced concrete beam result.

Reinforcement	Effective Area, mm^2	Vf, %	Ultimate Load, kN	Deflection, mm
BT_{(5cm)14}-Anch-2.6, 50k	80.7	0.57	11.8	14.5

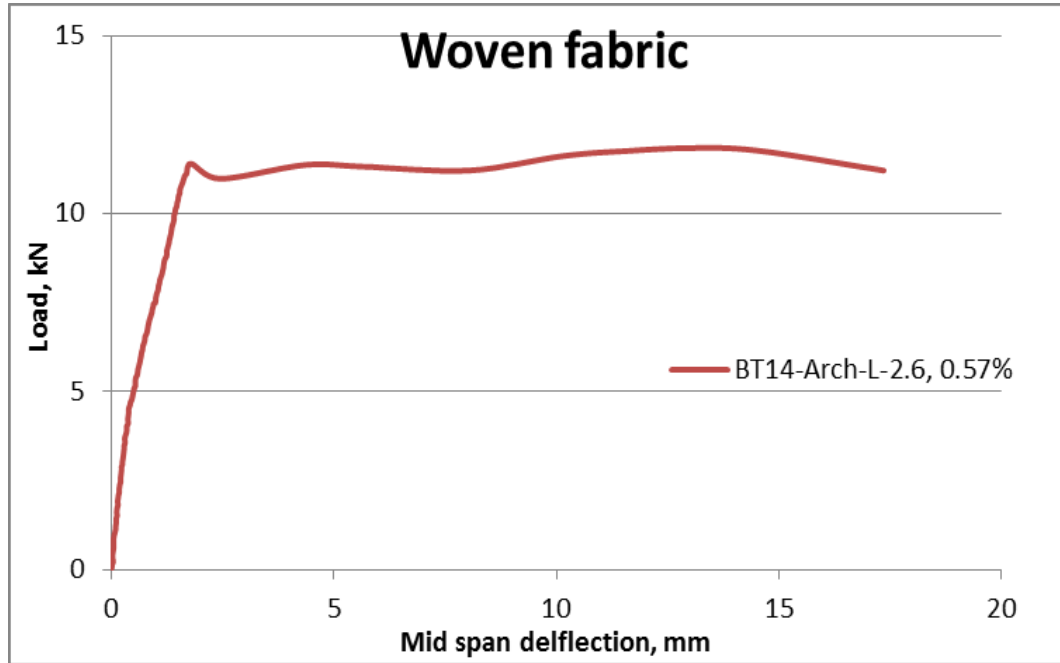


Figure 4-29 Load-Deflection behaviour at mid-span of woven textile at large scale beam.



Figure 4-30 Cracks patterns of BT_(5cm)14-Anch-2.6-L, 50k

4.4.2.2 Tow textile (uniaxial textile)

In this section, the results of uni-directional tow reinforced concrete beams are presented. The results are divided into two groups based on the anchorage of the reinforcement at the end of beam; first straight (not anchored) and the second group is anchored. The latter are classified into three sub-groups based on the cover thickness. Table 4.9 presents the results of uni-axial tow reinforced beam which was straight at the end of beam. Figure 4-31 shows the behaviour of uni-axial reinforcement with straight edge at different layouts. Figure 4-32 and Figure 4-33 demonstrate the cracks formation of both beams.

Table 4.9 Edge straight uni-axial tow textile reinforced beam.

Reinforcement	Effective Area, mm²	Vf, %	Ultimate Load, kN	Deflection, mm
UT₈-2.6, 50k	61.5	0.25	13.8	9.0
UT₈-L-2.6, 50k	61.5	0.25	14.4	15.7

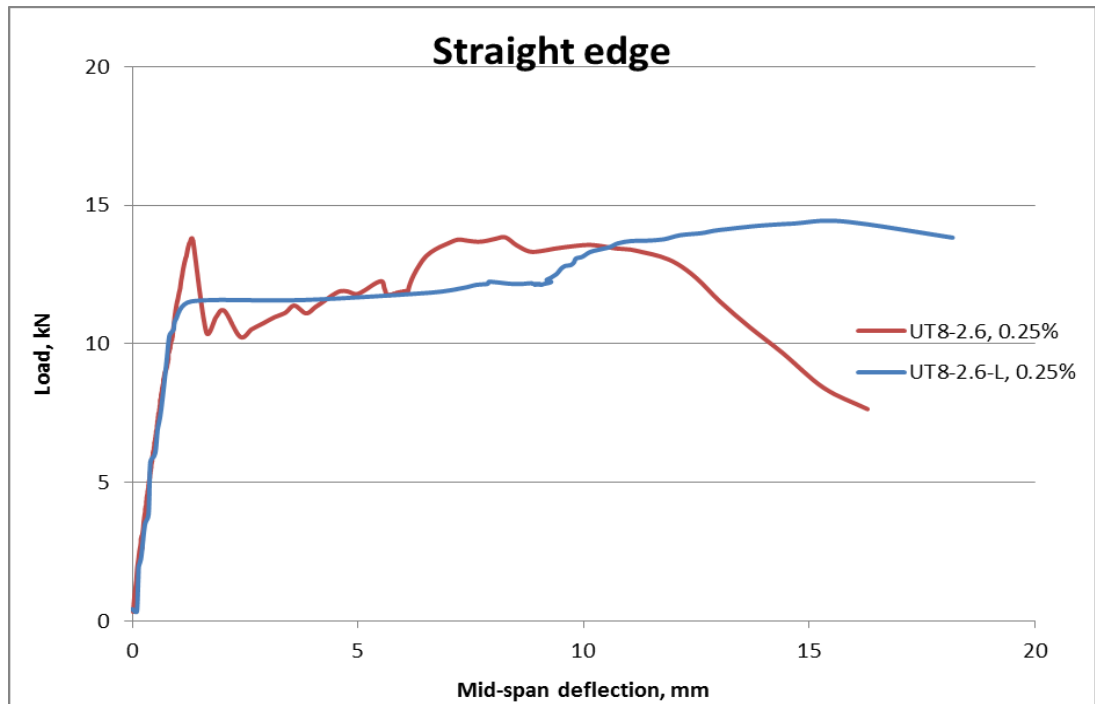


Figure 4-31 Load-Deflection behaviour at mid-span of uni-axial textile reinforcement at different layers.

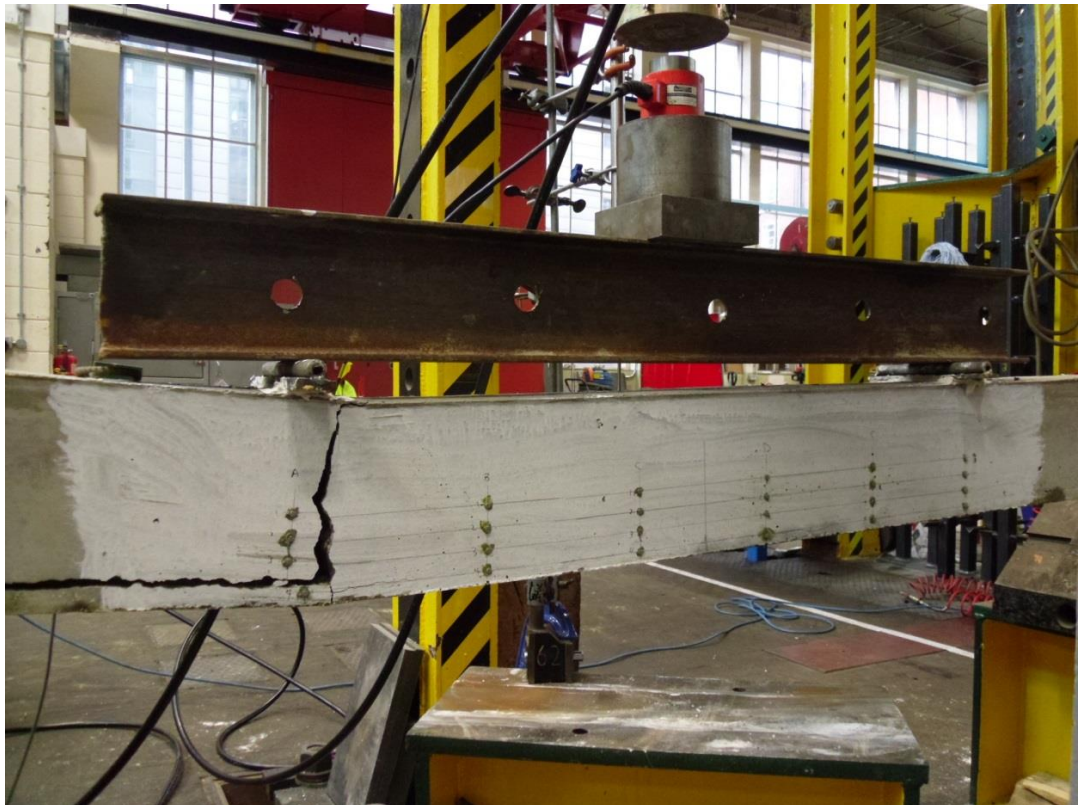


Figure 4-32 Cracks patterns of UT₈-2.6, 50k.



Figure 4-33 Cracks patterns of UT₈ -L-2.6, 50k.

Table 4.10 presents the results of uni-axial textile reinforced beam which was anchored at the end of beam. It can be seen that there are variety of lay outs of textile reinforcement mainly in the number of layers. L means the reinforcement was divided into two layers with 1.5 cm spacing, however, if L is not mentioned that means all tows are in one layer. $3L_3$ means that the reinforcement was divided into 3 layers (subscript) with 1.5 cm spacing between layers and 3 before L means that the number of uniaxial tows in each layer is 3 (if not mentioned the default is 4 in each layer). The cover thickness is 30 mm unless it is mentioned as C15 and C60 which is 15 mm and 60 mm the cover thickness. From Table 4.10, it can be seen that the results of the ultimate load varies considerably at the same quantity of fibre. The discussion chapter will investigate the explanation of these changes. Figure 4.32 shows the change in the behaviour as a result of change in the layouts of uni-axial textile which is anchored at the edge.

Table 4.10 Results of anchored uni-axial tow reinforced beam.

Reinforcement	Effective Area, mm²	V_f, %	Ultimate Load, kN	Deflection, mm
UT8-Anch-2.6, 50k	61.5	0.25	16.5	11.0
UT8-Anch-L-2.6, 50k	61.5	0.25	18.2	15.6
UT₁₂-Anch-3L₃-2.6, 50k	61.5	0.25	19.5	16.0
UT₁₂-Anch-L-2.6, 50k	92.3	0.37	16.2	17.0
UT₁₅-Anch-3L₃-2.6, 50k	92.3	0.37	39.3	23.6
UT₁₅-Anch-3L₃-2.6, 50k	92.3	0.37	33.7	17.8
UT₁₅-Anch-3L₃-2.6-C15	92.3	0.37	32.5	22.7
UT₁₅ -Anch-3L₃-2.6-C60	92.3	0.37	21.5	16.7

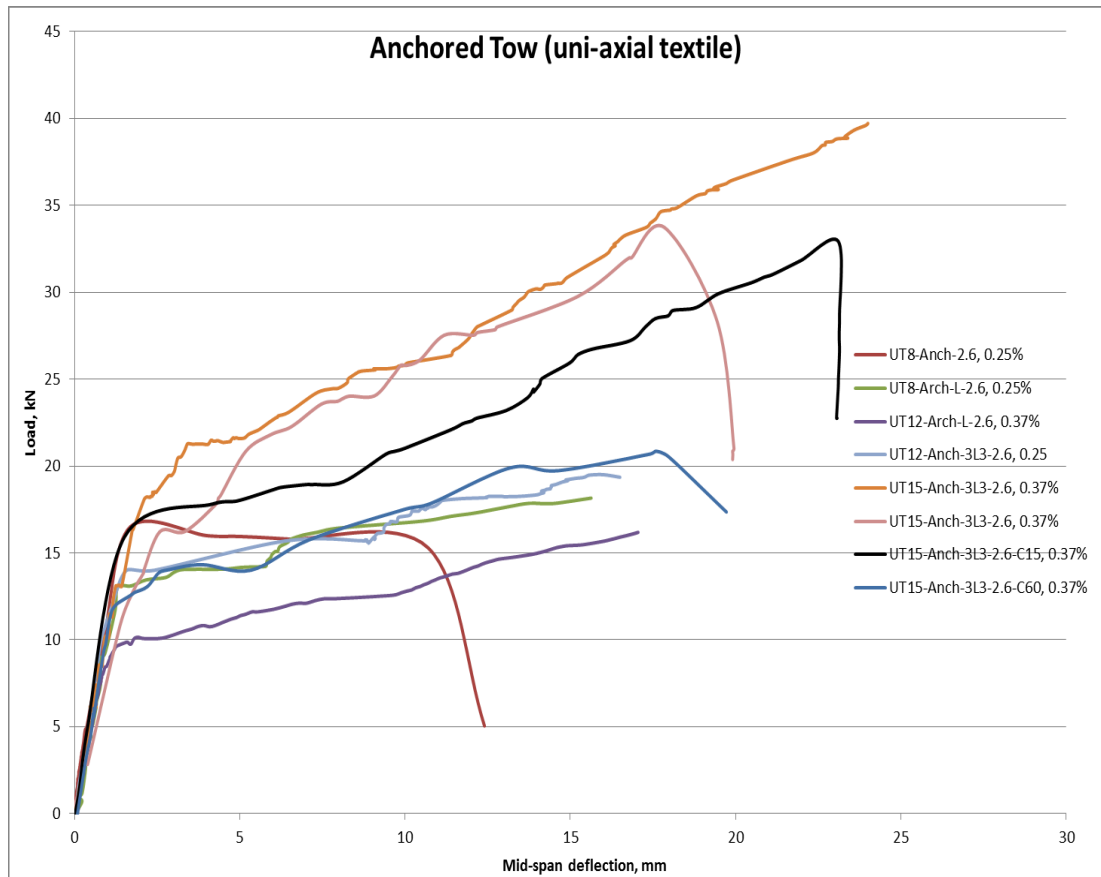


Figure 4-34 Load-Deflection behaviour at mid-span of anchored uni-axial reinforcement at different layouts.

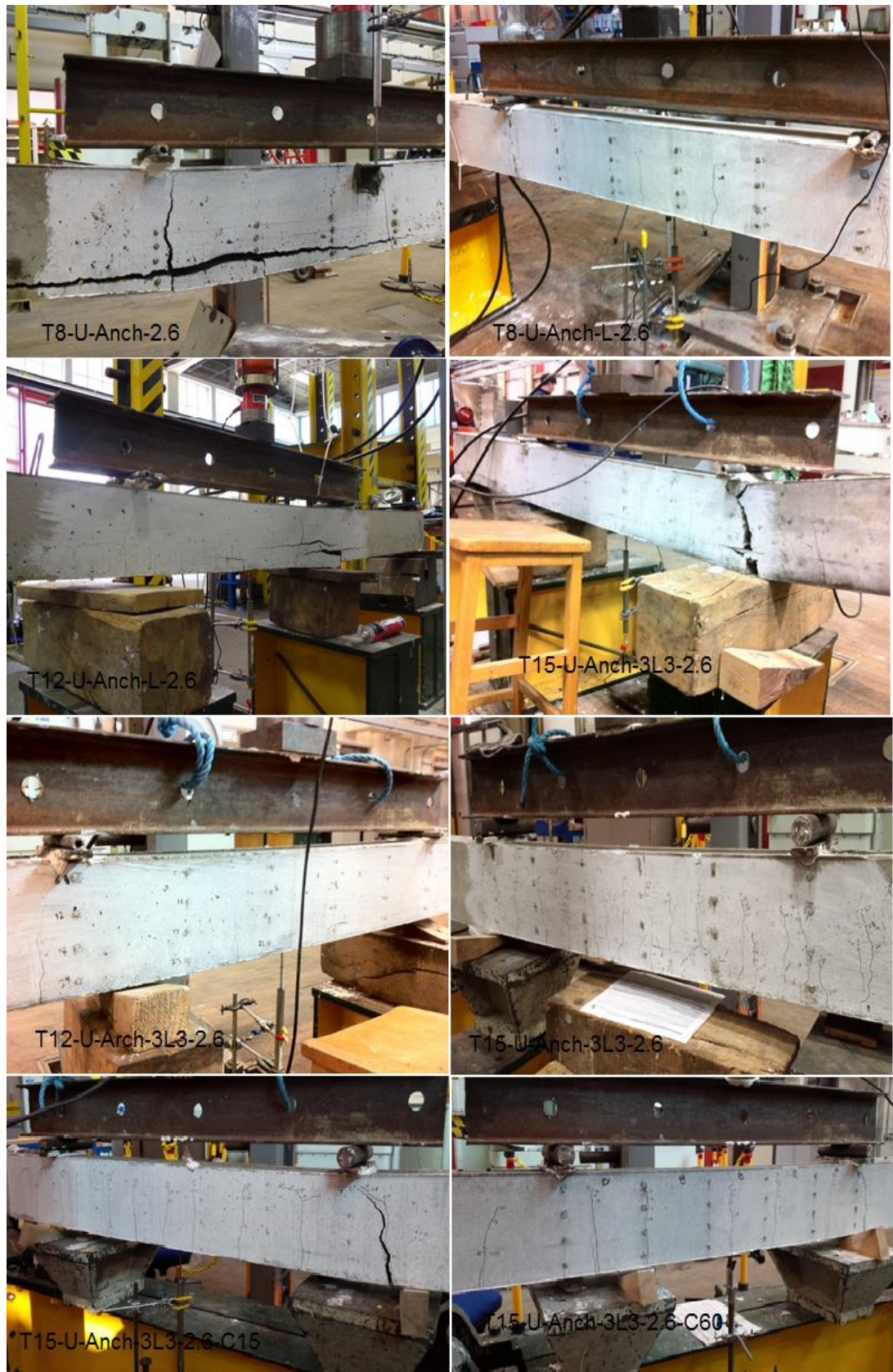


Figure 4-35 Crack patterns of different layouts of uni-axial textile reinforced concrete beams.

4.4.2.3 Steel

Control steel reinforced concrete beam was tested to compare the behaviour with TRC. Two steel bars with 8 mm diameter were used to reinforce beam. The results are presented in Table 4.11. The steel was anchored and the cover thickness at the bottom was 30 mm. Figure 4-36 shows the behaviour of steel reinforced concrete beam. The crack formations are illustrated in Figure 4-37.

Table 4.11 Results of steel reinforced beam.

Reinforcement	Area, mm ²	V _f , %	Ultimate Load, kN	Deflection, mm	Failure Mode
SRC	100.5	0.42	24.5	40.5	Flexural failure

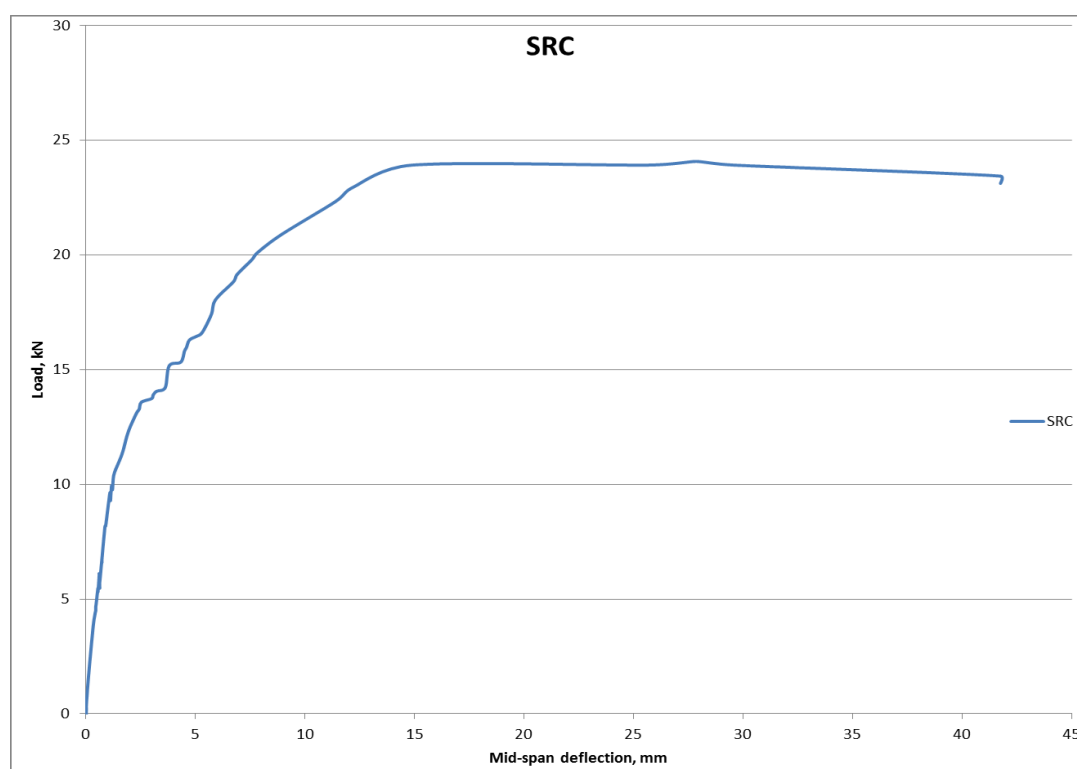


Figure 4-36 Load-Deflection behaviour at mid-span of steel reinforced concrete beam.

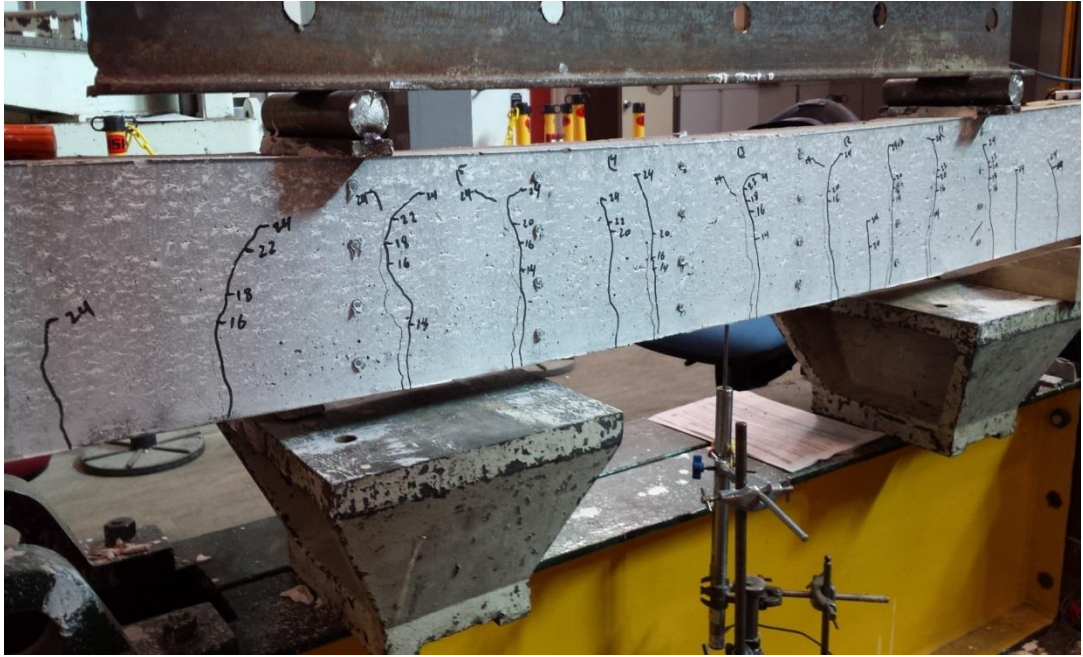


Figure 4-37 Crack pattern of steel reinforced concrete.

CHAPTER 5

DISCUSSION AND ANALYSIS

The effect of changing different parameters on the behaviour of carbon textile reinforced concrete will be discussed. In this chapter, the explanations of the results which were presented in the previous chapter will be investigated.

5.1 The effect of textile geometry and lay out

In this section, different geometries, lay outs, and types of textile reinforcement will be investigated to study how the change in the lay outs and geometry affects the TRC behaviour. Therefore, the findings will contribute to determining the optimum lay out and geometry for reinforcing the concrete beam using textile reinforcement. All beam dimensions in this section are *100 mm x 100 mm x 500 mm*.

5.1.1 The effect of the voids ratio of a textile

In order to compare between the roving densities the voids ratio is calculated. The voids ratio of a roving (warp or weft) is the voids in the cross sectional area relative to the area of the cross section of the roving. It presents the percentage of voids in the roving cross section. An increase in the ratio leads to an increase in penetration as a result of the increase in the voids. Figure 5-1 demonstrates the approximate textile reinforcement boundary dimensions. Accordingly, the effect of widening or narrowing the width of the roving could be measured. For the same number of filaments, the voids ratio may vary due to changes in the cross sectional area of the roving (warp, weft or tow).

$$\rho_v = \frac{A_g - A_f}{A_g}$$

where,

ρ_v is the voids ratio.

A_g is the cross sectional area of the roving (including the voids).

A_f is the filament area multiplied by the number of filaments in the roving or tow.

Thus, the increase in the cross sectional area of the roving for the same number of filaments leads to an increase in the voids ratio. In another words, the higher voids ratio means that additional filaments have a higher probability of coming into contact with the matrix. In contrast, a low voids ratio for a roving means the filaments are consolidated which reduces the roving area; therefore, the area in contact with the matrix is lowered. The bi-axial textile which is used to reinforce concrete has the same number of filaments in both directions (warp and weft). However, in the warp direction the filaments are stitched which leads to a lower voids ratio and in the weft direction is higher voids ratio, as shown in Figure 3.1. The results in Table 5-1 demonstrate that there is no significant effect of reinforcing in the weft direction (higher voids ratio) in comparison with the warp direction (lower voids ratio). The differentiation between warp and weft voids ratios is small which could explain the similarity in the capacity. However, the increase in the load capacity as a result of increasing the voids ratio in UT₄ can be clearly seen. The load strength increased by 12% in comparison with BT₄, however, the ductility is the same. Therefore, increasing the voids ratio is positive as the result is an increase in the load capacity and ductility is maintained.

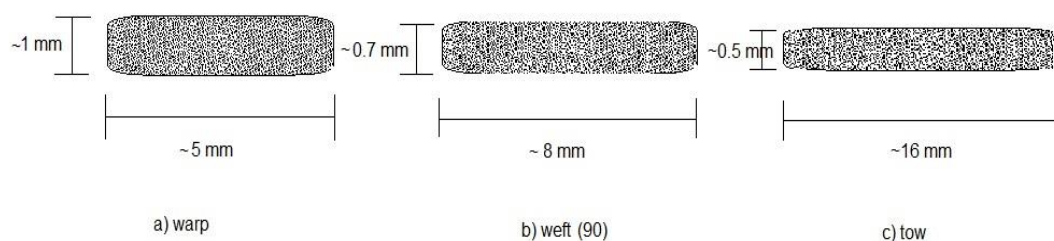


Figure 5-1 The width of different reinforcement rovings.

Table 5-1 Average ultimate load and deflection of a bi-axial textile in both directions.

Reinforcement	Area, mm ²	V _f , %	Voids Ratio	Average Ultimate Load, kN	Average Deflection, mm
BT ₃ , 50k	23.1	0.46	0.61	15.2	0.2
BT ₃₋₉₀ , 50k			0.65	16.9	0.6
BT ₄ , 50k	30.8	0.62	0.61	24.6	1.8
BT ₄₋₉₀ , 50k			0.65	24.0	1.5
UT ₄ , 50k	30.8	0.31	0.76	27.5	1.9

5.1.2 The effect of layering reinforcement

In conventional reinforced concrete, another layer(s) of tension reinforcement is added when the required number of steel bars is more than the minimum spacing between bars in one layer. However, the increase in the number of layers leads to a decrease in the effective depth (d) which results in a reduction in the beam capacity in comparison with the same area of

reinforcement in one layer. Therefore, this section investigates the influence of dividing TRC into two separated layers on the behaviour of TRC. In this study, the woven fabric was divided into two layers with *15 mm* spacing, see Figure 3.17. From Table 5-2, it can be seen that there is no clear influence of layering the reinforcement in case of reinforcing in warp direction on the ultimate load. However, BT_{L4} exhibits high deflection which is a result of the slipping which occurred in the inner filaments of the warp rovings after the sleeve filaments began to break. In BT_{L4-90}, the cause of the reduction in the deflection is the area of outer (sleeve) filaments in the weft rovings extending toward the core filaments which minimized the slippery of the inner filaments. Therefore, the ductility was restrained due to the reduction in the number of inner filaments. The expected decrease in the capacity was compensated for by the increase in the contact area of the textile due to dividing the fabrics into two layers. Also, the filaments in the warp direction were stitched, which reduced the penetration. However, in the weft direction the ultimate strength was considerably improved. The percentage increase was 36% which can be accounted for by the increase in the contact area with the concrete (already the weft direction was wider than the warp) which led to exploitation of the roving strength.

Table 5-2 Average ultimate load and deflection of a layered bi-axial TRC beam.

Reinforcement	Area, mm²	V_f, %	Average Ultimate Load, kN	Average Deflection, mm
BT₄, 50k	30.8	0.62	24.6	1.8
BT_{L4}, 50k			24.2	3.3
BT_{L4-90}, 50k			33.5	2.0

5.1.3 The effect of cover thickness

One of the main uses of the cover in steel reinforced concrete is to protect steel reinforcements from environmental conditions which could cause corrosion. Also, it is needed to guarantee the bond that is required to prevent the reinforcement from slipping, so that high tensile strength can be achieved. Therefore, the cover is theoretically not needed in the case of carbon textile reinforcement as it can naturally survive under various conditions, as mentioned in the literature. The increase in the thickness entails a decrease in the effective depth which results in a lower capacity of reinforced beam. In this section, the influence of the cover thickness will be investigated. The section details are shown in Figure 3.18. The average results for two beams are presented in Table 5-3. Increasing the cover thickness to *25 mm* shows no negative effect on the ultimate load as a result of the reduction in effective depth. The result indicates that the bond was improved due to the increase in the cover thickness as the ultimate load of BT_{C3}-90-25 is similar to BT₃-90. Therefore, the bond improvement cancels out the effect of the decrease in the effective depth. However, in terms of the deflection, the rise in the cover thickness appears to enhance the ductility because the tensile strength of BT_{C3}-90-25 is higher for the same area because of the bond; thus, the deformation in the beam is higher.

Table 5-3 Average ultimate load and deflection of different TRC cover thicknesses.

Reinforcement	Area, mm ²	V _f , %	Average Ultimate Load, kN	Average Deflection, mm
BT ₃ -90-15mm, 50k	23.1	0.46	16.9	0.6
BT _{C3} -90-25mm, 50k			16.3	1.8

5.1.4 The effect of the orientation

The change in the direction of the textile reinforcement with loading direction was investigated to study how it could affect TRC behaviour. The reinforcement was oriented in $\pm 45^\circ$ directions. Table 5-4 presents the average results of $\pm 45^\circ$ TRC. It is apparent from this table that the deviation of the direction of the loading causes a significant drop in the reinforced beam capacity. Hegger and Voss (2004) stated that once the angle of reinforcement increases, the ultimate load decreases. From the table, the reduction in the ultimate load due to locating the textile reinforcement at $\pm 45^\circ$ is 38%. The drop in the load capacity of carbon textile reinforced concrete due to 45° orientation is 60% in Hegger and Voss (2004) results (see Figure 2.29). The increase in the capacity in this study in comparison with Hegger's findings can be attributed to the improvement in the number of activated filaments. Also, the ductility experienced a substantial fall in deflection by 89%. The bending moment strength and deflection show that the textile reinforcement at $\pm 45^\circ$ works in a similar way to chopped fibre because of the discontinuity in the textile in this case. This may explain the reduction in the ultimate load and deflection. Therefore, it can be concluded that the deviation of textile reinforcement from the loading direction leads to a significant drop in the capacity of the reinforced beam.

Table 5-4 Ultimate load and deflection of $\pm 45^\circ$ TRC.

Reinforcement	Area, mm ²	V _f , %	Average Ultimate Load, kN	Average Deflection, mm
BT ₄ , 50k	30.8	0.62	24.6	1.8
BT _{4+45/-45} , 50k			15.3	0.2

5.1.5 The effect of the increase in the number of rovings at the same layer

T_n is defined as T , the textile, and n , the number of warp or weft layers, see Figure 3.15. Theoretically, the capacity will improve as a result of the increase in the volume fraction of fibre and the cross sectional area, however, the bond issue in textile reinforcement may have a counteracting effect. The increase in the number of rovings at the same area means an increase in the number of inner filaments that are not in direct contact with the matrix. Therefore, the bond between matrix and filaments is a matter which appears to need investigation. This section will look at the increase in the number of woven fabric layers at the same level and how it affects the TRC performance. Table 5-5 presents the effect of increasing the number of woven fabric (piled on top of each other) on the ultimate load and deflection of TRC. The results indicate that increasing the number of filaments improves the average ultimate load of bi-axial TRC, which is as expected. This is in agreement with Yin, Lü and Xu (2013) who found that, before cracking, the stiffness of a beam reinforced with textiles is not influenced by increasing the number of textile layers, but, after cracking the stiffness is improved by such an increase. However, from a closer look it appears that the percentage increase is quite low for a high number of rovings at the same layer in comparison with a lower one. For example, at low number of rovings at the same layer, the improved percentage at BT_4 in comparison to BT_3 is 63%, however, there is only one layer (33% increase in the area) more at BT_4 . The increase in the strength in comparison with the increase in area is considered to be high. The ultimate strength of BT_3 is low which causes this noticeable difference between BT_3 and BT_4 . On the other hand, at high numbers of rovings at the same number of layer, the increase in the number of woven fabric at the same layer of BT_7 is 3 (75% increase in the area) in comparison with BT_4 , however, the improvement is 21%. The improvement does not represent the percentage increase in the area. Therefore, more woven fabrics lead to improvement in the ultimate load but not as it should be as a result of this high number of woven fabrics. This can be accounted for by the increase in the number of inner filaments that are not efficiently utilized, which is seen in the increase in

the deflection of BT₇ due to the slippage in inner filaments. Also, the decrease in the contact area of BT₇ relative to the increase in the number of woven fabrics as a result of piling the rovings on top of each other. It should be mentioned that there is an increase in the contact area of the outer filaments, however, the increase is small relative to the increase in non-contact inner filaments. Therefore, some inner warp rovings which resisting load are practically not activated to resist applied load, however, it provides ductility because of filaments slipping. In addition to this, the concrete penetration of the rovings becomes more difficult, again due to the congestion which occurs due to the piling of the fabrics.

Table 5-5 Average ultimate load and deflection of TRC for different numbers of rovings at the same layer.

Reinforcement	Area, mm²	V_f, %	Average Ultimate Load, kN	Average Deflection, mm
BT₂, 50k	15.4	0.37	14.2	0.2
BT₃, 50k	23.1	0.46	15.2	0.2
BT₄, 50k	30.8	0.62	24.6	1.8
BT₇, 50k	53.9	1.08	29.7	2.6

5.1.6 The effect of weft rovings

In this section, the study investigates how the weft rovings could influence the behaviour of TRC. Thus, the same reinforcement details of the bi-axial direction textile were applied for the uni-axial direction (tow no weft rovings). Table 5-6 presents the results for the bi-axial and uni-axial textile reinforced beams. From the table, it can be seen that the effect of weft rovings on the ultimate load is insignificant. In both cases, UT₄ and UT₇, the average ultimate load is improved in comparison with BT₄ and BT₇, respectively.

At flexural load, the reinforcement that resisted the generated stresses because of the bending was the roving in the loading direction. From the table, the ultimate load is increased as a result of eliminating the weft rovings. These findings can be explained by the bond enhancement and the improvement in the penetration due to the reducing in the reinforcement congestion. Also, the perimeter of tow reinforcement is more than warp rovings of biaxial reinforcement. The tow width was ~ 16 mm while the warp width of the biaxial textile was ~ 5 mm. Because of this, there was an increase in the ductility of the bi-axial direction reinforcement for high numbers of woven fabrics (BT₇) as a result of slipping inner filaments.

Table 5-6 Average ultimate load and deflection of uni and bi-axial TRC beams.

Reinforcement	Area, mm²	V_f, %	Average Ultimate Load, kN	Average Deflection, mm
BT₄, 50k	30.8	0.62	24.6	1.8
UT₄, 50k		0.31	27.5	1.9
BT₇, 50k	53.9	1.08	29.7	2.6
UT₇, 50k		0.54	32.9	2.1

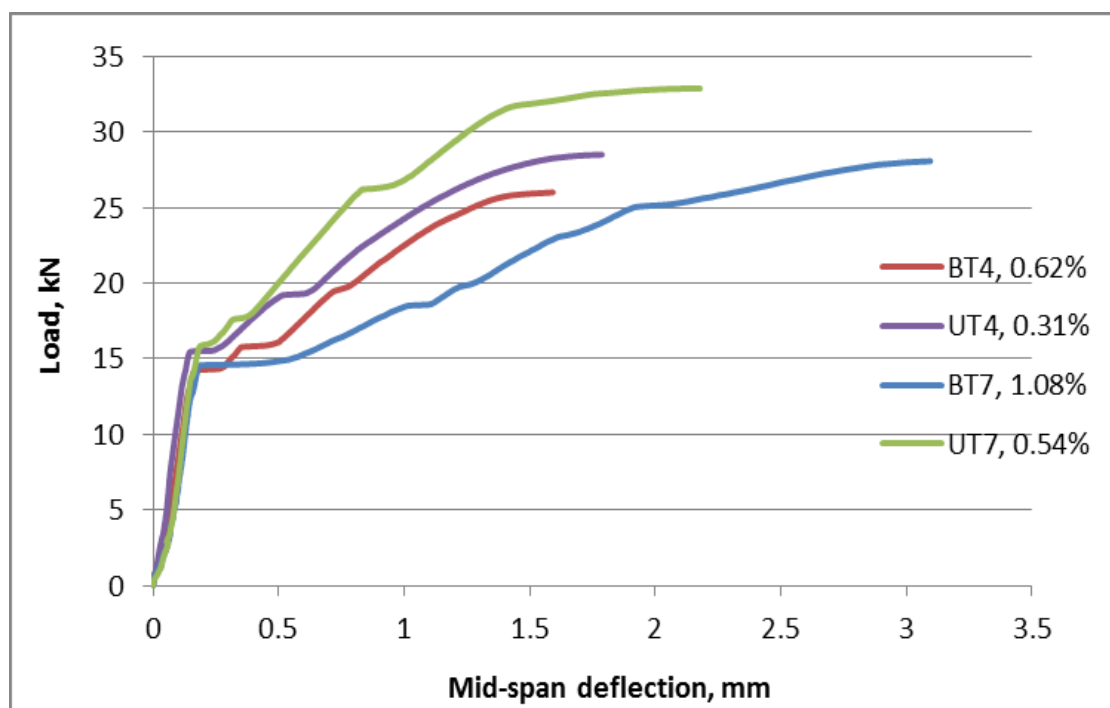


Figure 5-2 Load-deflection behaviour at mid-span of textile reinforcement with and without weft rovings.

From the figure, it can be said that the textile without weft rovings exhibits a stronger capacity in comparison with the textile with weft rovings. Both UT₄ and UT₇ provide high initial strength at the first crack as a result of good bonding which is attributed to good contact between matrix and fibre.

5.1.7 The effect of the volume fraction

Many studies (Contamine *et al.* 2010; Hartig *et al.* 2010; Silva *et al.* 2011) have investigated the performance of textile reinforced concrete (TRC) in terms of mechanical behaviour. In most of these studies, volume fraction of fibre V_f is used to express the quantity of fibre in the concrete member and the capacity (load and deflection) of textile-reinforced concrete beams which has been shown to increase with increasing volume fraction of the fibre (Papanicolaou and Papantoniou 2010). However, Abdulmajeed *et al.* (2011) found that an increase in volume fraction of fibre will not necessarily lead to

an increase in the flexural strength of the composite. Therefore, it appears that the use of volume fraction as a design parameter may actually result in inefficient design. Basically, volume fraction-based approaches consider all the fibres in the concrete member, regardless of fibre orientation. This approach may be fundamentally incorrect, as in TRC, some of the fibres (those acting perpendicular to the span of the beam and those in the middle of the batch of fibres) are not utilized in resisting loading. Table 5-6 (previous section) shows the results for different volume fractions for the same cross sectional area on the ultimate load. It can be seen that there is an insignificant effect of increasing volume on the improvement of the ultimate load. The volume fraction of BT₄ is 0.62% and of UT₄ is 0.31% at the same cross sectional area, however, there is no increase in the ultimate flexural load, although, the volume fraction is doubled. Contrarily, the ultimate flexural load decreased due to the increase in volume fraction for the same area which can be accounted for by the reduction in the penetration due to the increase in unnecessary fibre which leads to increased volume fraction, and possible congestion. Exactly the same effect was observed for BT₇ at 1.08% and UT₇ at 0.54%; the ultimate flexural load decreased as a result of increased volume fraction for the same area. Therefore, it can be concluded that ultimate load does not appear to be linearly related to the volume fraction parameter, which has been traditionally used in fibre reinforced concrete (FRC) design. In fact, the results show that increasing the amount of fibre whilst keeping the same cross sectional area of reinforcement may actually lead to a reduction in the ultimate flexural load of a beam.

5.1.8 The effect of the cross sectional area

As mentioned in the previous section, using a volume fraction based approach may lead to incorrect design in TRC. Therefore, this section will investigate the relationship between the mechanical behaviour of TRC beams and the cross sectional area-based parameter in order to illustrate which is more reliable in comparison with the volume fraction parameter. From Table 5-6, it is interesting to note that the improvement in the ultimate load was mainly due to the increase in the cross sectional area. On initial inspection, an increase

in volume fraction does appear to suggest an increase in failure load (i.e. compare UT₄ ($V_f = 0.31\%$) with UT₇ ($V_f = 0.54\%$), the ultimate load increases from 27.5kN to 33.5kN). However, taking a closer look at these results suggests that the orientation of the fibres is more significant than the total volume fraction and that this and the ultimate load is better defined using the cross sectional area approach. For instance, considering beams BT₄ and UT₇, there is a reduction in volume fraction (13%), however, there is an increase in cross sectional area of approximately 75% and an increase in ultimate load of 36%. Again, consider beam BT₄ with $V_f = 0.62\%$ and UT₄ with $V_f = 0.31\%$; these beams have the same area (30.8 mm²) however the ultimate flexural load reduces. Therefore, the cross sectional area based-approach should be considered in the flexural beam design methodology. The volume fraction parameter is suitable for use with fibre reinforced concrete (FRC) which is short and randomly distributed, and where the cross sectional area cannot be calculated. Because of this, the volume fraction should only be used to calculate the quantity of fibre in a beam.

5.1.9 The effect of a change in geometry

One of the advantages of textile reinforcement is that, unlike steel reinforcement, it can be easily formed into different geometries, for example, twisted, braided, or bundled. Figure 5-3 and Table 5-7 show how the different layouts of individual reinforcement elements – straight tows (control), bundled tows (b), braided tows (br) and twisted tows (t) (see Figure 3.21) – affect the ultimate load P_u and load-deflection curve at the same volume fraction and cross sectional area.

When the tow is used as it is, without changing the geometry, as in UT₄, the average ultimate load is 27.5 kN. Nevertheless, when the carbon fibre tows were divided into bundles (UT_{b4}) the ultimate load increased by 18%, therefore, the average ultimate load was raised to 32.7 kN and the ductility was also improved, as shown in Figure 5-3. This can be accounted for by the clear increase in the contact area between the matrix and filaments which agrees with the expectations of Peled, Bentur and Yankelevsky (1998). For

braided tows, three pieces of fibre were intertwined (UT_{br4}). The average ultimate load decreased by 14%. However, the ductility significantly increased to almost double that of UT_4 . Due to the complicated contact, the partial failure in the filaments may explain the decrease in ultimate load and the increase in the deflection. When the carbon rovings were twisted (UT_{t4}) the average ultimate load dropped significantly to *13.75 kN*; a 50% reduction in the ultimate load factor in comparison with UT_4 .

The failure here was brittle, indicating that the arrangement was such that the effective volume fraction of fibre dropped below the critical value (Figure 5-3). The failure suddenly occurred after the concrete began to crack. This can be attributed to the decrease in the contact area and the complexity of the cross section along the rovings. However, the exact behaviour of twisted roving is complicated and not fully understood.

Table 5-7 The bond efficiency factor for various fibre geometries.

Textile Geometry	Area, mm²	V_f, %	Average Ultimate Load, kN	Average Deflection, mm
UT_{t4}, 50k	30.8	0.31	13.8	0.1
UT_{br4}, 50k			23.8	2.6
UT_4, 50k			27.5	1.9
UT_{b4}, 50k			32.7	3.0

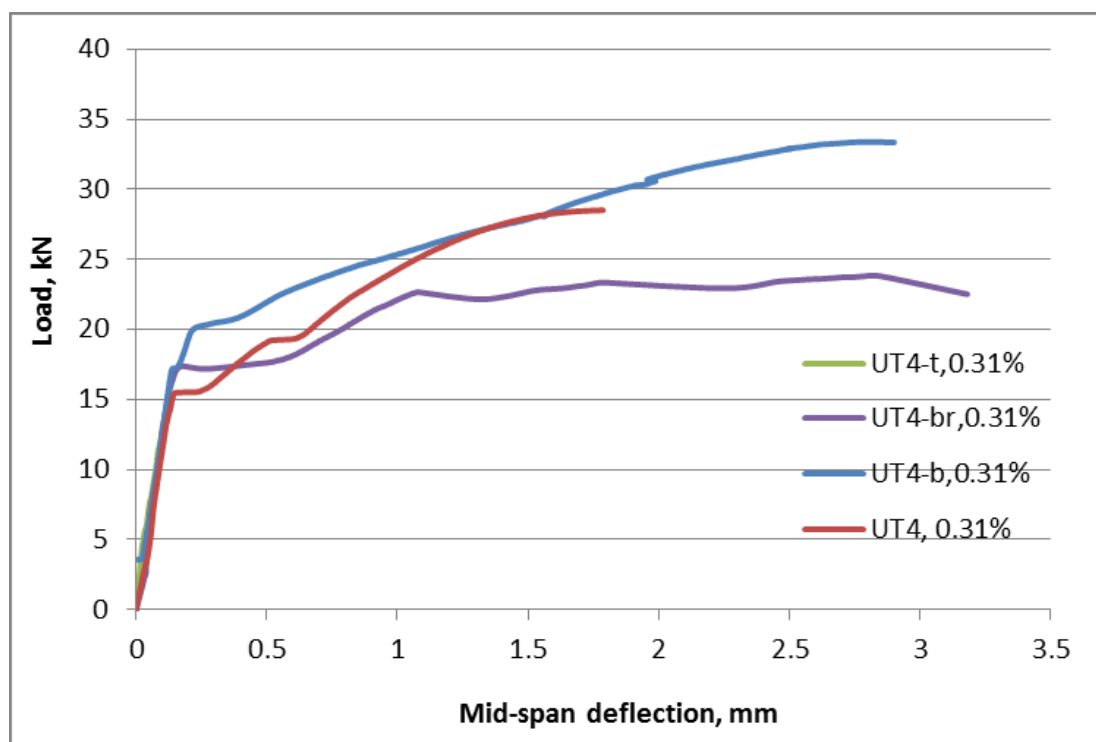


Figure 5-3 Load-deflection curves at mid-span for different roving geometries at the same volume fraction.

The findings confirm the effect mentioned by Peled and Bentur (2000) and Voss *et al.* (2006a) who found that the textile geometry significantly influenced the behaviour of textile reinforced concrete. However, in the case of twisted rovings, the findings are in contrast with the results found by Peled and Bentur (2000).

5.1.10 FRC vs TRC

Fibre reinforced concrete (FRC), unlike textile reinforced concrete (TRC), is normally dispersed randomly without paying attention to where the tensile stresses are located. Therefore, the fibres are not fully exploited as they may be placed in compression zones or orientated in a direction that is not experienced to tensile stresses. Sri Ravindrarajah and Tam (1984) stated that the existence of short fibres in the compression zones of concrete beams does not influence the strength of FRC. On the other hand, Papanicolaou and

Papantoniou (2010) reported that TRC is located at the required stresses which results in an effective utilization. In this section, a comparison will be made between FRC and TRC to investigate the differences in terms of ultimate strength and deflection. From Table 5-8, Figure 5-4, and Figure 5-5, it can be seen that TRC is considerably more efficient than FRC. At $V_f = 0.62\%$ and 1.08% the ultimate load for TRC is nearly double that for FRC which clearly indicates that locating the fibre at the required location provides perfect resistance to the tensile stresses. Also, the ductility of FRC is notably low when compared to TRC. This can be accounted for by the pull out that occurs in FRC once cracking begins. Also, the results confirm that the volume fraction approach is inaccurate for determining the load bearing capacity in comparison with the cross sectional area approach.

Table 5-8 Average ultimate load and deflection of FRC and TRC beams.

Reinforcement	Area, mm ²	V _f , %	Average Ultimate Load, kN	Average Deflection, mm
F-0.62%, 50k	-	0.62	13.4	0.3
BT4, 50k	30.8		24.6	1.8
F-1.08%, 50k	-	1.08	17.0	0.4
BT7, 50k	53.9		29.7	2.6

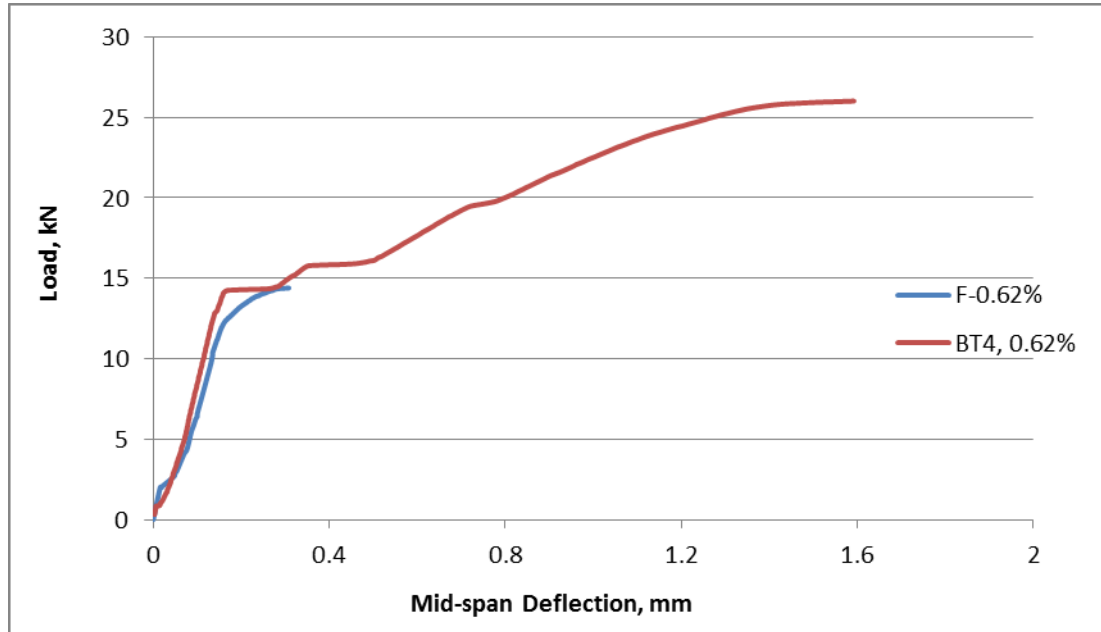


Figure 5-4 Load-deflection behaviour at mid-span of TRC vs FRC at 0.62% volume fraction.

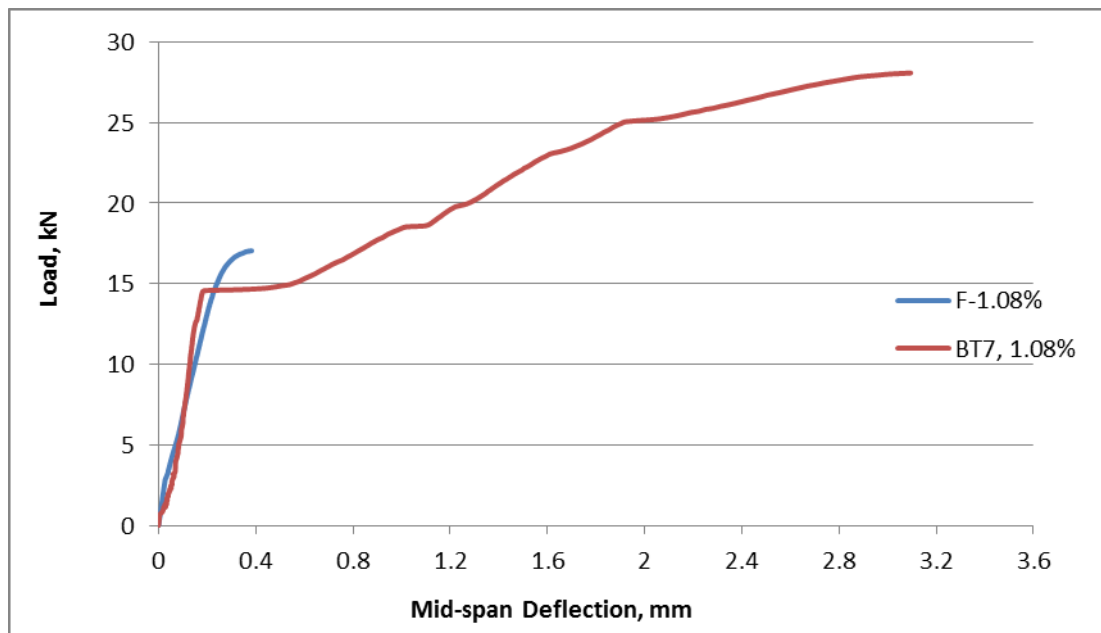


Figure 5-5 Load-deflection behaviour at mid-span of TRC vs FRC at 1.08% volume fraction.

5.2 Influence of reinforcement type

Four different kinds of carbon textile reinforcement were used to reinforce concrete beams. The reinforcement types were bi-axial fabric at 2.5 cm spacing between warps (50k), bi-axial fabric at 5 cm between warps (50k), uni-axial reinforcement (tow) with 50k, and uni-axial reinforcement (tow) with 24k. The comparison between different types of carbon textile reinforcements of the same cross sectional area ($A_r \sim 31 \text{ mm}^2$) is shown in Figure 5-6. It can be seen that the first crack was at around 15 kN, apart from for the beam reinforced by bi-axial reinforcement with 5 cm warp spacing (BT_{8(5cm)}, 50k), which was at 13.5 kN. In addition, the post behaviour of BT_{8(5cm)}, 50k varies from the others which can be attributed to the way that the woven fabrics were piled over one another. Eight fabrics were piled one over the other, which made it hard for the matrix to penetrate the filaments and resulted in an increase in the number of filaments that were not directly in contact with the matrix. Once the crack occurred, because there were 8 fabrics, this caused free movement of the inner fabric that had a weak bond with the matrix. With increased load, the inner fabrics began to resist the applied load which interprets the improvement in the capacity of BT_{8(5cm)} after it is dropped when the crack occurred.

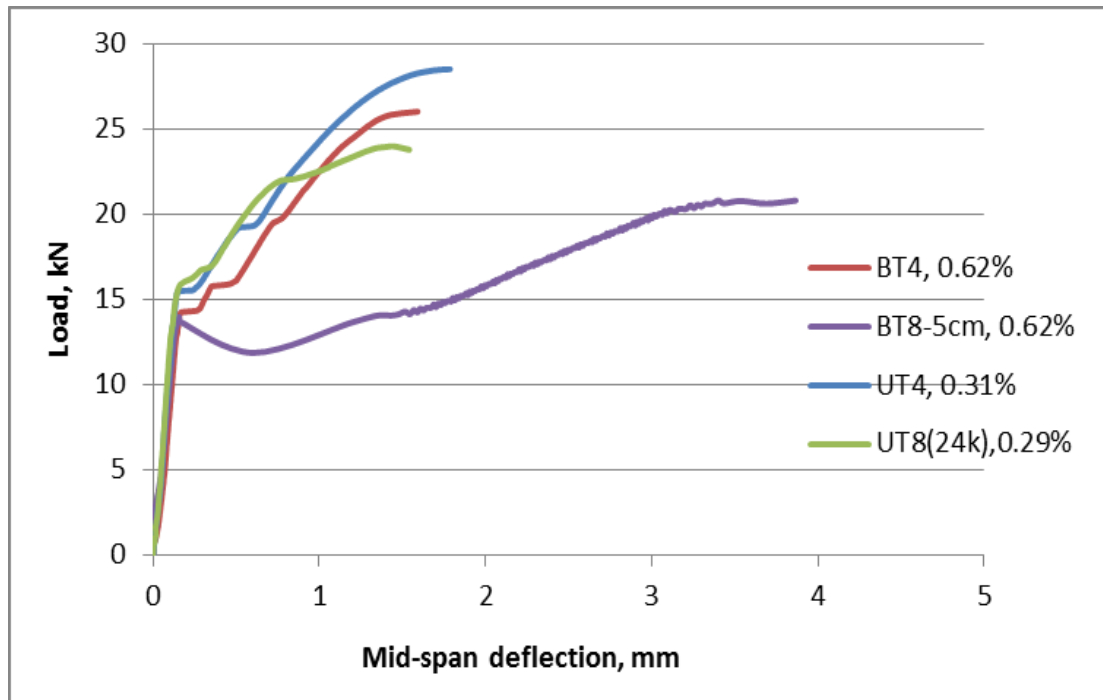


Figure 5-6 Load-deflection behaviour at mid-span of different types of reinforcement of the same area.

On the other hand, the rest of the beams behaved similarly with little difference in the ultimate load. The differences are also a result of the bond. The increase in the number of filaments that are in contact with the matrix leads to an increase in the capacity which can be seen in the figure. UT₈, 24k had the lowest ultimate load, because of the number of tows laid over each other (8 tows), followed by BT₄, 50k, due to stitching in the warp direction which logically reduced the penetration. Clearly, it can be concluded that, once the area of textile in contact with the matrix is increased, the bond is increased as a result of this improvement in the contact area. Thus, the bond is a vital factor in TRC behaviour. Also, TRC capacity increases as a result of enhanced bonding which leads to better utilization of textile properties.

5.3 Large scale beam

In this section, a large scale beam ($120\text{ mm} \times 200\text{ mm} \times 2600\text{ mm}$) will be investigated to gain a better understanding of textile reinforced concrete behaviour. Different parameters, such as cover thickness, anchorage, and variable layouts, were considered. Most beams cover thicknesses were 30 mm unless otherwise stated. Normal concrete was used in order to be more industrial.

5.3.1 The effect of anchored roving

The straight and anchored textile reinforced concrete beams were tested in order to study the performance of the beam. Table 5-9 shows the flexural results of straight and anchored reinforcement at the same cross sectional area. The reinforcement details are shown in Figure 5-7, with the reinforcement laid down in one layer. From Table 5-9, it can be seen that the loading capacity of UT₈-Anch-2.6 is increased as a result of anchoring the reinforcement. The load of UT₈-Anch-2.6 increased by 24% to 16.5 kN in comparison with UT₈-2.6 in which the reinforcement is straight. The result was expected as the filaments were prevented from slipping freely due to the anchoring of the tows. In UT₈-2.6, the tows slipped due to the flexural loading which led the tows to maintain the same length. The slipperiness could be attributed to the straight end of the reinforcement which was not able to produce development length, the small contact area between matrix and reinforcement, and the fine texture of the carbon fibre.

Table 5-9 Straight and anchored textile reinforced concrete.

Reinforcement	Area, mm ²	V _f , %	Ultimate Load, kN	Deflection, mm
UT ₈ -2.6, 50k	61.5	0.25	13.8	9.0
UT ₈ -Anch-2.6, 50k	61.5	0.25	16.5	11

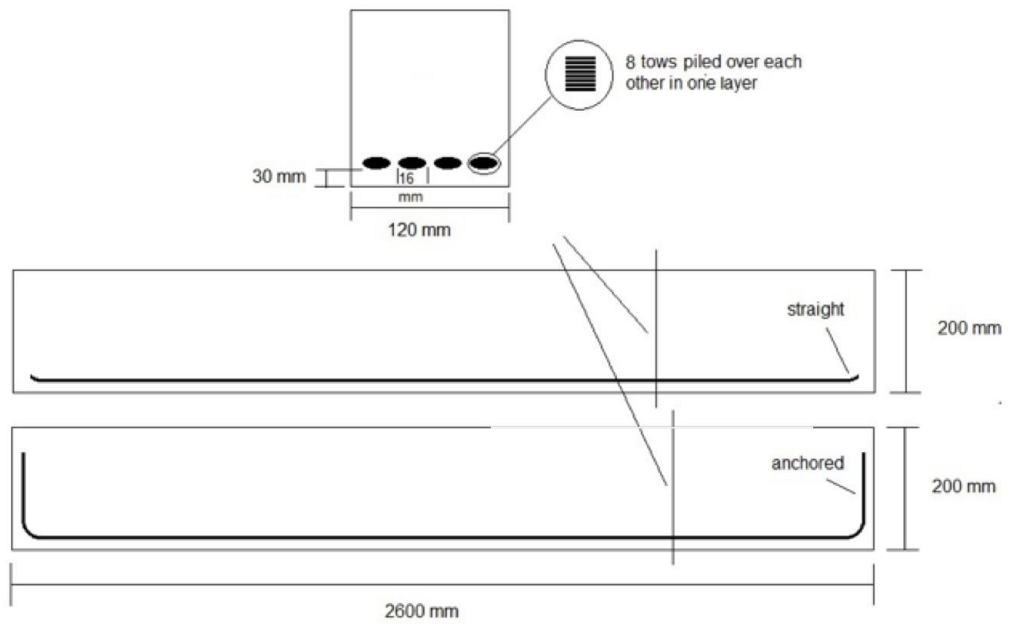


Figure 5-7 Reinforcement details of T₈, straight and anchored.



Figure 5-8 UT₈-Anch-2.6 cracks.

However, even for UT₈-Anch-2.6 the ultimate carbon fibre strength was not exploited because of delamination failure, as can be seen in Figure 5-8. The delamination crack is dominating the crack behaviour which is a result of piling the rovings over each other. This will be discussed in the next section.

5.3.2 The effect of layering

As shown in the previous section, UT₈-Anch-2.6 failed at an early stage of loading because the tows were over each other and this caused penetration difficulty and reduction in the contact area with the matrix. Therefore, at the same cross sectional area, the tows were divided into two layers and each layer had a number of tows (4 tows), which were laid over each other, and 4 horizontal uniaxial directions. Also, to improve our understanding of the effect of layering, which will increase the contact area, the tows were divided into three layers and three horizontal uniaxial directions, see Figure 5-9. The thickness of the tows was considered to be negligible in the effective depth calculation. Theoretically, the bearing load capacity will reduce as a result of reduction in the effective depth (d). However, the experimental results show that the layering and reforming of the reinforcement layouts improved the ultimate flexural load of TRC. Table 5-10 shows that UT₁₂-Anch-3L₃-2.6 exhibited the highest capacity in terms of strength and deflection. It was increased by 18%, while UT₈-Anch-L-2.6 was increased by 10% in comparison with UT₈-Anch-2.6, and all of them were anchored. Also, ductility was improved because of the reinforcement layering. Therefore, the bearing capacity was increased due to dividing the textile tows into layers, although, the effective depth was reduced because of the layering. This can be accounted for by the increase in the fibre contact area with the concrete matrix. The separation of tow reinforcement into two or three layers leads to an increase in the exposed filaments that are able to make contact with the concrete which improves the bond, therefore, the number of inner filaments is decreased. Also, dividing the tow reinforcement into three horizontal direction instead of 4 makes it possible to spread the width of the roving to *20 mm* instead of *16 mm*, as shown in Figure 5-9. This also increased the exposed area which was able to make contact with the matrix. Thus, the increase in

the bond compensates for the reduction in the capacity that was expected as a result of the reduction in the effective depth. In addition, the failure mode changed from delamination in UT₈-Anch-2.6 to flexural failure for UT₈-Anch-L-2.6 and T₁₂-U-Anch-3L₃-2.6. Also, the number of cracks increased to 4 and 5 cracks for UT₈-Anch-L-2.6 and UT₁₂-Anch-3L₃-2.6, respectively. This change in the crack behaviour provides assurance that the improvement in the bond between filaments and matrix is crucial.

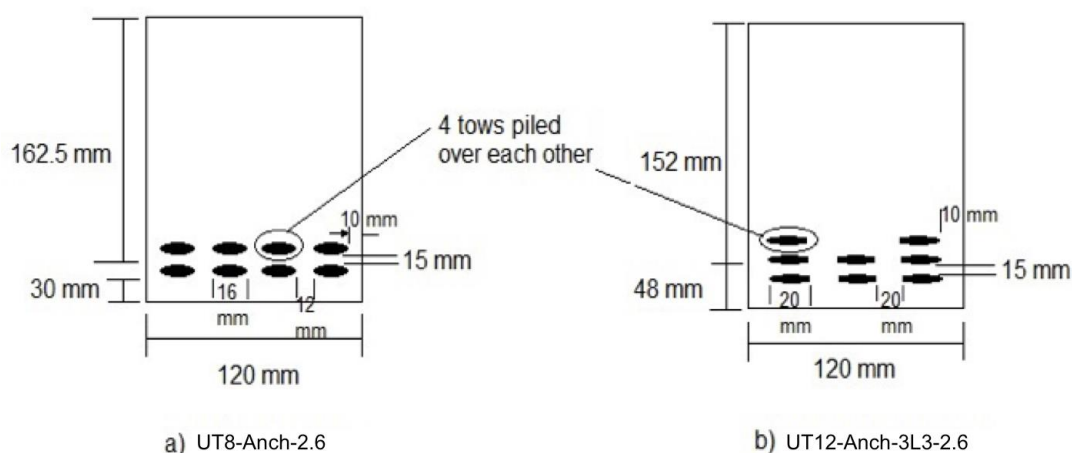


Figure 5-9 Reinforcement details of UT₈-Anch-2.6 and UT₁₂-Anch-3L₃-2.6.

Table 5-10 Results for TRC with different layers of the same cross sectional area.

Reinforcement	Area, mm ²	V _f , %	Ultimate Load, kN	Deflection, mm
UT ₈ -Anch-2.6, 50k	61.5	0.25	16.5	11
UT ₈ -Anch-L-2.6, 50k	61.5	0.25	18.2	15.6
UT ₁₂ -Anch-3L ₃ -2.6, 50k	61.5	0.25	19.5	16

5.3.3 The effect of volume fraction

The influence of the volume fraction of fibre on the behaviour of TRC was discussed with regard to the small scale beam (section 5.1.7). The results have shown that there is no effect due to increasing the volume fraction V_f , in fact, the capacity decreased as a result of increased volume fraction of the same cross sectional area. In order to confirm that there is no effect of V_f on TRC behaviour, different amounts of V_f were studied on a large scale beam. Table 5-11 provides the experimental results of changing the volume fraction (V_f). $BT_{(5cm)14}$ -Anch-L-2.6 is a bi-directional carbon textile reinforcement with 5 cm warp spacing reinforced concrete beam. It is apparent from this table that the volume fraction has no effect on the bearing capacity. In fact, the ultimate flexural load of $BT_{(5cm)14}$ -Anch-L-2.6 was significantly lower when compared to UT_8 -Anch-L-2.6. The volume fraction was increased by 128%, however, the load did not increase. This increase caused fibre congestion which prevented the concrete from penetrating and making contact with the filaments. Also, the stitch of warp direction can be added as another reason for this fall in capacity. In addition, the weft direction shows no influence on the beam performance. Accordingly, the use of bi-axial reinforcement to reinforce concrete is a waste of resources. The initial crack load was also lower which confirms that the bond between matrix and fibre was weak. Consequently, there is no sign of transferred stresses from concrete into textile reinforcement.

Therefore, the volume fraction of fibre must not be used to determine the flexural load of textile reinforced concrete. Unlike short fibre, the cross sectional area of continuous fibre can be calculated, which provides a more reliable parameter for design than volume fraction.

Table 5-11 Result of changing volume fraction.

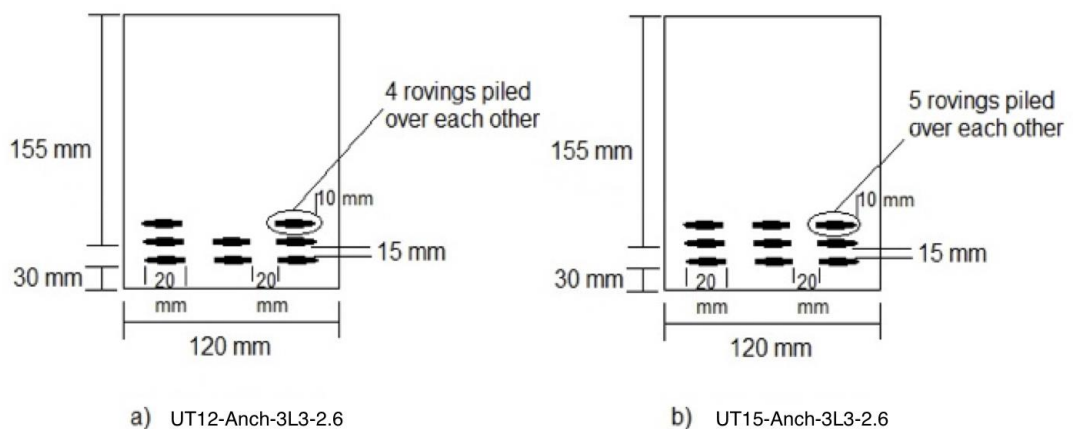
Reinforcement	Area, mm ²	V _f , %	Initial Crack Load, kN	Ultimate Load, kN	Deflection, mm
UT ₈ -Anch-L-2.6, 50k	61.5	0.25	13.0	18.2	15.6
BT _{(5cm)14} -Anch-L-2.6, 50k	80.7	0.57	11.4	11.8	14.5

5.3.4 The effect of cross sectional area

The cross sectional area of filaments in the direction of loading has a significant effect on the behaviour of TRC, as discussed in the small scale beam section (5.1.8). The same concept is applied here for large scale beams to show that the cross sectional area parameter should be used to compute the flexural properties. The results obtained from the experimental test are shown in Table 5-12. It can be clearly seen that the increase in the cross sectional area (A_f) leads to a considerable improvement in the load bearing capacity. The cross sectional area increased by 50%, and the ultimate flexural load increased by 100% which is double the load of UT₁₂-Anch-3L₃-2.6. As a result of the increase in load capacity, the ductility also improved. Also, 50% increase in the area significantly raised the initial crack load by 26%. Therefore, the results proved that the area of reinforcement is one of the main parameters that should be taken into account in the study of TRC behaviour. However, the textile reinforcement layout (see Figure 5-10) should not be neglected as it played a noticeable role in increasing the contact area of the fibre with the matrix.

Table 5-12 Results for increased cross sectional area.

Reinforcement	Area, mm ²	V _f , %	Initial Crack Load, kN	Ultimate Load, kN	Deflection, mm
UT ₁₂ -Anch-3L ₃ -2.6, 50k	61.5	0.25	14	19.5	16
UT ₁₅ -Anch-3L ₃ -2.6, 50k	92.3	0.37	17.7	39.3	23.6

Figure 5-10 Reinforcement details of UT₁₂-Anch-3L₃-2.6 and UT₁₅-Anch-3L₃-2.6.

In addition, the number of cracks changed noticeably. For UT₁₂-Anch-3L₃-2.6, the number of cracks before failure was 5, while for UT₁₅-Anch-3L₃-2.6 this jumped to 13 major cracks. Thus, it can be said that the increase in the cross sectional area of reinforcement with proper layout can produce excellent TRC behaviour, as shown in Figure 5-11.

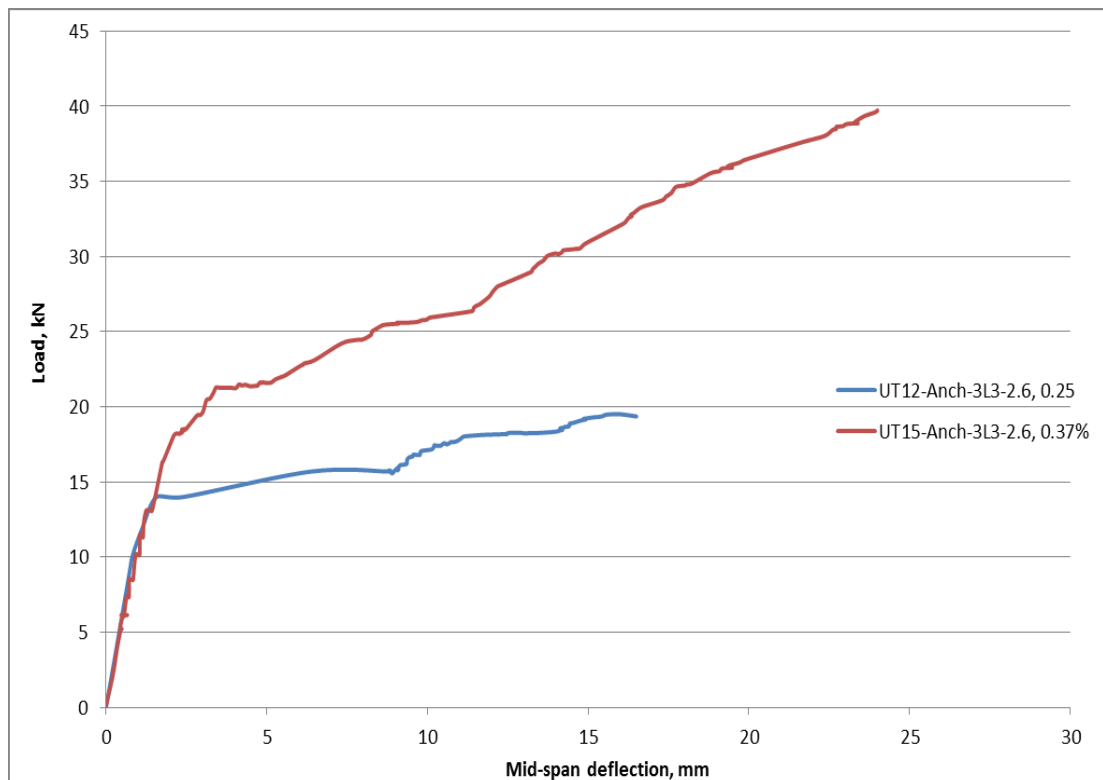


Figure 5-11 Load-deflection behaviour at mid-span of UT₁₂-Anch-3L₃-2.6 and UT₁₅-Anch-3L₃-2.6.

5.3.5 The effect of increase in the number of tows at the same layer

An increase in the number of tows at the same layer means an increase in cross sectional area. This section will study how the increase in the number of tows at the same layer can influence the flexural properties. Reinforcement details of the textiles used in this study are shown in Figure 5-12. The experimental results for textile reinforced concrete with different numbers of tows at the same layer are presented in Table 5-13. As this table shows, adding more reinforcement without considering the proper layout produces undesirable results. Although, the cross sectional area is increased in UT₁₂-Anch-L-2.6, the ultimate flexural load is reduced. These results can be

accounted for by the increase in the number of filaments (inner filaments) which are not in direct contact with concrete. However, the outer filaments is the same with UT₈-Anch-L-2.6 as there is no significant change in the number of outer filaments that are in direct contact with the concrete. Therefore, as the loading increased, the inner filaments slipped which explains the higher deflection of UT₁₂-Anch-L-2.6. Also, as can be seen from Table 5-13, the initial crack load dropped due to the increase in the number of tows at the same layer, therefore, the increase in the number of the inner filaments which may indicate a reduction in the bond between the fibre and matrix. Accordingly, if the textile layout is not well designed with a view to exposing more fibre surface to the concrete, adding more layers will not enhance the load capacity of TRC.

Table 5-13 The effect of increasing the thickness of roving/tow.

Reinforcement	Area, mm²	V_f,%	Initial Crack Load, kN	Ultimate Load, kN	Deflection, mm
UT₈-Anch-L-2.6, 50k	61.5	0.25	13.0	18.2	15.6
UT₁₂-Anch-L-2.6, 50k	92.3	0.37	9.7	16.2	17

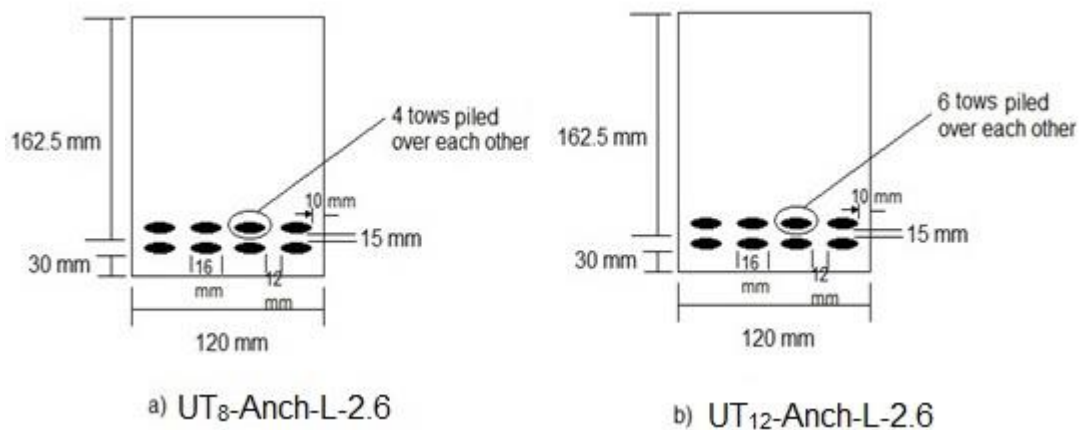


Figure 5-12 Reinforcement details of UT₈-Anch-L-2.6 and UT₁₂-Anch-L-2.6.

5.3.6 The effect of cover thickness

One of the advantages of textile reinforcement is corrosion resistance which means the cover thickness can be decreased. This reduction in thickness saves money as a result of a reduction in the required quantity of concrete. However, the effect of reducing or increasing the cover thickness on the flexural behaviour of textile reinforced concrete is not clear, so this section investigates the effect of cover thickness. Table 5-14 presents the results obtained from the experimental test for different cover thicknesses of TRC. The notations C15 and C60 stand for *15 mm* and *60 mm* cover thickness, respectively. Reinforcement details and cover thickness are illustrated in Figure 5-13. The cover thickness for UT₁₅-Anch-3L₃-2.6 is *30 mm*. From the table it can be seen that the load bearing capacity is negatively affected by increasing or decreasing the cover thickness.

Table 5-14 Flexural results for different cover thicknesses.

Reinforcement	Area, mm ²	V _f , %	Ultimate Load, kN	Deflection, mm
UT ₁₅ -Anch-3L ₃ -2.6, 50k	92.3	0.37	39.3	23.6
UT ₁₅ -Anch-3L ₃ -2.6-C15, 50k	92.3	0.37	32.5	22.7
UT ₁₅ -Anch-3L ₃ -2.6-C60, 50k	92.3	0.37	21.5	16.7

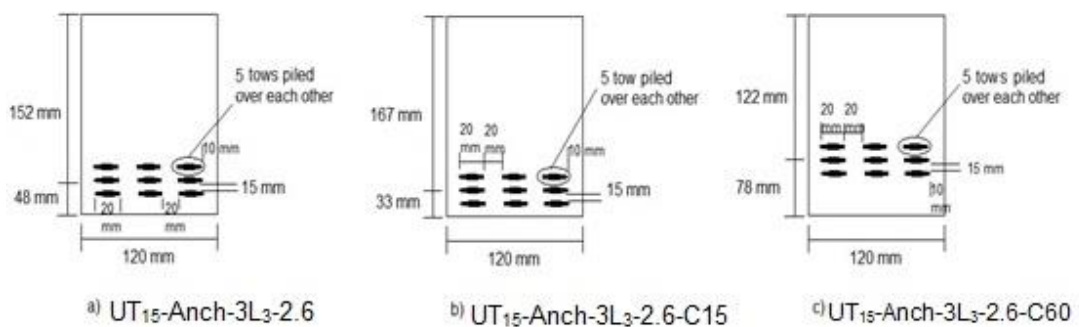


Figure 5-13 Different cover thicknesses of textile reinforcements.

For UT₁₅-Anch-3L₃-2.6-C15 the ultimate flexural load decreased by 17% in comparison with that for UT₁₅-Anch-3L₃-2.6. The same layout geometry was applied apart from the cover thickness which was 15 mm. Theoretically, the load capacity could be expected to increase because of the increase in the effective depth to 167 mm rather than 152 mm. A possible explanation for this result may be the lack of adequate bonding due to the small cover thickness. Therefore, the textile is unable to reach the ultimate tensile stress because of the bond reduction. On the other hand, the load for the thick cover UT₁₅-Anch-3L₃-2.6-C60 was considerably lower. The load dropped by 45% relative to the beam has 30 mm cover thickness (UT₁₅-Anch-3L₃-2.6). The bond issue

regarding cover thickness does not exist, therefore, this result may be explained by the fact that the reduction in the effective depth leads to a reduction in the load capacity of the reinforced beam.

From Figure 5-14, it can be seen that the initial crack is also influenced by the thickness or thinness of the concrete cover. It is clear that the thick cover has the lowest initial crack load. It seems possible that this result is due to the fact that 60 mm from the bottom of the tension zone of a loaded beam is unreinforced. This means that once the concrete reaches the cracking moment it will begin to crack, until cracks approach the textile reinforcement, then the load is transferred to the reinforcement. On the other hand, the initial crack load of the thin cover (15 mm) is also lower than 30 mm cover but higher than 60 mm . This observed decrease in the first cracking load could be attributed to the reduced bond due to the thin cover.

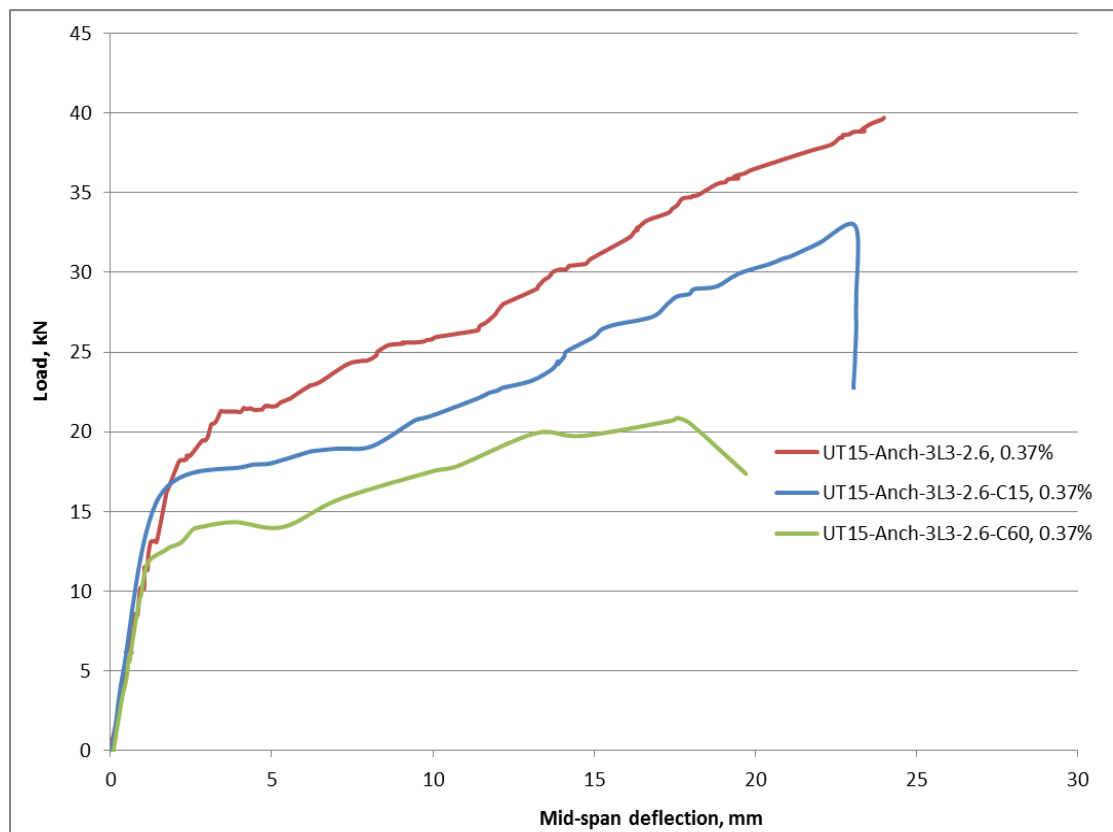


Figure 5-14 Load-deflection behaviour at mid-span of TRC with different cover thicknesses.

The cover thickness also affects the behaviour of the cracks in terms of their number and width. Figure 5-15 demonstrates the crack pattern of UT₁₅-Anch-3L₃-2.6-C15 and UT₁₅-Anch-3L₃-2.6-C60. It can be clearly seen that the thin cover is more cracked than the thick cover, with 9 cracks for the 15 mm cover and 6 for the 60 mm cover, while the number of major cracks for the 30 mm cover was 13, which represents a good bond. In addition, the crack width is smaller for UT₁₅-Anch-3L₃-2.6-C15 than for UT₁₅-Anch-3L₃-2.6-C60, which is as expected because the increase in the cover thickness leads to wider crack widths.

Therefore, it can be said that the 30 mm concrete cover is the optimum thickness of TRC as it seems to provide the proper and required bond to enable textile reinforcement to maximize the utilization of the tensile stress of reinforcement which results in high flexural resistance to the applied load.

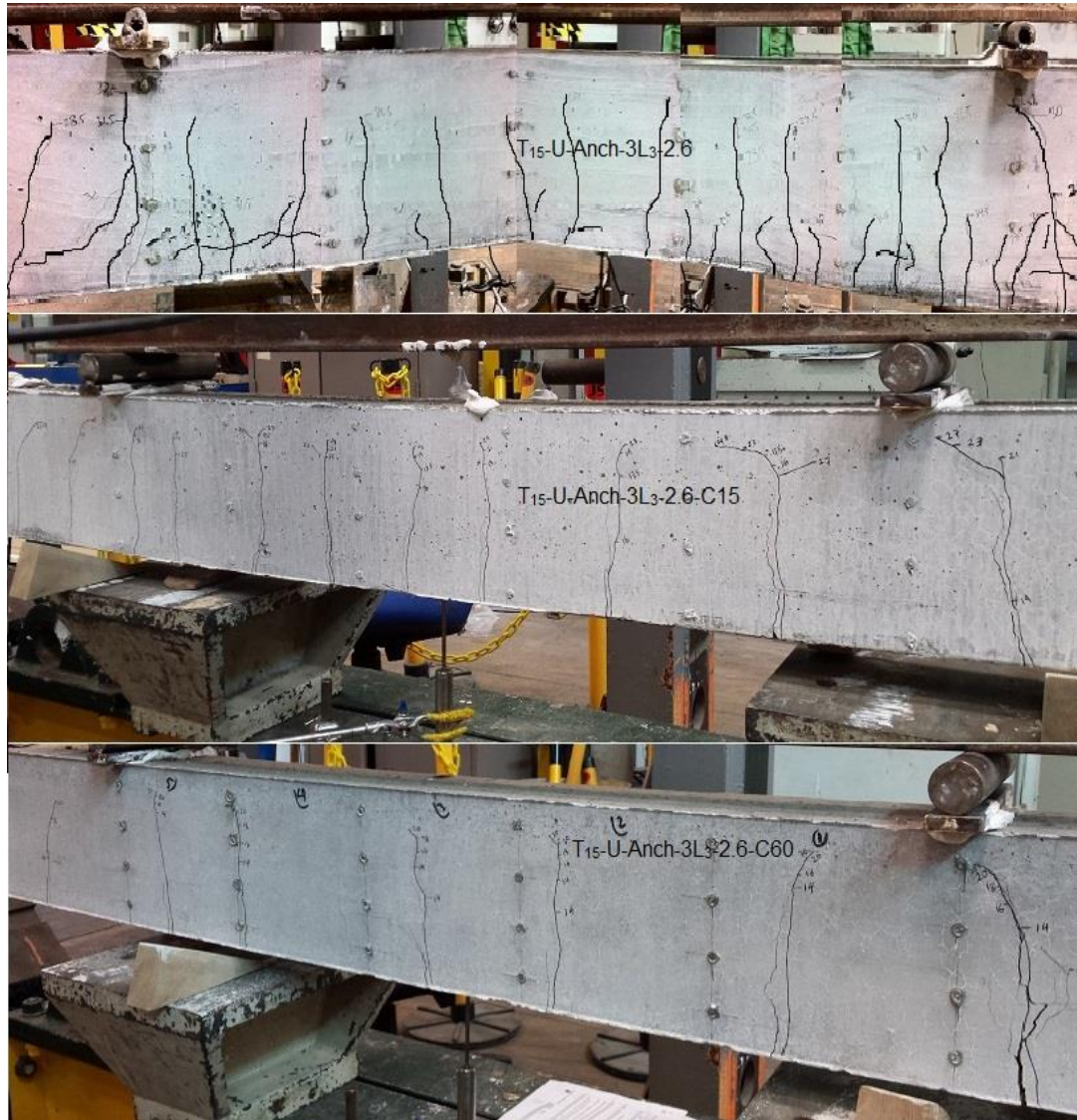


Figure 5-15 Cracking pattern of TRC with different cover thicknesses.

5.4 Conclusions

This section summarises the main findings in this chapter as follows:

- This study has shown that the tensile strength of a roving is significantly lower than that of a single filament.
- The pull out strength of TRC is considered to be low as a result of the slippage which occurs in the inner filaments.

- The geometry and layout of carbon textile reinforcement in TRC could negatively or positively influence its performance. An example of a positive effect is that the layering reinforcement increases the capacity as a result of increasing the contact area.
- Increasing the cover thickness leads to an increase in the bond strength around the carbon textile reinforcement.
- Bundling the roving notably increases the capacity.
- Anchoring the reinforcement at the end activates more filaments to resist the load because it prevents them from slipping.
- A large increase in volume fraction or cross sectional area of reinforcement without adjusting the layout may lead to a decrease in capacity as a result of an increase in inactivated filaments.
- Twisting the reinforcement reduces the capacity significantly.
- Comparison between different types of textile shows that tow reinforcement exhibits higher ultimate load which can again be attributed to the increase in the bond.
- There was a considerable difference between the TRC and FRC beams at the same volume fraction in favour of TRC. Placing the fibres where the tensile stress is present almost doubled the capacity at the same volume fraction.

CHAPTER 6

TEXTILE REINFORCED CONCRETE (TRC) BEAM VERSUS STEEL REINFORCED CONCRETE (SRC) BEAM

In the previous chapter, the effect of several parameters on the performance of TRC beams was discussed. In this chapter, the performance of TRC beams will be compared with conventional SRC beams. The load-deflection behaviour of TRC and SRC beams, its stiffness and cracking behaviour, will be the main performance criteria used in the comparison.

6.1 Flexural behaviour

In this section a comparison between TRC and SRC load-deflection behaviour will be made. The comparison will be in terms of moment curvature, stiffness, toughness, and cracks.

6.1.1 Moment curvature

For a large scale beam ($120\text{ mm} \times 200\text{ mm} \times 2600\text{ mm}$) and using an area of textile reinforcement, $A_t = 92.3\text{ mm}^2$, and steel reinforcement, $A_s = 100.5\text{ mm}^2$, the experimental moment-curvature curve of a TRC beam and SRC beam can be generated by measuring concrete strain, reading Demec points which are periodically taken at different load stages (see Figure 6-1). The beam curvature at each load stage can be calculated by dividing strain over neutral axis depth ($\frac{\epsilon_c}{x}$), as shown in Figure 6-2. Therefore, from the moment and the curvature at different loads, the moment-curvature curve can be drawn, as shown in Figure 6-3.

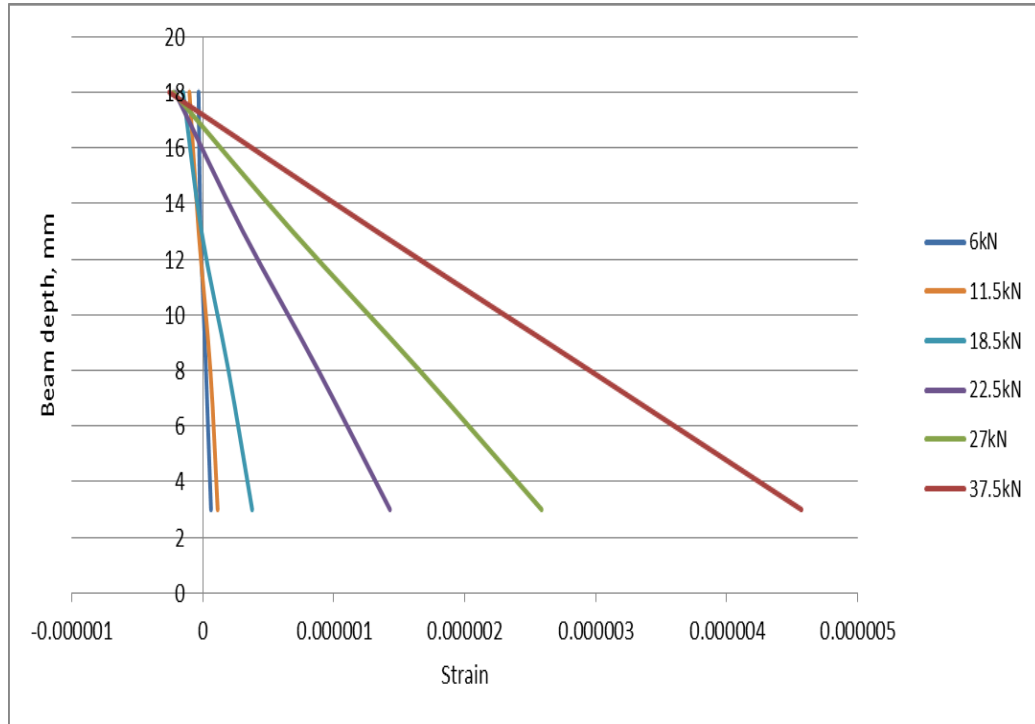


Figure 6-1 Surface strain of TRC beams obtained by reading demec points.

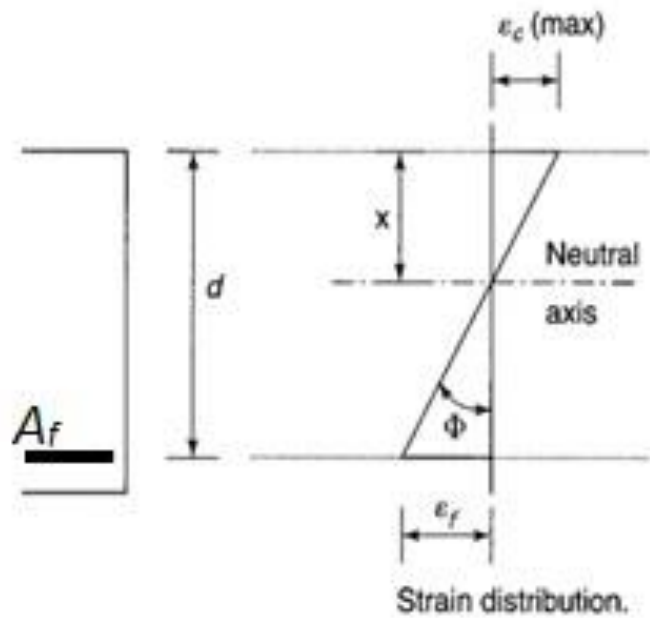


Figure 6-2 Calculation of beam curvature.

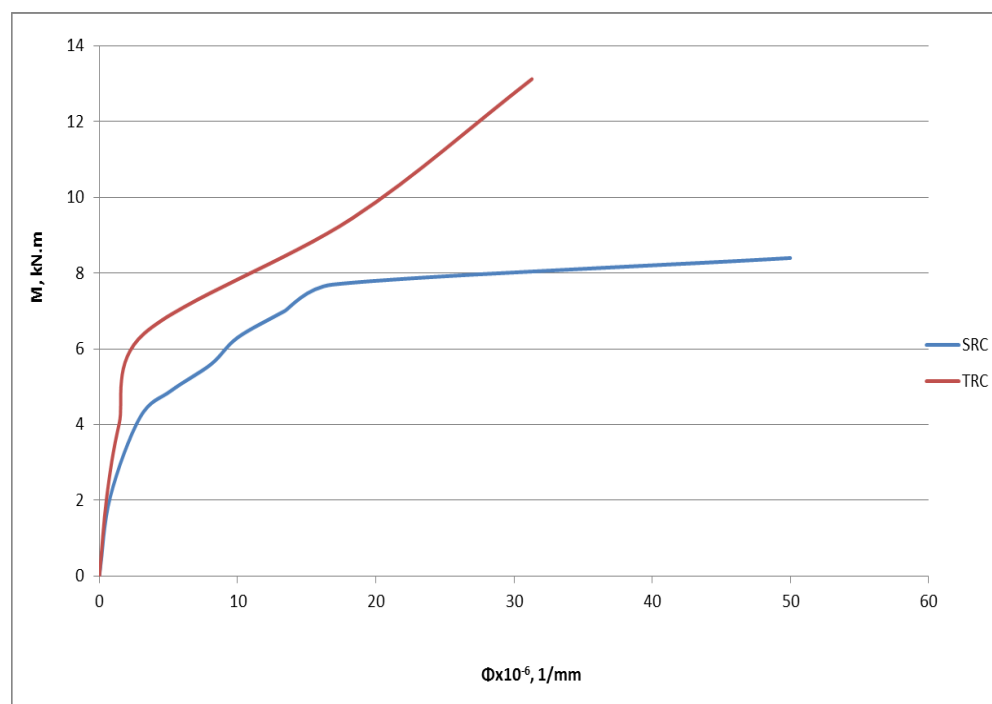


Figure 6-3 Moment-curvature relationship of TRC and SRC beams.

By comparing the SRC and TRC moment-curvature in Figure 6-3, it can be seen that the SRC beam exhibits significantly more plasticity after yielding. However, the TRC beam moment capacity is greater than that of the SRC beam. It can be said that the moment-curvature behaviour is similar until the cracking point of the SRC. Then, at the cracking formation region the behaviour of the TRC beam exhibits a higher stiffness than the SRC beam. At yielding point (lower than 8 kN.m), the TRC beam curvature is lower than that of the SRC beam by 50%. The SRC beam shows an increase in ductility at the same load, however, the TRC beam exhibits a higher stiffness relative to the SRC as it continues to increase in strength capacity with increase in ductility until the failure load. At the ultimate load of both TRC and SRC beams, the TRC curvature is lower than SRC by 37%, however, the TRC strength is higher by 56%. By comparing the curvature at the ultimate moment of SRC and TRC, it can be said that the stiffness of TRC is significantly higher than that of SRC. TRC therefore resists higher moment with lower curvature which can be accounted for by the high tensile strength of the textile and its lower strain formation.

6.1.2 Comparison of TRC and SRC beams containing identical reinforcement areas

In order to make an accurate comparison between the TRC and SRC beam performance, the same areas of reinforcement were used for both steel and textile reinforcements. Figure 6-4 shows the behaviour of uniaxial reinforcement (tow) and steel reinforced concrete beams with the same area $\sim 50 \text{ mm}^2$. The beams are considered to be small scale beams ($100 \text{ mm} \times 100 \text{ mm} \times 500 \text{ mm}$). From the figure, it can be seen that the SRC beam deflects more than the TRC beam. The TRC beam was less plastic in comparison with the steel reinforced beam. Before cracking, the two beams behaved similarly. The SRC beam first began to crack 14% earlier than the TRC beam. After both beams cracked, both had the same slope during the cracking formation stage until the steel began to yield. At that stage, the SRC beam exhibited high plasticity at nearly the same load, while, the TRC beam curve continued to increase. The TRC beam exhibited what ultimately appeared to be a horizontal shear failure. Figure 6-5 illustrates the crack performance of the uniaxial reinforcement (tow) of a carbon reinforced concrete beam, UT₇, 50k. It can be seen that the failure is a horizontal shear failure. Two flexural cracks were formed with small horizontal cracks at the level of the textile reinforcement. Once the flexural crack occurred, a shear horizontal crack formed. After increasing the applied load, the two cracks widened and the horizontal crack lengthened mostly towards the support. Then, and because of the separation between reinforcement and matrix, the failure occurred between the textile reinforcement and concrete above the reinforcement as a result of the weak bond which can be attributed to the thin cover thickness and low matrix penetration due to piling the tows over each other. Because of that, there were a high number of filaments (inner filaments) not in contact with the surrounding concrete which resulted in them not being activated to resist any of the internal forces. The textile reinforcement after failure was still holding the beam which implies that the inner filaments were intact. Therefore, this behaviour (as seen in Figure 6-4 and the reinforcement method) is not representative of true ultimate load and deflection. However, it can be seen that the first crack of the TRC beam is higher than that of the SRC beam by

nearly 15%. Also, at service loads, the TRC beam slope curve is similar to that of the SRC beam, however, it deflects lower than the SRC beam.

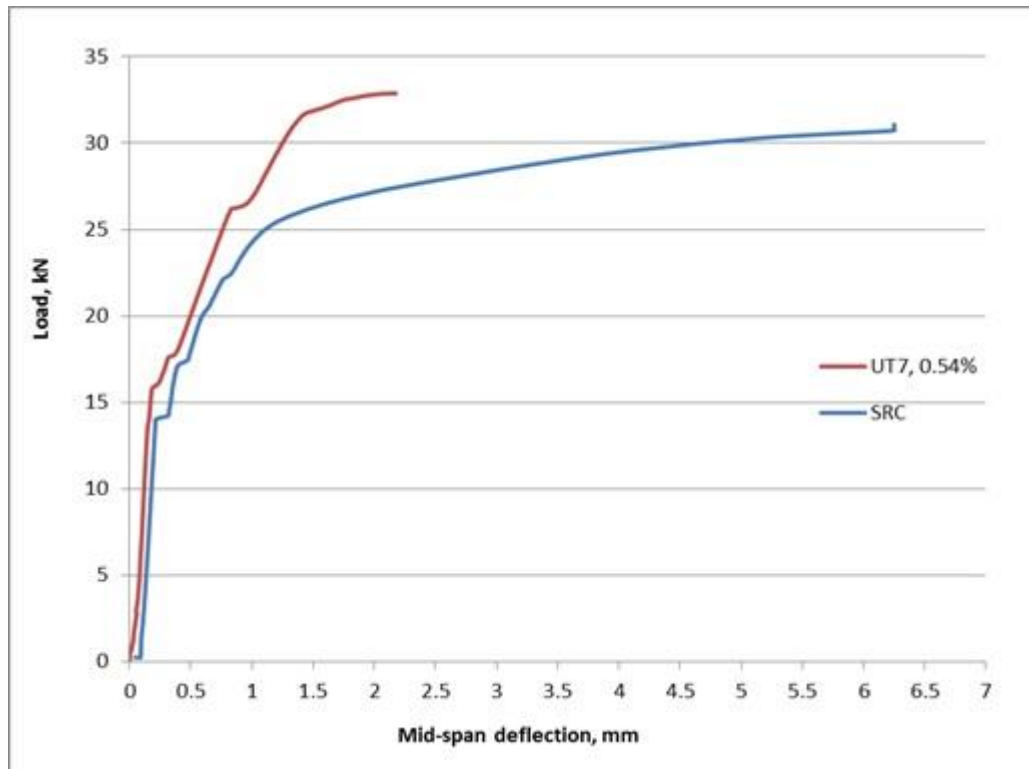


Figure 6-4 Load-deflection behaviour at mid-span of uniaxial tow and steel reinforced concrete beams of the same area.



Figure 6-5 Failure mode of UT₇,50k.

Figure 6-6 shows the deflection behaviour of large scale beams ($120\text{ mm} \times 200\text{ mm} \times 2600\text{ mm}$). The beams were reinforced with either uniaxial reinforcement of carbon (tow) or steel reinforcement. The area of reinforcement was nearly the same ($A_f = 92.3\text{ mm}^2$ and $A_s = 100.5\text{ mm}^2$). It is apparent from this figure that the ultimate flexural load capacity of the carbon tow reinforced concrete beam is considerably higher than that of the steel reinforced beam. UT₁₅-Anch-3L₃-2.6 strength capacity is approximately 60% greater than for the SRC beam. In addition, the TRC beam exhibits higher stiffness than the SRC beam. The figure shows the steel reinforced beam is more plastic at post cracking formation. It can be seen that the ultimate deflection of UT₁₅-Anch-3L₃-2.6 is lower than for the SRC beam by 40%. This is due to the yielding deformation of the steel reinforcement. From the figure, the ultimate steel reinforcement strength becomes steady after reaching yielding strength until the failure point is reached, which is controlled by the ultimate strain of the steel. Meanwhile, for the carbon reinforced beam, the beam strength continues to increase after all the primary cracks have occurred until the failure point which is controlled by the ultimate strain of the textile reinforcement. However, the deflection at the service loads of the TRC beam is lower than for the SRC beam. The deflection of the TRC beam is nearly 50% lower than for the SRC beam, although both beams have the same slope at service loads.

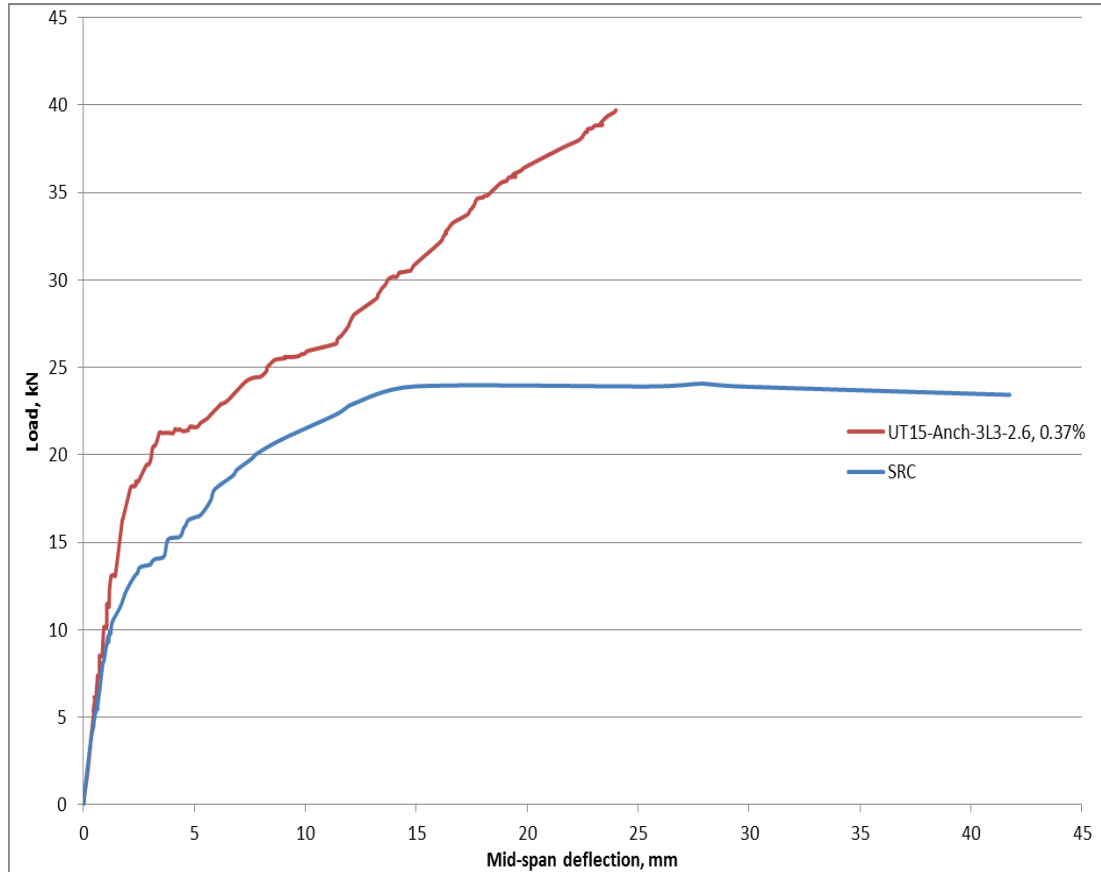


Figure 6-6 Load-deflection behaviour at mid-span of uniaxial reinforcement (tow) and steel reinforced concrete beams.

6.1.3 Comparison of TRC and SRC beams containing identical reinforcement stiffness

An attempt has been made to monitor TRC and SRC beams ($100\text{ mm} \times 100\text{ mm} \times 500\text{ mm}$) containing reinforcement with equivalent stiffness. The axial stiffness of steel and textile reinforcement is represented by EA (where $E = 200\text{ GPa}$ and 235 GPa , and $A = 50.2\text{ mm}^2$ and 42.3 mm^2 for the SRC and TRC, respectively). Hence, the equivalent textile area is as follows:

$$A_s E_s = A_f E_f$$

$$A_f = \frac{A_s E_s}{E_f} \quad (6.1)$$

where,

A_s is the steel reinforcement area;

A_f is the fibre reinforcement area;

E_s is the modulus of elasticity of steel reinforcement;

E_f is the modulus of elasticity of fibre reinforcement.

Figure 6-8 shows the behaviour of the TRC and SRC beams containing reinforcement with the same stiffness. The cross sectional area (A_f) of uniaxial reinforcement of carbon (tow) is 42.3 mm^2 and the area of steel reinforcement is 50.2 mm^2 . From the figure, it can be seen that the ultimate flexural strength failure of both beams is the same, however, the SRC beam is significantly more plastic after yielding deformation. After formation of the first crack in TRC UT_{5.5}, the behaviour continues to be similar to that of the concrete beam reinforced with steel until the steel reaches the yielding point. Then, the SRC curve tends to be horizontal with high plasticity and low stiffness, while, the UT_{5.5} curve keeps increasing in strength with increase in ductility until, just before failure, the curve begins to flatten out (this is thought to be as a result of increase in the crack width). However, the ultimate failure was not a flexural failure; it was due to horizontal shear failure which separated the textile reinforcement from the concrete. The ultimate deflection of UT_{5.5} is lower than for the SRC beam by 60%. This marked difference in deflection may be a result of the type of failure that occurred in the TRC. The horizontal shear failure mode prevented UT_{5.5},50k from continuing to increase in terms of strength and deflection; the results also suggest that the ultimate tensile strength of UT_{5.5},50k is not fully utilized. This failure again indicates a weakness in the bond between the concrete and the fibre which is a result of the thin cover thickness (15 mm), which seems unable to provide sufficient bond. It also again points towards the lack of concrete connectivity with all the fibre strands. Late in the TRC beam test, the horizontal crack at the reinforcement began to lengthen and spread within the constant moment

region, therefore, the textile reinforcement was not fully confined. The textile fibre was only partially broken which indicated that the ultimate tensile strength of the whole cross-section of fibre was not used. Therefore, textile reinforcement could exhibit higher ultimate failure strength and enhanced ductility if a suitable layout of fibres and sufficient cover could be achieved.

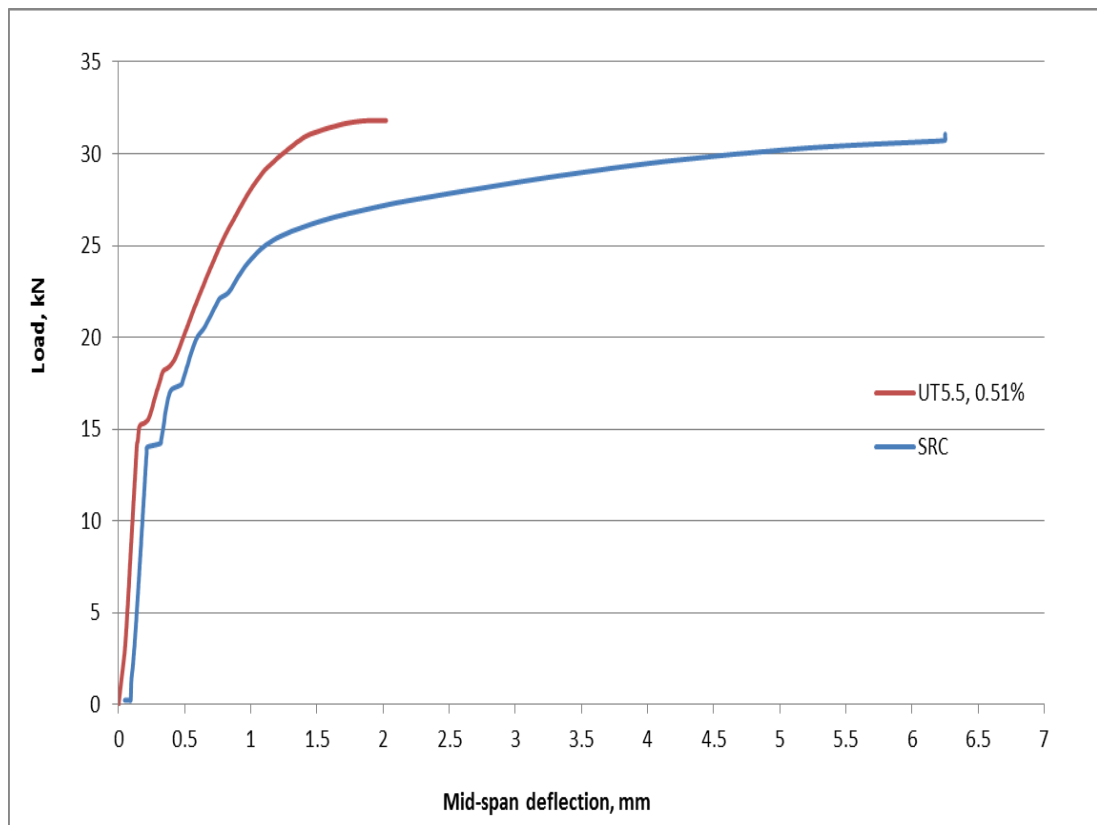


Figure 6-7 Load-deflection behaviour at mid-span of uniaxial reinforcement of carbon (tow) and steel reinforced concrete beams of the same stiffness.



Figure 6-8 Failure mode of UT_{5.5,50k}.

6.1.4 Cracking

This section investigates the cracking behaviour of textile reinforced concrete beams and compares it with that of steel reinforced concrete beams. First crack, crack spacing, crack development, and crack width will be discussed. The beam dimensions in this section are *120 mm x 200 mm x 2600 mm*.

6.1.4.1 First crack

The tensile strength of concrete is about 10% of its compressive strength. Traditionally, cracking is related to the tensile strength of the concrete. Therefore, predicting the tensile strength of concrete with reasonable accuracy is important. Because of the experimental difficulties of determining an accurate tensile strength, the modulus of rupture (f_r) is used to measure the tensile stress of concrete (it is recognised that this will provide an over-estimate of the direct or true tensile strength of the concrete)(Nilson, Darwin and Dolan 2009). The modulus of rupture (f_r) equation, as presented in ACI-08 section 9.5, is:

$$f_r = 0.7\sqrt{f'_c} \quad (6.2)$$

Therefore, the moment that will cause the section to crack is:

$$M_{cr} = \frac{f_r I_g}{y_t} \quad (6.3)$$

Where,

f'_c is the concrete compressive strength;

M_{cr} is the cracking moment;

I_g is the gross moment of inertia;

y_t is the distance from the centroid to the tension edge.

It can be seen from the equation that the effect of reinforcement is neglected at this stage. The moment which will produce the first crack (M_{cr}) can be calculated based on the elastic analysis of a homogeneous section (uncracked). By comparing the cracking moment obtained during the modulus of rupture test with that for the small reinforced beams the effect of the fibre reinforcement on first crack can be assessed. The theoretical cracking load ($f'_c = 50 \text{ MPa}$) is 11 kN (equation 6.2); the MoR tests provided experimental values of 12.95 kN and a deflection is 0.2 mm . Table 6-1 presents the load at which the first crack was observed for each beam (different layouts and geometries). The first crack load of the concrete beams reinforced with steel is 14 kN ; thus, the effect of reinforcement is evident. However, the increase is only approximately 8% greater than the MoR test results (although it is 27% greater than the theoretical cracking load). The effect of textile reinforcement on the first crack load is more significant. The average cracking load of beams reinforced by a variety of textile reinforcements is 15.91 kN . This load is greater than the theoretical cracking load by 45% and greater than that of the tested unreinforced concrete by 23%. In addition, it is 14% greater than that for first crack of the SRC beam. This increase in TRC beam first crack can be

accounted for by the surface area of the textile reinforcement which is in contact with the matrix. The results indicate that the surface area of the roving/tow which is in contact is greater than for the steel reinforcement which leads to greater incorporation of the filaments into the concrete.

Table 6-1 First crack load and deflection of steel reinforced concrete, and textile reinforced concrete.

Reinforcement	Area, mm²	V_f, %	First Experimental Crack Load, kN	First Experimental Crack Deflection, mm
SRC	50.2	0.50	14.00	0.30
BT₃₋₉₀	23.1	0.46	17.00	0.33
BT₄	30.8	0.62	14.00	0.35
BT_{L4}	30.8	0.62	14.30	0.34
BT₄₋₉₀	30.8	0.62	17.30	0.30
BT_{L4-90}	30.8	0.62	14.60	0.28
UT₄	30.8	0.31	16.00	0.34
UT_{br4}	30.8	0.31	17.00	0.21
UT_{b4}	30.8	0.31	17.10	0.21
BT₇	53.9	1.08	16.20	0.35
UT₇	53.9	0.54	15.55	0.37

6.1.4.2 Crack spacing

There are several factors which influence crack spacing in reinforced concrete spanning elements; typically, these are: member thickness (depth),

reinforcement ratio, cover thickness, and bond strength. The spacing between cracks observed in the TRC and SRC beams was experimentally measured. Figure 6-9 shows the crack pattern produced in the steel reinforced concrete. There are 10 primary cracks (stabilised at an applied load of 20 kN) within the constant moment zone; the average crack spacing is 11.3 cm (the spacing ranges between 6 and 15 cm). Cracking is completely stabilised at nearly 85% of ultimate load and 20% of ultimate deflection. Figure 6-10 illustrates the crack pattern produced in the TRC beam test. There are 13 primary cracks (stabilised at an applied load of 26 kN) with an average crack spacing of 9 cm (ranging between 6 cm and 15 cm). It is completely stabilised at nearly 70% of ultimate load and 30% of ultimate deflection. Moreover, it can be seen that the TRC beam is different from the SRC beam in terms of minor cracks. TRC exhibits many minor and horizontal cracks in comparison with the steel reinforced beam. Regarding the horizontal cracks, this can be explained by the horizontal cover thickness (side thickness) which is thin (10 mm), therefore, these cracks appear to be secondary/bond cracks.



Figure 6-9 Crack pattern of the steel reinforced concrete beam.

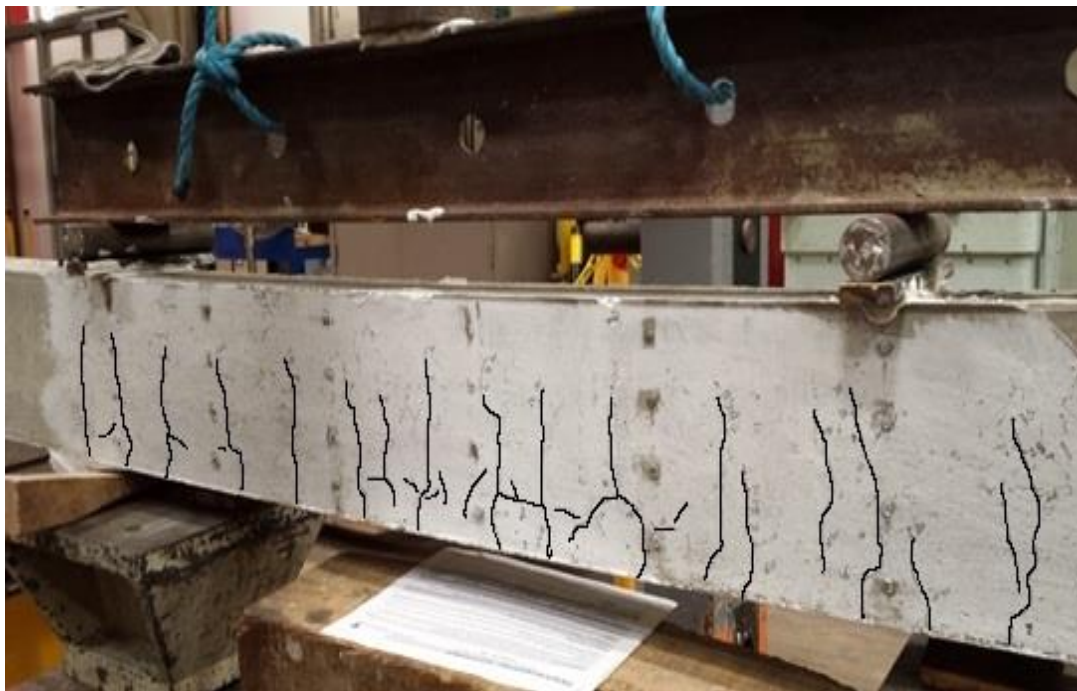


Figure 6-10 Crack pattern of the TRC beam.

The additional cracks in the TRC beams are interesting as they suggest that the bond stress between the fibres and the concrete can develop more quickly (over a shorter distance) than between the steel and the concrete. This degree of improvement in the bond was not perhaps expected as earlier indications suggested reduced bond/contamination of the fibres with the concrete. In these large beam tests, the situation could be enhanced because of the layout of the fibres within the beam cross-section (see Figure 5.13b).

6.1.4.3 Crack development

This section compares the development (number and length) of cracks, after first cracking, which occurred in both the textile reinforced concrete and steel reinforced concrete beams. Figure 6-11 shows the theoretical development of cracks in a reinforced concrete prism subjected to an axial tension load. It illustrates that the concrete will crack once the tensile stress of the concrete reaches the maximum tensile strength for the concrete (f_{ct}). Where the concrete cracks, the load is completely carried by the reinforcement. Also, there is a re-distribution of stress, such that the overall level of stress in the concrete is reduced. As the external load is increased, the tensile stress within

the sample increases again until it reaches the maximum tensile strength capacity of the concrete once again at another location away from the first crack. This process continues until there is insufficient space between the cracks to generate a tensile stress in excess of the tensile stress capacity of the concrete.

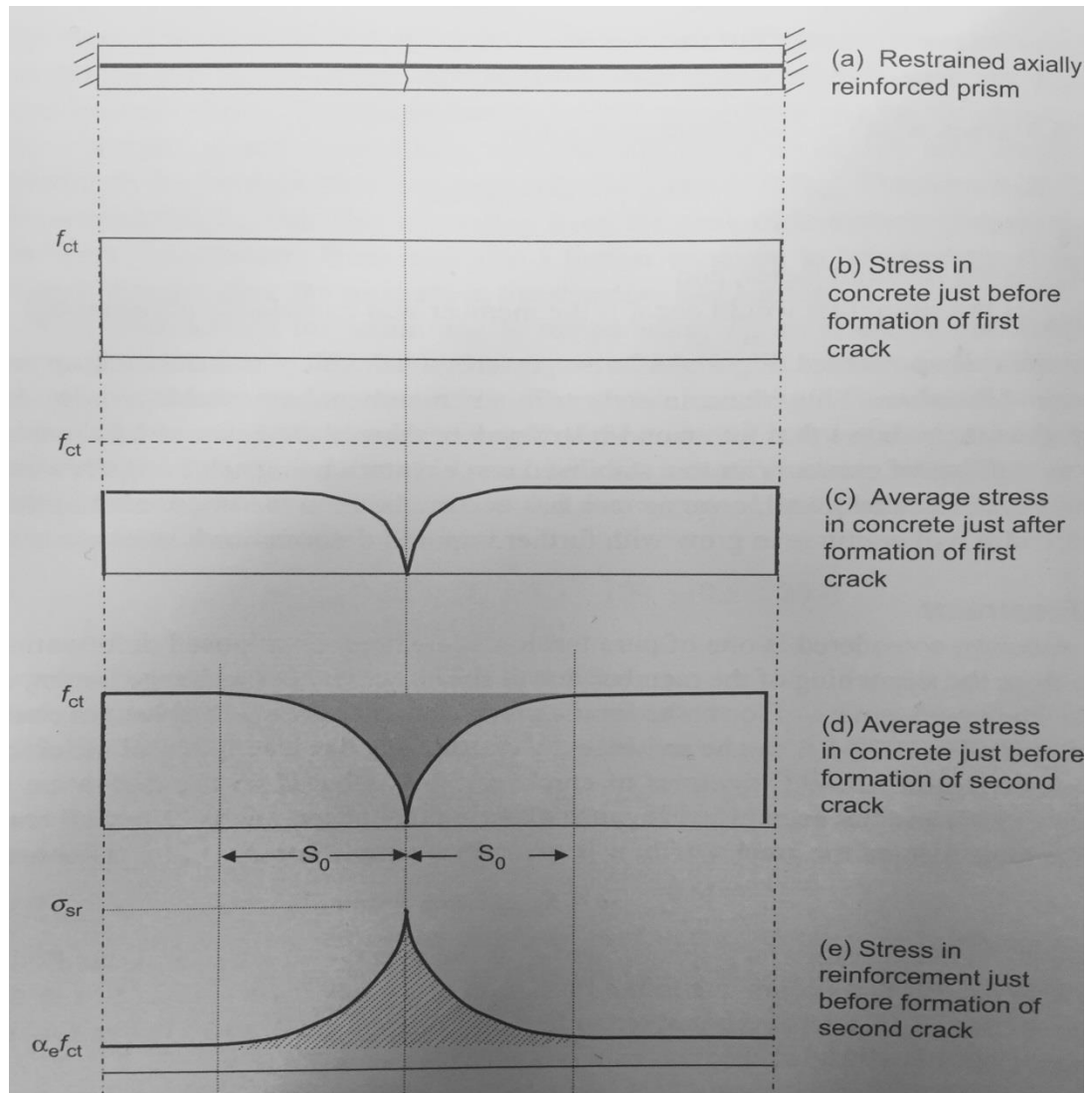


Figure 6-11 Stress distribution between cracks (Forth and Martin 2014).

At this stage, no more primary cracks will form (a stabilised crack pattern is produced). Reinforcement stress and strain are not constant along its length and are at a maximum at the cracks. Also, between the cracks, the concrete is in tension, the level of tension depending on the bond between the reinforcement and the concrete. Table 6-2 presents the experimentally

determined number of cracks and average length of crack observed in the textile reinforced and steel reinforced concrete beams (with the same reinforcement area). From the table, there are a number of observations that are apparent. First, the first crack occurred at *14 kN* and *16 kN* for the SRC

Table 6-2 The development in number of cracks and average crack length of TRC and SRC.

Load, kN	SRC		TRC	
	No. of Primary Cracks	Average Crack Length, cm	No. of Primary Cracks	Average Crack Length, cm
14	6	~8	0	-
16	8	~11	7	~5.5
18	8	~12	9	~7
20	10	~13	9	~8.5
22	10	~15	11	~10
24	10	~18	12	~12
26	failure	-	13	~12
28	=	-	13	~14
30	=	-	13	~15
32	=	-	13	~15
34	=	-	13	~15
36	=	-	13	~15
38	=	-	13	~16

and TRC beams, respectively. Secondly, the length of crack is greater in the SRC beam than in the TRC beam. For example, at *18 kN*, the average crack length in the SRC beam is around *12 cm* while in the TRC beam it is around *7 cm*. Thirdly, at the ultimate load of the SRC beam (*24 kN*) the number of cracks was 10 and the depth was around *18 cm* whilst at the failure load of the TRC beam (*>38 kN*), the number of cracks was 13 and the crack depth was around *16 cm*. Therefore, the crack spacing is smaller in the TRC beam.

These results suggest that the TRC beam is stiffer than the SRC beam as the latter exhibited higher curvature than the TRC beam most likely due to the stress-strain properties of steel reinforcement.

6.1.4.4 Crack width

Crack widths are important in matters of appearance, leakage, and durability. The minimum measured crack width of the steel reinforced concrete beam ($120\text{ mm} \times 200 \times 2600\text{ mm}$) before failure was 0.76 mm ; the maximum was 2 mm . For the TRC beam, the minimum crack width was 0.22 mm ; the maximum was 0.42 mm . There are several prominent equations used to calculate crack width of SRC beam. First is the CEB-FIP Model Code 1990, which determines crack widths based on the slip between the concrete and steel reinforcement.

$$w = l_{s,max}(\varepsilon_{sm} - \varepsilon_{cm} - \varepsilon_{cs}) \quad (6.4)$$

Where,

w is the crack width.

$l_{s,max}$ is the maximum distance over which slip between the concrete and steel occurs.

ε_{sm} is the average steel strain within $l_{s,max}$.

ε_{cm} is the average concrete strain within $l_{s,max}$.

ε_{cs} is the concrete shrinkage strain.

This equation is not suitable for use with TRC beams because of the constitution of the textile reinforcement. The slip is hard to determine as a result of the slip which also occurs within the roving itself between the inner and outer filaments. Second is the Gergely and Lutz (1968) equation which is based on the statistical analysis of experimental data. It is adopted by the ACI Code (ACI 318-11) and applied here for ease of use and also because all of

the parameters can be applied to a TRC beam. Table 6-3 presents the experimentally measured increasing crack width with increasing load for the steel reinforced concrete and carbon textile reinforced concrete beams. The predicted crack width is also included in the table (using the Gergely and Lutz (1968) equation):

$$w = 0.076\beta f_s^3 \sqrt{d_c A} \quad (6.5)$$

where,

w is maximum width of crack, thousands inches.

f_s is the steel stress at a particular load, *ksi*.

d_c is the concrete cover thickness until the centre of the bar closest to that face, *in*.

β is h_2/h_1 .

A is effective tension area divided by number of bars, *in²*.

Figure 6.12 defines the variables above.

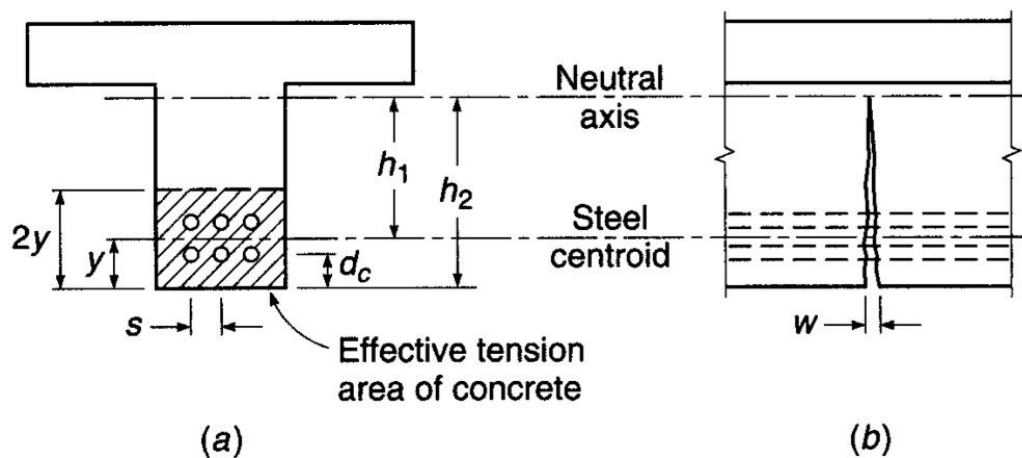


Figure 6-12 Definition of variables for the crack width calculations (Nilson, Darwin and Dolan 2009).

Table 6-3 Crack width with increasing applied load for the SRC and TRC beams.

Load, kN	SRC			TRC		
	Crack Width, mm			Crack Width, mm		
	Minimum	Maximum	Calculated at Service Load	Minimum	Maximum	Calculated
14	0.04	0.08	0.21	-	-	-
16	0.08	0.14	0.25	0.02	0.04	0.21
18	0.08	0.2	0.28	0.04	0.06	0.24
20	0.12	0.28	0.31	0.04	0.08	0.27
22	0.18	0.36	0.34	0.06	0.16	0.3
23	0.3	1.38	-	0.06	0.2	0.31
24	0.32	1.4	-	0.06	0.22	0.32
24.5	0.76	2	-	0.1	0.22	0.33
26	failure		-	0.14	0.26	0.35
28	=		-	0.14	0.28	0.38
30	=		-	0.2	0.38	0.41
32	=		-	0.22	0.42	0.43
34	=		-	0.23	0.43	0.48
36	=		-	0.25	0.45	0.49
38	=		-	0.25	0.46	0.52

At the ultimate load of the SRC beam (24.5 kN), the maximum crack width is 2 mm ; at this load the crack width measured in the TRC beam was 0.22 mm (9 times less). At nearly the ultimate load of the TRC beam (38 kN), the maximum crack width was 0.46 mm , still significantly less than the maximum measured in the SRC beam. The TRC beam is clearly more stiff than the SRC beam. From an aesthetic viewpoint, the TRC beam can be considered a suitable option because of the small crack width relative to the SRC beam.

Applying the Gergely and Lutz equation to calculate the crack width of the steel reinforced concrete beam shows good correlation with the measured crack width especially at service load. As the yield load is approached, the equation can no longer be applied because it markedly underestimates the crack width. However, when applying the same equation to predict the crack width of the carbon textile reinforced concrete it can be seen that the prediction formula is more accurate at ultimate, and less so under serviceability, conditions. The difference between the two results is large (especially under serviceability conditions) which shows the need to derive an equation that is able to determine the crack width of TRC with different geometries. In Chapter 7, a crack width equation for TRC beam will be investigated.

6.1.5 Tension stiffening

Tension stiffening is the contribution of the concrete in the tension zone, after cracking, to the stiffness of the reinforced concrete section (Khalfallah and Guerdouh 2014). Therefore, tension stiffening varies along the beam span and is at a maximum approximately midway between the two primary cracks, and zero at the cracked section. Deflection of beams is a function of loads, spans, and supports divided by flexural stiffness. The flexural stiffness of a cross section of a steel reinforced concrete beam is represented by EI . The stiffness of a cracked section is decreased as a result of a decreased moment of inertia (I) at the crack. Therefore, the deflection is significantly influenced by the moment of inertia. The flexural stiffness of a steel reinforced concrete beam varies in relation to the bending moment as follows:

If $M \leq M_{cr}$, the moment of inertia is I_g which is the gross moment of inertia.

$M \geq M_{cr}$, if the beam is still cracking (within the crack formation stage), the moment of inertia is called the effective moment of inertia (I_{eff}), however, if the beam is fully cracked, the moment of inertia is called the cracked moment of inertia I_{cr} (ACI 318 2011).

Figure 6-13 and Figure 6-14 show the short term behaviour of the steel and textile reinforced concrete (UT₁₅-Anch-3L₃-2.6) beams ($120\text{ mm} \times 200\text{ mm} \times 2600\text{ mm}$) of the same area with a fully uncracked (EI_g) and cracked section (EI_{cr}). It can be seen from Figure 6-13 that the SRC beam begins to lose its stiffness once cracking has occurred at 4.5 kN.m . With increased moment, the stiffness deviates from uncracked behaviour towards cracked behaviour which results in an increase in curvature. Under serviceability conditions, the contribution of concrete is evident as can be seen in the difference between the experimental and fully cracked curve. At the ultimate load, the SRC beam is completely cracked and all the tensile stress is resisted by steel reinforcement. Figure 6-14 shows that the TRC beam also begins to lose stiffness after cracking has occurred at 6 kN.m . After cracking, the TRC beam stiffness deviates from uncracked behaviour towards cracked behaviour. With increasing load, the curvature increases and the section loses more stiffness until the ultimate load is reached.

By comparing the contribution of tension stiffening in SRC and TRC beams, it can be seen that the effect of tension stiffening is higher in the TRC beam than in the SRC beam. At service moment (e.g. 7 kN.m), the contribution of tension stiffening to the behaviour is significant in the TRC beam. It is nearly 7 times greater than tension stiffening in the SRC beam. At ultimate moment in the SRC beam (nearly 8 kN.m), the contribution of concrete is zero while at the same load in the TRC beam the contribution is considerable. Despite the secondary cracks that appeared when the load approached the ultimate load, the concrete still contributes to the resistance of the tensile stress. Therefore, the contribution of concrete with regard to the tensile stresses is greater in TRC than in SRC. This may explain the shorter crack spacing of TRC and the

shorter cracked length in the TRC beam. The significant contribution of tension stiffening may be attributed to the high tensile strength of carbon textile reinforcement, and also to the layout that was used to improve the bond between concrete and reinforcement which increases the interaction between filaments and concrete. This produced a good bond between textile and matrix.

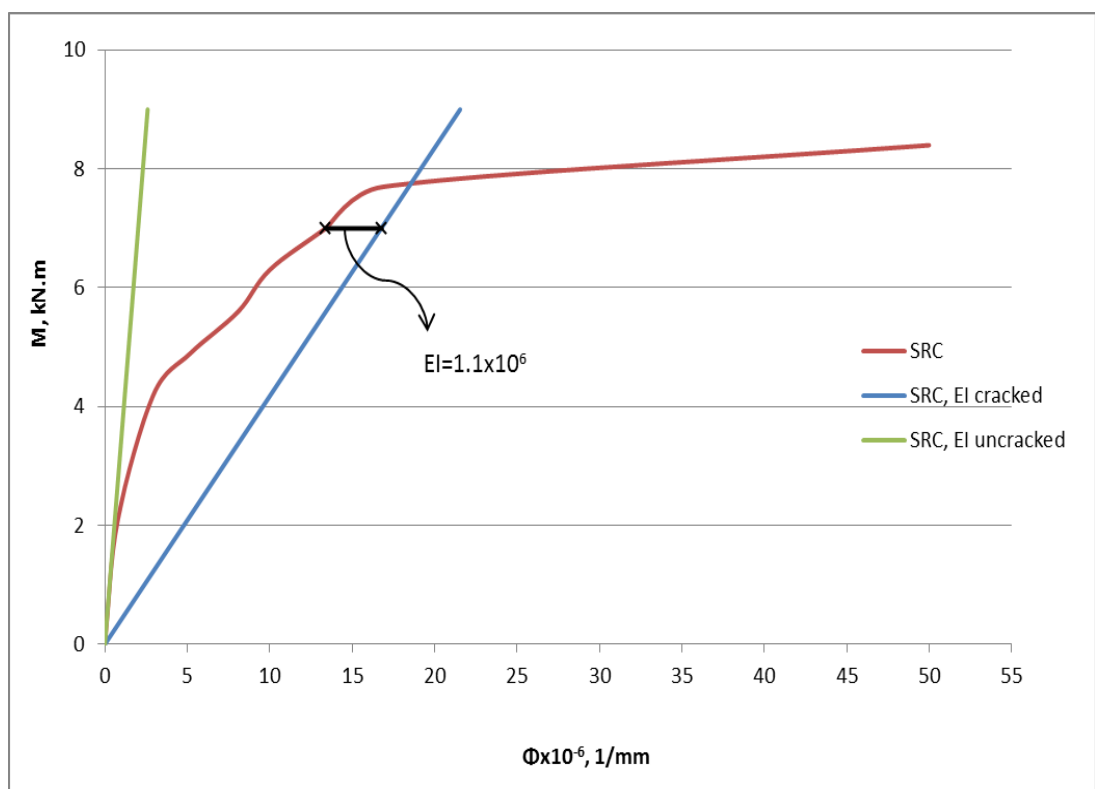


Figure 6-13 Tension stiffening of SRC beam.

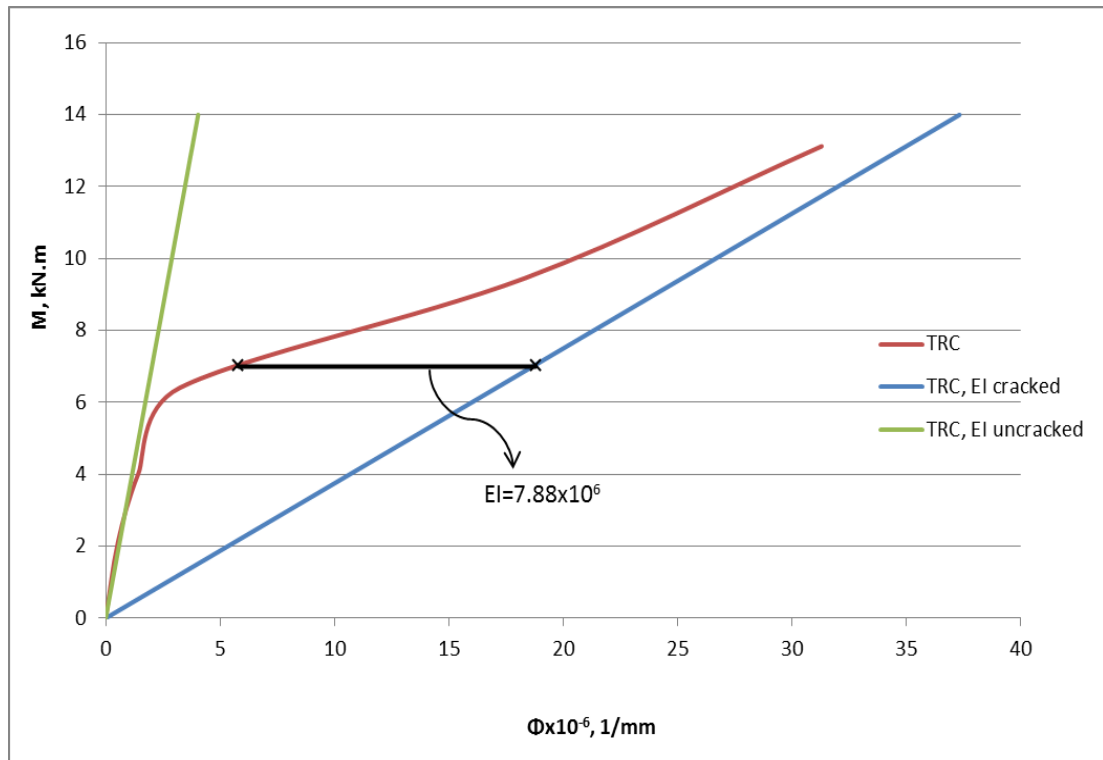


Figure 6-14 Tension stiffening of TRC beam.

6.2 Conclusions

The main conclusions that can be drawn from the work discussed in this chapter are summarised as follows:

- The TRC beam behaviour is different from the SRC beam in terms of moment-curvature, deflection, cracking, and tension stiffening.
- At the yielding point of the SRC beam, the TRC beam curvature is lower than that of the SRC beam by 50%. However, the TRC beam continues to resist the applied loading as the TRC beam capacity is higher than that of the SRC beam by 56% for the same area of reinforcement.
- The ultimate deflection of the TRC beam is lower than that of the SRC beam by 37%.

- In cases where the cover thickness is too small the failure mode of the TRC beam is horizontal shear failure at the level of the textile reinforcement due to the lack of bond.
- The first crack in the TRC beam is at a higher load than occurs in the SRC beam and the number of primary cracks is greater than in the SRC beam.
- The crack widths in the TRC beam are smaller than those in the SRC beam.
- The crack lengths in the TRC beam are less than those in the SRC beam by ~17%.
- These results for crack behaviour pour in favour of structural aesthetic.
- The contribution of the concrete in the tension zone (tension stiffening) in the TRC beam appears to be greater than in the SRC beam. The results indicate that the surface contact area of textiles is greater than that for steel reinforced concrete beams. This results in an enhancement in the interaction between filaments and concrete.
- The use of the steel reinforced concrete code for textile reinforced concrete beams is shown not to provide a good correlation of the theoretical results with experimental data, and this supports the need to work on a new standard for TRC.

CHAPTER 7

TEXTILE REINFORCED CONCRETE DESIGN METHODOLOGY

Textile reinforcements are considered to be new materials in terms of being used as the main reinforcement in reinforced concrete members. Therefore, there is currently no specific code that can be used to design textile reinforced concrete (TRC) beams. However, it may be possible to use the design codes for steel reinforced concrete (SRC) as long as the differences between steel and textile reinforcement, i.e. primarily bond behaviour and yielding point, are taken into account. Voss (2006) also stated that steel reinforced concrete design cannot be applied directly to TRC because of the differences between the steel and textile reinforcement. The design of a structural concrete member must meet the requirements of safety, serviceability, economy, and functionality. This chapter will develop a design method for carbon textile reinforced concrete beams, with regard to safety, using the design methods currently utilized in SRC design.

7.1 Design concepts

In a singly reinforced concrete composite section, the concrete resists the compression forces and the reinforcement resists the tension forces. The principle of design is that the allowable resistance load must be greater than the applied load. There are several prominent codes based on this concept. One of these is the ACI 318-11 Code, which provides guidance to achieve this aim, thus:

required strength \leq design strength (ACI 318-11)

$$M_u \leq \Phi M_n \quad (7.1)$$

where,

M_u is the external factored moment.

M_n is the nominal moment.

Φ is the strength reduction factor.

The ultimate moment, M_u , is the moment from the factored loads. The nominal moment, M_n , is the theoretical beam capacity which can be calculated from the static equilibrium of the concrete and reinforcement theoretical capacities and the beam dimensions.

7.1.1 Design assumptions

The experimental data suggests that the TRC beams can be designed based on the same assumptions made for SRC beams. Nilson *et al.* (2009) and Wight and MacGregor (2009) stated that the following assumptions must apply in order to simplify the analysis and design of reinforced concrete elements:

- 1- Plane sections before loading remain plane after loading.
- 2- Perfect bond between concrete and reinforcement, therefore, the extension is the same for both.
- 3- Concrete in the tension zone does not resist tensile load.
- 4- Stress-strain curves of concrete and reinforcement can be used to determine the stresses from the strains.

However, it should be mentioned that the perfect bond between concrete and reinforcement is practically correct for uncracked sections. After the beam is cracked, a slip in reinforcement has occurred and also at the cracked section the extension is different between concrete and reinforcement. Also, concrete can to some extent resist tensile stress even with the existence of hairline cracks. Concrete before cracking and between cracks is able to resist small magnitude tensile stresses. These assumptions are a simplification of the actual behaviour of a reinforced concrete beam.

7.2 Analysis and design of carbon textile reinforced concrete

In this study, the beams were designed to fail under tension; i.e. the reinforcement was designed to fail. Therefore, the design procedures developed in this section use the tension failure of the reinforcement as a basis for design.

7.2.1 Tension failure

In order to fail under tension, the textile reinforcement ratio (ρ_f) must be less than the balanced reinforcement ratio (ρ_b); the latter can be determined by considering the equilibrium of a balanced section in which the concrete strain is at the ultimate (ε_{cu}) while at the same time, the textile reinforcement strain is at its ultimate (ε_{fu}), see Figure 7-1. Thus, from the equilibrium equation, the compression force equals the tension force, $C=T$:

$$\rho_{fb} \cdot b \cdot d \cdot f_{fu} = \gamma f'_c ab$$

$$\rho_{fb} \cdot b \cdot d \cdot f_{fu} = \gamma \beta_1 f'_c c_b b \quad (7.2)$$

where;

ρ_{fb} is the balanced fibre reinforcement ratio.

b is the beam width.

d is the beam effective depth.

c_b is the distance from extreme compression fibre to neutral axis at balanced strain condition.

f'_c is compressive strength of concrete.

f_{fu} is the ultimate tensile strength of textile fibre.

β_1 is a coefficient that depends on the compressive strength of concrete.

γ is the stress intensity factor.

γ is the empirical factor (0.85) found by (Whitney 1937) to replace the actual parabolic stress distribution of concrete in compression with an equivalent rectangular stress block. This factor is adopted by the ACI committee. However, it is based on a steel reinforced concrete beam, but will be applied here to a TRC beam, as it is assumed to have the same concrete compression behaviour as an SRC beam.

c can be determined from strain distribution:

$$c_b = \frac{\varepsilon_{cu}}{\varepsilon_{cu} + \varepsilon_{fu}} d \quad (7.3)$$

$$\rho_{fb} = 0.85\beta_1 \frac{f'_c}{f_{fu}} \left(\frac{\varepsilon_{cu}}{\varepsilon_{cu} + \varepsilon_{fu}} \right) \quad (7.4)$$

where,

ε_{cu} is the ultimate strain of concrete (0.003).

ε_{fu} is the ultimate strain of fibre f_{fu}/E_f .

E_f is the modulus of elasticity of fibre.

From ACI 318-11, section 10.2, it can be computed as follows:

$$\beta_1 = 0.85 \text{ if } f'_c \leq 27.5 \text{ MPa} \quad (7.5a)$$

$$\beta_1 = 0.85 - 0.05 \left(\frac{f'_c - 27.5}{7} \right) \quad (7.5b)$$

However, β_1 is not less than 0.65.

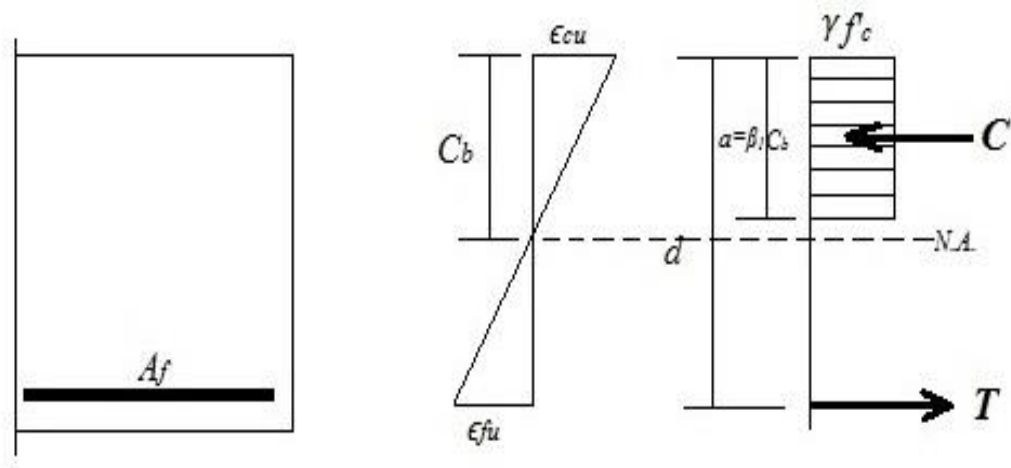


Figure 7-1 Balanced section.

7.2.2 TRC beam behaviour

Initially, the behaviour of the TRC beam was very similar to that of the SRC beams during the uncracked (elastic) phase of loading. Therefore, for this uncracked phase the concepts adopted for the design of SRC beams will be used for the TRC beam design, with the necessary material property adjustments, see Figure 6.5.

7.2.2.1 Uncracked section

Theoretically, the section is considered uncracked when the tensile stress in the concrete due to the applied load is smaller than the tensile strength of the concrete modulus of rupture (f_r); i.e., the concrete alone is able to resist the compression and tension stresses. However, the reinforcement is also resisting the tensile forces; the stress in the reinforcement is n (modular ratio) times the tensile stress in the concrete. Figure 7-2 suggests the typical stress and strain distributions at this stage. Therefore, the bending stress can be determined using:

$$f = \frac{My}{I} \quad (7.6)$$

where,

f is the bending stress at a distance y from the neutral axis.

M is the bending moment.

I is the second moment of inertia of the cross section around the neutral axis.

The location of the neutral axis can be calculated either by neglecting the effect of the reinforcement or by taking its effect into consideration (i.e. a transformed section). In a transformed section, the area of the reinforcement is replaced by the equivalent concrete area, which is nA_f .

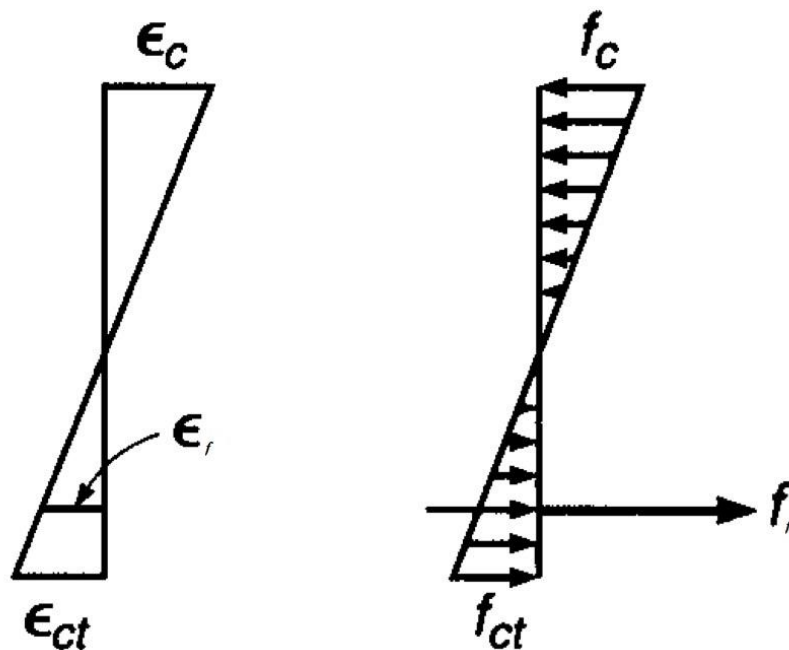


Figure 7-2 Stress and strain distribution of an elastic section.

7.2.2.2 Cracked section

With increasing load, the tensile stress in the concrete exceeds the tensile strength of the concrete, leading to the formation of cracks. Also, the neutral axis rises and sits just above the tip of these cracks. At a cracked section, it is assumed that the concrete does not resist any tensile stress, thus, the tension force is completely resisted by the reinforcement. It can be said that the stress-strain curve of concrete is nearly linear to almost $f'_c/2$, which represents the service load of a steel reinforced concrete beam (Nilson, Darwin and Dolan 2009). This means that up to this value the concrete behaves elastically, and with regard to the carbon fibre, it is elastic until failure. Therefore, the theoretical strain and stress distribution at the cracked section is shown in Figure 7-3, up to $f'_c/2$. A transformed section can then be used to calculate the stresses and strains of the section. It should be mentioned that the concrete resistance under tension is neglected as shown in Figure 7-3b.

The neutral axis (kd) can be determined by considering the first moment area theorem.

$$b \cdot kd \left(\frac{kd}{2} \right) = nA_f(d - kd) \quad (7.7)$$

$$b \cdot \frac{(kd)^2}{2} - n\rho_f b d(d - kd) = 0$$

$$k = \sqrt{(\rho_f n)^2 + 2\rho_f n} - \rho_f n \quad (7.8)$$

Where,

ρ_f is the fibre reinforcement ratio.

n is the modular ratio.

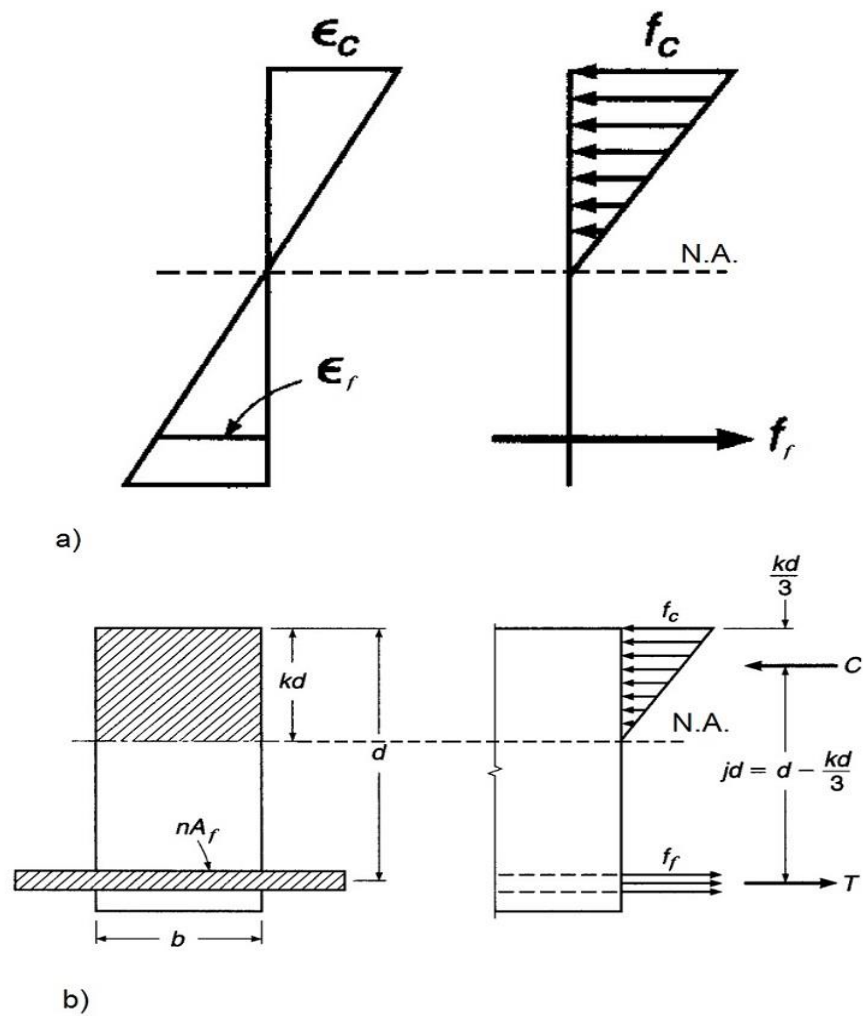


Figure 7-3a) Stress and strain distribution at elastic cracked section, b) at cracked transformed section (Nilson, Darwin and Dolan 2009).

However, not all of the area of textile reinforcement is activated due to the inactive bond of the inner filaments (see section 5.1). Therefore, the bond efficiency factor is indirectly related to the effective area ($A'_f = \eta_\tau A_f$) that is resisting the load:

$$k = \sqrt{(\eta_\tau \rho_f n)^2 + 2\eta_\tau \rho_f n} - \eta_\tau \rho_f n \quad (7.9)$$

Thus M is,

$$C = T \quad (7.10)$$

$$\frac{1}{2} f_c b k d = \eta_\tau A_f f_f \quad (7.11)$$

$$M = \eta_\tau A_f f_f (j d) \quad (7.12)$$

$$j d = d - \frac{k d}{3} \quad (7.13)$$

where,

$j d$ is the internal lever arm between C and T .

f_f and f_c can be determined as follows:

$$f_f = \frac{M}{\eta_\tau A_f j d} \quad (7.14)$$

$$f_c = \frac{2M}{k j b d^2} \quad (7.15)$$

With increasing load (to failure or near ultimate capacity), the stress and strain behaviour can no longer be considered elastic. The calculation of stresses and strains in this (non-elastic) stage is explained in the next section.

7.2.3 Design of TRC beams using tension control

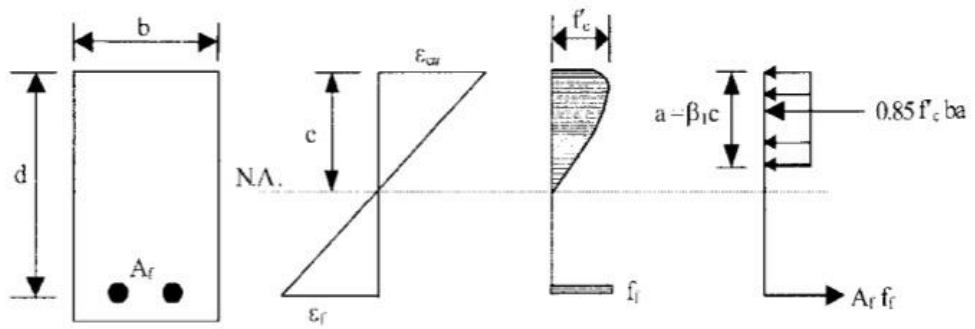
When $\rho_f < \rho_b$, the failure occurs in the textile reinforcement and is deemed a tension failure. ACI 440.1R states that when $\rho_f < \rho_b$ for an FRP reinforced concrete beam, the rectangular stress block cannot be applied because the maximum strain in concrete is not reached. As such, an equivalent stress block is required to approximate the stress in the concrete. There are two parameters that are unknown at failure; the concrete strain ε_c and the depth

of the neutral axis c . Therefore, determining the actual nominal moment strength is complicated. Hence, a conservative capacity can be computed at the balanced neutral axis as shown in Figure 7-4 (ACI 440.1R). Therefore, the ultimate strain of concrete and FRP are reached.

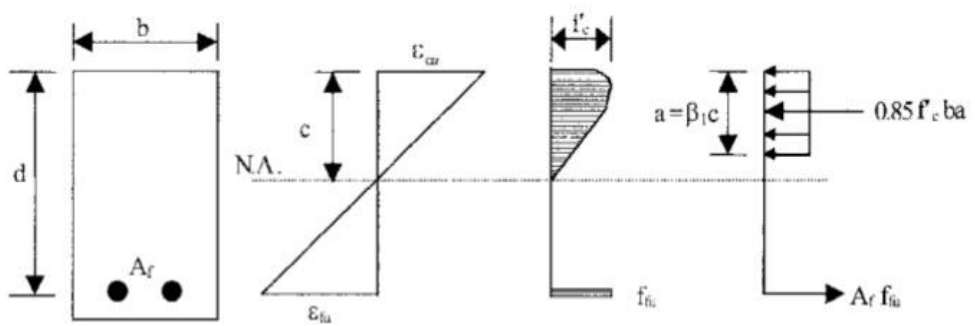
$$M_n = A_f f_{fu} \left(d - \frac{\beta_1 c_b}{2} \right) \quad (7.16)$$

$$c_b = \left(\frac{\varepsilon_{cu}}{\varepsilon_{cu} + \varepsilon_{fu}} \right) d \quad (7.3)$$

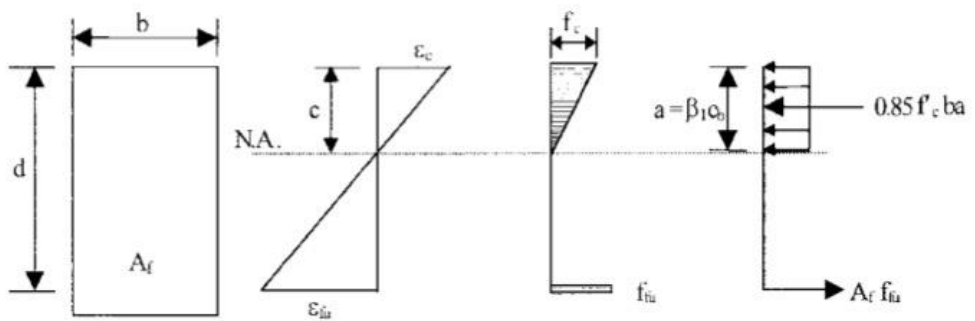
The nominal moment strength recommended by ACI 440.1R is conservative at low reinforcement ratios because it uses the balanced reinforcement. Consequently, this study tries to determine the design bending moment more accurately. As the design is under reinforced ($\rho < \rho_b$), failure is in the textile reinforcement, which means that the ultimate tensile strength and ultimate strain of the reinforcement are attained. However, the strain in the concrete is unknown as the concrete may not have reached the ultimate strain. Figure 7-5 shows the theoretical stress distribution of a TRC beam cross section at the textile ultimate load.



(a) Failure governed by concrete crushing



(b) Balanced failure condition



(c) Failure governed by FRP rupture (concrete stress may be nonlinear)

Figure 7-4 Stress and strain distribution (ACI-440 2006).

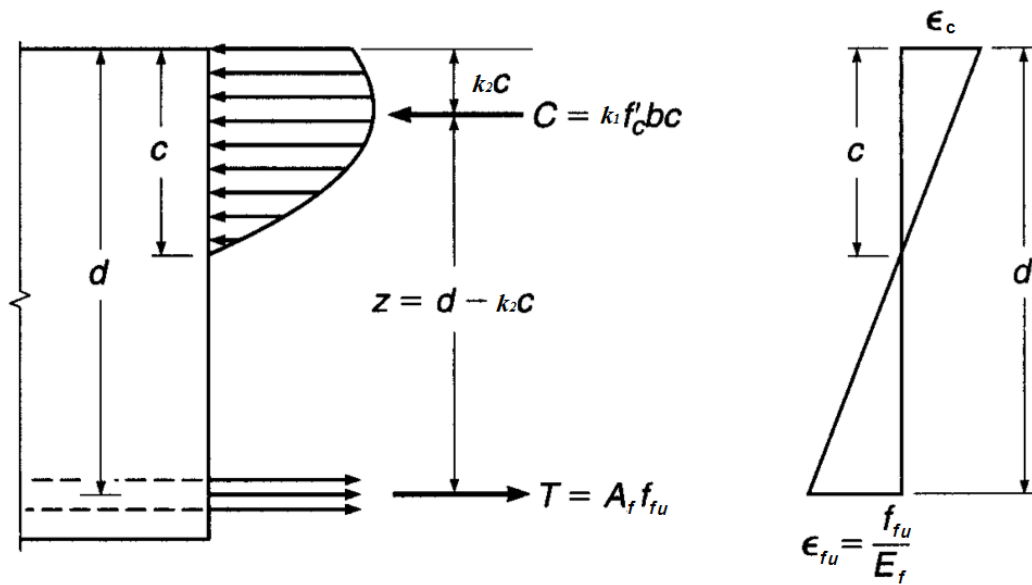


Figure 7-5 Stress and strain distribution of a TRC control beam.

Hognestad, Hanson and McHenry (1955) determined k_1 and k_2 as illustrated in Figure 7-6. Therefore, the neutral axis can be calculated from the equilibrium equation:

$$A_f f_{fu} = k_1 f'_c b c \quad (7.17)$$

where,

k_1 is the ratio of the distance between the extreme compression fibre and the resultant of the compressive force to the depth of neutral axis;

The effect of bonding is also taken into account here, thus:

$$c = \frac{\eta_\tau A_f f_{fu}}{k_1 f'_c b}, \quad A'_f = \eta_\tau A_f, \quad A_f = \rho b d$$

$$c = \frac{\eta_\tau \rho f_{fu} d}{k_1 f'_c} \quad (7.18)$$

where,

η_τ is the bond efficiency factor.

Hence, the nominal bending moment can be determined:

$$M_n = \eta_\tau A_f f_{fu} (d - k_2 c) \quad (7.19)$$

$$M_n = \eta_\tau \rho b d f_{fu} \left(d - \frac{k_2 \eta_\tau \rho f_{fu} d}{k_1 f'_c} \right) \quad (7.20)$$

where,

k_2 is the ratio of the average compressive stress to the maximum stress of concrete.

At different concrete strengths, it can be said that $\frac{k_2}{k_1}$ is constant:

$$\frac{k_2}{k_1} \approx 0.59$$

$$M_n = \eta_\tau \rho b d^2 f_{fu} \left(1 - 0.59 \frac{\eta_\tau \rho f_{fu}}{f'_c} \right) \quad (7.21)$$

Therefore,

$$\Phi M_n \geq Mu \quad (7.22)$$

As mentioned in the literature review, TRC behaviour differs from that of steel reinforced concrete, the main difference being the bond behaviour. Therefore, the effect of the bond is accounted for and the actual tensile strength of the textile yarn (not a single filament) must also be quantified. The tensile strength of the textile yarn was experimentally measured and presented in Section 4.2. Thus, the activated textile area is considered by multiplying the bond efficiency

factor by the textile area as in equation 7.21. The bond efficiency factor and the reduction factor are determined in the next sections.

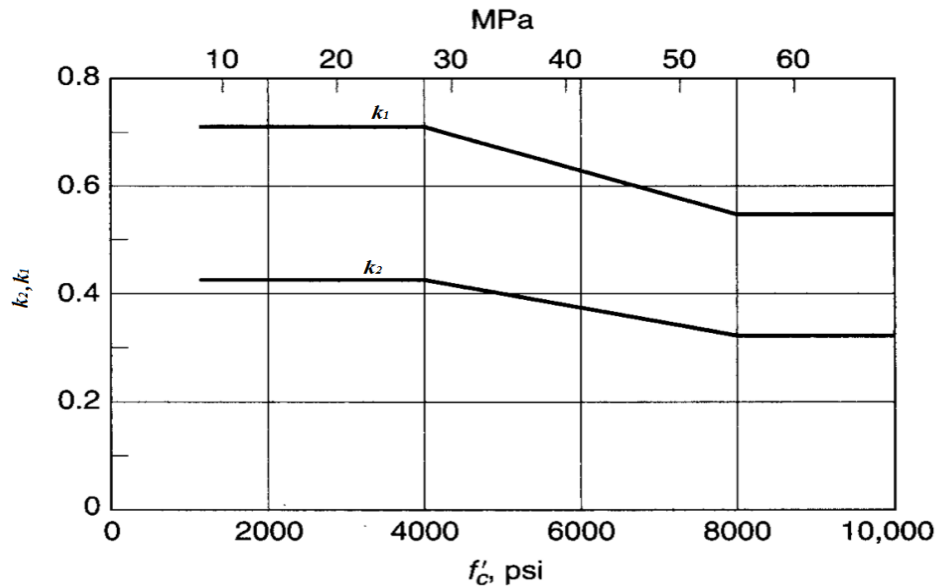


Figure 7-6 k_1 and k_2 relative to concrete strength.

7.2.3.1 Bond efficiency factor

To determine the bond efficiency factor, the nominal moment is calculated using the methodology explained previously in section 7.2.3. Equation 7.21 will be used. The bond efficiency factor can then be determined by dividing the actual experimental moment, M_u , as measured during the four-point bending tests of the small beams, by the computed theoretical nominal moment M_n (i.e. assuming that the bond efficiency factor is unity); since moment is proportional to load, this is equal to P_u/P_n .

In this study, volume fraction and textile geometry were the parameters considered in order to investigate how the bond efficiency factor may vary for the small scale beams.

7.2.3.1.1 Volume fraction

The volume fraction (V_f) is the quantity of fibre in the concrete member. Table 7.1 shows the effect of volume fraction on the bond efficiency of carbon textile reinforced concrete. Theoretically, when the volume fraction of a textile is increased, it has a direct effect on the capacity of the composite section; that is, the strength is increased. In practice, incorporating more textile (not in the loading direction) leads to a reduction in the overall bond, which limits the achievable increase in capacity (see section 5.3.7). It can be seen from Table 7-1 that the bond efficiency factor decreased when the volume fraction of fibre was increased; the average bond efficiency factor of UT_{4,24k} was 0.64 at $V_f = 0.15\%$, while the average bond efficiency factor of BT_{7,50k} was 0.35 at $V_f = 1.08\%$. This could be attributed to the reduction in the contact area between the concrete and textile owing to congestion, which progressively prevents the concrete from fully penetrating between the rovings and filaments as V_f increases. However, on closer inspection, it can be observed that using UT_{7,50k}, which has the same textile area as BT_{7,50k}, apart from the weft rovings, improved the bond efficiency factor by 13%, up to 0.40. It is suggested that there is an inverse linear relationship between V_f and η_τ (see Figure 7-7) (the trend being derived from the results obtained from the 16 beam tests). It can be seen that the regression (R^2) is low. This is a result of different parameters were applied of the same and different volume of fraction. For example, at 0.60 volume fraction, 4 beams were tested with different geometries. However, the trend shows that the increase in the volume fraction leads to a decrease in the bond efficiency factor.

Table 7-1 The bond efficiency factor for various volume fractions and numbers of layers.

Textile Geometry	$V_f, \%$	Bond Efficiency Factor (min – max) η_r
UT ₄ , 24k	0.15	0.64 (0.64-0.64)
UT ₈ , 24k	0.29	0.49 (0.45-0.53)
BT ₂ , 50k	0.31	0.54 (0.53-0.54)
UT ₄ , 50k	0.31	0.54 (0.52-0.56)
UT ₇ , 50k	0.54	0.40 (0.39-0.40)
BT ₄ , 50k	0.62	0.49 (0.46-0.51)
BT _{8-(5cm)} , 50k	0.62	0.39 (0.33-0.44)
BT ₇ , 50k	1.08	0.35 (0.33-0.37)
	Average	0.48

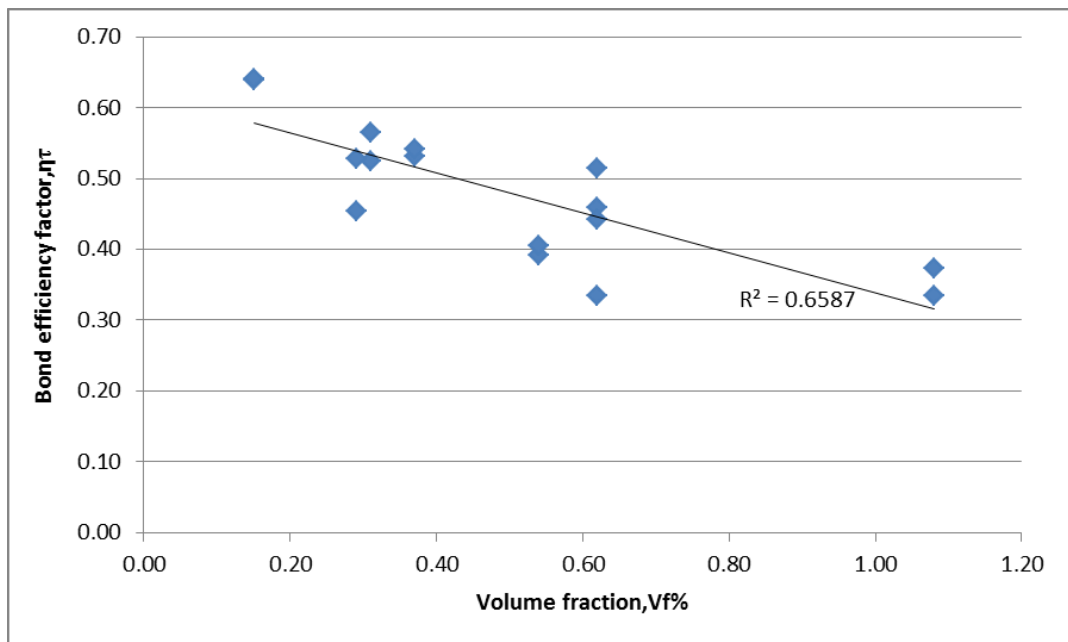


Figure 7-7 Bond efficiency factor with volume fraction.

7.2.3.1.2 Textile geometry

Table 7-2 and Figure 7-8 show how the different layouts of individual reinforcement elements affect the bond efficiency factor (the volume fraction is kept constant).

When the tow is used as it is, without changing the geometry as in UT₄, the average bond efficiency (η_τ) is 0.54 and the average ultimate load is 27.5 kN. If the bond efficiency factor is lower than 1, this means the ultimate flexural load of a specific beam will be lower than the theoretical design load. The best bond efficiency factor was achieved with the bundled textile (UT_{b4}) reinforced beam which has η_τ equal to 0.65; this is as a result of the increase in the number of filaments that are in direct contact with the concrete. When the carbon tows were twisted rather than woven (UT_{t4}), the average efficiency factor dropped significantly to 0.27, which is equivalent to 73% lower than the design (theoretical) load. This can be accounted for by the decrease in the contact area and the complexity of the cross section along the tow.

Table 7-2 The bond efficiency factor for various fibre geometries.

Textile Geometry	$V_f, \%$	Average Ultimate Load, kN	Bond Efficiency Factor (min – max) η_τ
UT _{t4} , 50k	0.31	13.75	0.27* (0.27-0.28)
UT _{4c} , 50k	0.31	20.3	0.41 (0.40-0.41)
UT _{4br} , 50k	0.31	23.8	0.47 (0.47-0.47)
UT ₄ , 50k	0.31	27.5	0.54 (0.52-0.56)
UT _{4b} , 50k	0.31	32.7	0.65 (0.63-0.66)
		Average	0.52

* This value is not included in the average.

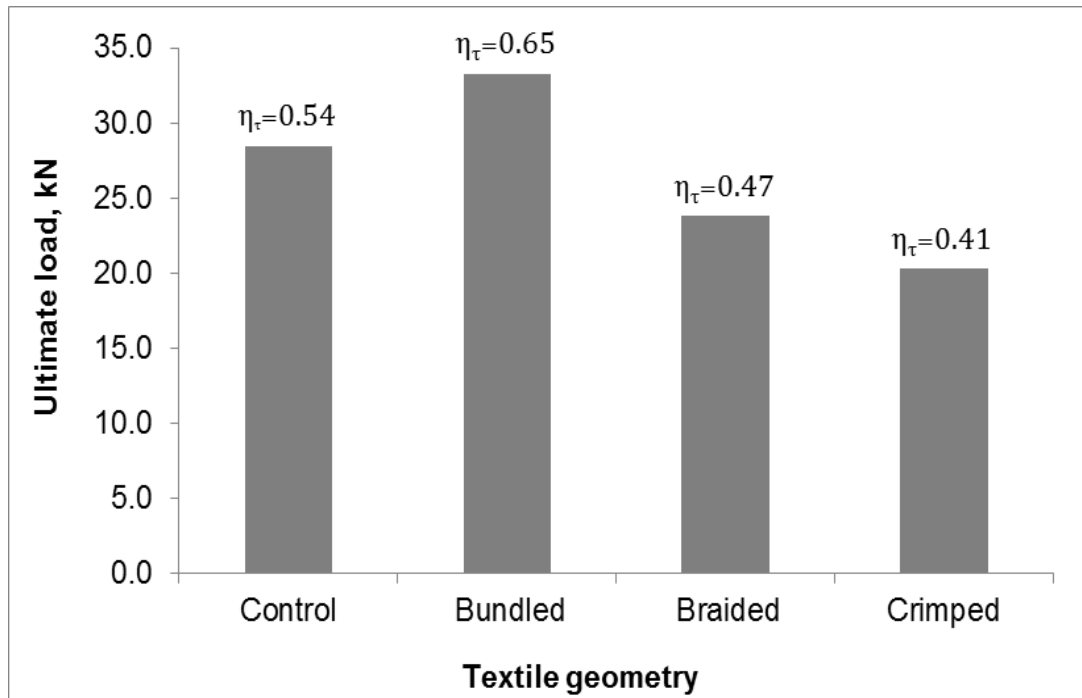


Figure 7-8 Bond efficiency factor and ultimate load with the same volume fraction ($V_f = 0.31$) and 4 layers for all beams with different geometries.

Therefore, the bond efficiency factor η_{τ} is 0.48 in the case of woven fabric or tow reinforcement and 0.52 if different textile geometries are used. It is believed that these reductions in experimental moment capacity, compared with the theoretical values, can be linked to the area of fibres not activated by the bond with the concrete as the inner filaments are not bonded directly to the concrete matrix. Therefore, it could be said that the activated area is 48% in the case of woven fabric and 52% in the case of different textile geometries.

7.2.4 Reduction factor

Häußler-Combe and Hartig (2007) stated that the exact properties of filaments cannot be used due to: early filament failure, the production processes, the fact that some filaments are broken, alignment change, and change in fibre orientation. Therefore, the reduction factor needs to be applied in order to account for the variations in the composite properties of TRC. In carbon TRC, textile carbon reinforcement has no plasticity, so this also needs to be accounted for by a further reduction factor in TRC design, to increase the safety of the concrete member. The bond efficiency factor can be considered

an additional reduction factor to that already used in the design method in the previous section (7.2.3).

The design method developed in the previous section was applied to 49 experimental beams. Statistical calculations were performed to show the accuracy of the equation. Figure 7-9 shows the normal distribution of the predicted bending moment over the measured bending moment of TRC beams. From the figure, it can be said that 95% of calculated/experimented moment is over 0.60. According to this result, the use of reduction value (ϕ) of 0.60 could ensure that the designed structural concrete beam is 95% safe.

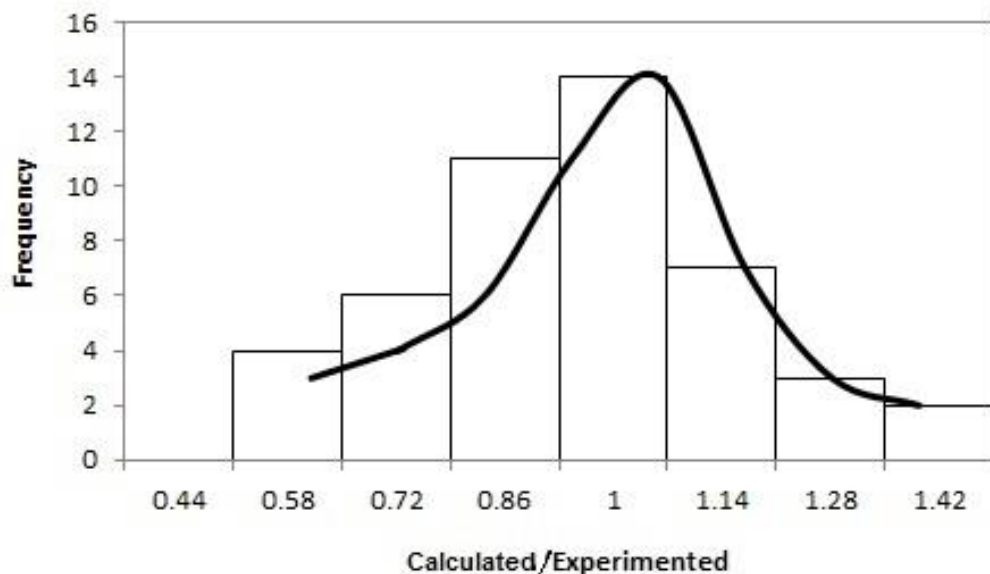


Figure 7-9 Normal distribution of designed capacity over the experimental capacity of beams reinforced by carbon textile.

7.2.5 Moment-curvature prediction

In Chapter 6 (section 6.1.1) the moment-curvature of a textile reinforced concrete beam was experimentally measured and compared with a steel reinforced concrete beam. It was clear that the moment-curvature behaviour

of the TRC beam was different to that of the SRC beam, especially beyond service loading. According to the design methodology proposed earlier that utilised the effective area, the moment-curvature is theoretically predicted:

$$\phi = \frac{M}{E_c I} \quad (7.23)$$

where,

I is the moment of inertia.

With reference to the moment-curvature of the tested TRC beam, the gross moment of inertia is used during the elastic stage and the effective moment of inertia after cracking has occurred. The same effective moment of inertia used in the calculations for the SRC beam (from ACI-318,11) is utilized for the TRC beam:

$$I_g = \frac{bh^3}{12} \quad (7.24)$$

$$I_{eff} = \left(\frac{M_{cr}}{M_a}\right)^3 I_g + \left[1 - \left(\frac{M_{cr}}{M_a}\right)^3\right] I_{cr} \quad (7.25)$$

$$I_{cr} = \frac{bc^3}{12} + bc\left(\frac{c}{2}\right)^2 + n\eta_\tau A_f (d - c)^2 \quad (7.26)$$

Where;

M_{cr} is the cracking moment;

M_a is the service moment.

Figure 7-10 compares the predicted moment-curvature of a TRC beam with the experimental beam behaviours. Beam1 and Beam2 layouts were shown in Figure 5-13a with 30 mm cover thickness. Beam3-C15 and Beam4-C60 layouts were shown in Figure 5-13b and c with 15 mm and 60 mm cover

thicknesses, respectively. At the uncracked stage, it can be seen that the slope of the predicted moment-curvature is similar to that of the measured beam. However, after cracking has occurred, the moment-curvature behaviour is not identical to that of the measured beams. The variety between the measured beams is due to the bond and the number of activated filaments, and between the predicted and measured beams is a result of the prediction of tension stiffening. In general, the predicted behaviour can be considered to calculate the moment-curvature of the TRC beam. However, it can be seen that the slope of the predicted curve after cracking is similar to the measured beams' behaviour. For Beam3-C15 and Beam4-C60, the curvature at specific moments is significantly different from the that of the predicted beam although the slope is nearly the same. This can be attributed to the difference in the initial crack which is a result of the variation in the cover thickness (15 mm and 60 mm). At 8 kN.m , the predicted curvature is 8×10^{-6} while for Beam1 and Beam2 it is 13.5 and 11×10^{-6} , respectively. The difference is quite significant especially for Beam1. However, with the increase in the moment and curvature, the difference is reduced to 11 kN.m 10% and 4% for Beam1 and Beam2, respectively. It can be seen that there is a clear difference between the model and measured beams at the early stage of cracking. However, this differentiation narrows down at the later stage of loading. This variation may be accounted for the effective moment of inertia. It is to some extent inaccurate at the early cracking stage whilst the accuracy increases as the ultimate load is approached. In addition to that, there is variation between the bonds of two similar beams, as was shown in the result of the regression (R^2) (see section 7.2.3.1).

Therefore, it can be said that the predicted moment-curvature is not sufficiently accurate for use when the cover thickness is lower or higher than 30 mm , or when large numbers of filaments are not activated as a result of improper layout. Thus, this developed method for predicting moment-curvature is limited to beams that have sufficient cover thickness and a proper layout which provides adequate bonding.

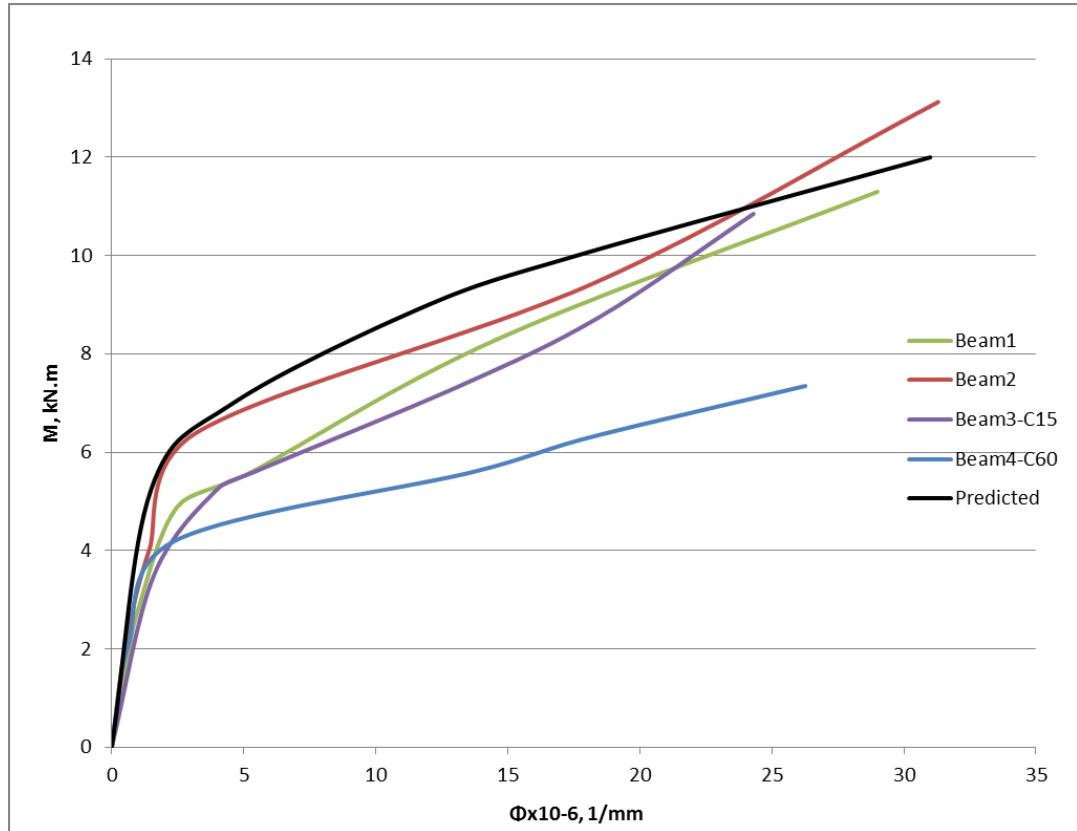


Figure 7-10 Predicted moment-curvature of a TRC beam against 4 experimentally beams measured.

7.2.6 Predicting crack width

As discussed in section 6.1.4.4, applying directly the same equation used for steel reinforced concrete beams overestimates the crack width of textile reinforced concrete beams. Equation 6.6 was produced based on experimental observations. Therefore, it can be adjusted to suit TRC beams by modifying the factor. The crack width of an experimental beam is calculated by using the design methodology presented in the cracked section (see section 7.2.2.2). Then, it is compared with the measured width observed in the TRC beam, as shown in Table 7-3.

Table 7-3 Measured and calculated crack width of a TRC beam.

Load, kN	TRC		
	Crack Width, mm		Measured/Calculated
	Measured Crack at Service Load	Calculated Crack	
16	0.04	0.40	0.10
18	0.06	0.45	0.13
20	0.08	0.50	0.16
22	0.16	0.55	0.29
24	0.22	0.60	0.37
26	0.26	0.65	0.40
28	0.28	0.70	0.40
30	0.38	0.76	0.50
32	0.42	0.81	0.52

It can be seen from Table 7-3, that the calculated crack width, based on the same factor that was provided in the equation for SRC beams, overestimates the crack width. By dividing the measured crack width by the calculated crack width, it can be observed that this ratio increases with load. To find the adjustment factor that needs to be included in Eq. 6.6, the relationship between the load and the measured crack width ratio is plotted in Figure 7-11. From this figure, it can be seen that the increase in the measured/calculated crack width ratio is approximately linear with load. Therefore, Eq. 6.6 becomes:

$$w = 0.076(0.028P - 0.3538)\beta f_f^3 \sqrt{d_c A} \quad (7.27)$$

$$w = (0.00213P - 0.00269)\beta f_f^3 \sqrt{d_c A} \quad (7.28)$$

where,

w is the crack width at the specific load;

P is the load.

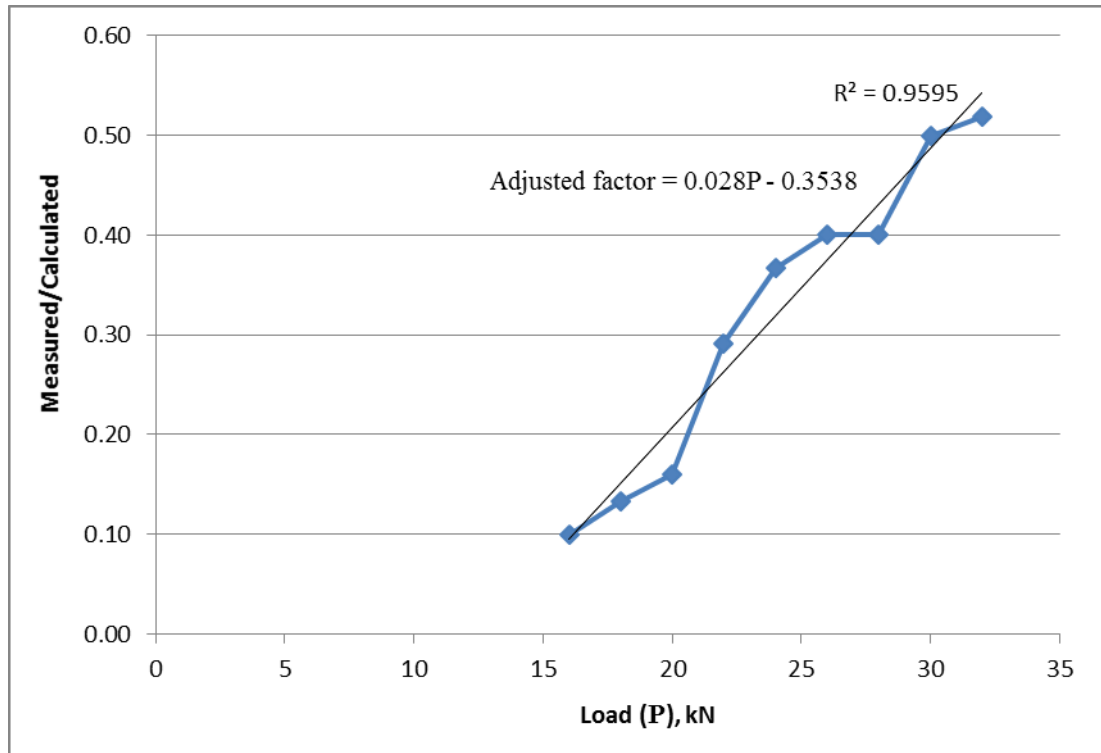


Figure 7-11 The relationship between the measured/calculated crack and the load of the TRC beam.

Table 7-4 shows the measured crack width of other TRC beams tested and compared with the predicted crack width based on the new equation. After cracking load, the increase in the load leads to further cracks and also widening in the crack width until the primary cracks are completely formed and stabilized. Then, with the increase in the load, more width is added to the formed crack.

Table 7-4 indicates that the calculated crack width is in good agreement with the measured crack width of Beam1 and Beam2. The predicted crack width shows this widening of cracks with a good correlation with the crack width of

experimental beams (Beam1 and Beam2). However, approaching failure load, the accuracy of crack width prediction is a little low as shown for Beam2. From the results for Beam1 and Beam2, it can be said that the predicted crack width is in good agreement with the experimental beams up to the stabilized crack load. After the stabilized cracking load, the prediction equation still exhibits predicted crack widths which are close to the measured ones with only slightly lower or higher predictions. However, in the case of Beam3-C15 (cover = 15 mm) and Beam4-C60 (cover = 60 mm), this developed equation could not predict the crack width. The measured crack widths are significantly higher than predicted, as shown in the table. This can be accounted for the change in the cover thickness. The crack width for a small cover thickness is expected to be lower in comparison to a 30 mm cover, however, as a result of the lack of bonding and a reduction in the number of activated filaments, the measured crack widths were higher. While, the crack width of larger cover thicknesses is expected to increase which the experimental results are showed it. However, the measured crack widths were very high because the 60 mm tension zone was unreinforced.

Therefore, it can be said that the developed crack width equation should be restricted to TRC beams with 30 mm cover thickness. In addition to that, proper reinforcement layout should be applied to obtain accurate results.

Table 7-4 Measured crack width of a TRC beam and calculated crack width based on the new proposed equation.

Load, kN	TRC										
	Crack width, mm										
	Beam1- C30	Beam2- C30	Calculated Crack	Beam1 Measured/ Calculated	Beam2 Measured/ Calculated	Beam3- C15	Calculated Crack	Beam3 Measured/ Calculated	Beam4- C60	Calculated Crack	Beam4 Measured/ Calculated
14	-	-	-	-	-	-	-	-	0.14	0.02	7.00
16	0.045	0.04	0.04	1.13	1.00	0.08	0.03	2.67	0.24	0.06	4.00
18	0.07	0.06	0.07	1.17	0.86	0.15	0.05	3.00	0.35	0.10	3.50
20	0.11	0.09	0.11	1.22	0.82	0.25	0.08	3.13	1.00	0.16	6.25
22	0.16	0.14	0.15	1.14	0.93	0.33	0.11	3.00	1.40	0.21	6.67
24	0.22	0.20	0.21	1.10	0.95	0.40	0.14	2.86	-	-	-
26	0.26	0.24	0.25	1.08	0.96	0.45	0.18	2.50	-	-	-
28	0.28	0.27	0.31	1.04	0.87	0.54	0.22	2.45	-	-	-
30	0.38	0.32	0.37	1.19	0.86	0.62	0.27	2.30	-	-	-
32	0.42	0.37	0.44	1.14	0.84	0.70	0.32	2.19	-	-	-
34	-	0.40	0.52	-	0.77	-	-	-	-	-	-
36	-	0.44	0.60	-	0.73	-	-	-	-	-	-
38	-	0.50	0.69	-	0.72	-	-	-	-	-	-

7.3 Examples

The following example shows theoretical calculations for the nominal moments of carbon textile reinforced concrete beams and compares them with the experimental beam results. Also, the reinforcement is assumed to be in three layers to ensure a good bond:

Compressive strength (f'_c) = 87 MPa.

Beam width (b) = 120 mm.

Beam depth (h) = 200 mm.

Carbon tensile strength of roving or tow (f_f) = 1550 MPa.

Area of carbon (A_f) = 92.5 mm².

Span length (l) = 2400 mm.

In order to find M_n , equation 7.21 is applied:

$$M_n = (\eta_\tau \rho) b d^2 f_{fu} \left(1 - 0.59 \frac{\eta_\tau \rho f_{fu}}{f'_c}\right)$$

The first step is to check whether the failure is a tension failure by ensuring the reinforcement ratio (ρ) is lower than the reinforcement balance (ρ_b):

$$\rho_b = 0.85 \beta_1 \frac{f'_c}{f_{fu}} \left(\frac{\varepsilon_{cu}}{\varepsilon_{cu} + \varepsilon_{fu}}\right)$$

$$\varepsilon_{cu} = 0.003$$

$$\varepsilon_{fu} = \frac{f_{fu}}{E_{fu}} = 0.02$$

Because f'_c is greater than 55 MPa:

$$\beta_1 = 0.65$$

So, ρ_b is 0.003

$$\rho = \frac{\eta_\tau A_f}{bd}$$

$$d = 200 - (30 + 2 + 15 + 1) = 152 \text{ mm}$$

The bond efficiency factor (η_τ) is 0.52, thus:

$$\rho \text{ is } 0.0026$$

Therefore, $\rho < \rho_b$

Tension is controlled, that means the tensile strength in textile can reach the ultimate (f_{fu}).

Hence M_n is:

$$M_n = 11.0 \text{ kN.m}$$

The theoretical analysis shows that the beam will resist 11.0 kN.m.

The same properties were experimentally tested and the nominal moment of two beams was found to be 11.8 and 13.8 kN.m. It can be said that the increase is a result of an increase in the activated area of fibres due to the increase in the number of activated filaments achieved with the reinforcement layout.

Because the failure is tension controlled, the design moment is:

$$\phi M_n = 0.60 \times 11.0 = 6.6 \text{ kN.m}$$

The following table illustrates the calculated nominal moment, and experimental nominal moment of the different TRC beams.

Table 7-5 The results for calculated and experimental nominal moment.

Reinforcement	Area, mm ²	Calculated M_n , kN.m	Experimental M_n , kN.m	Normalized
UT ₈ -2.6-C15, 50k	61.5	8.1	4.8	0.59
UT ₈ -Anch-2.6-C15, 50k	61.5	8.1	5.8	0.72
UT ₈ -Anch-L-2.6, 50k	61.5	7.3	6.4	0.88
UT ₁₂ -Anch-3L ₃ -2.6, 50k	61.5	6.84	6.8	1.0
UT ₁₂ -Anch-L-2.6, 50k	92.3	10.86	5.7	0.52
UT ₁₅ -Anch-3L ₃ -2.6, 50k	92.3	11.0	13.8	1.25
UT ₁₅ -Anch-3L ₃ -2.6, 50k	92.3	11.0	11.8	1.07
UT ₁₅ -Anch-3L ₃ -2.6-C15, 50k	92.3	11.2	11.4	1.02
UT ₁₅ -Anch-3L ₃ -2.6-C60, 50k	92.3	8.11	7.5	0.92

From the table, the experimental moment over the calculated nominal moment is the normalized value. Less than one means the experimental moment is lower than calculated and higher than one means the experimental moment is higher than calculated. It can be seen that there are five beams with values lower than one which means the calculations overestimated the capacity. However, on closer inspection, for the same area and properties of fibre but with the layout of textile reinforcement spread into three layers as in UT₁₂-Anch-3L₃-2.6, the experimental moment was greater than calculated. In addition, the cover thickness was increased from 15 mm to 30 mm which provided sufficient bonding around the reinforcement. This implies that the bond is improved because the number of filaments that are in direct contact with concrete is increased and a cover of sufficient thickness has been applied. All of the beams that were reinforced with three layers had an

experimental capacity greater than or similar to the calculated moment. This was further confirmed by looking at UT₁₂-Anch-L-2.6, which had two layers, and comparing its results with the other beams reinforced with three layers. The results show that with two layers the experimental moment was significantly reduced in compare with calculated moment.

Using the derived reduction factor will ensure that the actual capacity is greater than the ULS (Ultimate Limit State) design value. Thus, the structural member is safe, as a result of $\phi M_n \geq M_u$.

7.4 Conclusions

The main conclusions of the design methodology chapter are as follows:

- The investigation shows that a steel reinforced concrete beam design methodology cannot be directly applied to textile reinforced concrete beams.
- The same can also be said for the FRP reinforced concrete beam methodology.
- This is because of the bond; rovings/tows are divided into outer and inner filaments, which means that not all filaments are bonded well with the concrete. Also, the TRC mechanism is different from that for SRC and FRP reinforced concrete.
- TRC beams can, however, adopt the methodology used for SRC beams and FRP reinforced beams with several adjustments.
- The bond efficiency factor is applied to determine the area that is effectively resisting flexural load.
- The analysis and design methodology is based on the effective area of textile reinforcement.
- The analysis of TRC beam behaviour at the uncracked section is similar to that for the uncracked SRC beam.
- At the cracked section and up to half of compressive strength, the analysis is developed to represent the actual behaviour of a TRC beam.

- A TRC beam design methodology is developed and showed good agreement with experimental beams when a proper reinforcement layout and sufficient cover depth were used.
- The reduction factor is statistically calculated in order to ensure design safety.
- The proposed moment-curvature prediction method shows an acceptable accuracy in determining the moment-curvature behaviour especially at the late stage of behaviour.
- An equation for computing the crack width of a TRC beam is suggested. Unlike the SRC beam equation, it shows a high degree of correlation with the measured TRC beam up to failure.

CHAPTER 8

CONCLUSIONS AND RECOMMENDATIONS FOR FUTURE STUDIES

8.1 Introduction

In this study, carbon textile reinforced concrete (TRC) beams were investigated in order to develop a structural design methodology which could incorporate textile reinforcement. Therefore, textile reinforced concrete beams of various sizes, reinforced with different textile layouts and types, were studied. In addition, steel reinforced concrete (SRC) beams were tested to provide 'control' data. Experimentally, the crack width and propagation, beam behaviour in terms of load and deflection, beam failure mode, and tension stiffening of both TRC and SRC beams were investigated. In addition, the study was extended to investigate the tensile strength and pull out strength of textile reinforcement. This chapter summarises the main findings of this research and presents recommendations for future work.

8.2 Conclusions

The main findings of this study can be summarised as follows:

- The flexural results for TRC beams using normal concrete mixes show that textile reinforcement can be used to reinforce normal concrete and not just fine grained concrete mixes.
- The experimental tensile strength of a roving/tow is significantly lower than the tensile strength of a single filament; this is because not all filaments are stressed to the same level. Effectively, it was found that not all filaments are activated. Therefore, the tensile strength of a single filament must not be used to represent the textile strength in composite.
- The test to determine the stress-strain behaviour of textile reinforcement needs a special set up to avoid shear or partial failure of the filaments.

- Pull out strength is hard to measure because of the 'slippery' inner filaments.
- TRC beams exhibited a considerable increase in performance compared with FRC beams for the same volume fraction of fibre.
- Textile geometry and layout have a direct influence on the bond between concrete and reinforcement. Loose rovings/tows (as in bundled fibre) lead to a better bond as a result of the increase in the interaction between the concrete and reinforcement and therefore an increase in the number of activated filaments. Therefore, the TRC beam (with loose rovings/tows) performed much better in terms of load capacity and deflection.
- Textile reinforcement is corrosion-resistant which could encourage the design of smaller cover thicknesses. However, a small cover thickness may lead to premature failure or horizontal shear failure due to the reduced capacity for stress transfer between the reinforcement and the concrete. The optimum cover thickness in this study was found to be *30 mm*.
- The cross sectional area of the textile reinforcement in the loading direction, rather than the volume fraction of fibre, should be used to determine the mechanical properties of textile reinforced concrete.
- TRC beams differ from SRC beams with regard to moment-curvature behaviour because of the difference between the textile and steel reinforcement properties. The main difference in the properties between textile and steel reinforcement is the stress-strain behaviour.
- Bond, and specifically the surface contact between the concrete and textile reinforcement, are significant. The increase in the contact surface area leads to an improvement in the stiffness and toughness of TRC beams.
- As a result of improving the contact surface area of the textile reinforcement, the first crack in a TRC beam occurs at a higher load by approximately 14% than in an equivalent SRC beam. Also, when the stabilised crack pattern is achieved, the number of primary cracks in a TRC beam is greater than that in an SRC beam.

- TRC beams can exhibit a greater stiffness than SRC beams, consequently the crack width in TRC beams can be almost 50% lower. This could be a positive advantage of textile reinforcement over steel reinforcement in terms of aesthetic appearance.
- For the same area of reinforcement, the ultimate load of TRC beams could be up to 56% greater than that of SRC beams. Also, the ultimate deflection is 37% lower than that of an SRC beam. However, at SLS (Service Limit State), the deflection of TRC beams is significantly lower (62%) than that of SRC beams.
- Textile reinforced concrete beams possess a significant degree of tension stiffening. At SLS, it is up to 7 times that observed in SRC beams.
- Owing to the nature of the bond and the failure mode exhibited by TRC beams, the design methodology used in steel reinforced concrete beam codes cannot be directly applied to the design of textile reinforced concrete beams.
- For textile reinforced concrete beam design methodology the effective area of the active filaments is determined based on the bond efficiency factor.
- The proposed TRC beam design methodology is reasonably successful in predicting nominal moments. The method of predicting the moment capacity is enhanced when an appropriate bond efficiency factor is derived which better represents specific layouts of reinforcement and cover thickness.
- A design reduction factor can be statistically computed in order to ensure that the design capacity of the TRC beam is safe. This factor was found to be 0.60.
- A crack width equation has been developed which accurately predicts the width of crack in a TRC beam up to failure. This is an improvement on the traditional theory for steel reinforced concrete which is only accurate up to the crack stabilization stage.

8.3 Recommendations for further study

There are several areas in this research which need more investigation in order to ensure a better and more comprehensive understanding of textile reinforced beams and the reinforcement itself. It is recommended that further research is undertaken in the following areas:

- Pull out strength behaviour; in particular, further understanding is required of the test set up, including the mould dimensions.
- Research is required to determine the optimum textile geometry and layout that needs to be used to activate more filaments in the roving/tow. Also, the cover thickness which will allow adequate transfer of stresses between the two elements of the composite needs to be better understood.
- Further investigation is required to study the effect of the increase in the volume fraction on the behaviour of TRC beams.
- Investigation is required into the contribution of the second and third layer (if present) of reinforcement in TRC beams to the load capacity and deflection of the beam, especially at failure. In addition, this investigation could be extended to study the behaviour of textile reinforced concrete beams when over-reinforced.
- The phenomenon of surface contact between the concrete and the textile needs to be fully understood. Furthermore, calculation of the number of activated filaments would help to understand the behaviour for different layouts and geometries.
- Data on the actual tensile stress of the textile reinforcement during flexural bending tests would provide further understanding of TRC beam behaviour.
- The long term behaviour of TRC beams needs to be quantified in order to determine the degradation mechanisms and influences on the filaments.
- Design reduction factors could be further optimized.

- Shear design of textile reinforced concrete also needs to be investigated.

REFERENCE

- Abdulmajeed, A. A., T. O. Närhi, P. K. Vallittu and L. V. Lassila. 2011. The effect of high fiber fraction on some mechanical properties of unidirectional glass fiber-reinforced composite. *Dental Materials*,**27**(4), pp.313-321.
- Aci-440, C. 2006. *440.1R-06: Guide for the Design and Construction of Structural Concrete Reinforced with FRP Bars*.
- Aci 318, C. 2011. *ACI 318-11: Building Code Requirements for Structural Concrete and Commentary (318-11)*. American Concrete Institute, First Edition edition.
- Aci 544, C. 1996. *ACI 544.1R-96 State of the Art on Fiber Reinforced Concrete*. American Concrete Institute
- Al-Jamous, A., R. Ortlepp, S. Ortlepp, M. Curbach, J. Hegger, W. Brameshuber and N. Will. 2006. Experimental investigations about construction members strengthened with textile reinforcement. *In: J. HEGGER, W. BRAMESHUBER and N. WILL, eds. ICTRC'2006 - 1st International RILEM Conference on Textile Reinforced Concrete*. RILEM Publications SARL, pp.161-170.
- Aldea, C., T. Gries and A. Roye. 2006. Definitions. *In: W. BRAMESHUBER, ed. Textile Reinforced Concrete - State-of-the-Art Report of RILEM TC 201-TRC*. RILEM Publications SARL.
- Alrshoudi, F. and P. Purnell. 2015. Bond efficiency factor at different textile geometries reinforced concrete beams. *In: Second International Conference on Advances in Civil, Structural and Construction Engineering - CSCE 2015, Italy, Rome*.
- Aveston, J., G. A. Cooper and A. Kelly. 1971. Single and multiple fracture: the properties of fiber composites. *In: Conference proceedings of NPL Conference: IPC Science and Technology Press*, pp.15-24.
- Banholzer, B. 2006. Bond of a strand in a cementitious matrix. *Materials and structures*,**39**(10), pp.1015-1028.
- Bartos, P. 1981. Review paper: Bond in fibre reinforced cements and concretes. *International Journal of Cement Composites and Lightweight Concrete*,**3**(3), pp.159-177.
- Bayer, D. and M. Richter. 2010. On the Crack Opening in Textile Reinforced Concrete with Regard to Fibre Bridging. *In: International RILEM*

Conference on Material Science, Aachen, Germany. RILEM Publications SARL.

- Bentur, A. and S. Mindess. 2006. *Fibre Reinforced Cementitious Composites* Second Edition ed. Taylor & Francis.
- Brameshuber, W. and T. Brockmann. 2006. Introduction. In: W. BRAMESHUBER, ed. *Textile Reinforced Concrete - State-of-the-Art Report of RILEM TC 201-TRC*. RILEM Publications SARL.
- Brameshuber, W., T. Brockmann, M. Curbach, C. Meyer, G. Vilkner, B. Mobasher, A. Peled, H. W. Reinhardt, M. Krüger and J. Wastiels. 2006. Concrete/Matrix. In: W. BRAMESHUBER, ed. *Textile Reinforced Concrete - State-of-the-Art Report of RILEM TC 201-TRC*. RILEM Publications SARL.
- Brandt, A. M. 1995. *Cement-based Composites: Materials, Mechanical Properties and Performance* First edition ed. Spon Press
- Brockmann, T. 2005. *Mechanical and fracture mechanical properties of fine grained concrete for textile reinforced composites*. thesis, Universitätsbibliothek.
- Brockmann, T. and W. Brameshuber. 2005. Matrix development for the production technology of textile reinforced concrete (TRC) structural elements. In: *composites in construction 2005 - third international conference*, Lyon, France.
- Butler, M., M. Lieboldt and V. Mechtcherine. 2009. Application of Textile-Reinforced Concrete (TRC) for structural strengthening and in prefabrication. *Advances in Cement-Based Materials*. CRC Press, pp.127-136.
- Butler, M., V. Mechtcherine and S. Hempel. 2010. Durability of textile reinforced concrete made with AR glass fibre: effect of the matrix composition. *Materials and structures*, **43**(10), pp.1351-1368.
- Cheyrezy, M., J. I. Daniel, H. Krenchel, H. Mihashi, J. Pera, P. Rossi and Y. Xi. 1996. Specific production and manufacturing issues In: A. E. NAAMAN and H. W. REINHARDT, eds. *High Performance Fiber-reinforced Cement Composites 2 (HPFRCC 2)*. Spon Press, p.528.
- Cohen, Z., A. Peled, Y. Pasder, A. Roye and T. Gries. 2006. Effects of warp knitted fabrics made from multifilament in cement-based composites. In: *ICTRC'2006 - 1st International RILEM Conference on Textile Reinforced Concrete*, Aachen, Germany. RILEM Publications SARL, pp.23 - 32.

- Colombo, I., A. Magri, G. Zani, M. Colombo and M. Di Prisco. 2013. Textile Reinforced Concrete: experimental investigation on design parameters. *Materials and structures*,**46**(11), pp.1933-1951.
- Contamine, R., A. S. Larbi and P. Hamelin. 2010. Tensile Identification of Textile Reinforcement Concrete Behaviour. *In: International RILEM Conference on Material Science: RILEM Publications SARL*, pp.105-110.
- Cuypers, H. and J. Wastiels. 2006. A Stochastic Cracking Theory For The Introduction of Matrix Multiple Cracking in Textile Reinforced Concrete Under Tensile Loading. *In: Textile Reinforced Concrete*, Aachen, Germany. RILEM Publications SARL.
- Dolatabadi, M. K., S. Janetzko, T. Gries, B.-G. Kang and A. Sander. 2010. An Analytical Investigation of Cement Penetration within Bundle of Fibers. *In: International RILEM Conference on Material Science*, Aachen, Germany. RILEM Publications SARL.
- Forth, J. P. and A. J. Martin. 2014. *Design of Liquid Retaining Concrete Structures*. 3rd edition ed. Whittles Publishing.
- Freitag, S., M. Beer, F. Jesse, S. Weiland, J. Hegger, W. Brameshuber and N. Will. 2006. Experimental investigation and prediction of long-term behavior of textile reinforced concrete for strengthening. *year: 2006*, pp.121-130.
- Gergely, P. and L. A. Lutz. 1968. Maximum crack width in reinforced concrete flexural members. *In: Causes, mechanism and control of cracking in concrete.*, Detroit, Michigan, 48219, USA,. American Concrete Institute, pp.87–117.
- Ghali, E., V. S. Sastri and M. Elboudjaini. 2007. *Corrosion prevention and protection: practical solutions*. John Wiley & Sons.
- Graf, W., A. Hoffmann, B. Möller, J. U. Sickert and F. Steinigen. 2007. Analysis of textile-reinforced concrete structures under consideration of non-traditional uncertainty models. *Engineering Structures*,**29**(12), pp.3420-3431.
- Gray, R. J. and C. D. Johnston. 1987. The influence of fibre-matrix interfacial bond strength on the mechanical properties of steel fibre reinforced mortars. *International Journal of Cement Composites and Lightweight Concrete*,**9**(1), pp.43-55.
- Greszczuk, L. B. 1969. Theoretical studies of the mechanics of the fiber matrix interface of composites

- Interfaces in Composites*. Philadelphia: American Society for Testing and Materials, pp.42-45.
- Gries, T., A. Roye, P. Offermann and A. Peled. 2006. Textiles. In: W. BRAMESHUBER, ed. *Textile Reinforced Concrete - State-of-the-Art Report of RILEM TC 201-TRC*. RILEM Publications SARL.
- Hanisch, V., A. Kolkman, A. Roye and T. Gries. 2006. Influence of machine settings on mechanical performance of yarn and textile structures. In: *ICTRC'2006 - 1st International RILEM Conference on Textile Reinforced Concrete*, Aachen, Germany. RILEM Publications SARL, pp.13 - 22.
- Hannant, D. J. 2003. 6 - Fibre-reinforced concrete. In: J. NEWMAN and B. S. CHOO, eds. *Advanced Concrete Technology Set*. Oxford: Butterworth-Heinemann, pp.1-17.
- Hartig, J., F. Jesse, U. Häußler-Combe and W. Brameshuber. 2010. Evaluation of experimental setups for determining the tensile strength of Textile Reinforced Concrete. In: *International RILEM Conference on Material Science*: RILEM Publications SARL, pp.117-127.
- Hartig, J., F. Jesse, K. Schicktanz and U. Häußler-Combe. 2012. Influence of experimental setups on the apparent uniaxial tensile load-bearing capacity of Textile Reinforced Concrete specimens. *Materials and structures*, **45**(3), pp.433-446.
- Häußler-Combe, U. and J. Hartig. 2006. Uniaxial structural behavior of TRC – A one-dimensional approach considering the transverse direction by segmentation. In: *ICTRC'2006 - 1st International RILEM Conference on Textile Reinforced Concrete*, Aachen, Germany. RILEM Publications SARL.
- Häußler-Combe, U. and J. Hartig. 2007. Bond and failure mechanisms of textile reinforced concrete (TRC) under uniaxial tensile loading. *Cement and Concrete Composites*, **29**(4), pp.279-289.
- Hegger, J., O. Bruckermann and R. Chudoba. 2004. A smeared bond-slip relation for multi-filament yarns embedded in fine concrete. In: *6th International RILEM Symposium on Fibre Reinforced Concretes*: RILEM Publications SARL.
- Hegger, J., M. Horstmann and M. Zell. 2008. Textile Reinforced Concrete - Realization in applications. *Tailor Made Concrete Structures*. CRC Press, pp.98-98.

- Hegger, J. and S. Voss. 2004. Textile reinforced concrete under biaxial loading. *In: 6th International RILEM Symposium on Fibre Reinforced Concretes*: RILEM Publications SARL.
- Hegger, J. and S. Voss. 2008. Investigations on the bearing behaviour and application potential of textile reinforced concrete. *Engineering Structures*,**30**(7), pp.2050-2056.
- Hegger, J., S. Voss and O. Bruckermann. 2005. Textile Reinforced Concrete - Bearing Behaviour, Design, Application. *In:Composites in Construction 1005 - Third International Conference, Lyon, France*. pp.1139-1146.
- Hegger, J., N. Will, C. Aldea, W. Brameshuber, T. Brockmann, M. Curbach and J. Jesse. 2006a. Applications of textile reinforced concrete. *In: W. BRAMESHUBER, ed. Textile Reinforced Concrete - State-of-the-Art Report of RILEM TC 201-TRC*. RILEM Publications S.A.R.L., pp.237-266.
- Hegger, J., N. Will, A. Bentur, M. Curbach, F. Jesse, B. Mobasher, A. Peled and J. Wastiels. 2006b. Composite materials - 6.2 Mechanical behaviour of textile reinforced concrete. *In: W. BRAMESHUBER, ed. Textile Reinforced Concrete - State-of-the-Art Report of RILEM TC 201-TRC*. RILEM Publications SARL.
- Hegger, J., N. Will, O. Bruckermann and S. Voss. 2006c. Load-bearing behaviour and simulation of textile reinforced concrete. *Materials and structures*,**39**(8), pp.765-776.
- Hinzen, M. and W. Brameshuber. 2009. Improvement of serviceability and strength of Textile Reinforced Concrete by using short fibres. *In: Textile reinforced structures. Proceedings of the 4th colloquium on textile reinforced structures (CTRS4), Dresden*, pp.261-272.
- Hognestad, E., N. W. Hanson and D. Mchenry. 1955. Concrete stress distribution in ultimate strength design. *Journal of the American Concrete Institute*,**Part 1. Vol. 27**.
- Jesse, F. and G. Curbach. 2003. Strength of continuous AR-glass fibre reinforcement of cementitious composites. *In: International Workshop High Performance Fiber Reinforced Cement Composites*: RILEM Publications SARL.
- Jesse, F., N. Will, M. Curbach and J. Hegger. 2008. Load-bearing behavior of textile-reinforced concrete. *ACI Special Publication*,**250**.

- Johnston, C. 2000. *Fiber-Reinforced Cements and Concretes*. Taylor & Francis.
- Kabele, P., L. Novák, J. Nemecek and L. Kopecký. 2006. Effects of chemical exposure on bond between synthetic fiber and cementitious matrix. *In: ICTRC'2006 - 1st International RILEM Conference on Textile Reinforced Concrete*: RILEM Publications SARL.
- Keil, A., H. Cuypers and J. Wastiels. 2008. study of the bond in textile reinforced concrete: influence of matrix and interface modification. *In: Challenges for Civil Construct*, Portuga, Porto.
- Khalfallah, S. and D. Guerdouh. 2014. Tension stiffening approach in concrete of tensioned members. *International Journal of Advanced Structural Engineering (IJASE)*,6(1), pp.1-6.
- Ko, F. K. 1993. Advanced topics in materials science and engineering. *In: J. L. MORÁN-LÓPEZ and J. M. SANCHEZ*, eds. Plenum Press.
- Köksal, F., F. Altun, İ. Yiğit and Y. Şahin. 2008. Combined effect of silica fume and steel fiber on the mechanical properties of high strength concretes. *Construction and Building Materials*,22(8), pp.1874-1880.
- Kruger, M., H.-W. Reinhardt and M. Fichtlscherer. 2001. BOND BEHAVIOUR OF TEXTILE REINFORCEMENT IN REIN-FORCED AND PRESTRESSED CONCRETE. *Otto-Graf-Journal*,12, p33.
- Kwan, W. H., M. Ramli and C. B. Cheah. 2014. Flexural strength and impact resistance study of fibre reinforced concrete in simulated aggressive environment. *Construction and Building Materials*,63(0), pp.62-71.
- Laws, V. 1971. The efficiency of fibrous reinforcement of brittle matrices. *Journal of Physics D: Applied Physics*, 4, pp.1737-1746.
- Laws, V., P. Lawrence and R. W. Nurse. 1971. Reinforcement of brittle matrices by glass fibres *Journal of Physics D: Applied Physics*,**Volume 6**, pp.523-537.
- Lieboldt, M., R. Hempel, H. Schorn, G. Franzke and U. Helbig. 2005. Textile reinforced concrete and polymer pipes. *In: Fibre Reinforced Concrete in Practice: 1st Central European Congress on Concrete Engineering*, Graz, Austria. Österr. Vereinigung für Beton- und Bautechnik.
- Majumdar, A. J. 1974. The role of the interface in glass fibre reinforced cement. *Cement and Concrete Research*,4(2), pp.247-268.

- Mashima, M., D. J. Hannant and J. G. Keer. 1990. Tensile Properties of Polypropylene Reinforced Cement with Different Fiber Orientations. *Materials Journal*,**87**(2), pp.172-178.
- Mindess, S., J. F. Young and D. Darwin. 2003. *Concrete*. Prentice Hall.
- Mobasher, B. 2011. *Mechanics of Fiber and Textile Reinforced Cement Composites*. CRC Press
- Mobasher, B. and C. Y. Li. 1996. Effect of interfacial properties on the crack propagation in cementitious composites. *Advanced Cement Based Materials*,**4**(3), pp.93-105.
- Mumenya, S., R. Tait and M. Alexander. 2011. Evaluation of toughness of textile concrete. *Materials and structures*,**44**(1), pp.279-289.
- Naaman, A. 2007. Tensile strain-hardening FRC composites: Historical evolution since the 1960. In: C. GROSSE, ed. *Advances in Construction Materials 2007*. Springer Berlin Heidelberg, pp.181-202.
- Neville, A. M. 1995. *Properties of Concrete*. Pearson Education.
- Neville, A. M. and J. J. Brooks. 2010. *Concrete Technology*. Second edition 2010 ed. Pearson Education Limited.
- Nilson, A., D. Darwin and C. Dolan. 2009. *Design of Concrete Structures*. McGraw-Hill
- Ohno, S. and D. Hannant. 1994. Modelling the stress–strain response of continuous fiber reinforced cement composites. *ACI Materials Journal*,**91**(3), pp.306-312.
- Papanicolaou, C. G. and I. C. Papantoniou. 2010. Mechanical Behavior of Textile Reinforced Concrete (TRC)/Concrete Composite Elements. *Journal of Advanced Concrete Technology*,**8**(1), pp.35-47.
- Peled, A. and A. Bentur. 2000. Geometrical characteristics and efficiency of textile fabrics for reinforcing cement composites. *Cement and Concrete Research*,**30**(5), pp.781-790.
- Peled, A. and A. Bentur. 2003. Fabric structure and its reinforcing efficiency in textile reinforced cement composites. *Composites Part A: Applied Science and Manufacturing*,**34**(2), pp.107-118.
- Peled, A., A. Bentur and D. Yankelevsky. 1998. Effects of Woven Fabric Geometry on the Bonding Performance of Cementitious Composites:

- Mechanical Performance. *Advanced Cement Based Materials*,7(1), pp.20-27.
- Peled, A., A. Bentur and D. Yankelevsky. 1999. Flexural performance of cementitious composites reinforced with woven fabrics. *Journal of materials in civil engineering*,11(4), pp.325-330.
- Peled, A., Z. Cohen, Y. Pasder, A. Roye and T. Gries. 2008. Influences of textile characteristics on the tensile properties of warp knitted cement based composites. *Cement and Concrete Composites*,30(3), pp.174-183.
- Peled, A., E. Zaguri and G. Marom. 2008. Bonding characteristics of multifilament polymer yarns and cement matrices. *Composites Part A: Applied Science and Manufacturing*,39(6), pp.930-939.
- Prull, W. 1995. One-Coat Stucco. *The Journal of Light Construction*
- Purnell, P. 2010a. Interface and bonding. In: P. DOMONE and J. ILLSTON, eds. *Construction Materials: Their Nature and Behaviour*. Fourth Edition ed. CRC Press, p.375.
- Purnell, P. 2010b. Mechanical behaviour of FRC. In: P. DOMONE and J. ILLSTON, eds. *Construction Materials: Their Nature and Behaviour*. 4th ed. London and New York: Spon Press, p.567.
- Purnell, P. 2010c. Reinforcement layouts. In: P. DOMONE and J. ILLSTON, eds. *Construction Materials: Their Nature and Behaviour*. London: Spon Press, p.567.
- Raupach, J. B. M. 2002. Durability Investigations On Textile Reinforced Concrete.
- Reinhardt, H.-W., M. Krüger, A. Bentur, W. Brameshuber, B. Banholzer, M. Curbach, F. Jesse, B. Mobasher, A. Peled and H. Schorn. 2006a. Composite materials - 6.1 Bond. In: W. BRAMESHUBER, ed. *Textile Reinforced Concrete - State-of-the-Art Report of RILEM TC 201-TRC*. RILEM Publications SARL, pp.83 - 131.
- Reinhardt, H.-W., M. Kruger, M. Bentur, W. Brameshuber, B. Banholzer, M. Curbach, F. Jesse, B. Mobasher, A. Peled and H. Schorn. 2006b. Composite Materials. In: W. BRAMESHUBER, ed. *Textile Reinforced Concrete, State-of-the-Art Report of RILEM TC 201-TRC*. Bagneux, France: RILEM Publications S.A.R.L., p.292.
- Rypl, R., M. Vo Echovský, B. Sköck-Hartmann, R. Chudoba and T. Gries. 2009. Effect of twist, fineness, loading rate and length on tensile

behavior of multifilament yarn. *In: 4th Colloquium on Textile Reinforced Structures (CTRS4), Dresden, Germany.*

Schlangen, E., H. Prabowo, M. G. Sierra-Beltran and Z. Qian. 2010. A model for building a design tool for ductile fibre reinforced materials. *Advances in Cement-Based Materials.*

Schwartz, M. M. 1997. *Composite Materials: Properties, nondestructive testing, and repair.* Prentice Hall PTR.

Shi-Lang, X. and L. He. 2006. Bond properties and experimental methods of textile reinforced concrete. *In: ICTRC'2006 - 1st International RILEM Conference on Textile Reinforced Concrete:* RILEM Publications SARL.

Sickert, J.-U., B. Möller, W. Graf and S. Freitag. 2006. Time-dependent reliability of strengthened RC structures. *In: ICTRC'2006 - 1st International RILEM Conference on Textile Reinforced Concrete,* Aachen, Germany. RILEM Publications SARL.

Silva, F. D. A., M. Butler, V. Mechtcherine, D. Zhu and B. Mobasher. 2011. Strain rate effect on the tensile behaviour of textile-reinforced concrete under static and dynamic loading. *Materials Science and Engineering: A*, **528**(3), pp.1727-1734.

Soranakom, C. and B. Mobasher. 2009. Geometrical and mechanical aspects of fabric bonding and pullout in cement composites. *Materials and structures*, **42**(6), pp.765-777.

Sri Ravindrarajah, R. and C. T. Tam. 1984. Flexural strength of steel fibre reinforced concrete beams. *International Journal of Cement Composites and Lightweight Concrete*, **6**(4), pp.273-278.

Steinigen, F., B. Möller, W. Graf and A. Hoffmann. 2006. Numerical simulation of textile reinforced concrete considering dynamic loading processes. *In: ICTRC'2006 - 1st International RILEM Conference on Textile Reinforced Concrete,* Aachen, Germany. RILEM Publications SARL.

Stucke, M. and A. Majumdar. 1976. Microstructure of glass fibre-reinforced cement composites. *Journal of Materials Science*, **11**(6), pp.1019-1030.

Swamy, R. N. 1975. Fibre reinforcement of cement and concrete. *Matériaux et Construction*, **8**(3), pp.235-254.

Swamy, R. N. and N. I. Fattuhi. 1974. Mechanics and properties of steel fibre reinforced concrete. *In: First Australian Conference on Engineering Materials,* Sydney. University of New South Wales

- Swamy, R. N. and M. W. Hussin. 1989. Woven polypropylene fabrics - an alternative to asbestos for thin sheet application. *In: Fibre reinforced cements and concretes: recent developments*: Elsevier Science Publishers, pp.p. 90-100.
- Swamy, R. N. and P. S. Mangat. 1974. A theory for the flexural strength of steel fiber reinforced concrete. *Cement and Concrete Research*,**4**(2), pp.313-325.
- Tysmans, T., S. Adriaenssens, H. Cuyper and J. Wastiels. 2009. Structural analysis of small span textile reinforced concrete shells with double curvature. *Composites Science and Technology*,**69**(11-12), pp.1790-1796.
- Vorechovský, M., J. Jerábek and R. Chudoba. 2006. Impact of scatter of material properties on the yarn performance in TRC. *In: ICTRC'2006 - 1st International RILEM Conference on Textile Reinforced Concrete*, Aachen, Germany. RILEM Publications SARL.
- Voss, S. 2006. DESIGN METHODS FOR TEXTILE REINFORCED CONCRETE. *In: T. VOGEL, N. MOJSILOVIĆ and P. MARTI, eds. 6th International PhD Symposium in Civil Engineering, August 23-26, 2006, Zurich*.
- Voss, S., J. Hegger, W. Brameshuber and N. Will. 2006a. Dimensioning of textile reinforced concrete structures. *In: ICTRC'2006-1st International RILEM Conference on Textile Reinforced Concrete*: RILEM Publications SARL, pp.151-160.
- Voss, S., J. Hegger, W. Brameshuber and N. Will. 2006b. Dimensioning of textile reinforced concrete structures. *year: 2006*, pp.151-160.
- Whitney, C. S. 1937. Design of reinforced concrete members under flexure or combined flexure and direct compression. *In: ACI Journal Proceedings*: ACI.
- Wight, J. K. and J. G. Macgregor. 2009. *Reinforced Concrete Mechanics and Design*. Fifth ed. Pearson Prentice Hall.
- Williams Portal, N., K. Lundgren and K. Malaga. 2014. Evaluation of Pull-out Behaviour in Textile Reinforced Concrete. *In: 10th fib International PhD Symposium in Civil Engineering*.
- [Www.Adbengineering.Com](http://www.adbengineering.com). *Concrete Reinforcing Steel Corrosion* [online]. [Accessed 05/08].
- Yang, L. 2008. *Techniques for corrosion monitoring*. Elsevier.

- Yin, S.-P., H.-L. Lü and S.-L. Xu. 2013. Properties and calculation of normal section bearing capacity of RC flexural beam with skin textile reinforcement. *Journal of Central South University*,**20**(6), pp.1731-1741.
- Yin, S. P., S. L. Xu and F. Wang. 2015. Investigation on the flexural behavior of concrete members reinforced with epoxy resin-impregnated textiles. *Materials and Structures*,**48**(1-2), pp.153-166.
- Zhu, W. and P. Bartos. 1997. Assessment of interfacial microstructure and bond properties in aged GRC using a novel microindentation method. *Cement and Concrete Research*,**27**(11), pp.1701-1711.